UCRL-ID-153750

LAWRENCE
LIVERMORE
NATIONAL
LABORATORY

Electron Transport Workshop, September 9-11, 2002

J. Edwards, S. Glenzar, E. Alley, R. Town, D. Braun, S. Kruer, B. Lasinski, A. Mackinnon, M. Haines, R. Kingham, N. Nicolai, E. Valco, S. Krasheninnikov

June 17, 2003

This work was performed under the auspices of the U.S. Department of Energy by University of California, Lawrence Livermore National Laboratory under Contract W-7405-Eng-48.

Electron Transport Workshop

Purple Orchid (www.purpleorchid.com) 925 606 8855

9-11 September 2002

Agenda

Monday 9th September

8:30	Introduction & Welcome	(Edwards)
9:00	Overview of issues for NIF	(Glenzer)
9:45	Physics of magnetic fields & Criterion for validity of linear transport	(Haines)
10:30	Break	
11:00	Hybrid electron transport package	(Alley)
11:45	Hohlraums according to lasnex	(Edwards)
12:30	Lunch	
1:30	Non-Local heat flow in FCI2	(Schurtz)
	Coupled MHD non-local model	(Schurtz)
2:30	Application of FCI2 to laser expts	(Nicolai)
3:30	Break	
4:00	Omega direct drive implosions	(Town)
4:30	Omega & NIF slab experiments	(Braun)
5:00	High intensity slab modeling with FCI2	(Nicolai)
5:30	**BBQ**	

Tuesday 10th September

8:30	Tidman and Shanny instability – viscosity or f2?	(Haines)
9:30	Filamentary structures	(Mackinnon)
10:00	Electro-thermal instability	(Haines)
10:30	Break	
11:00	Interface with LPI	(Kruer)
11:15	B-fields around a laser speckle	(Lasinski)
11:30	Detuning SBS	(Haines)
11:45	I/c driven fields in lasnex	(Edwards)
12:00	Collisional δf model	(Valeo)
12:30	Lunch	
1:30	2-D Fokker Planck with B	(Kingham)
2:30	2-D FP without B	(Town)
2:50	1-D FP with B & v^{-2}	(Haines)
3:30	Break	
4:00	An improved model of non-local heat flow in laser heated plasmas	(Matte)
4:45	A 3D model for non-local heat flow	(Krasheninnikov)

Wednesday 11th Septenber

Discussion sessions on future plans. This will shape up during the first two days

8:00 Future theory/computation

topics include:
Is 2D good enough?
Micro-turbulence
Simulations & code development (Fokker-Planck vs non-local)
Numerical benchmarks

11:00 Thomson scattering measurements of heat flow (Hawreliak)

12:00 lunch

1:00 Wash up discussions

Heat Transport in 2D Simulations of High Intensity, Direct Drive Ablation

David Braun, David Bradley, Gilbert Collins, John Edwards and Larry Suter

LLNL

High pressure shock experiments are required to verify equation of state models

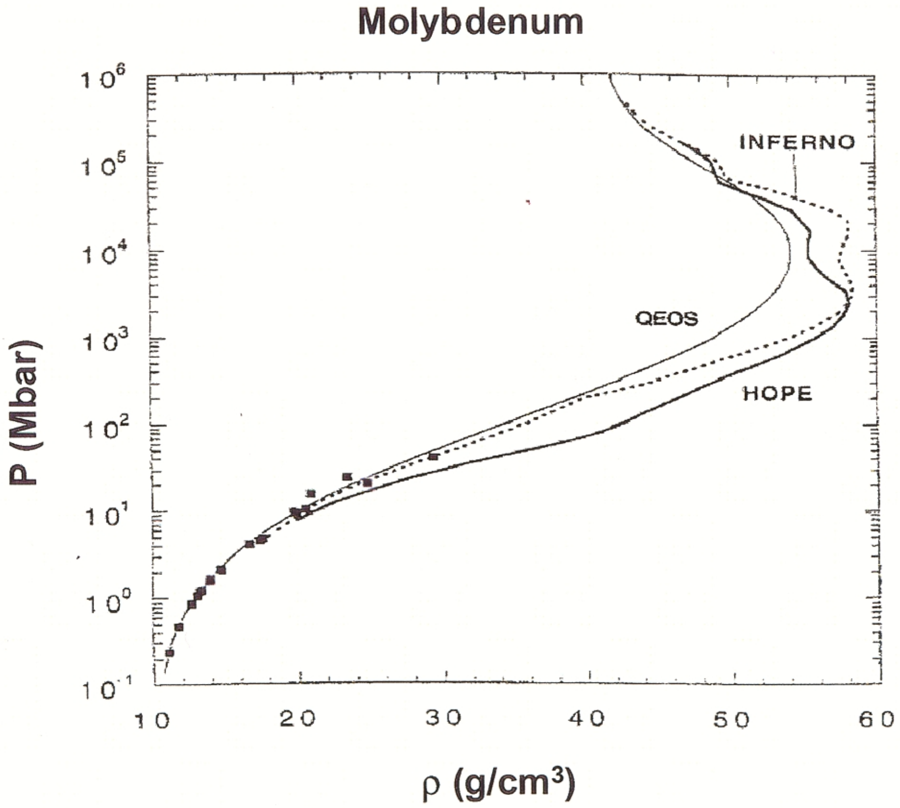

- Existing compression data from gas gun experiments is limited to pressures of less than 100 Mbar
- At ~1 Gbar, ionization effects dominate materials' equation of state
- Current eos models diverge in this regime
- High intensity, direct drive ablation experiments on the NIF will access the 1 Gbar regime

Initial experiments were performed last July at Omega, using a moderate laser intensity

relative eos experiment, compares the shock speed in the sample to that in Mo

- 6 beams from 22°, 6 from 48°
- spot radius of 412 μm, spreading to an ellipse on target
- intensity on target of 3.8e14 W/cm2
- shock breakout times were recorded using a reflectivity-based VISAR diagnostic

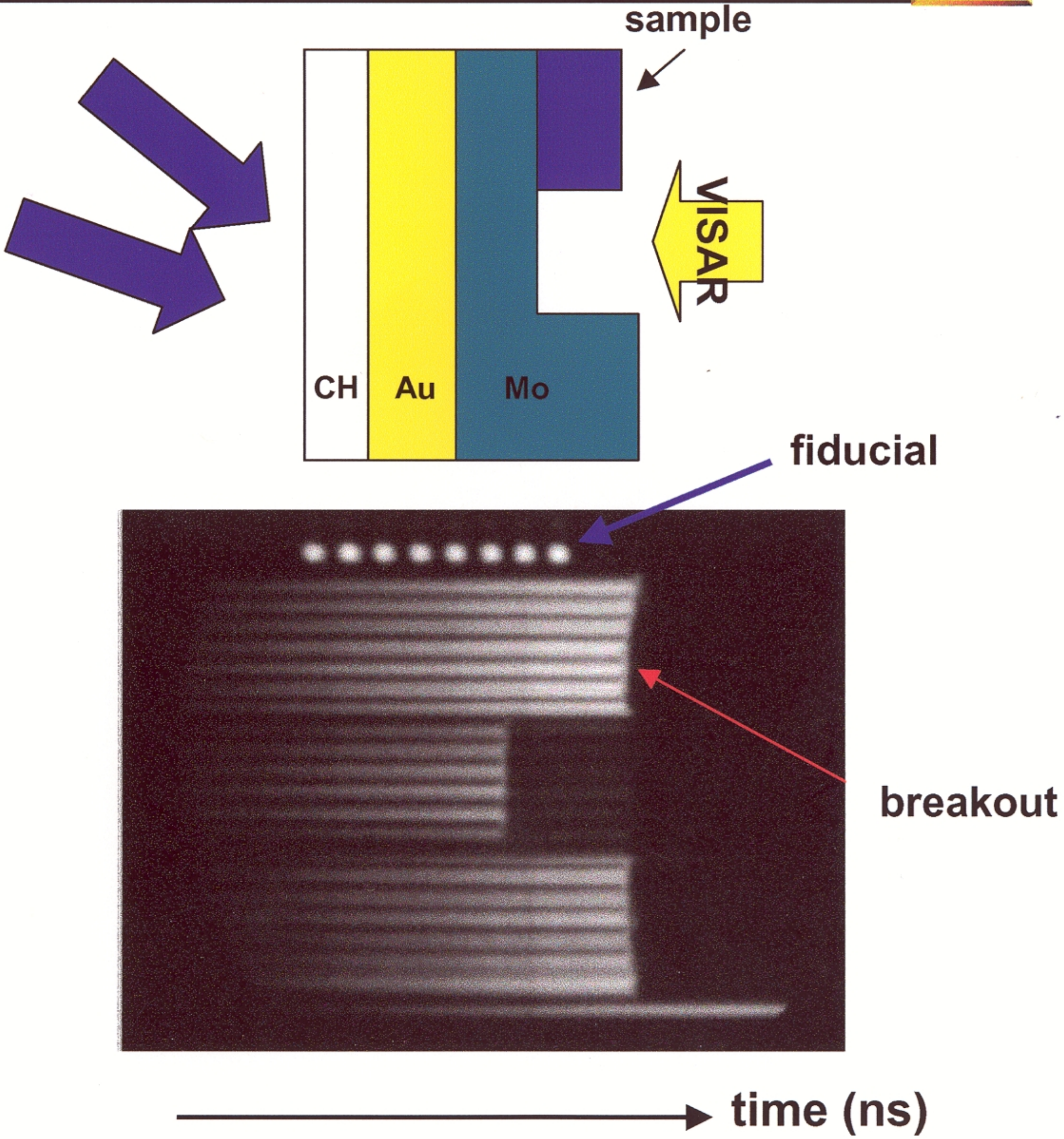

Measured shock breakout times were consistently longer than those predicted by 1D simulations

1D lasnex results vs measured shock breakout times

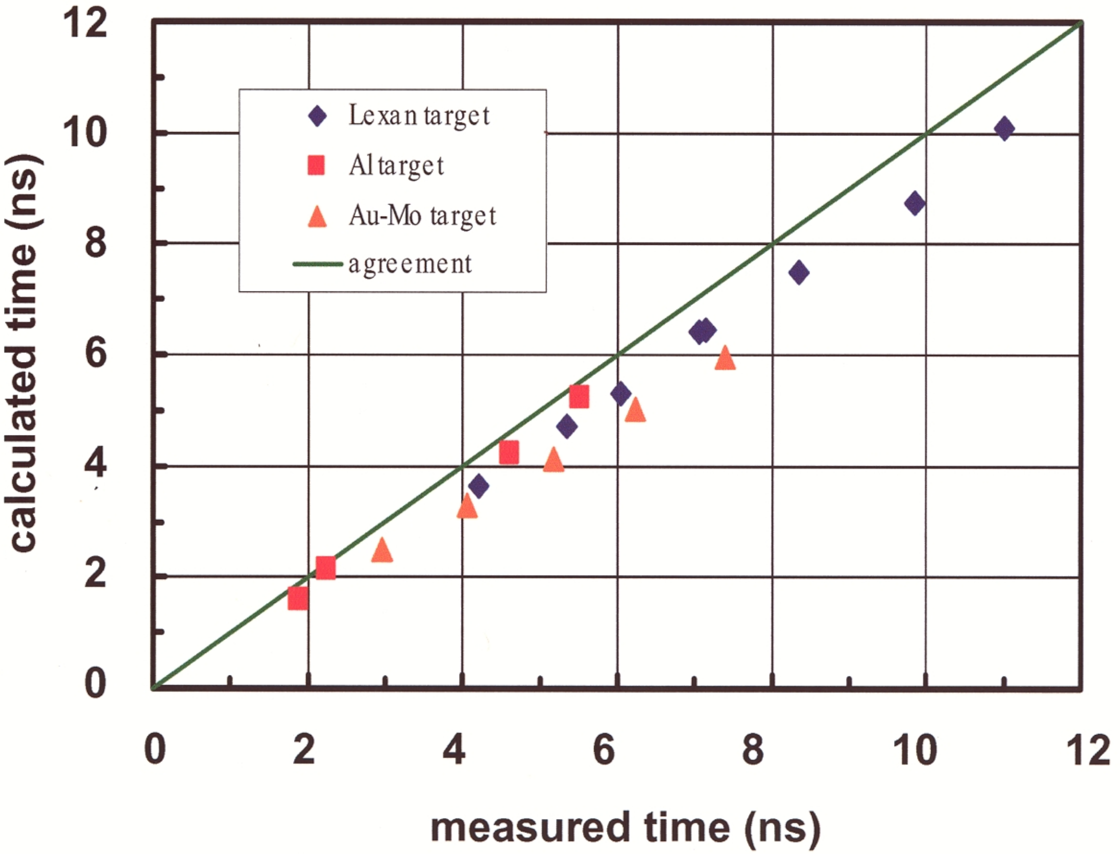

- results on Mo were consistent with a pattern obtained using various targets
- data includes shots with intensities from $2*10^{13}$ to $4*10^{14}$ W/cm^2
- simulations used measured laser pulses
- spot size based on measured beam profile
- agreement requires intensity reduction of 30-50%, which is beyond the experimental uncertainty

Good agreement has been obtained between 2D calculations and the measured shock speed

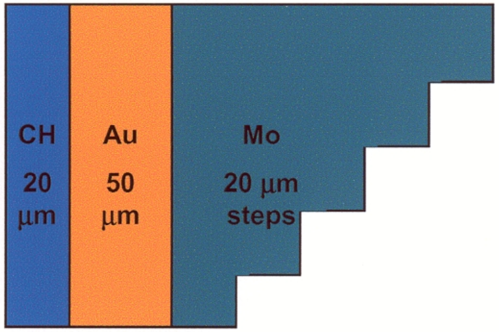

visar image

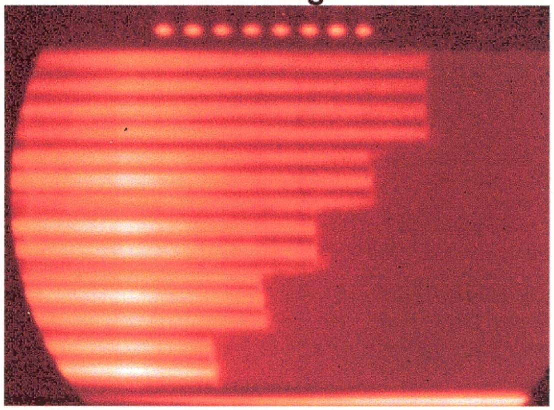

time (ns)

calculated vs measured shock breakout times in Mo

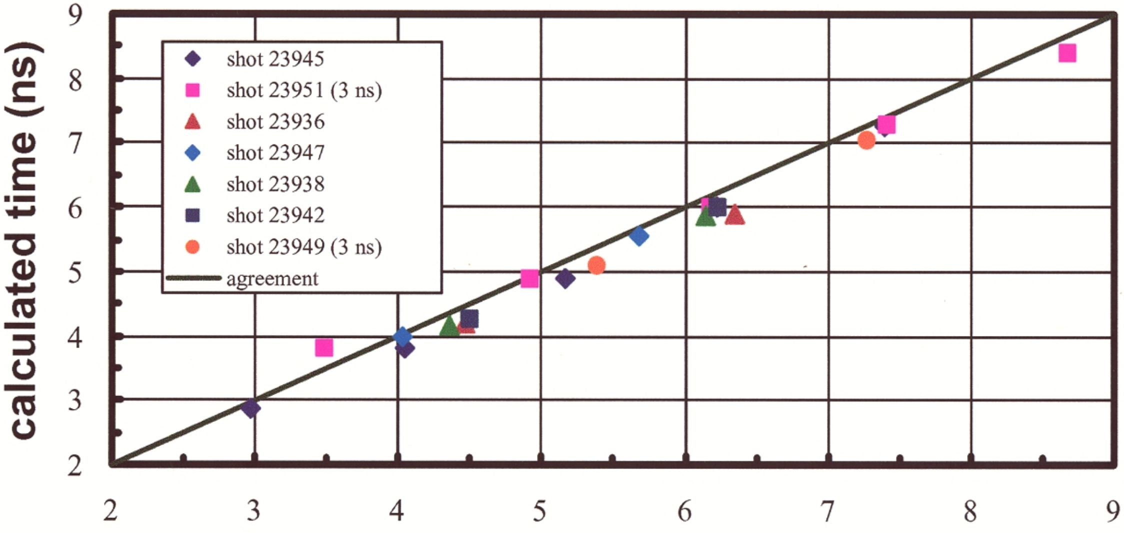

- 2D lasnex simulations, fully Lagrangian
- simulations use the measured laser pulse and beam spot size
- electron flux limiter = 0.1

2D simulations of the experiments show that radial energy loss dominates in the coronal plasma

Contours of Te (keV) at the end of a 2 ns pulse on a Au-Mo target

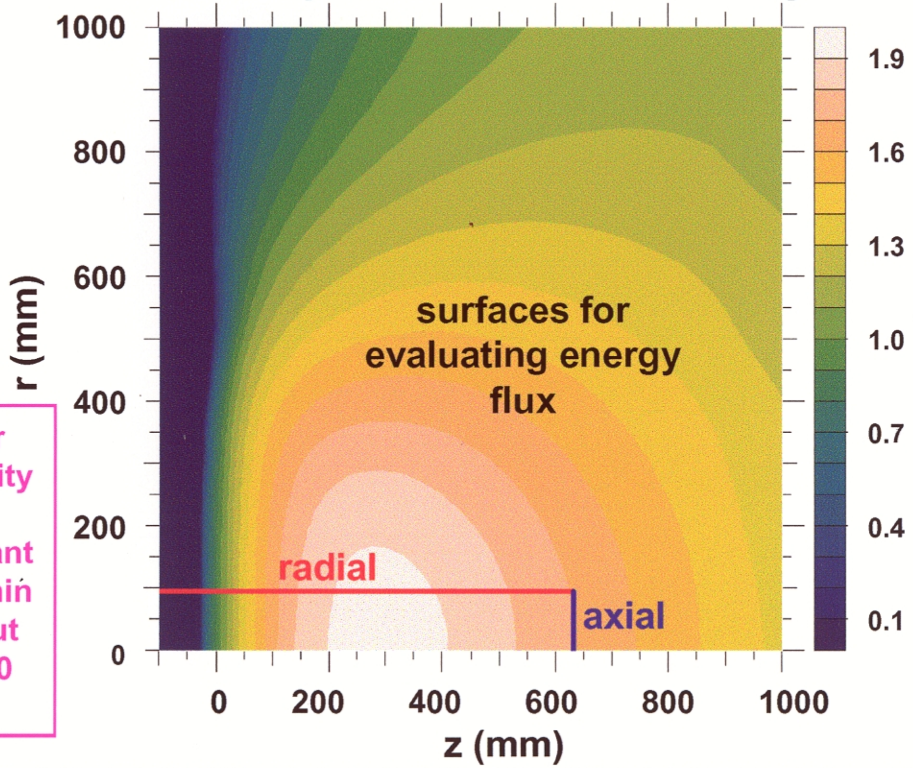

laser intensity is constant to within 2% out to 200 μm

Energy flux crossing the radial and axial surfaces vs time

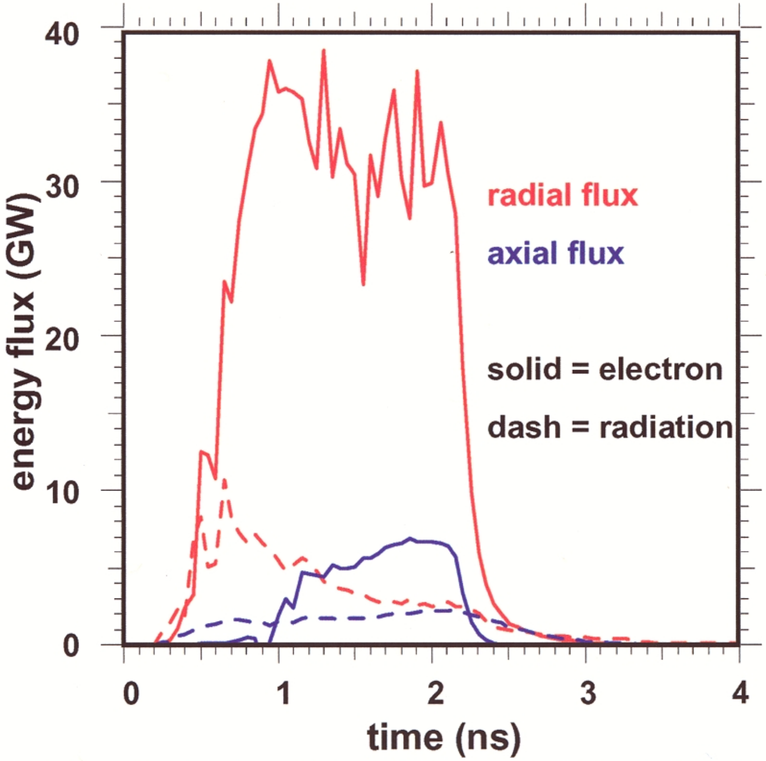

- Even at small radii, the gradients are sufficiently large so that, with the large surface area, radial energy loss dominates
- In a 1D simulation, the energy builds up until the gradient can drive an axial flux

Radial energy loss in the 2D simulation yields a lower plasma pressure for the same on-axis laser intensity

Contours of pressure (Mbar) at the end of a 2 ns pulse on a Au-Mo target

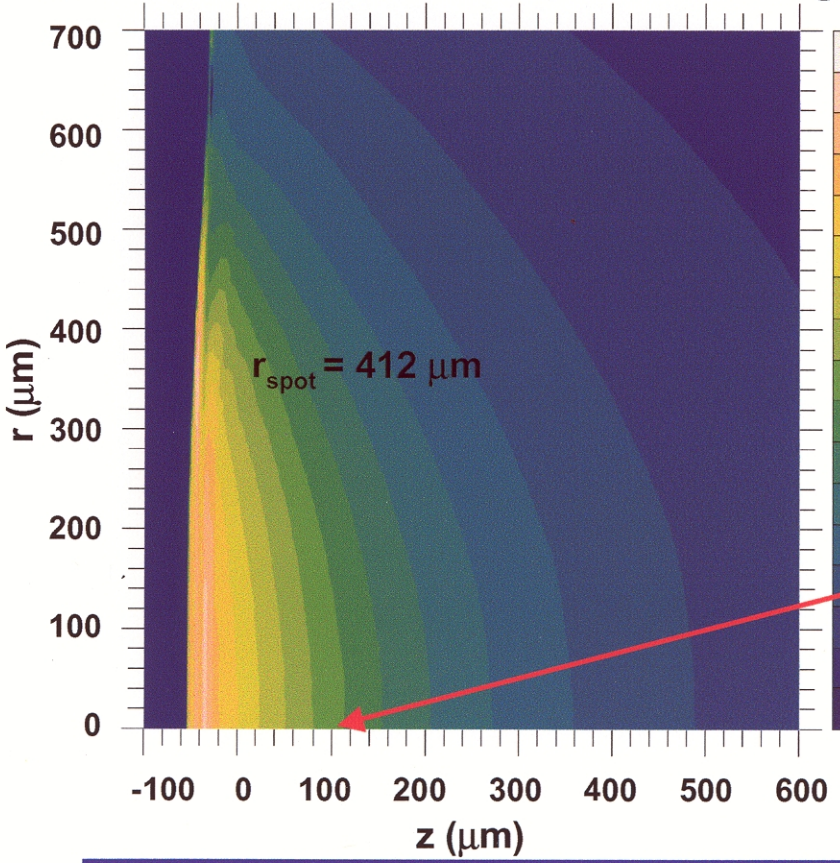

Pressure vs. time at a point on beam axis, z=100 um

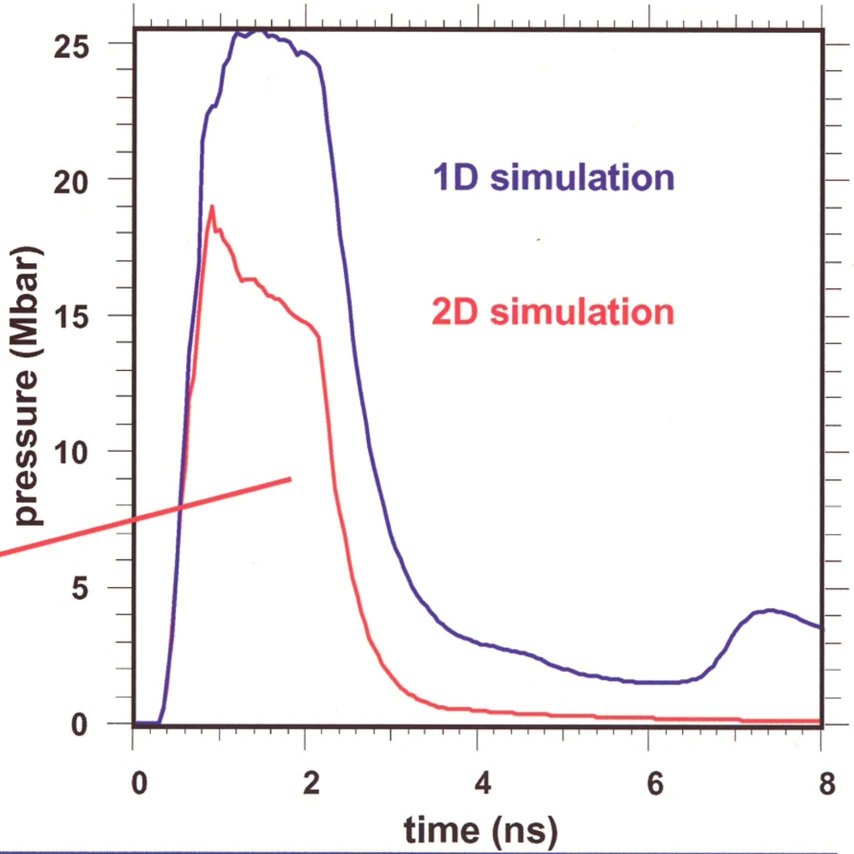

The 2D simulation pressure is 70% of the 1D calculation, producing the slower shock speeds consistent with the experiments

High-Z eos experiments proposed for NIF were designed to use laser intensities of 10^{16} W/cm^2

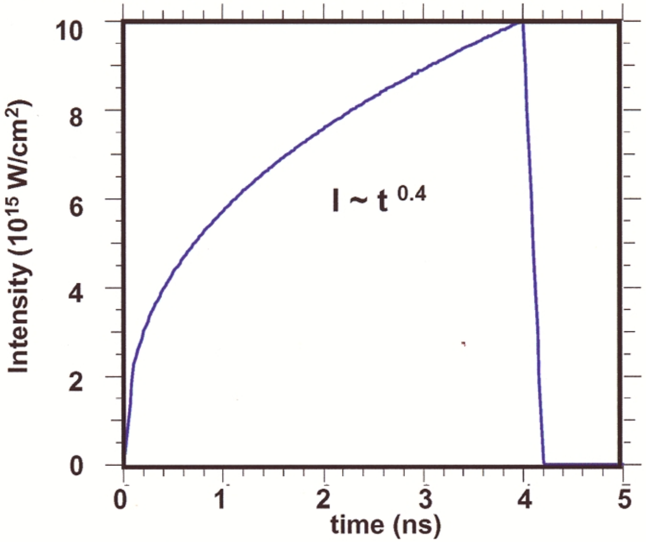

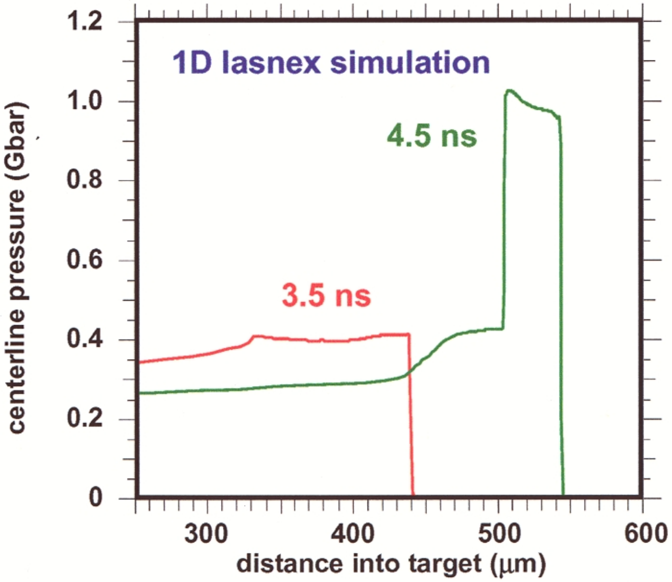

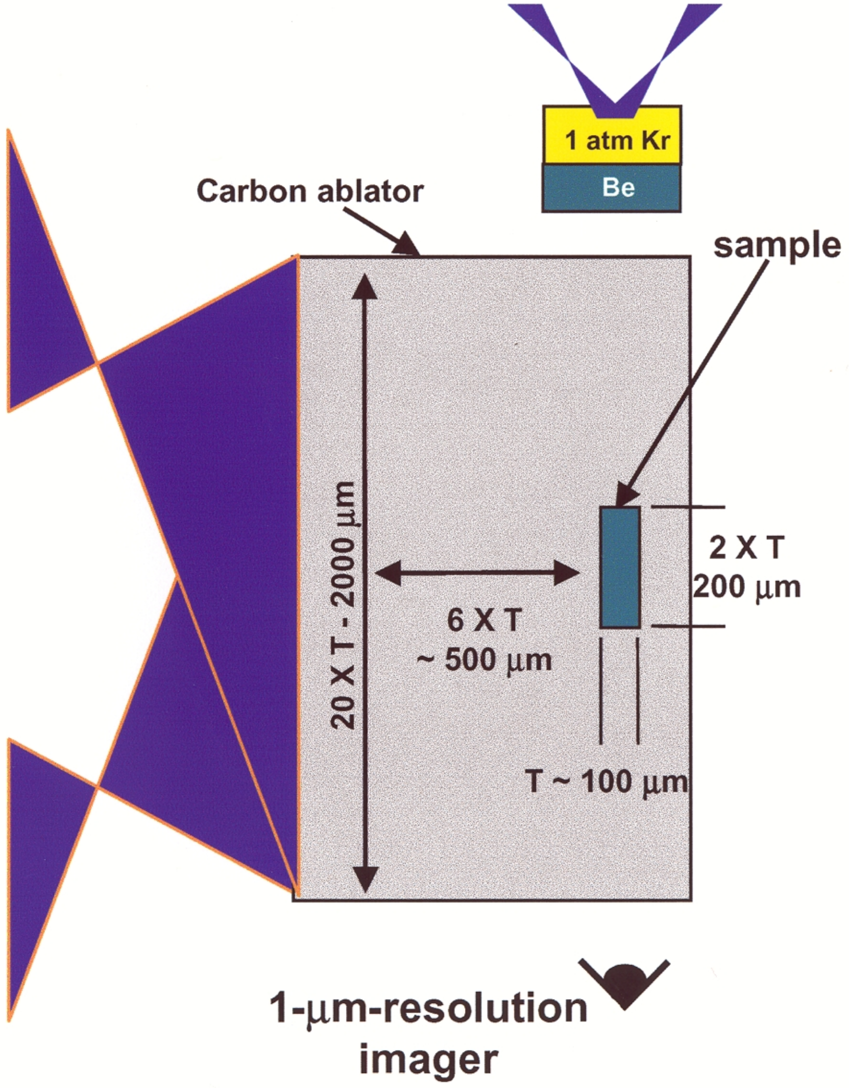

The difference between the 2D and 1D simulations is even greater in the proposed NIF experiment

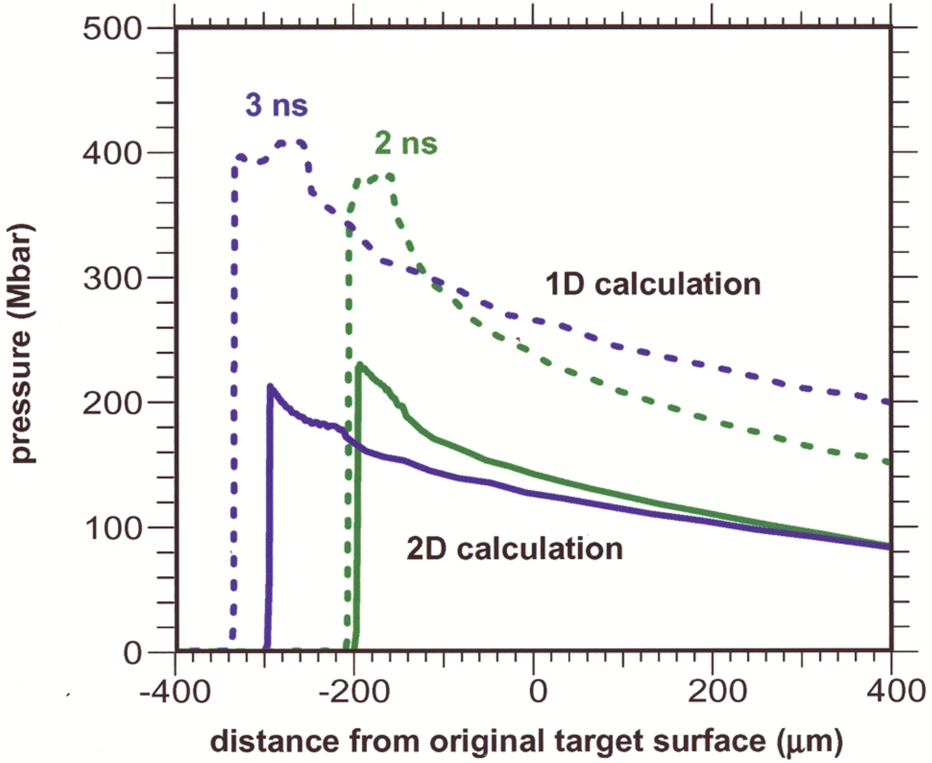

- both 1D and 2D simulations use a 4 ns ramped laser pulse to an intensity 10^{16} W/cm^2
- 2D calculation uses r_{spot} = 0.1 cm

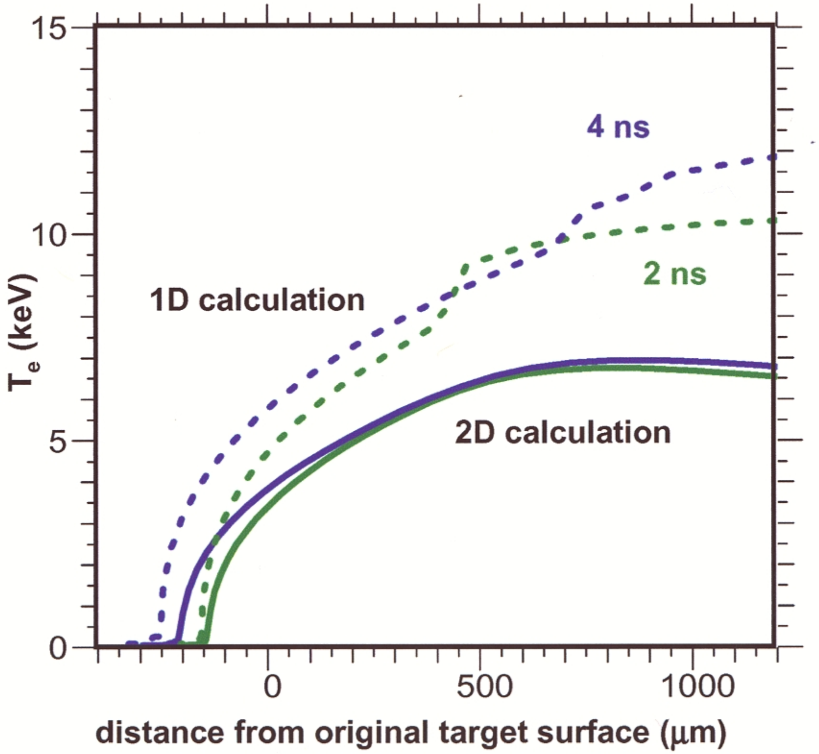

- shock pressure in the 2D simulation is a factor of 2 lower than predicted in the 1D calculation
- T_e is reduced from 12 keV in the 1D simulation to 7 keV

In the NIF experiment, the absorption region has moved out a distance comparable to the spot size

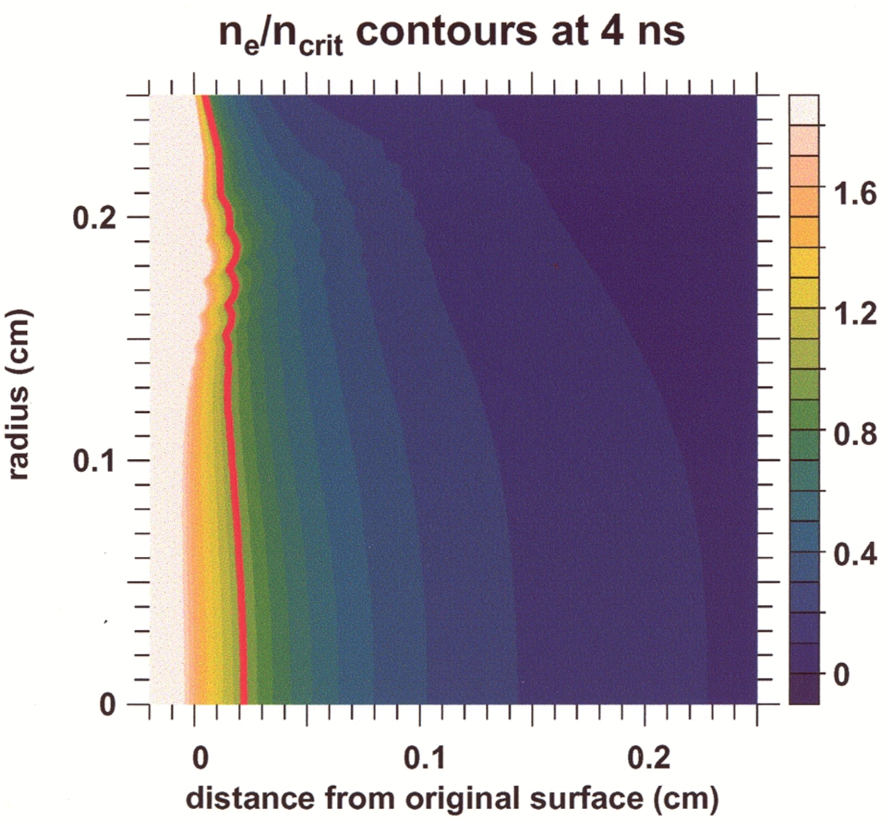

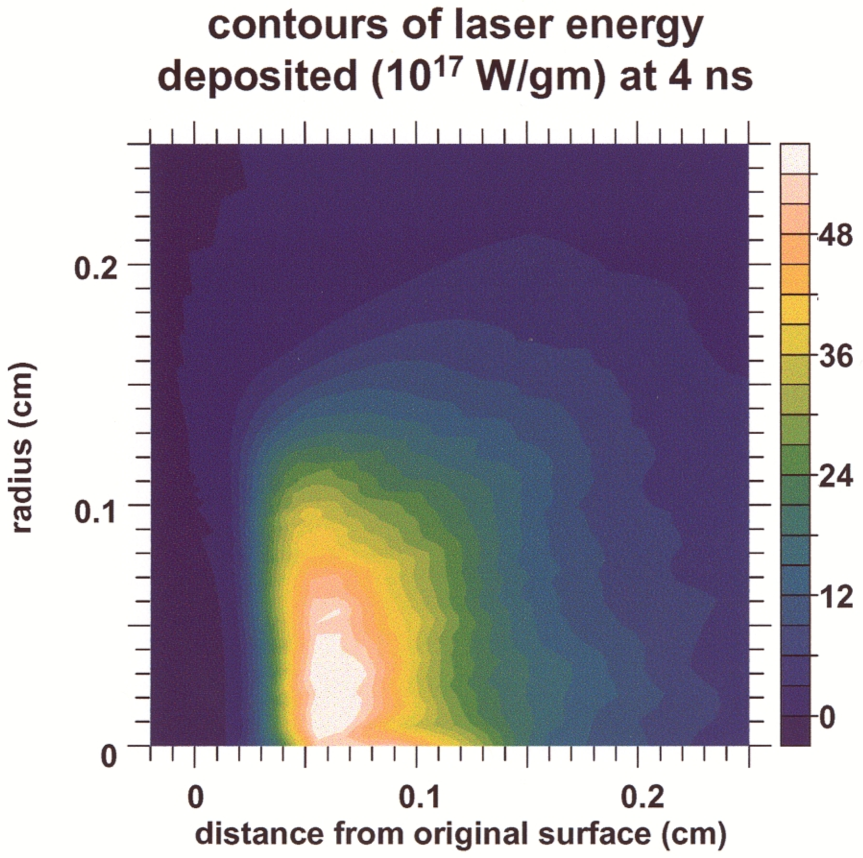

the region of laser absorption is comparable to the 0.1 cm radius spot, so that a 2D simulation is required

The deviation of the results from the 1D simulation scales with laser intensity

ratio of shock pressure in graphite, 2D / 1D

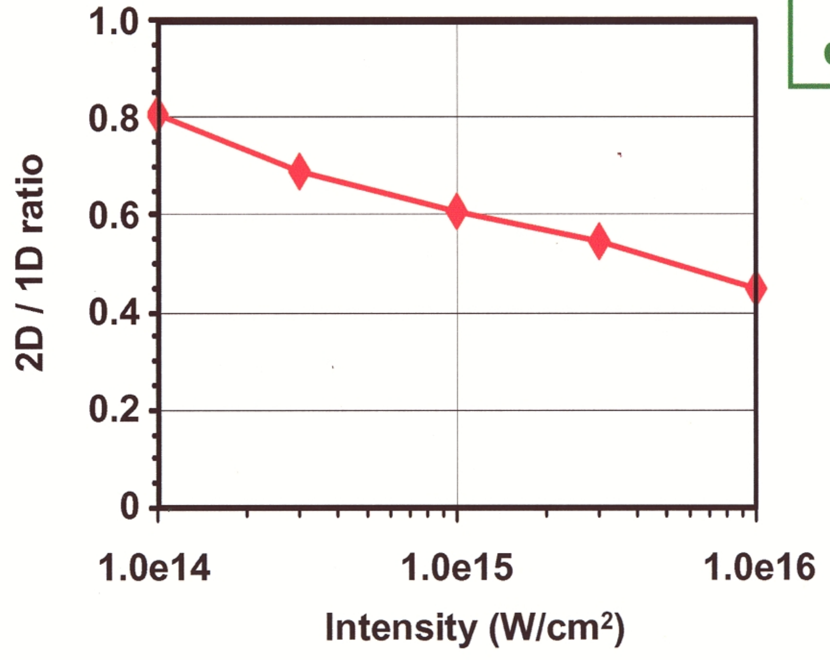

fixed 1000 μm spot, data at 4 ns

axial location of critical density in 2D simulations

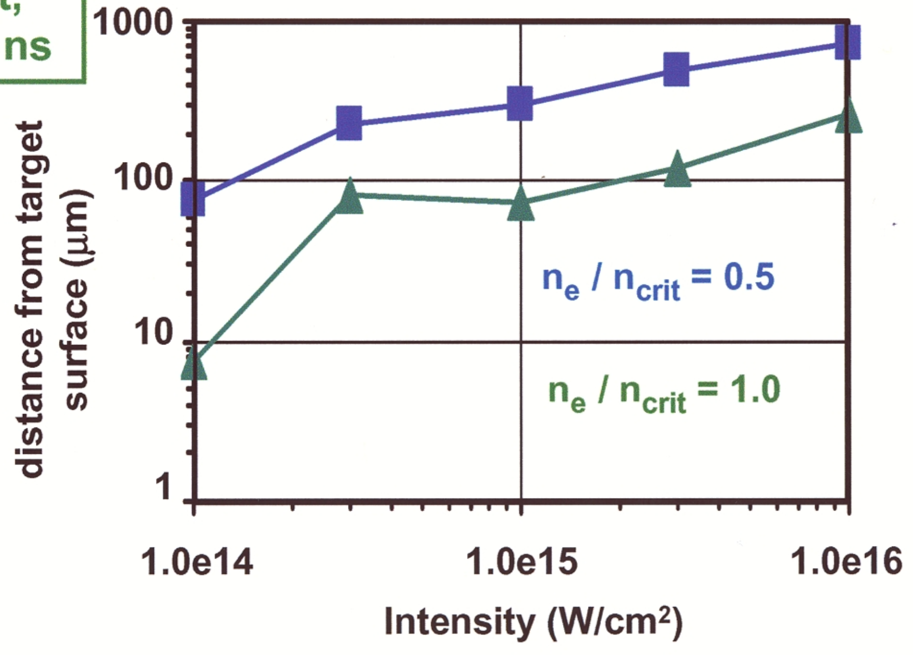

increased laser intensity → greater mass ablation rate → absorption further from surface → geometry more 2-dimensional

An order of magnitude increase of the spot size is required to recover the 1D results

2D simulations with laser ramp to I = 1.0e16 W/cm2 and variable spot size

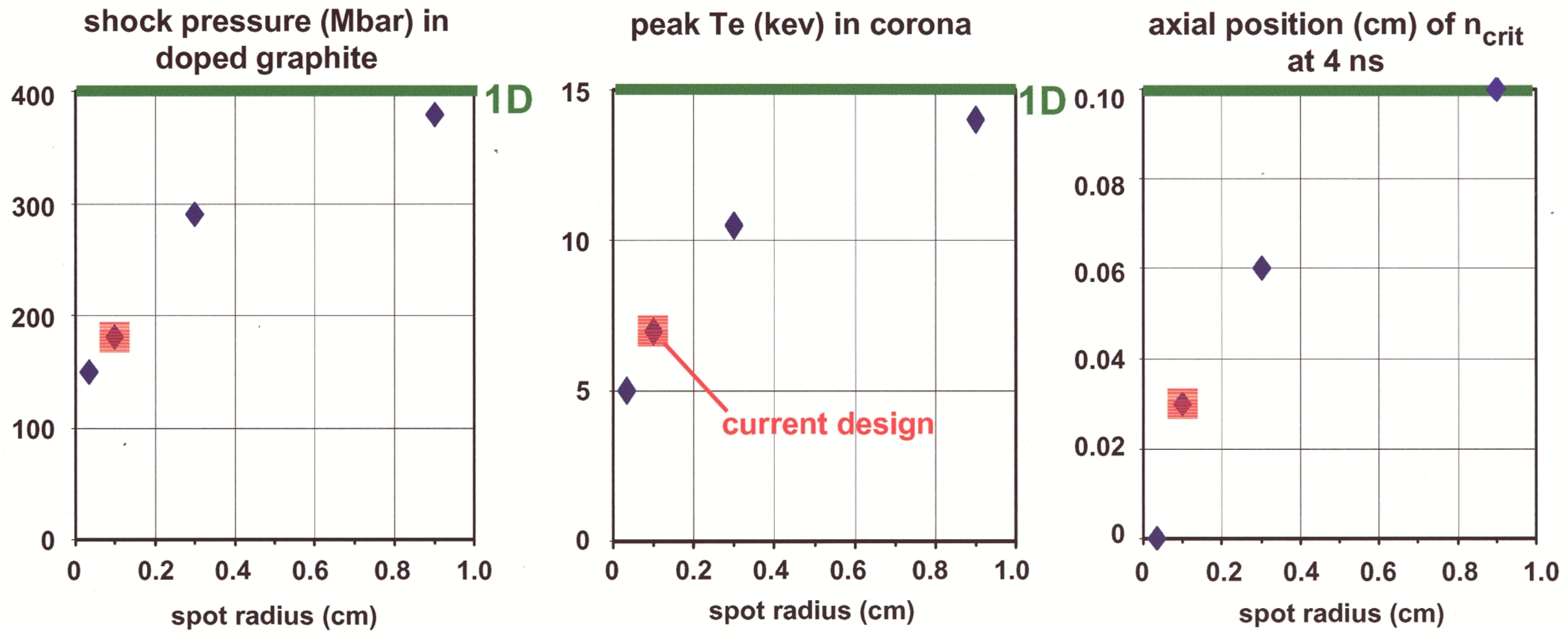

- at high intensity, power limitations prohibit even 2x increases in spot size
- the experiments are inherently 2D, their performance limited by radial transport

Dominated by radial transport, coronal plasma conditions depend on the value chosen for the flux limiter

- Lasnex limits the maximum electron energy flux to a fraction of its free-streaming value, $\Gamma^{max} = f * n_e v_e^{th}$
- Decreasing the flux limiter from 0.1 to 0.03 in the NIF experiment;

increases T_e in the corona,

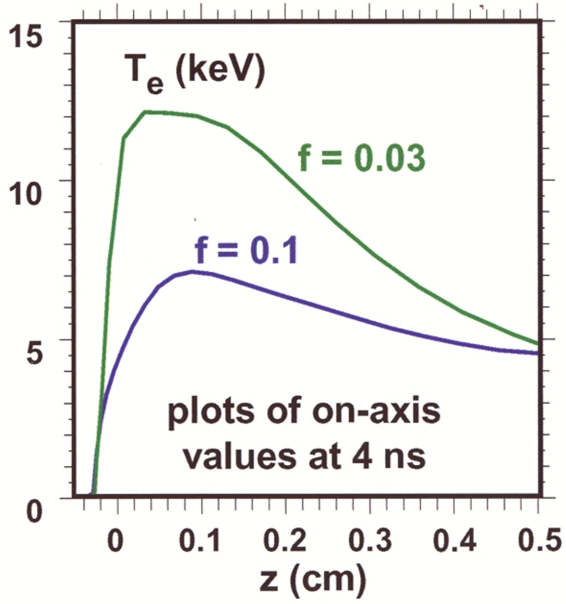

which causes the density to decreases,

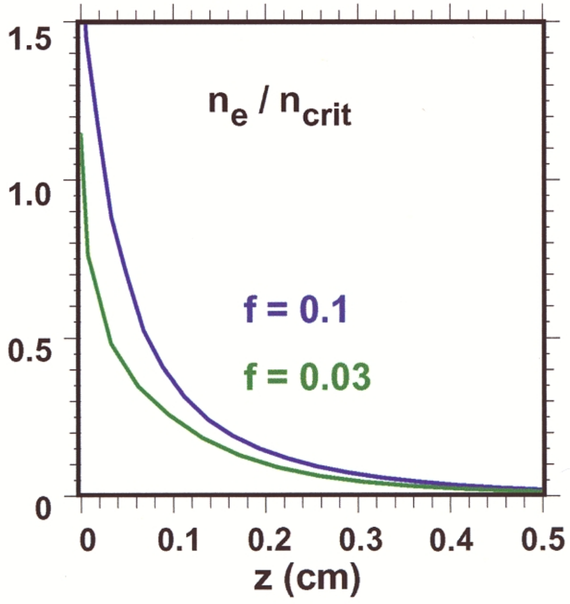

so that the pressure does not significantly increase

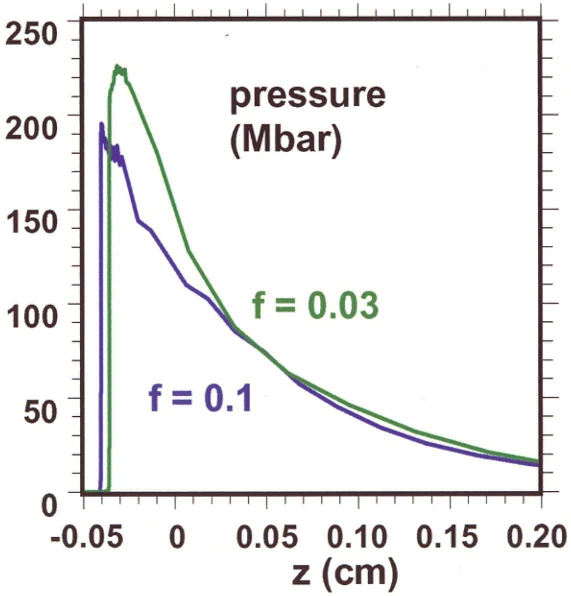

- Initial experiments at moderate intensity ($4*10^{14}$ W/cm^2) are well modeled by f=0.1
- A different flux limiter may be appropriate at the high intensity NIF experiments

Self-generated magnetic fields in the corona may restrict electron energy transport

- Ohm's law, balancing the ambipolar field and the pressure,

$$e\,n_e\,\vec{E} = -\vec{\nabla} p_e$$

combined with Faraday's law,

$$\frac{\partial \vec{B}}{\partial t} = -\vec{\nabla} \times \vec{E}$$

predicts magnetic field generation

$$\frac{\partial \vec{B}}{\partial t} = \frac{k\,\vec{\nabla} n_e \times \vec{\nabla} T_e}{e\,n_e}$$

- Magnetic field generation is greatest at the edge of the corona, where the gradients are not parallel

calculated magnetic field density (MG) at 4 ns for the NIF target

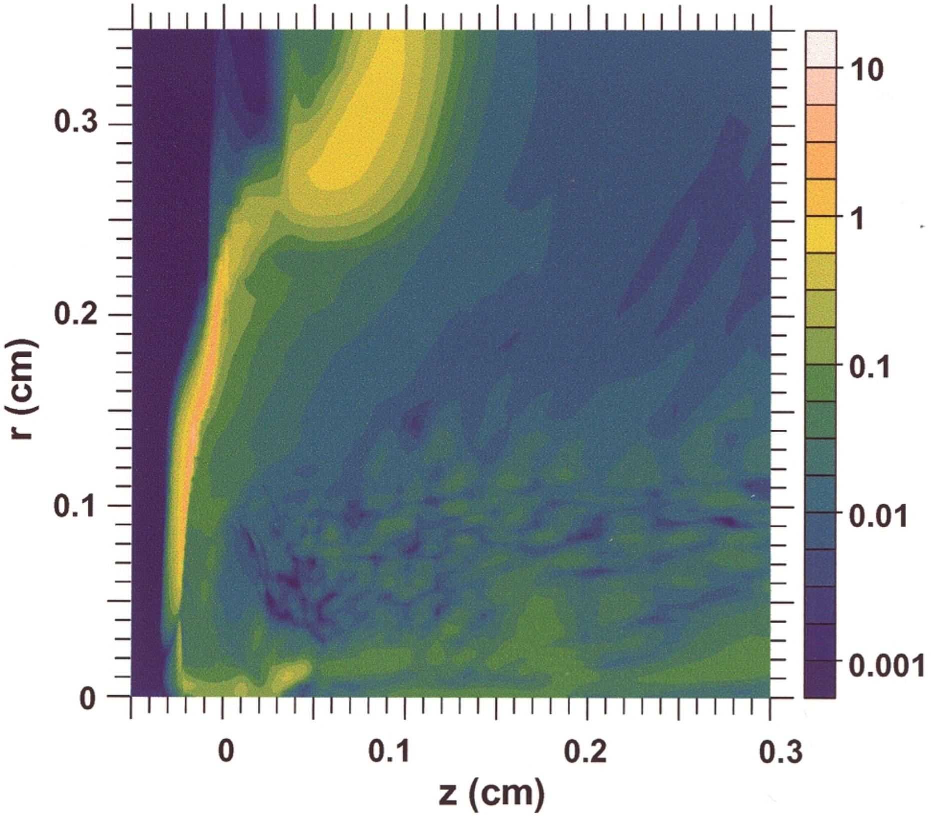

The generation of magnetic fields can also result in increased values of T_e in the corona

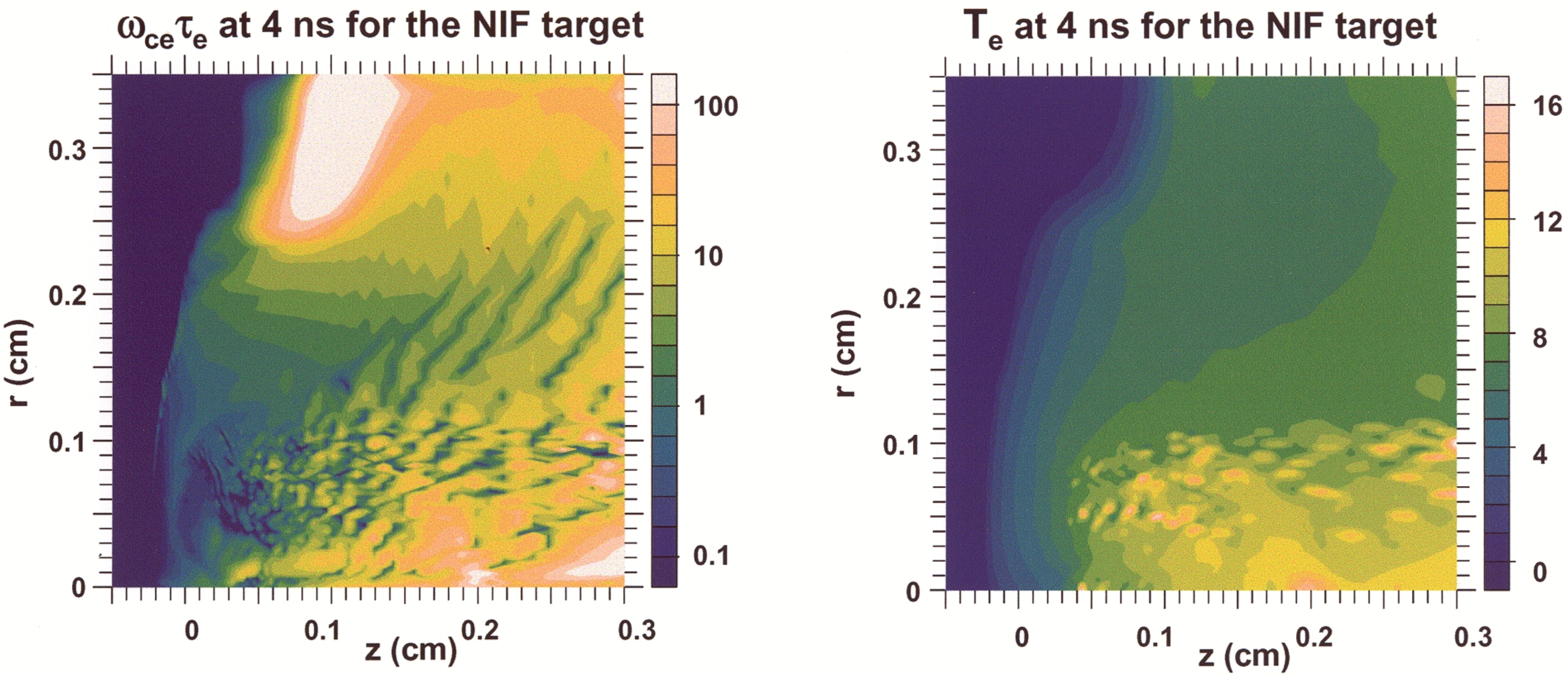

- T_e is increased from 7 to ~12 keV with this magnetic field model
- predicted increase in T_e is model dependent
- experiments are needed to verify the magnetic field model

X-rays generated in the corona degrade the experiment by preheating the high-Z sample

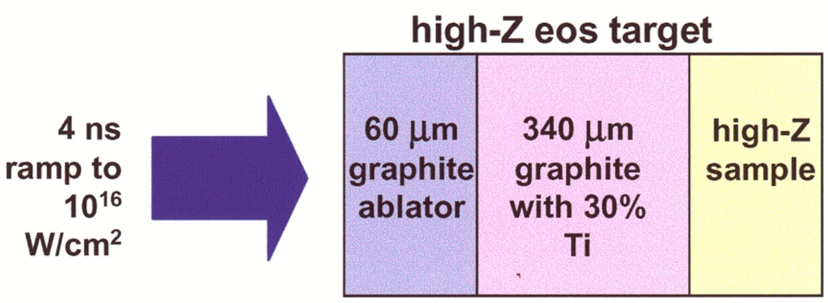

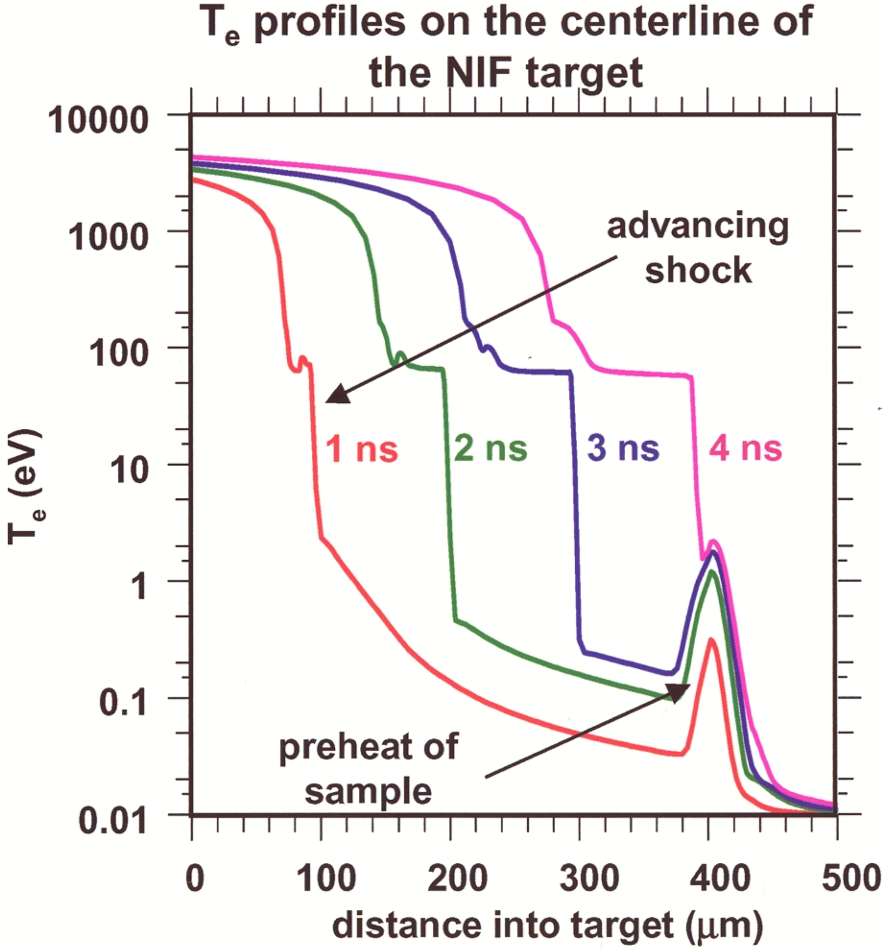

- dopant added to the graphite shields still permits penetration of high energy x-rays (>10 keV)
- desired preheat level is < 0.1 eV
- too much dopant can obstruct the backlighter image

success of the experiment depends on what value of the coronal T_e is produced at a given pressure

Summary

- Direct drive ablation experiments on the NIF will generate shock pressures above 100 Mbar for high-Z equation of state measurements
- Initial experiments at moderate laser intensities have been successfully modeled using LASNEX
- 2D simulations are required as radial transport dominates coronal energy losses, especially in the high intensity NIF experiments
- The value of T_e in the corona may vary by a factor of 2 depending on the transport model
- The experiment is very sensitive to the coronal T_e, as preheat of the high-Z sample by high energy x-rays degrades the experiment
- Validation of physics models at high intensity is needed for effective target design
  - electron heat transport
  - magnetic field generation

Magnetic fields & electron transport In high energy density hohlraums

Is our capability good enough?

Lawrence Livermore National Laboratory
1952-2002

John Edwards
Jim Hammer, Judy Harte, Ed Alley, George Zimmerman
Lawrence Livermore National Laboratory

Malcolm Haines
Imperial College, London, UK

This work was performed under the auspices of the U.S. Department of Energy by the University of California, Lawrence Livermore National Laboratory under contract No. W-7405-Eng-48.

Introduction

Electron transport workshop

9-11th Sepetmber

Purple Orchid Inn, Livermore 2002

So what's changed?

Despite all that, we have strong evidence B-fields are important in at least some aspects of hohlraums

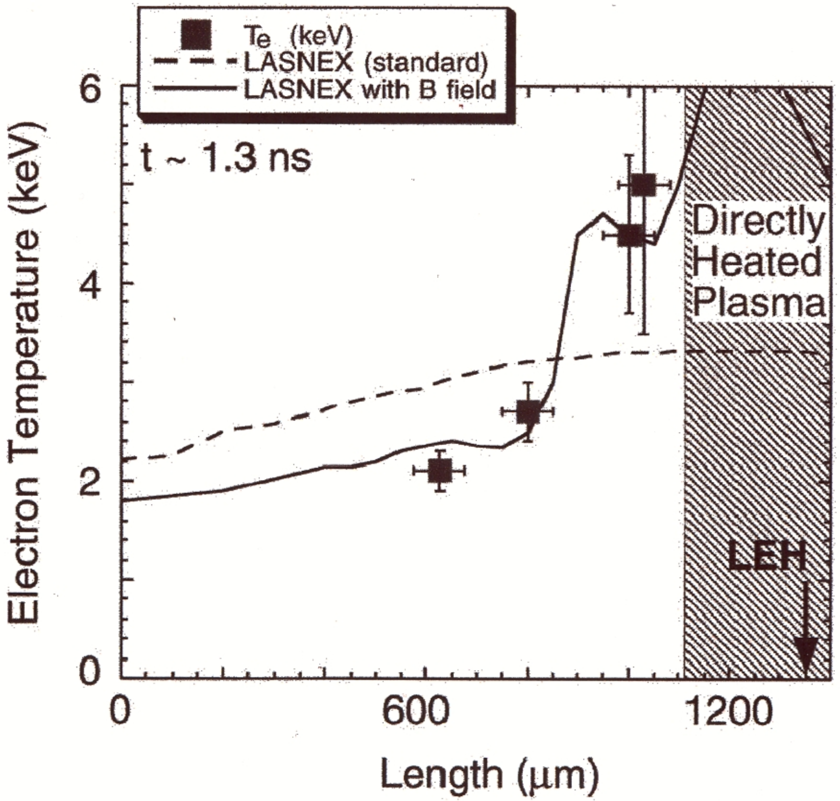

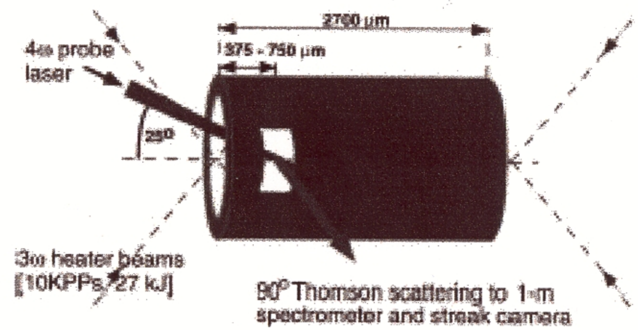

FIG. 5. Schematic of the 4ω TS experiments in Nova scale-1 hohlraums.

Is there really a problem?

In the early days of laser fusion:
Spitzer-Harm inapplicable
B via $\nabla n \times \nabla T$ recognized

At high intensities bad stuff began to happen with direct drive
=> so for this & other reasons we went to indirect drive

Nova was a spectacular success & led to NIF

There was no indication that non-local transport or B-fields were a big issue. Hohlraums worked just fine (with a flux limiter ~ 0.1) (exceptions are small hohlraums - we have no idea why yet!)

In the mean time the rest of the world plugged away with direct drive
Both this and LPI in hohlraums drove a very aggressive &
Very successful beam smoothing effort

So what's changed......?

NIF is very much closer now!
When we do something different there's often a surprise

We're planning to do much more with NIF than ignition and go into regimes that are far from our current experiences

The beam smoothing success has seduced us into thinking that maybe we can take advantage of better over all coupling into targets compared to indirect drive

Ultra-high intensity lasers => proton probing - electro-thermal-instability?

Short pulse lasers for physics studies

Workshop objectives

Our focus this time round is “long pulse” regime
especially for high energy density hohlraums & direct drive

What physics do we need to include?

What is a sensible way forward computationally?

- Fokker-Planck
- something else (eg Monte Carlo)
- reduced model

What developments & benchmarks do we need?

What should we do to test our ideas & models?

Theory & computation

Fokker-Planck for laser plasmas in 1D (Bell, 1981)
Then in 2D (Epperlein, 1988)
Now 2D with B to f_1 keeping df_1/dt (Kingham, 2002)

At the same time, driven by extreme cost of FP
People got busy making reduced non-local models
to use in hydrocodes (1D, Luciani, 1983; ....
2D, Schurtz, 2000)

We're now 20 years on

is it time to try FP in our design codes?
and if not, what?

The failure of Spitzer in laser plasmas is not news

We use $q \sim \kappa \nabla T$ **which we know breaks down**

To fix it we set $q \leq f q_{fs}$ **where typically f ~ 0.1**

Some results from 2D Fokker-Planck coupled to hydro are:

$$\frac{q}{q_{fs}} = \mathrm{g}(\vec{\mathrm{r}},\mathrm{t}) \qquad \frac{q}{q_{SH}} = h(\vec{\mathrm{r}},\mathrm{t}) \qquad q \nparallel \nabla T$$

And then there's magnetic fields…….

A simple estimate indicates we need to worry about non-local effects in all laser plasmas

$\frac{\lambda_{mfp}Z}{2}$ vs T_e for *thermal* electrons

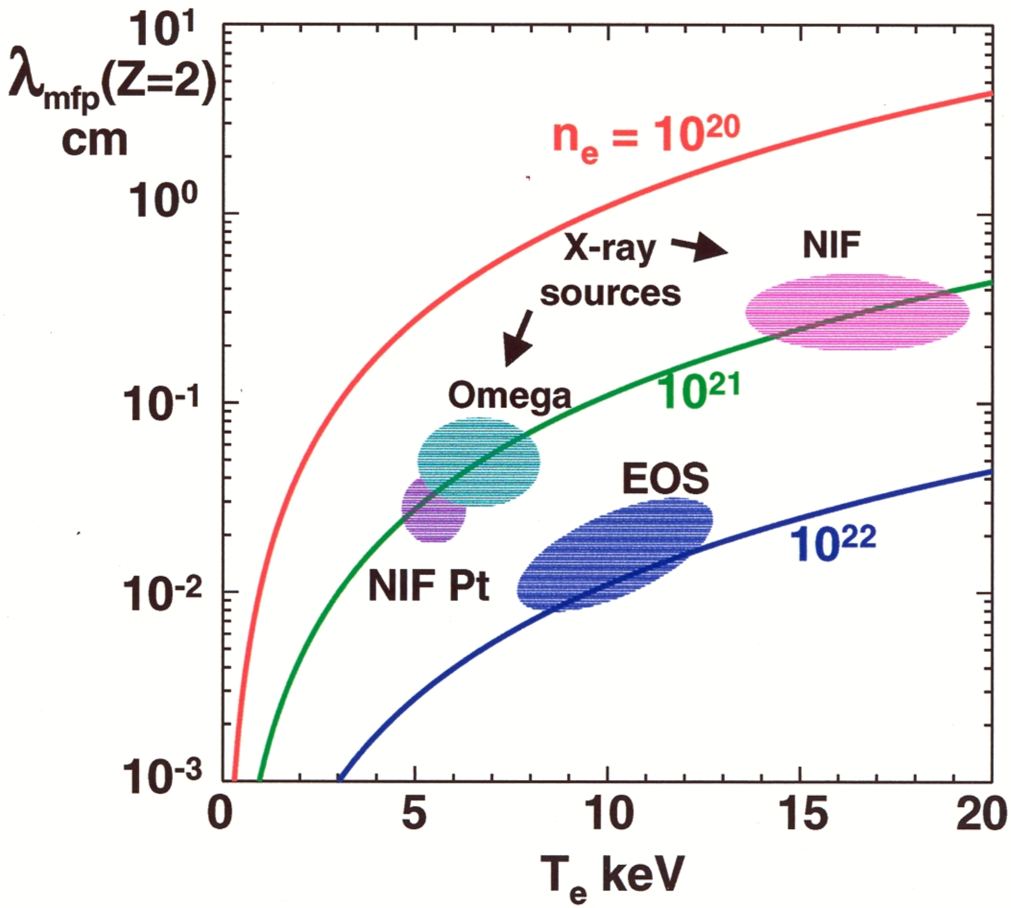

NB heat carrying e's have λ_{mfp} ~ 80x that of thermals

(because $\lambda(v) \sim v^4$)

Even a small field can effectively localize electrons

Lamour radius $a_e = \dfrac{m_e v}{eB}$

For thermals $v \sim (2kT/m_e)^{1/2}$ => $a_e = \dfrac{T_{e\,keV}^{1/2}}{B_{MG}}$ μm

Fields of ~ 1 MG are adequate to localize magnetized electrons for nearly all typical NIF plasmas

The magnetic field is generated (mainly) via ∇n x ∇T at the hohlraum wall

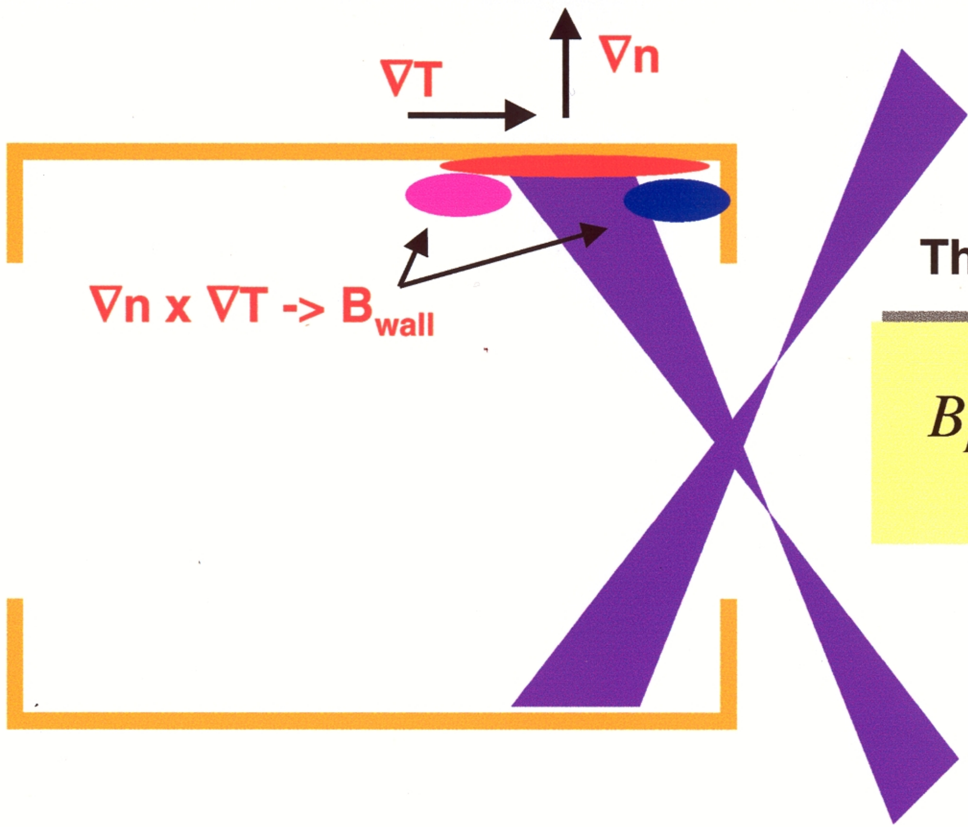

The source term is huge

$$B_{MG} \sim \frac{T_{e,keV}}{L_{n,100\mu m} L_{T,100\mu m}} t_{ns}$$

But convection rapidly limits the field near the wall to ~ 1 MG

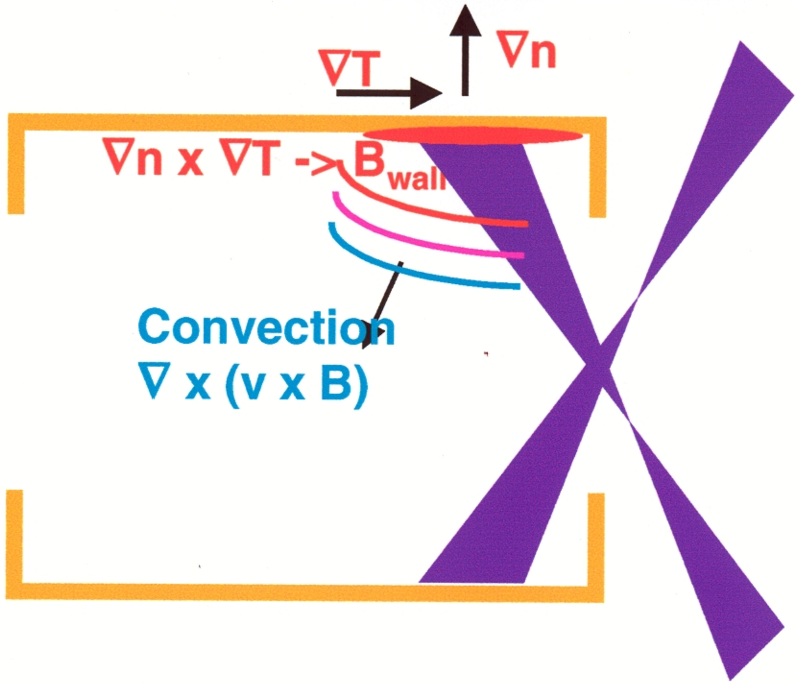

Balancing hydro & source
for B near the wall

$$B_{MG} \sim \frac{T_e}{c_s L_T} \sim \frac{1}{L_{T,100\mu m}} \frac{T_{e,keV}^{1/2}}{T_{R,heV}^{1/4}}$$

=> B_{MG} ~ 1 MG

This happens on a time scale

$$t_{ns} \sim \frac{L_n}{c_s} \sim \frac{L_{n,100\mu m}}{T_{R,heV}^{1/4} T_{e,keV}^{1/2}}$$

=> t < 1 ns

Indirect evidence of B fields in hohlraums was seen on Nova

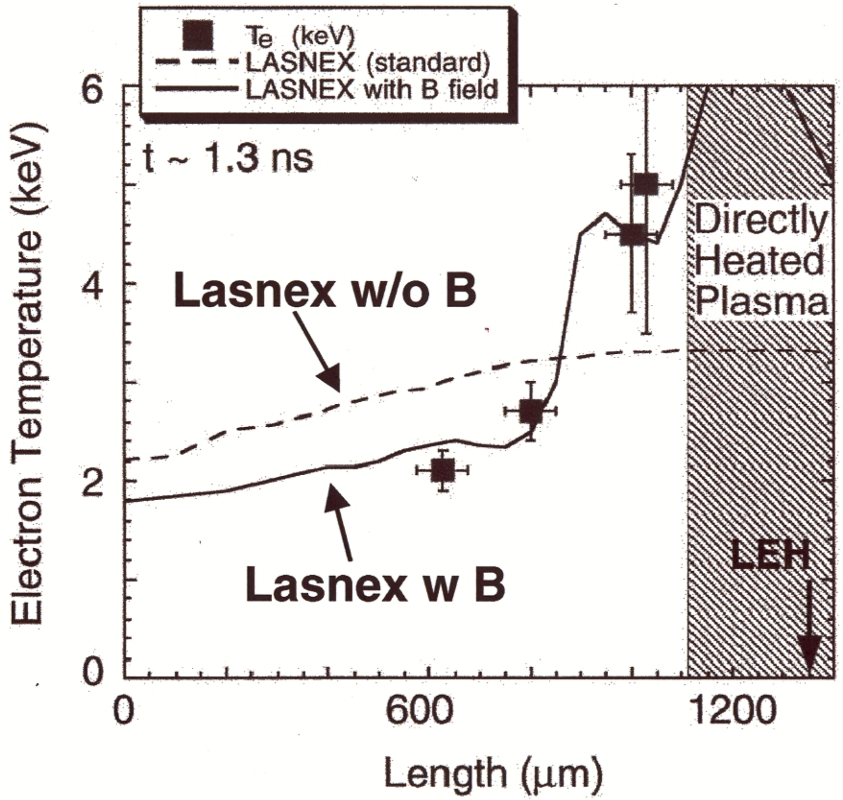

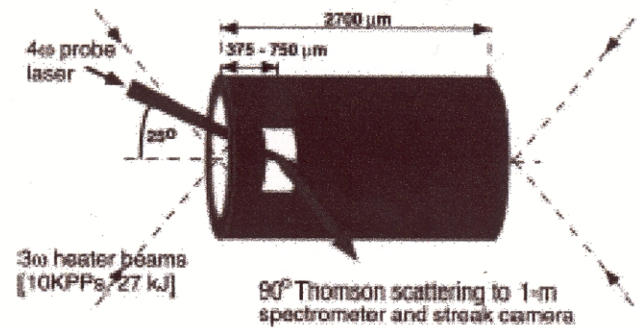

FIG. 5. Schematic of the 4ω TS experiments in Nova scale-1 hohlraums.

Siegfried Glenzer Nova measurement
Lasnex's from Jim Hammer & Kent Estabrook

This is what we expected/saw in studies based around this experiment

Relatively slow scaling of B in hot spots
No saturation in the volume (time scale too short)

$\omega\tau << 1$ in the gold
$\omega\tau >> 1$ in the gas

local heat flow approximation in general marginal

The major consequences of this for ICF are most likely to be related to eg beam pointing, LPI, hard X-ray asymmetry in double shell capsules

Based on a wide variety of recent hohlraum calculations from 10-500 TW we find

The major impact of including B
(rather independent of power or size):

$T_{e,LEH}$ (with B) ~ 2 x $T_{e,LEH}$ (without B)

T_R NOT affected

Possible knock on consequences need to be investigated
LPI, LEH beam energy transfer, hard X-ray production, beam pointing, drive symmetry, preheating

Local heat flow approximation appears marginal
need better heat flow - difficult problem!

We need good experiments that measure and correlate T_e & B

We'll consider just 2 gas filled examples to illustrate this

1)

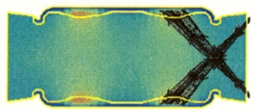

Nova scale 1 - 75% LEH
200 TW

(calculations
spanning 10-500 TW produce
very similar conclusions
with non-local effects becoming
gradually worse as power is
increased)

2)

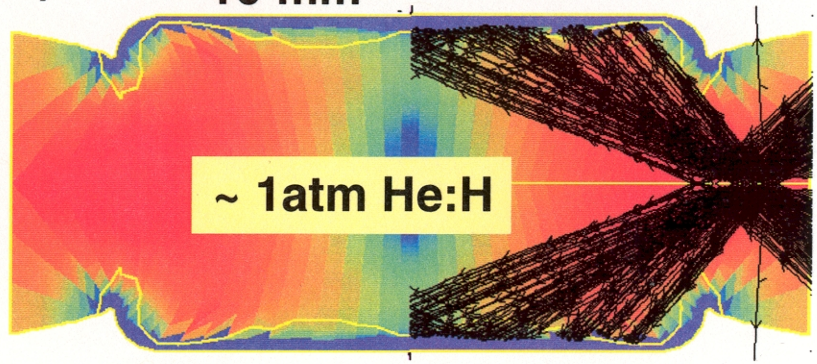

NIF ignition scale - 75% LEH
~400 TW

B field is formed at the wall & gradually convected into the hohlraum

200 TW: magnetic field evolution

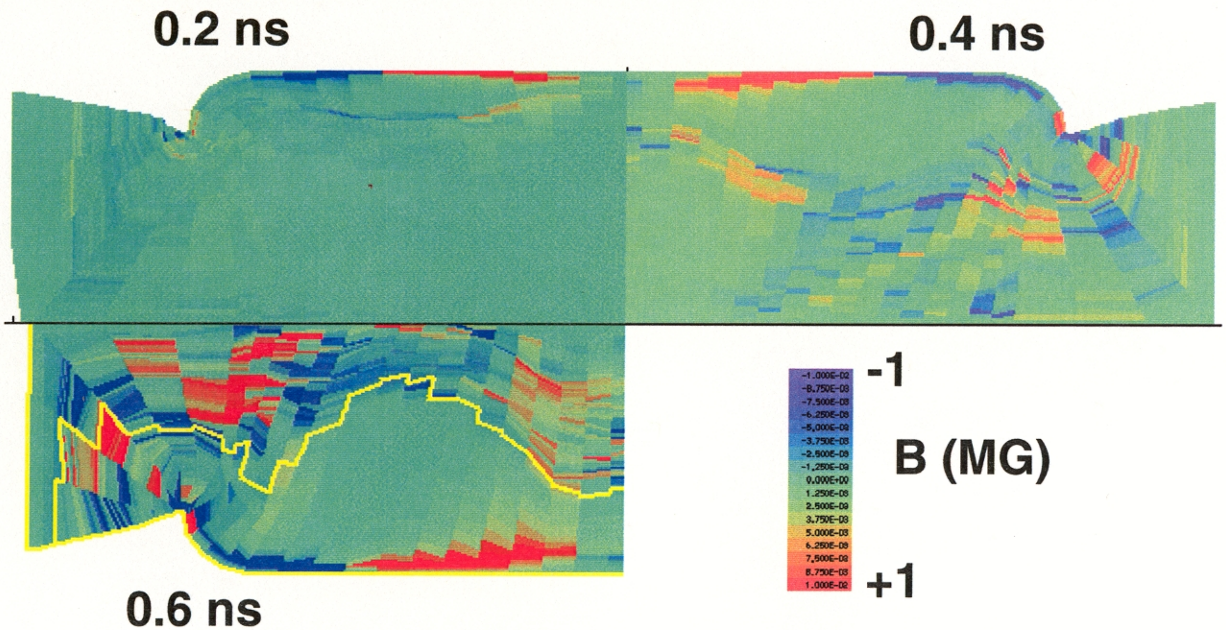

fields rapidly approach ~ 1MG

The main difference when B fields are included is a much higher T_e (~x2) in the LEH

0.6 ns; 200 TW

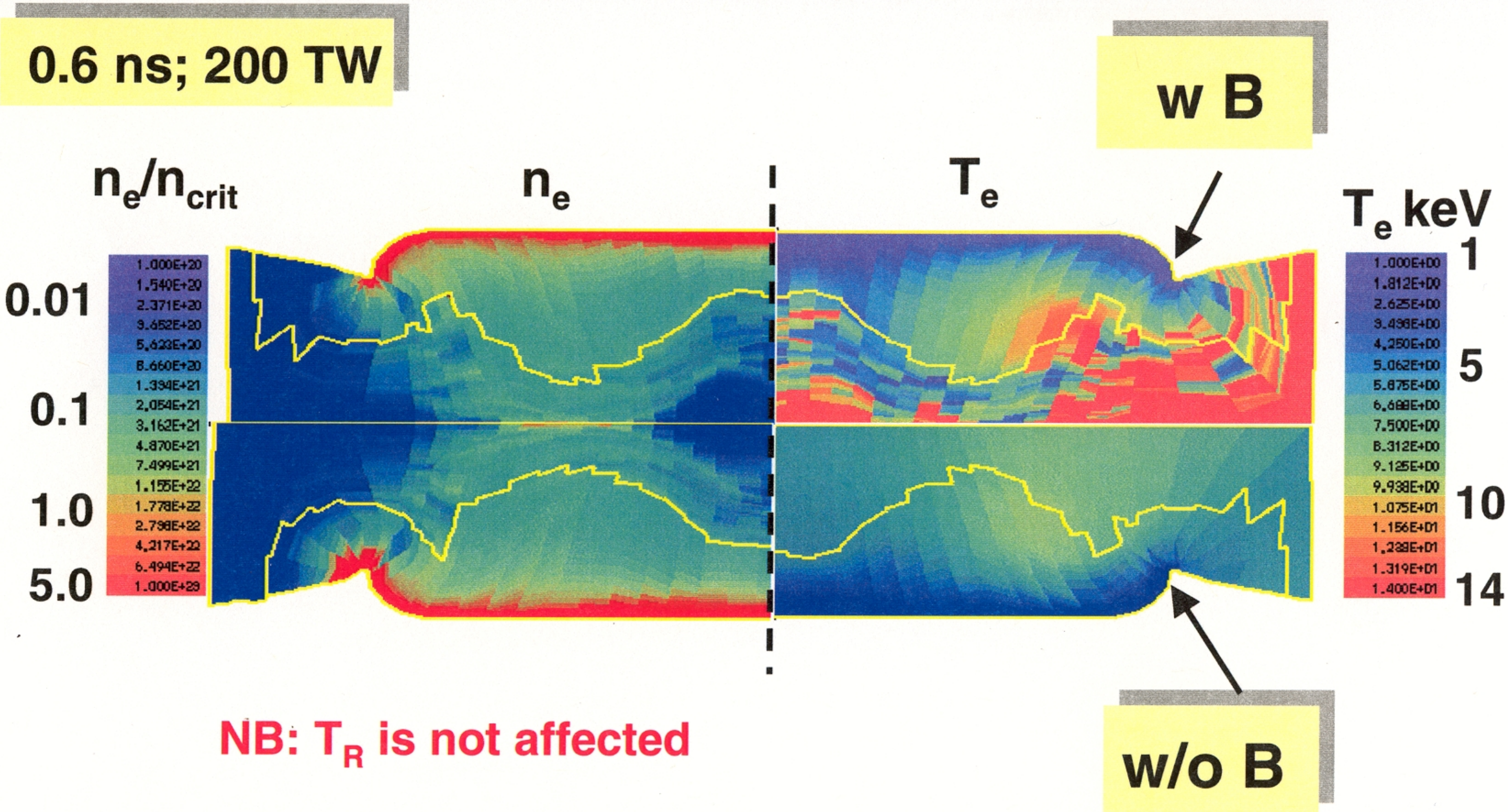

NB: T_R is not affected

We find this to be very typical of a wide variety of hohlraums

Righi-Leduc heat flow is responsible for this

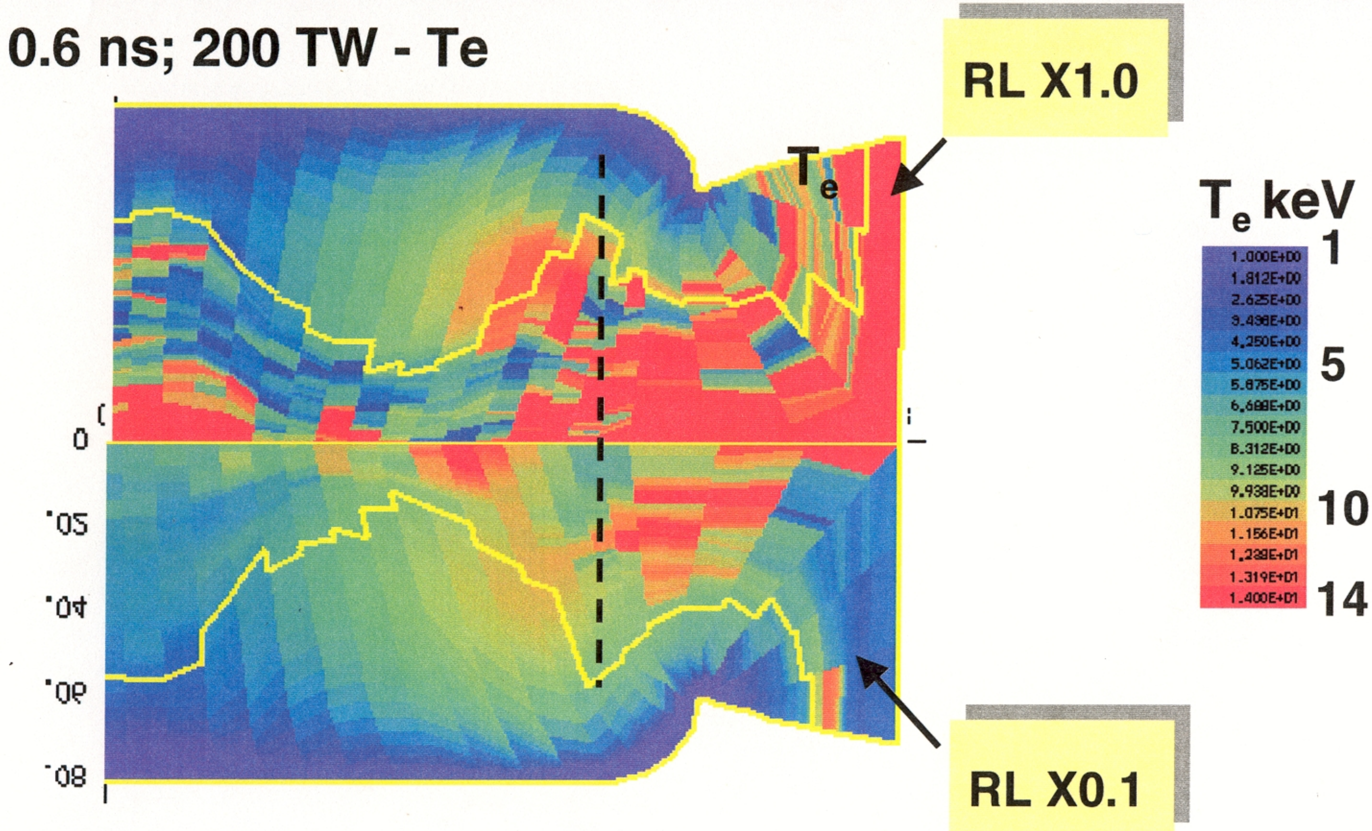

Despite significant B-fields local transport is questionable

0.6 ns; 200 TW

$$\frac{\lambda_{thermal}}{L_T}$$

$$V_c^6 = \frac{L_T^2}{2a_e^2} + \left[\frac{L_T^4}{4a_e^4} + \frac{L_T^2}{\lambda_e^2}\right]^{\frac{1}{2}}$$

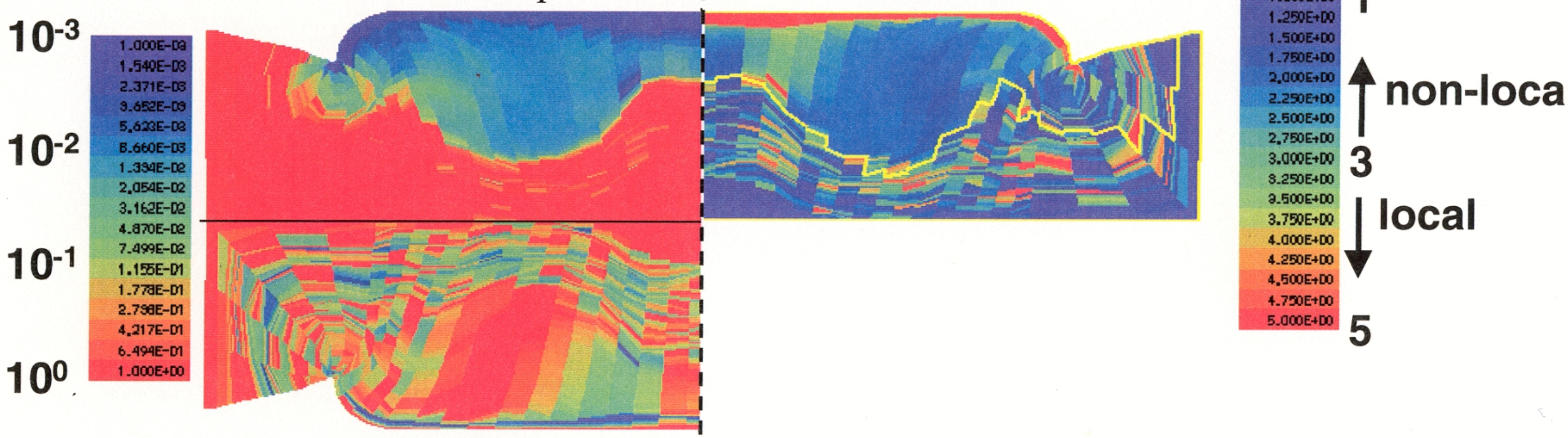

$$\frac{a_{thermal}}{L_T}$$

It slowly gets worse (more non-local) as the power goes up

V_{crit}

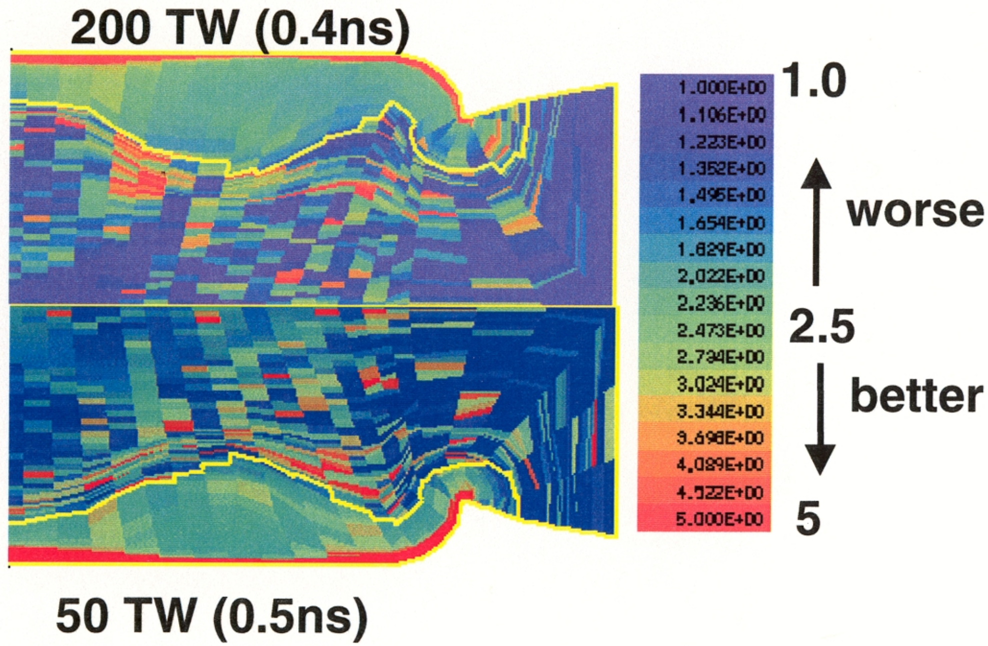

Righi-Leduc makes the calculation "noisy" & is often responsible for crashes, but IS needed

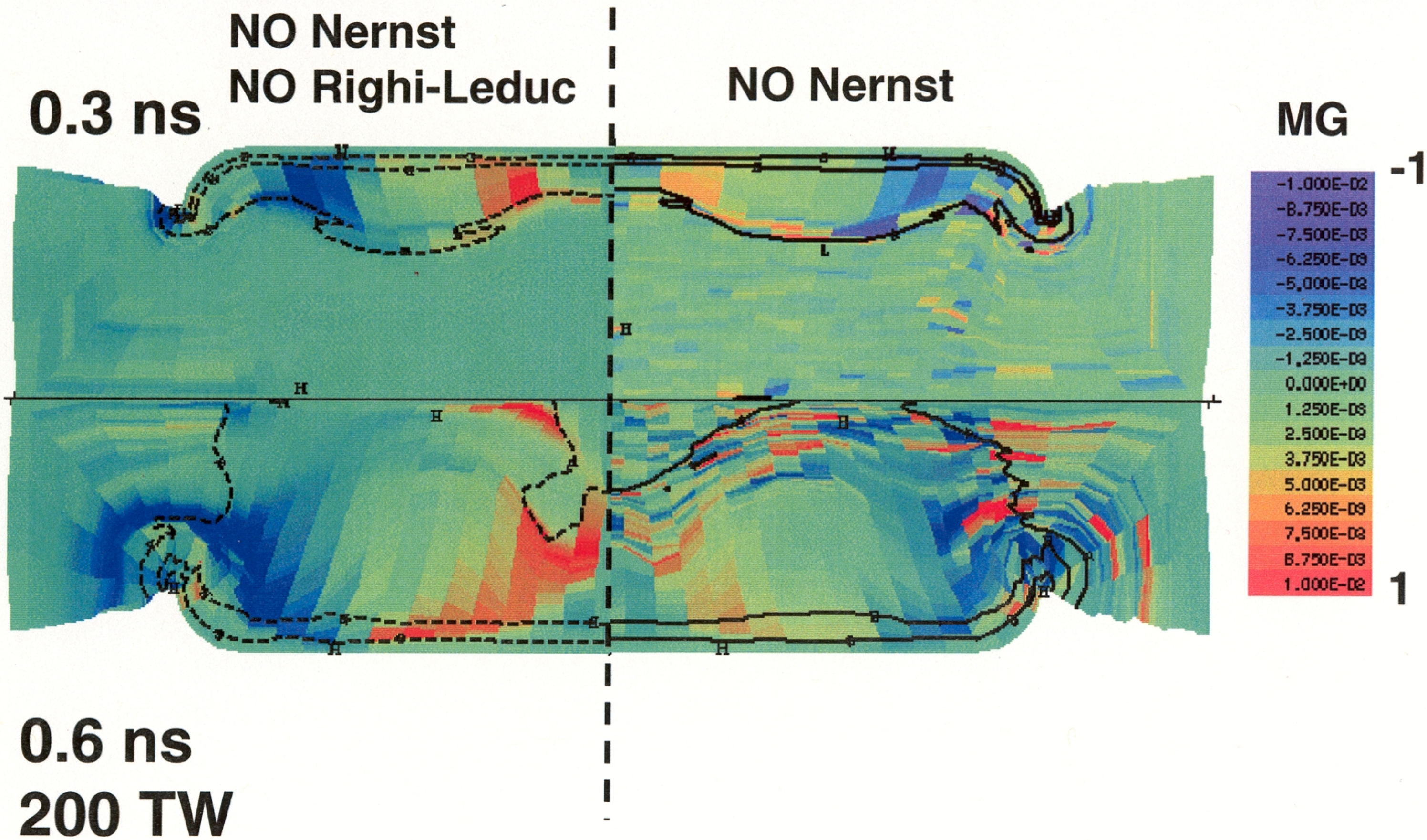

"Righi-Leduc" can also drive a thermomagnetic instability

A key point is that ∇T & ∇n are parallel: ∇T. ∇n > 0

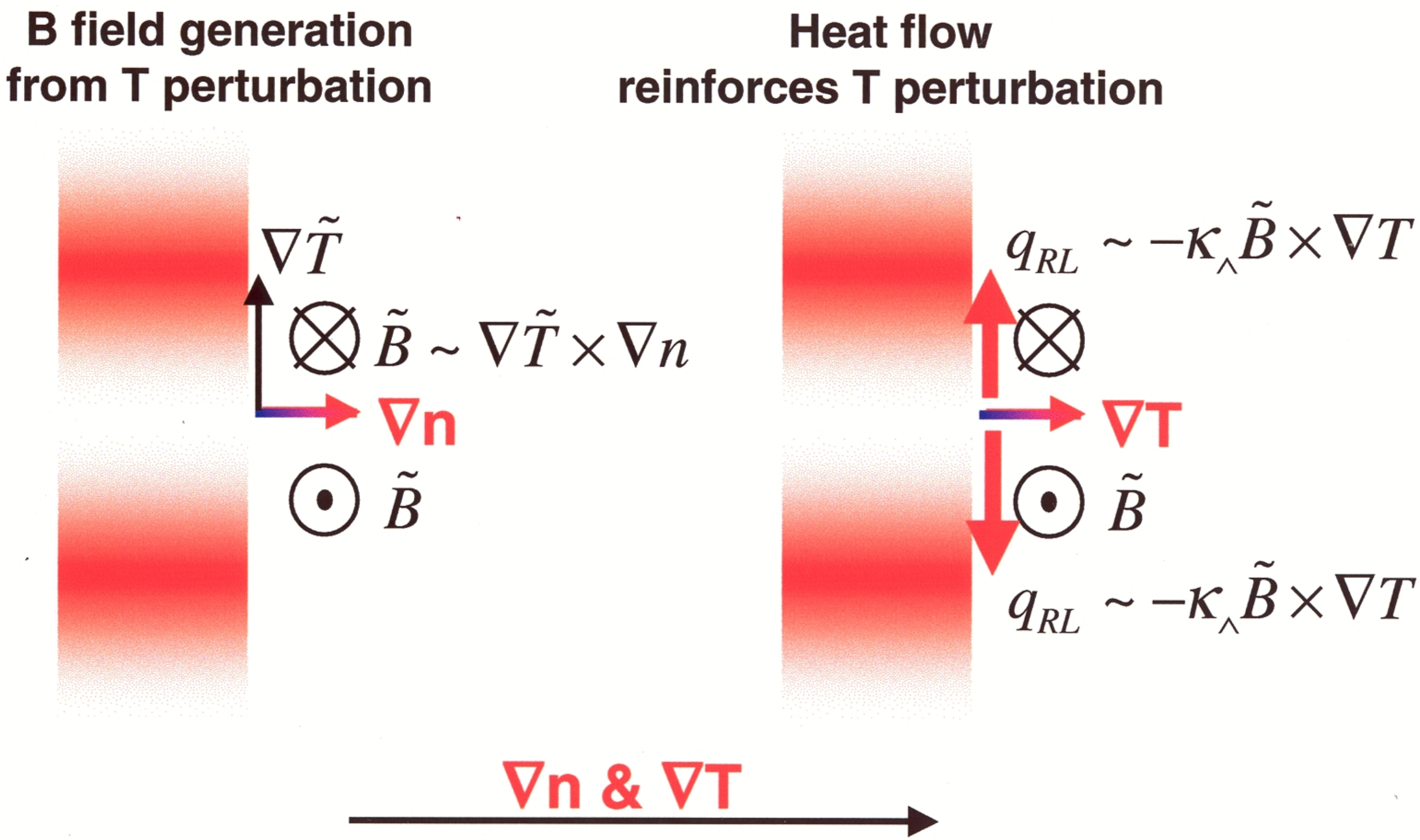

Tidman & Shanny 1974

Conditions in the gas are perfect for thermomagnetic instability!

cos (angle between ∇T & ∇n_e)

200 TW

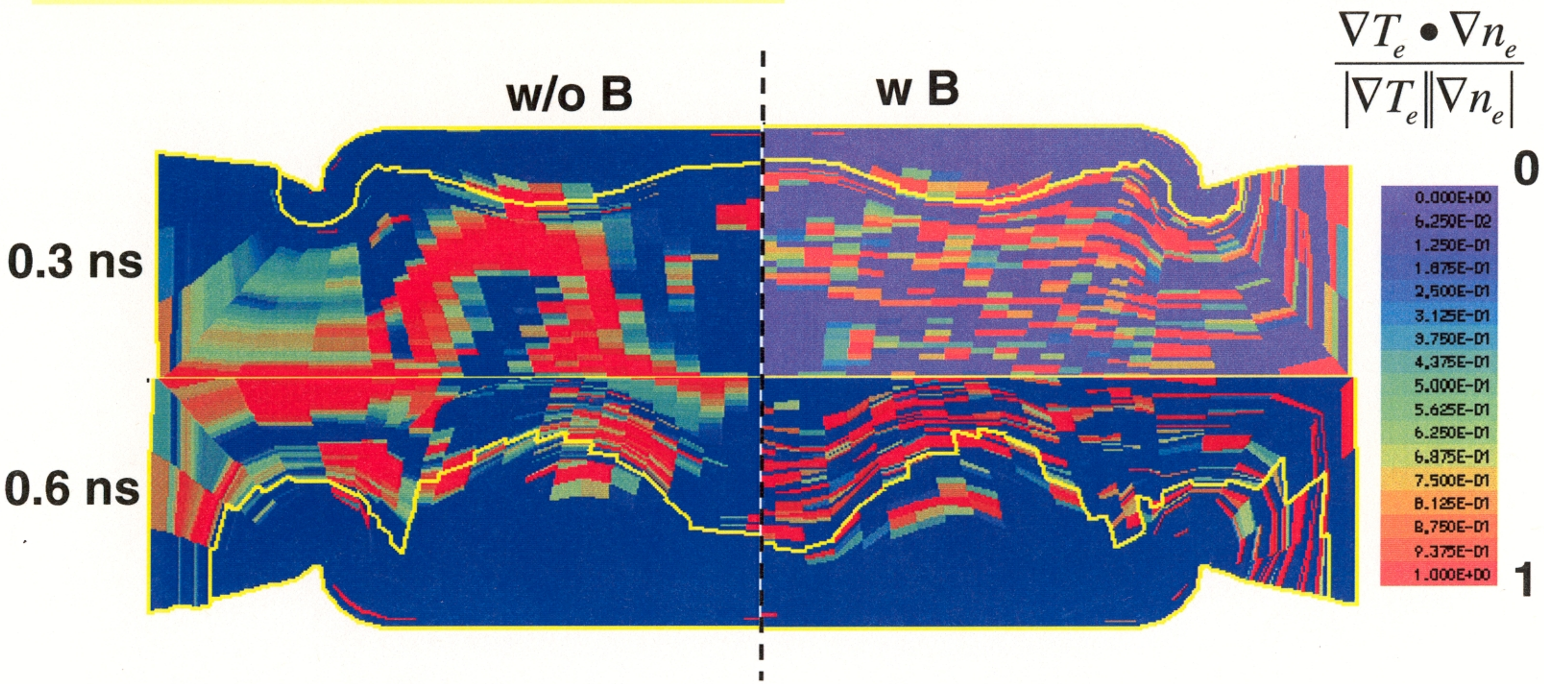

Thermomagnetic instability results 1 (Tidman & Shanny, 1974)

∇T & ∇n parallel: $\nabla T . \nabla n > 0$

High wavenumber cutoff driven by field diffusion

Theory needs:	$\lambda >> \lambda_e$	collisions
	$\lambda << L_n, L_T$	gradient supports wave
	$\dfrac{\omega}{k} >> c_s$	static ions

$$\lambda_M \sim \frac{1}{2}\phi^{1/2}(L_n L_T)^{1/2} \qquad \gamma \sim const \frac{T^{5/2}}{n_i Z^2 \ln\Lambda}\frac{1}{L_n L_T}$$

$$\phi = \frac{c \ln\Lambda}{v_e}\frac{Z}{n_e \lambda_D^3}$$

Thermomagnetic instability results 2 (Tidman & Shanny, 1974)

T ~ 10 keV;   Z ~ 3.5; n_e~ n_{ecrit}/4 ;   (lnΛ~8.5); L_n~L_T~0.02-0.2 cm

$$\lambda_M \sim \frac{1}{7}(L_n L_T)^{1/2} \qquad \gamma \sim \frac{7\times10^8}{(L_n L_T)_{cm^2}} s^{-1}$$

$$\lambda_M \sim 280\mu m \qquad 1/\gamma \sim 50\,ps$$

$$\lambda_e \sim 200\mu m$$

We see the same ~ x2 T_e elevation in ignition hohlraums

ignition hohlraum @ 16.2ns
near peak drive (~280eV in this case)

with B fields

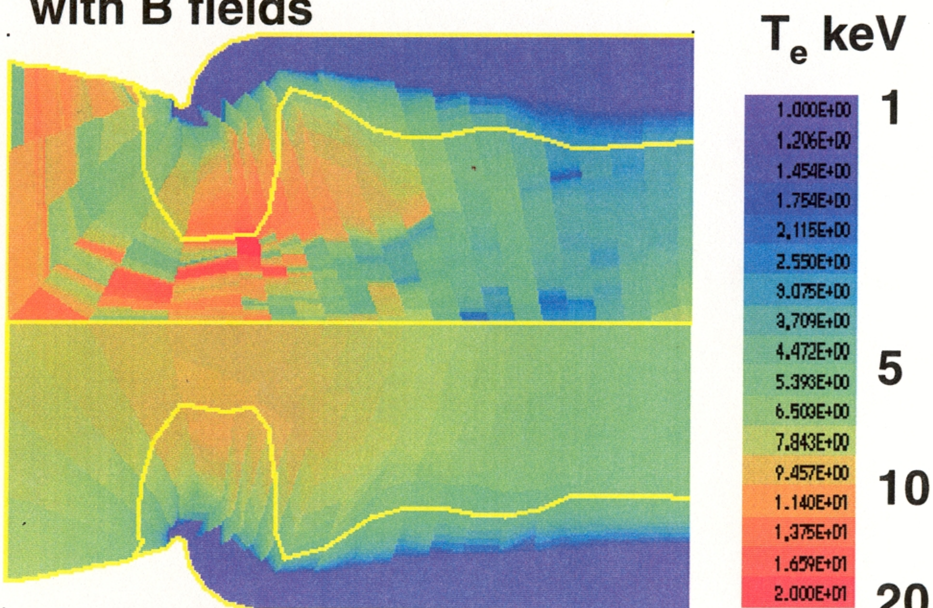

w/o B fields

- T_R is not affected
- Knock on consequences will most likely relate to
  - LPI
  - beam pointing
  - energy transfer
  - hard X-ray production

local transport appears equally questionable

Our general conclusions are rather independent of hohlraum or laser power

As expected the scaling is rather slow with

B_{VOL} shows no sign of saturation (expected)

If this is right B helps localize the electrons

BUT the local heat flow approximation appears marginal

The major impact of this appears to be in T_e distribution (~ x 2 at LEH when B is included); T_R NOT affected

This may affect:

LPI, symmetry, beam pointing, hard X-ray generation.....

For all this to be right we have to be modeling B correctly & this is linked to the heat flow model which in our case is local

Righi-Leduc is our main problem in running calculations

We need data! (correlate T_e with B)

Introduction

John Edwards

Electron transport workshop

9-11th Sepetmber

Purple Orchid Inn, Livermore 2002

Is there really a problem?

In the early days of laser fusion:

Spitzer-Harm inapplicable

B via $\nabla n \times \nabla T$ recognized

At high intensities bad stuff began to happen with direct drive
=> so for this & other reasons we went to indirect drive

Nova was a spectacular success & led to NIF

There was no indication that non-local transport or B-fields were a big issue. Hohlraums worked just fine (with a flux limiter ~ 0.1) (exceptions are small hohlraums - we have no idea why yet!)

In the mean time the rest of the world plugged away with direct drive
Both this and LPI in hohlraums drove a very aggressive &
Very successful beam smoothing effort

So what's changed?

Despite all that, we have strong evidence B-fields are important in at least some aspects of hohlraums

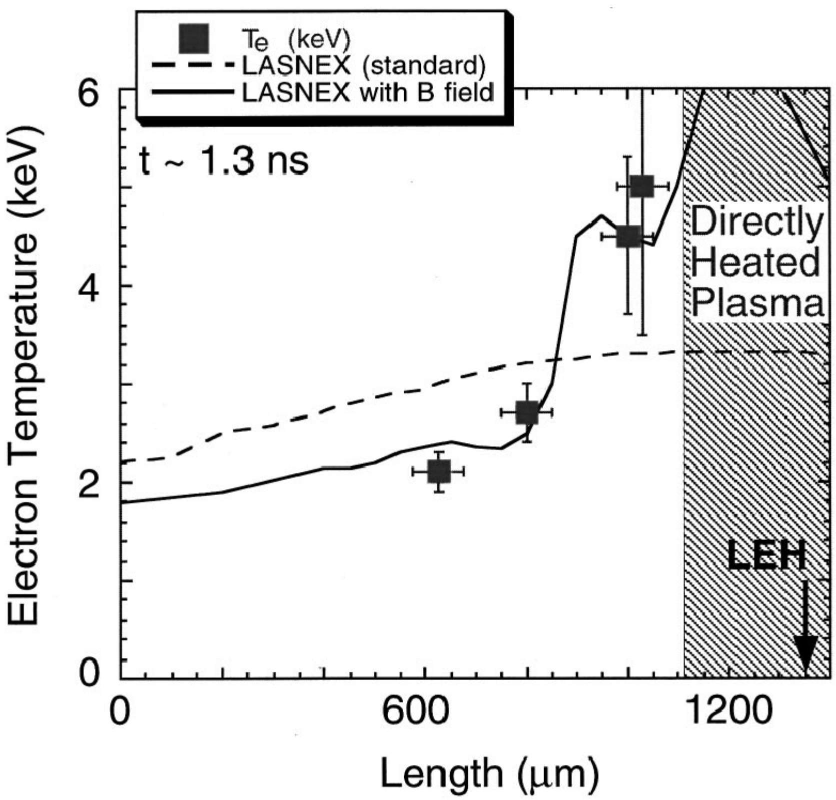

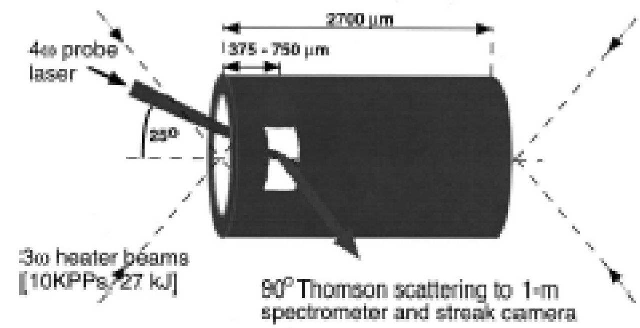

FIG. 5. Schematic of the 4ω TS experiments in Nova scale-1 hohlraums.

So what’s changed……?

NIF is very much closer now!
When we do something different there’s often a surprise

We’re planning to do much more with NIF than ignition
and go into regimes that are far from our current experiences

The beam smoothing success has seduced us into thinking that
maybe we can take advantage of better over all coupling into targets
compared to indirect drive

Ultra-high intensity lasers => proton probing - electro-thermal-instability?

Short pulse lasers for physics studies

Theory & computation

Fokker-Planck for laser plasmas in 1D (Bell, 1981)
Then in 2D (Epperlein, 1988)
Now 2D with B to f_1 keeping df_1/dt (Kingham, 2002)

At the same time, driven by extreme cost of FP
People got busy making reduced non-local models
to use in hydrocodes (1D, Luciani, 1983; ….
2D, Schurtz, 2000)

We're now 20 years on

is it time to try FP in our design codes?
and if not, what?

Workshop objectives

Our focus this time round is “long pulse” regime
especially for high energy density hohlraums & direct drive

What physics do we need to include?

What is a sensible way forward computationally?

> **Fokker-Planck**
> **something else (eg Monte Carlo)**
> **reduced model**

What developments & benchmarks do we need?

What should we do to test our ideas & models?

Physics of $\underline{B}$ generation

Ohm's law

$$\underline{E} + \underline{v}_e \times \underline{B} + \frac{\nabla p_e}{n_e} + \frac{\nabla \cdot \underline{\underline{\pi}}_e}{n_e} - \frac{m_e}{n_e e^2}\left(\frac{\partial \underline{J}}{\partial t} + \underline{v}_e \cdot \nabla \underline{J} + \underline{J} \cdot \nabla \underline{v}_e\right)$$

$$= \frac{1}{n^2 e^2}\Big[\underbrace{\alpha_{\parallel}\, \underline{b}\,(\underline{b}\cdot\underline{J})}_{\text{resistivity}} + \alpha_{\perp}\, \underline{b}\times(\underline{J}\times\underline{b}) - \underbrace{\alpha_{\wedge}\,(\underline{b}\times\underline{J})}_{\text{collisional Hall}}\Big]$$

$$- \frac{1}{e}\Big[\underbrace{\beta_{\parallel}\, \underline{b}\,(\underline{b}\cdot\nabla T_e)}_{\text{Thermoelectric}} + \beta_{\perp}\, \underline{b}\times(\nabla T_e\times\underline{b}) + \underbrace{\beta_{\wedge}\,(\underline{b}\times\nabla T_e)}_{\text{Nernst}}\Big]$$

Terms in green are extra to Braginskii

Faraday's law

$$\frac{\partial \underline{B}}{\partial t} = -\nabla \times \underline{E}$$

Include laser effects (see Can. J. Phys. $\underline{64}$, 912 (198?))

$$\underline{v}_e \rightarrow \underline{v}_e + \underline{\dot{\xi}}$$

quiver velocity

Extra terms $\langle \dot{\xi} \times \tilde{B} \rangle$ = radiation pressure due to absorption or reflection

$\langle\ \rangle$ time averaged

$$\frac{\nabla \cdot}{n_e} \langle n_e m_e \underline{\dot{\xi}}\, \underline{\dot{\xi}} \rangle = \text{ponderomotive force}$$

Source terms

(1) $$\nabla\times\left(\frac{\nabla p_e}{n_e e}\right) = \frac{\nabla T_e \times \nabla n_e}{n_e e}$$

Known as a dynamo in astrophysics

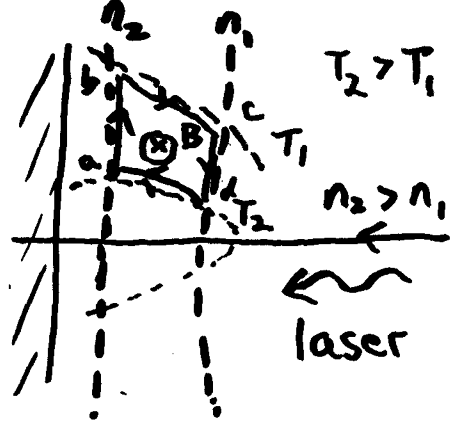

Consider line integral abcda

$$\int \frac{\nabla p}{n}.dl = \int_a^b \nabla T.\underline{dl} + \int_b^c T\frac{\nabla n}{n}\underline{dl} + \int_c^d \nabla T\,\underline{dl} + \int_d^a T\frac{\nabla n}{n}\,dl.$$

$$= -(T_2-T_1) - T_1 \ln\frac{n_2}{n_1} + (T_2-T_1) + T_2\ln\frac{n_2}{n_1}$$

$$= (T_2-T_1)\ln\frac{n_2}{n_1} \quad = \quad \frac{\partial B_\theta}{\partial t}\times \text{area.}$$

(2) $$\nabla\times\left(\frac{\nabla.\left[\underline{\underline{\tau}} + m_e n_e \underline{v}_e\underline{v}_e + m_e n_e \langle \dot{\underline{\xi}}\,\dot{\underline{\xi}}\rangle\right]}{\{n_e e\}}\right)$$

$\uparrow$ Weibel instability

$\uparrow$ e.g. resonance absorption

Convection and amplification of $\underline{B}$.

A good approximation to Ohm's law which holds for any f_0, including when nonlinear heat flow and other transport drives f_0 non-Maxwellian, is

$$\underline{E} + (\underline{V}_e + \underline{V}_T) \times \underline{B} + \frac{\nabla p_e}{n_e e} + \frac{\beta}{e}\nabla T_e = \eta \underline{J}$$

scalar

$$\underline{V}_T = \frac{\underline{q}_e}{5/2\, p_e} = \frac{\text{electron heat flux}}{5/2 \text{ electron pressure}}$$

We still need a good calculation of $\underline{q}_e$, but

$$\underbrace{\frac{\partial \underline{B}}{\partial t} + (\underline{V}_e + \underline{V}_T + \underline{V}_\alpha) \cdot \nabla \underline{B}}_{\text{convection}} = \underbrace{-\underline{B}\,\nabla \cdot (\underline{V}_e + \underline{V}_T)}_{\text{compression}} + \underbrace{\frac{\nabla T \times \nabla n}{n_e e}}_{\text{source.}}$$

$$+ \underbrace{\frac{\eta}{\mu_0}\nabla^2 \underline{B}}_{\text{diffusion}} + \underbrace{(\underline{B}\cdot\nabla)(\underline{V}_e + \underline{V}_T - \underline{V}_\alpha) + \nabla(\underline{V}_\alpha \cdot \underline{B})}_{\text{3D effects.}}$$

$$\underline{V}_\alpha = -\frac{\nabla \eta}{\mu_0}$$

Convection by $\underline{V}_T$ is because the magnetic field is more frozen to hot electrons than cold

If $\nabla \cdot \underline{V}_T < 0$, e.g. heat flow up a pressure gradient, amplification of $\underline{B}$ occurs. (Nishiguchi et al)

— also true nonlinearly (Kho + Haines) 1D F.P.

2 distinct cases

(1) $\nabla \times \underline{E} = 0$ at $t = 0$

Then there is still the possibility that $\underline{B}$ can be generated as a result of an instability

- Weibel instability
  - collisionless (PIC codes)
  - collisional (Epperlein et al)
- Thermomagnetic (Tidman + Shanny) $\lambda_{mfp} > c/\omega_{pe}$
- Electrothermal ; $\lambda_{mfp} < c/\omega_{pe}$ $E_z = \eta J_c$.
  - driven by heat flow (Haines)

(2) $\nabla \times \underline{E} \neq 0$ at $t = 0$ ie. 2-D state

- $\nabla T \times \nabla n$ generating $+B_\theta$ around a laser focal spot (+Z is direction of laser)
- In overdense plasma, especially in fast ignitor, generating $-B_\theta$ due to
  - $E_z(r) = \eta J_{cold}$ (need collisions) in contrast

to • Weibel instability $\Rightarrow$ filaments $\Rightarrow$ coalescence ; seen in PIC codes.

Validity of linear transport

For a tensor expansion of f

$$f(\underline{r},\underline{v},t) = f_0(\underline{r},v,t) + \underline{f}_1(\underline{r},v,t)\cdot\frac{\underline{v}}{v} + \underline{\underline{f}}_2(\underline{r},v,t):\frac{\underline{v}\,\underline{v}}{v^2} + \ldots$$

$\uparrow$ scalar

it has been shown that f_0 becomes non-Maxwellian for increasing f_1

For a Lorentz plasma + linear transport

$$\underline{F}_1 = \frac{F_m}{1+\Omega^2 V^6}\left(-V^4\underline{e} - \Omega V^7\underline{b}\times\underline{e} - V^6\underline{t} - \Omega^9\underline{b}\times\underline{t}\right)$$

where $F = \frac{4\pi v_T^3 f}{n}$, $V = \frac{v}{v_T}$, $v_T = \sqrt{\frac{2T}{m}}$, $\nu_T = \frac{3\sqrt{\pi}}{4\tau}$

$$\underline{e} = \frac{2e\underline{E}}{m_e v_T \nu_T} + \frac{v_T}{\nu_T}\frac{\nabla p_e}{p_e} - \frac{5}{2}\underline{t} \quad , \quad \underline{t} = \frac{v_T}{\nu_T}\frac{\nabla T_e}{T_e}$$

Taking $\underline{t}$ terms only, and $L = \left(|\nabla T|/T\right)^{-1}$ there is a critical velocity V_c at which

$$F_1 = F_m$$

$$V_c^6 = \frac{L^2}{2a_0^2} + \sqrt{\left[\frac{L^4}{4a_0^4} + \frac{L^2}{\lambda_{mfp}^2}\right]}$$

If $V_c \gg 1$ then linear transport holds. Consider 1-D heat flow

$$-1.5\sqrt{\pi}\,\underline{Q}_1 = \underline{t}\int_0^\infty V^{11}\exp(-V^2)\,dV + \underline{e}\int_0^\infty V^9\exp(-V^2)\,dV$$

High powers of V. High energy tail important. For $\underline{J} = 0$

$$\underline{e} = -4\underline{t}$$

thermoelectric field is set up

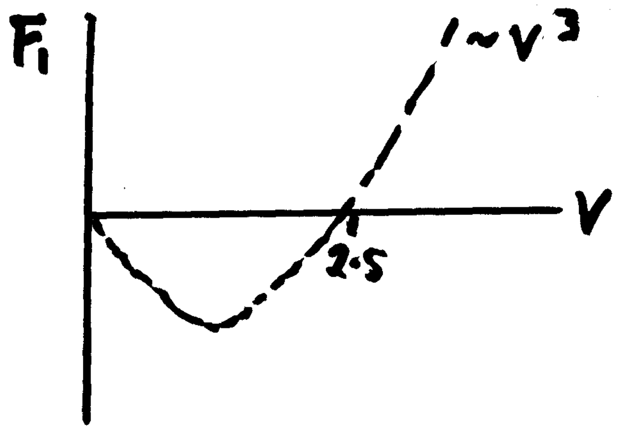

Reversal of F_1 (and heat flow) up to $V \simeq 2.5$. To capture 60% of q need $V=3$; 80%, $V=3.5$

Thermomagnetic instability

D.A. Tidman and R.A. Shanny '74 Phys. Fluids $\underline{17}$, 1207.

Could be occurring in LASNEX with linear transport and magnetic fields.

Equilibrium

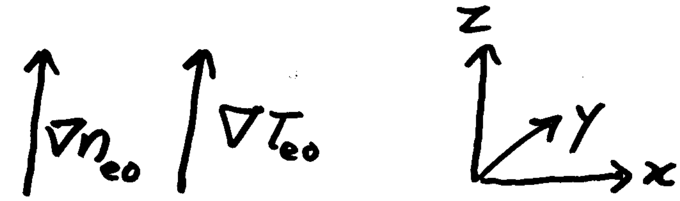

Perturbation $e^{\gamma t - ikx}$

$n_e \Rightarrow n_{eo} + n_1$ $\qquad T_e = T_{eo} + T_1$

$B_1 = (0, B_1, 0)$ $\qquad \underline{E}_1 = (0, 0, E_{z1})$

$\qquad \underline{J}_1 = (0, 0, J_{z1})$

Basic physics. $\quad$ Source of B is $\nabla n \times \nabla T$

$\frac{\partial B_1}{\partial t}$ from $- \frac{\partial T_1}{\partial x}\frac{\partial \ln n_0}{\partial z}$

$\frac{3}{2} n_0 \frac{\partial T_1}{\partial t}$ from $- \frac{\partial q_x}{\partial x}$ and $q_x = - K_{\wedge 1} \underline{b} \times \nabla T_0$

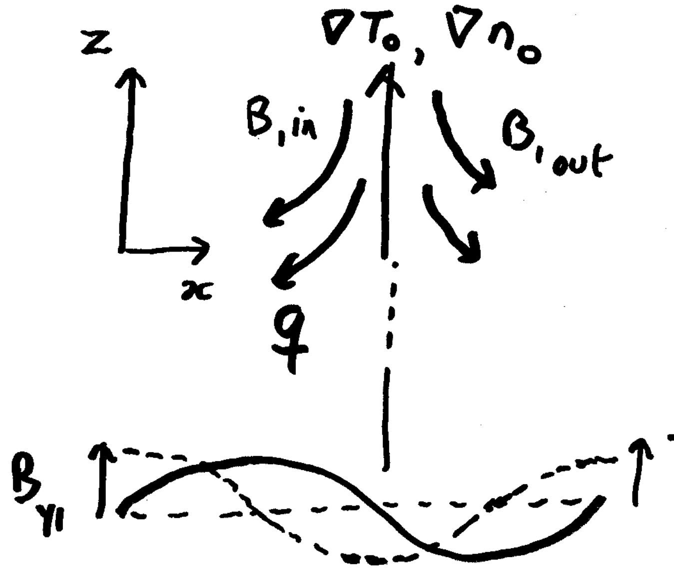

If $B_{y1} \sim \sin kx$

then $q_x \sim - \sin kx$

and $T_1 \sim \cos kx \sim J_{z1}$

$\rightarrow$ Positive feedback

$\rightarrow \frac{\partial B_{y1}}{\partial t} \sim \sin kx$

Tidman + Shanny included resistive diffusion and thermal diffusion

$$\frac{\partial B_1}{\partial t} = \frac{\partial E_{z1}}{\partial x} - \frac{\partial E_{x1}}{\partial z}$$

$$= \frac{\partial}{\partial x}\Big(-\frac{T_1}{n_e e}\frac{\partial n_0}{\partial z} + \underbrace{\eta_0}_{\text{resistive diffusion}} J_{z1}\Big) - \frac{\partial}{\partial z}\Big(-\underbrace{\frac{T_0}{n_0 e}\frac{\partial n_1}{\partial x}}_{\text{ignore } n_1 \text{ changes.}} - \underbrace{\frac{\partial \beta_\wedge}{\partial B}}_{\text{Nernst}} B_1 \frac{\partial T_0}{\partial z}\Big)$$

$$\frac{3}{2} n_0 \frac{\partial T_1}{\partial t} = -\frac{\partial q_x}{\partial x} - \frac{\partial q_z}{\partial z}$$

$$q_e = -\frac{n_e T_e \tau}{m_e}\Big[\underbrace{\kappa_\perp^c \nabla_\perp T}_{\text{thermal conduction}} + \underbrace{\kappa_\wedge^c \underline{b} \times \nabla T}_{\text{Righi-Leduc}}\Big] - \underbrace{\frac{T_e}{e}\beta_\perp^c \underline{J}_\perp}_{q_{z1}} - \underbrace{\frac{T_e}{e}\beta_\wedge^c \underline{b}}_{\text{Ettingshausen}}$$

(non-linear $\sim \hat{\underline{x}} \sin 2kx$

$$\therefore \gamma B_1 = \frac{ik}{n_0 e}\frac{\partial n_0}{\partial z} T_1 - k^2 \frac{m_e \alpha_\perp^c}{n_0 e^2 \tau \mu_0} B_1$$

$$\gamma T_1 = -\frac{2}{3}\frac{T_0 \tau_0}{m_e}\kappa_{\perp 0}^c k^2 T_1 - ik\,\gamma_{on}\frac{e\tau^2 T_0}{m_e^2}\frac{\partial T_0}{\partial z} B_1$$

with assumptions : (none of which are probably true!!)

1) Local approximation , $k \gg \frac{1}{L_n}, \frac{1}{L_T}$

2) No ion motion ; $n_1 = 0$

3) Linear transport holds ; $\lambda_{mfp} \ll 1/k$

4) $\underline{\underline{f}}_2$ – anisotropy negligible.

Dispersion relation

$$(\gamma + d_1 k^2)(\gamma + d_2 k^2) = d_1 d_2 k_c^2 k^2$$

where $d_1 = \dfrac{m_e \alpha_\perp^c}{n_0 e^2 \tau \mu_0}$, $d_2 = \dfrac{2}{3}\dfrac{T_0 \tau_0}{m_e} K_{\perp 0}^c$

$$k_c^2 = \frac{3\gamma_{0\wedge}}{2\alpha_\perp^c K_\perp^c} \cdot \frac{\tau^2 \mu_0 e^2}{m_e^2} \frac{n_0 T_0}{L_n L_T} = \frac{3}{2}\frac{\gamma_{0\wedge}}{\alpha_0 \delta_0} \frac{\lambda_{mfp}^2}{c^2/\omega_{pe}^2} \cdot \frac{1}{L_n L_T}$$

$$= \begin{matrix} 5.6 \\ \text{to} \\ 35 \end{matrix} \frac{\lambda_{mfp}^2}{c^2/\omega_{pe}^2} \cdot \frac{1}{L_n L_T} \quad \text{for } Z = 1 \text{ to } 10$$

Marginal stability is at $k = k_c$ - critical wave number (at $\gamma = 0$). Unstable for

$$0 < k \leq k_c \quad \text{and} \quad \nabla n_0 \cdot \nabla T_0 > 0$$

It follows that $\lambda_{mfp} \gg \frac{c}{\omega_{pe}}$ for $k^2 \sim k_c^2 \gg \frac{1}{L_n L_T}$

This is the opposite of condition for heat flux driven electrothermal instabilities $\left(\lambda_{mfp} < \frac{c}{\omega_{pe}}\right)$

Growth rate

$$\gamma = -\left(\frac{d_1 + d_2}{2}\right) k^2 + \sqrt{\left[\left(\frac{d_1 - d_2}{2}\right)^2 k^4 + d_1 d_2 k^2 k_c^2\right]}$$

This has a maximum at $k^2 = k_c^2 \dfrac{\sqrt{d_1 d_2}}{(\sqrt{d_1} + \sqrt{d_2})^2}$

At small k, $\gamma \rightarrow (d_1 d_2)^{1/2} k_c k$

In experiments, resistive diffusion is usually much less than thermal diffusion i.e. $\frac{d_1}{d_2} \equiv x \ll 1$

<u>Example</u>: $n_e = 3.5 \times 10^{20}\ cm^{-3}$

$T_e = 5\ keV$

$Z = 4$

$\ln\Lambda = 7.256$, $\tau = 1.2 \times 10^{-11}$

$\gamma_0 = 6.995$ $\alpha_0 = 0.3750$ $\gamma_{0\wedge} = 34.95$

$c/\omega_{pe} = 2.84 \times 10^{-7}\ m$ $\lambda_{mfp} = 356\ \mu m$

$\lambda_{mfp}(v = 3v_t) = 28.8\ mm$

$\therefore$ need non-local transport

$d_1 = .0282\ m^2/s$ $\frac{d_1}{d_2} = 3.2 \times 10^{-5}$

$d_2 = 880.8\ m^2/s$

$\left(\frac{\lambda_{mfp}}{c/\omega_{pe}}\right)^2 = 1.57 \times 10^6 \gg 1$ $k_c = \frac{5601}{(L_n L_T)^{1/2}}$

$$\frac{\gamma_{max}}{d_2 k_c^2} = \frac{x^{1/2}}{(1+\sqrt{x})^2}\left\{\sqrt{\left[\frac{1}{4} - \frac{1}{2}x + x^2 + x^{1/2}(1 + 2\sqrt{x} + x)\right]} - \frac{1}{2} - \frac{1}{2}x\right\}$$

$\rightarrow x$ for $x \ll 1$

$\therefore \gamma_{max} \simeq d_1 k_c^2$ at $k = k_c\left(\frac{d_1}{d_2}\right)^{1/4}$

For $L_n = L_T = 100\ \mu m$

$$\gamma_{max} = 8.85 \times 10^{13}\ s^{-1}$$

at $\lambda = \dfrac{2\pi}{k} = \dfrac{2\pi\,(L_n L_T)^{1/2}}{421.3} = 1.49\ \mu m.$

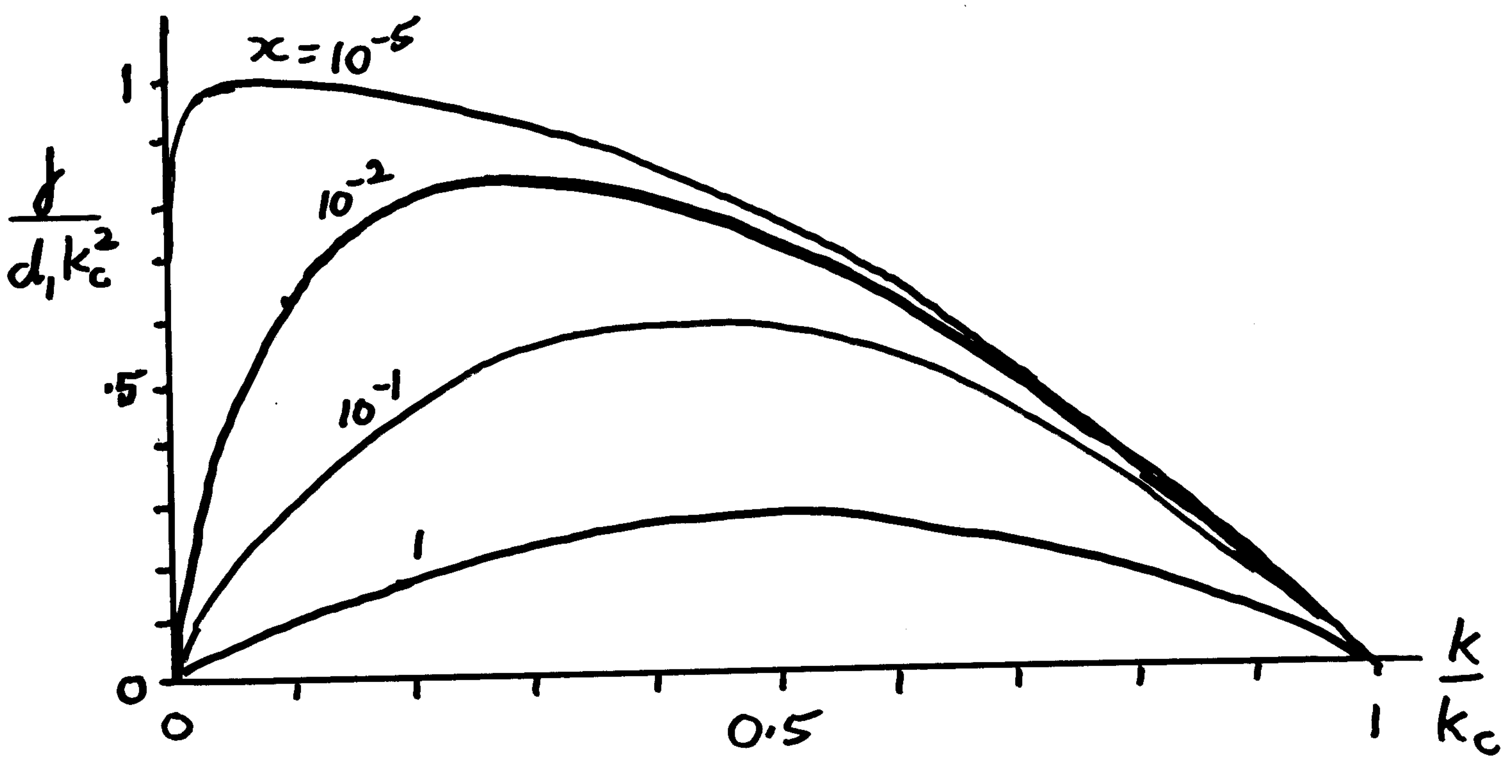

Conditions for validity

$$L_n, L_T \gg \lambda = \frac{2\pi}{k} \gg \lambda_{mfp} \gg c/\omega_{pe}$$

$100\ \mu m$ $\quad$ $1.49\ \mu m$ $\quad$ $356\ \mu m$ $\gg$ $0.28\ \mu m$

$1000\ \mu m$ $\quad$ $14.9\ \mu m$ $\quad$ still bad.

Include electron viscosity in Ohm's law

$$E_{z1} = \eta_0 j_{z1} - \frac{T_1}{n_0 e}\frac{\partial n_0}{\partial z} - \frac{1}{n_0 e}\frac{\partial}{\partial x}\left[\frac{n_0 T_0 \tau_{ee}}{n_0}\frac{\partial j_{z1}}{\partial x}\right]$$

$$= \frac{\eta_0}{\mu_0}\left(1 + k^2\lambda_{mfp}^2\right)\frac{\partial B_1}{\partial x} - \frac{T_1}{e L_n}$$

ie. replace d_1 by $d_1(1+k^2\lambda_{mfp}^2)$ and k_c^2 by $\frac{k_c^2}{1+k^2\lambda_{mfp}^2}$

Growth rate

$$\gamma = -\frac{1}{2}\left[(d_1+d_2)k^2 + d_1 k^4 \lambda_{mfp}^2\right]$$

$$+\sqrt{\left\{\frac{1}{4}\left[(d_1+d_2)k^2 + d_1 k^4 \lambda_{mfp}^2\right]^2 + d_1 d_2 k^2\left[k_c^2 - k^2 - k^4\lambda\right.\right.}$$

Example $\quad T_e = 10\,\text{keV}$

$n = \frac{1}{4} n_c = 0.25 \times 10^{22}\,\text{cm}^{-3}$

$L_n = L_T = 100\,\mu\text{m}. \qquad Z = 3.5$

$\Rightarrow \gamma_{max} = 5.3 \times 10^{-12}\,\text{s}^{-1}$ (only slightly less)

at $\lambda = 42.4\,\mu\text{m}$ for $\lambda_{mfp} = 193\,\mu\text{m}$.

But delocalisation by $\left[1 + (30 k \lambda_{mfp})^{4/3}\right]$

(Epperlein + Short PF B4, 2211 (1992))

should perhaps be applied to viscosity, thermal conduction and (maybe modified) to Righi-Leduc.

Electrothermal instability associated with nonlinear heat flow from the corona to the molten/vapour core of wire (or capsule)

References. M.G. Haines, J. Plasma Phys $\underline{12}$, 1 (1974)
($k \parallel B_0$) (for current driven ET instab. in θ pinch)

M.G. Haines, Phys. Rev. Lett. $\underline{47}$, 917 (1981)
(for nonlinear heat flow driven instability in ICF)

For ET instability in magnetised plasma with $\underline{k} \perp \underline{B}_0$
A. Tomimura and M.G. Haines, J. Plasma Phys.
M.G. Haines and F. Marsh, J. Plasma Phys.
+ IAEA

ET instability driven by heat flow

hot electrons $\longrightarrow$ $\longleftarrow$ $\qquad J_{cold} = \sigma E$

$\longrightarrow$ cold electrons $\longleftarrow$ $\qquad \downarrow \underline{k} \qquad \sigma = \alpha T^{3/2}$

$\longrightarrow E_{thermoelectric} \qquad \underline{k}$ is $\perp$ to q

$\longrightarrow q$ heat flux

Basic instability is Joule heating of cold electrons by the return (cold) current. Where $T' \sim e^{ikx}$ is higher, J + heating increases, so raising T'. Include damping by transverse thermal conduction and $\nabla \times \underline{E}' = -\dfrac{\partial B'}{\partial t}$ + ion motion

Then found to be unstable if

$$\lambda_{mfp} < c/\omega_{pe}$$

and if Joule heating is sufficiently strong e.g. would create $T_e > 1.32\, T_i$

$$T_e\,(^\circ K) \leq 0.1\, n_e^{1/4}(m^{-3})\, Z^{1/2} \left(\frac{\ln\Lambda}{5}\right)^{1/2}$$

Growth rate $\quad \alpha = 2.8 \times 10^{-8} \dfrac{n_e Z}{A\, T_{e0}^{3/2}}$

at wavelength $\quad \lambda = 2.4 \times 10^{10} \dfrac{T_e^{2}(^\circ K)\, A^{1/2}}{n_e(m^{-3})\, Z} \quad (m)$

Perturbed magnetic fields, surrounding each filament reduce thermal condution, relaxes $\lambda_{mfp} < c/\omega_{pe}$, and filaments get frozen in.

A more rigorous theory requires a F.P. model including F_0' and the $\underline{E}.\underline{F}_1$ terms (heating of colds and cooling of hots, and possibly $\underline{\underline{F}}_2$.

In hybrid model the hot electrons have perturbed orbits in the $\underline{E}'$ and B' fields

The parameter h describing the hot electrons is zero if $J_{hot} = n_h e (kT_h/m_e)^{1/2}$

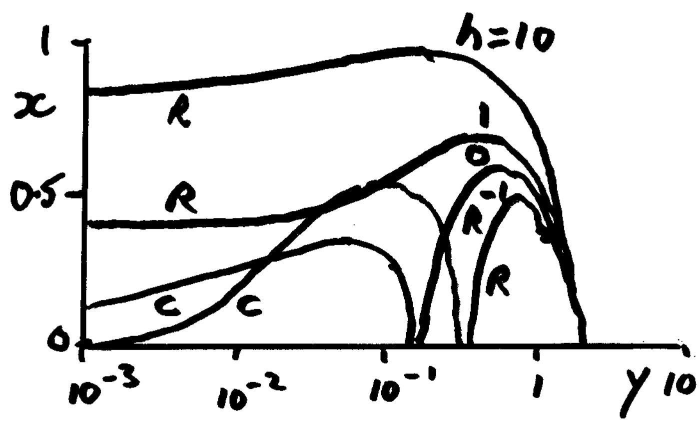

Unstable roots of the dispersion equation

$x \propto$ growth , $y \propto k^2$

R = real ~~root~~ root C = complex root

Curtailment of SBS by localised magnetic field generation

M.G. Haines, Imperial College.

laser

back scatter

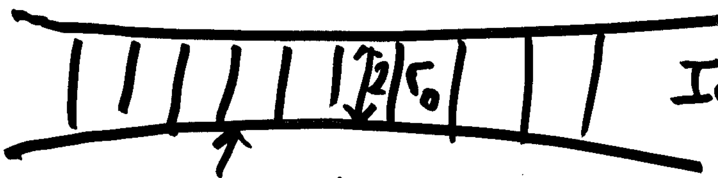

Speckle

Ion acoustic wave.

Ponderomotive force on electrons from photon momentum (absorbed + reflected)

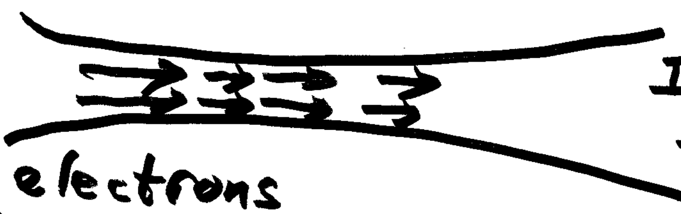

Induced $\underline{E}$ transfers force to ions ($\lambda_{ii} \gg r_0$)

$\underline{E} = -\nabla\Phi$ in 1-D

$\underline{E} = -\nabla\Phi - \frac{\partial \underline{A}}{\partial t}$ in general

$\nabla \times \underline{E} \neq 0$

$= -\frac{\partial \underline{B}}{\partial t}$

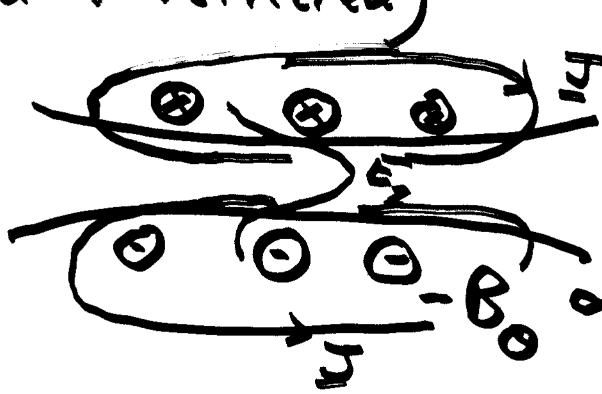

$B_\theta \propto r$

Ion sound waves replaced

$c_A^2 = \frac{B^2}{\mu_0 \rho}$

by magnetosonic fast wave $\sqrt{c_s^2 + c_A^2} \simeq c_s(1 + A(t) r^2)$

Coherent plane wave of IAW broken up

Driving currents and azimuthal Magnetic fields from photon momentum

Effective Ohm's law

$$n_e m_e \frac{\partial v_{ez}}{\partial t} = -n_e e E_z - n_e e (\underline{v}_e \times \underline{B})_z + \frac{\alpha I_z}{cL} - n_e m_e \nu_{ei} v_{ez} - \nabla_\alpha P_{\alpha z}$$

where I_z = radiation intensity in z direction

$\alpha = \alpha_{abs} + 2\alpha_{refl}$ over length L

$\frac{\alpha I_z}{cL} = \langle \tilde{\underline{J}} \times \tilde{\underline{B}} \rangle_z$ average radiation pressure

But $\frac{\partial E_z}{\partial r} = \frac{\partial B_\theta}{\partial t}$ and $\frac{1}{r}\frac{\partial}{\partial r}(r B_\theta) = -\mu_0 n_e e v_{ez}$

For a laser heater pulse in a gas-bag or gas-filled hohlraum at LLNL

Neglect electron inertia and e-i collisions

$$E_z \simeq \frac{\alpha I}{n_e e c L} \quad \text{and} \quad B_\theta \simeq -\frac{\tau}{r_0}\frac{\alpha I}{n_e e c L}$$

For $L = 5\,mm$, $I = 3.10^{15}\,W.cm^{-2}$, $n_e = 10^{20}\,cm^{-3}$

$r_0 = 30\,\mu m$, $\tau = 5\,ns$, $\alpha = 0.5 \Rightarrow B_\theta = 104$ tesla

$\alpha = \alpha_{absorbed} + 2\alpha_{reflected}$

Siegfried Glenzer's experiment

For a parabolic profile $I = I_0(1 - r^2/r_0^2)$

average intensity $\bar{I} = \frac{1}{2} I_0$

If $r_0 = 125 \mu m$ $\qquad I_0 = 2\bar{I} = 3.10^{15}\ W cm^{-2}$

$L = 1.6\ mm$ $\qquad t = 1.5\ ns$

$\alpha = \alpha_{abs} + 2\alpha_{refl} = 0.3 + 2 \times 0.2 = 0.7$

$n_e = 5 \times 10^{20}\ cm^{-3}$

$\Rightarrow B_\theta = 13.1$ tesla (131 KG)

Cavitation time for CH

$\bar{Z} = 3.5 \qquad \bar{m}_i = 6.5\ m_p$

$$t_c = \left(\frac{9}{2} \frac{n_e m_i r_0^2}{Z \alpha_{abs} I_0} \right)^{1/3}$$

$$= 2.3 \times 10^{-9}\ s$$

n_e is reduced by $\sim \exp\left(-\frac{t}{t_c}\right)$

$\sim e^{-1.5/2.3} = 0.52$

Then $B_\theta \simeq 26$ tesla (260 KG)

But larger r_0, smaller α leads to much reduced B_θ. Instead consider speckles and self focusing.

Speckle

Harvey Rose (Phys. Plasmas 4, 437 (1997))
proposed saturation of SBS by ion flows
driven by photon momentum deposition.
But λ_{mfp} of ions >> spot radius
$10 - 40\,\mu m >> 2\,\mu m$.
and will receive a kick from E_z as
they move through speckle
$\partial E_z / \partial r$ will generate B_θ and will convert
c_s to $(c_s^2 + c_A^2)^{1/2}$ where $\frac{c_A^2}{c_s^2} = \frac{B^2}{\mu_0 P_e} = \frac{2}{\beta}$
which will vary strongly over the speckle radius
r_0 and cause sound waves to break up.

Use $B_\theta = -\frac{2r}{r_0^2} \frac{\alpha I t}{n_e e c L}$ and $v_z = \frac{\alpha I t}{n_i m_i c L}$

$I = 6 \times 10^{15}\,W cm^{-2}$, $L = 50\,\mu m$, $r_0 = 1.8\,\mu m$, $t = 100\,ps$
$n_e = 10^{21}\,cm^{-3}$ for $Z = 1$, $m_i = m_p$, $T_e = 2.10^3\,eV$

$B_\theta = 1.4 \times 10^3$ tesla $\quad v_z = 1.2 \times 10^5\,m/s$
$(c_s = 4.4 \times 10^5\,m/s)$

$\frac{V_t}{c_s} = 2.42$

· B- Field is dominant

Because $B_\theta < 0$, the $v_r B_\theta$ and $\frac{q_r B_\theta}{3/2\, P_e}$ electric field terms will amplify the magnetic field.

But the 'Nernst' term is only valid for λ_{mfp}/L small as it represents the velocity dependence of the collision frequency.

q_r however exists and is known in gas bag experiment. $\lambda_{mfp} \sim 44\,\mu m$ and for $V \sim 3$, $\lambda_{mfp} \sim 4$ mm

Use results of diode problem with plasma between plates at T_L and T_R with variable λ_{mfp}/L.

Kho + Bond, J. Phys D 14, L117 (1981)
Bond, Kho + Haines, Plasma Phys. 24, 1133 (1982)

$$q_{collisionless} = \frac{n_e}{\pi^{1/2}} \frac{(2k_B)^{3/2}}{m_e^{1/2}} T_L^{1/2} T_R^{1/2} \left(T_L^{1/2} - T_R^{1/2}\right)$$

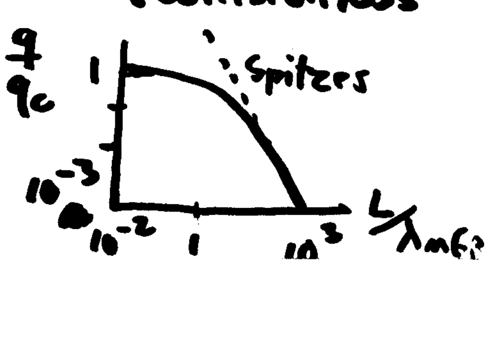

For gasbag $q_r/q_{FS} \simeq .04$

or $T_R \sim .93\, T_L$ if collisionless

Nonlinear electron transport in magnetized laser plasmas

T. H. Kho and M. G. Haines Phys Fluids $\underline{29}$, 2665 (1986)

(Also PRL $\underline{55}$, 825 (1985))

1-D model with transverse B_y applied + constant at $z = 0$

(Langdon)
v_0 = quiver vel.

$$\underline{F}_1 = (F_1^x, 0, F_1^z)$$

$$\partial_t f_0 + \frac{1}{3v^2}\partial_z(v^3 f_1^z) = \frac{1}{v^2}\partial_v\left\{\frac{v^3}{3}\underline{a}\cdot\underline{f}_1 + Y\left[Cf_0 + \left(D + \frac{nZv_0^2}{6v}\right)\partial_v f_0\right]\right\}$$

$$f^x = -\frac{\tau}{1+\chi^2}\left[v\chi\,\partial_z f_0 - (a_x + \chi a_z)\,\partial_v f_0\right]$$

$$f^z = -\frac{\tau}{1+\chi^2}\left[v\,\partial_z f_0 + (\chi a_x - a_z)\,\partial_v f_0\right]$$

where $\underline{a} = \frac{e\underline{E}}{m_e}$, $\chi(v) = \frac{eB}{m}\tau(v)$, $\tau = \frac{v^3}{(Z+1)nY}$

$$Y = \frac{4\pi e^4 \ln\Lambda}{(4\pi\epsilon_0 m_e)^2}, \quad C = f_0 I_0^0, \text{ and } D = \frac{v}{3}\left(I_2^0 + J_{-1}^0\right)$$

$$I_j^i = \frac{4\pi}{v^j}\int_0^v f^i u^{j+2}\,du \quad \text{and} \quad J_j^i = \frac{4\pi}{v^j}\int_v^\infty f^i u^{j+2}\,du$$

a_z adjusted for $J_z = 0$. $\nabla T = \frac{\partial T}{\partial z}$, J_x, q_x, q_z non zero

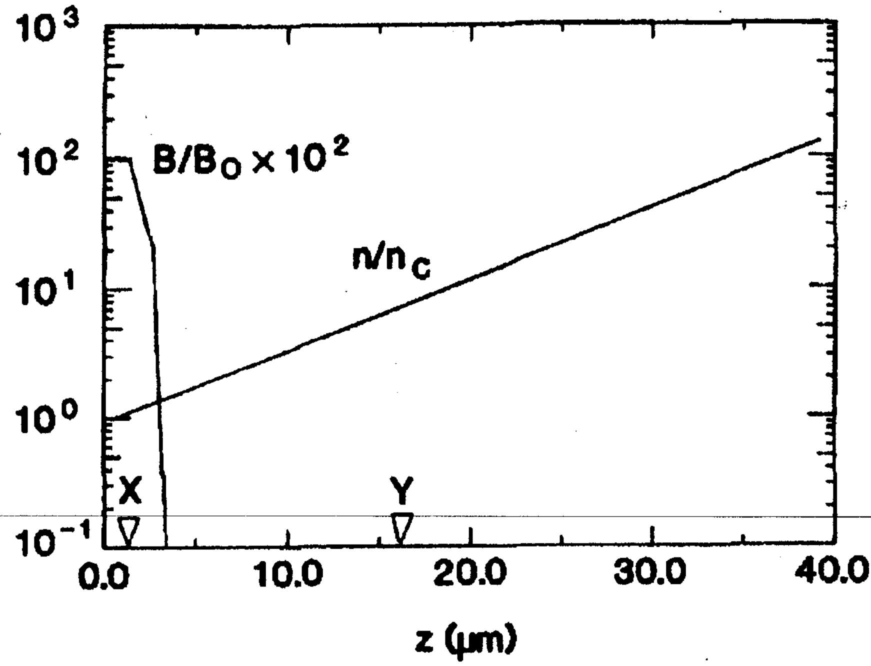

FIG. 1. Fixed exponential density, normalized to critical density n_c, and initial (normalized) magnetic field B/B_0, which vanishes for $z > 4\,\mu$m. Inverse bremsstrahlung absorption takes place from $z = 0$ to $z = X$. Over the same region, the "source" magnetic field B_0 is kept constant in time.

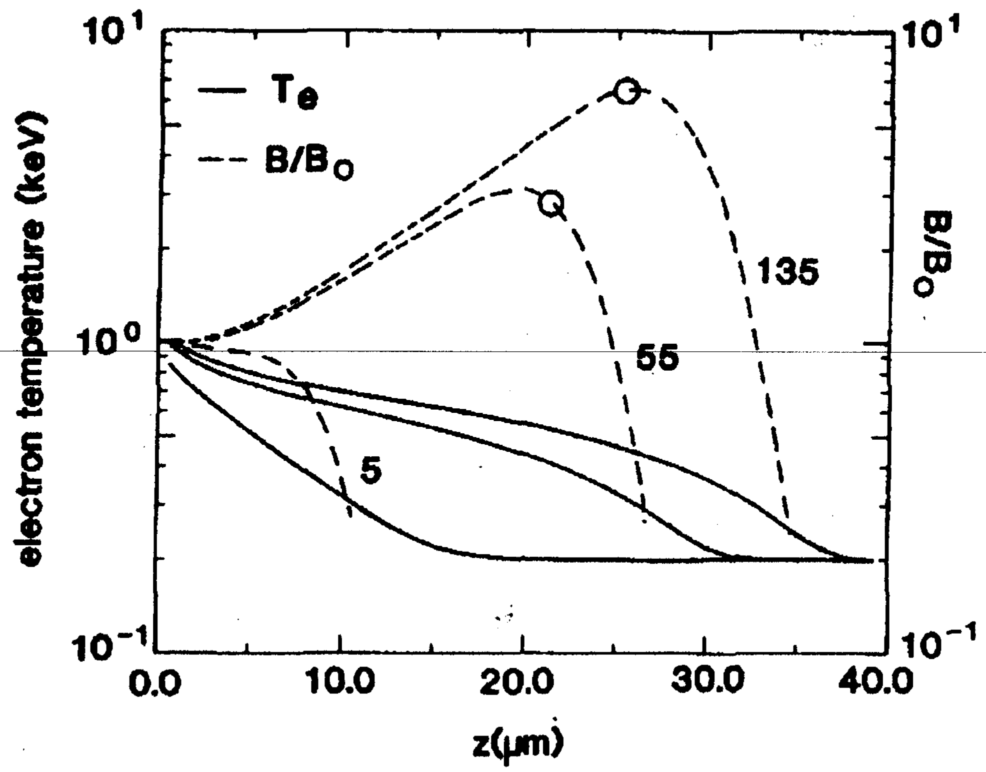

FIG. 2. Temperature T_e (solid lines) and magnetic field B/B_0 (dotted lines) at 5, 55, and 135 psec (from left to right). Circle on the B/B_0 curves indicate positions where $(\lambda_e/\lambda_s) = 1$.

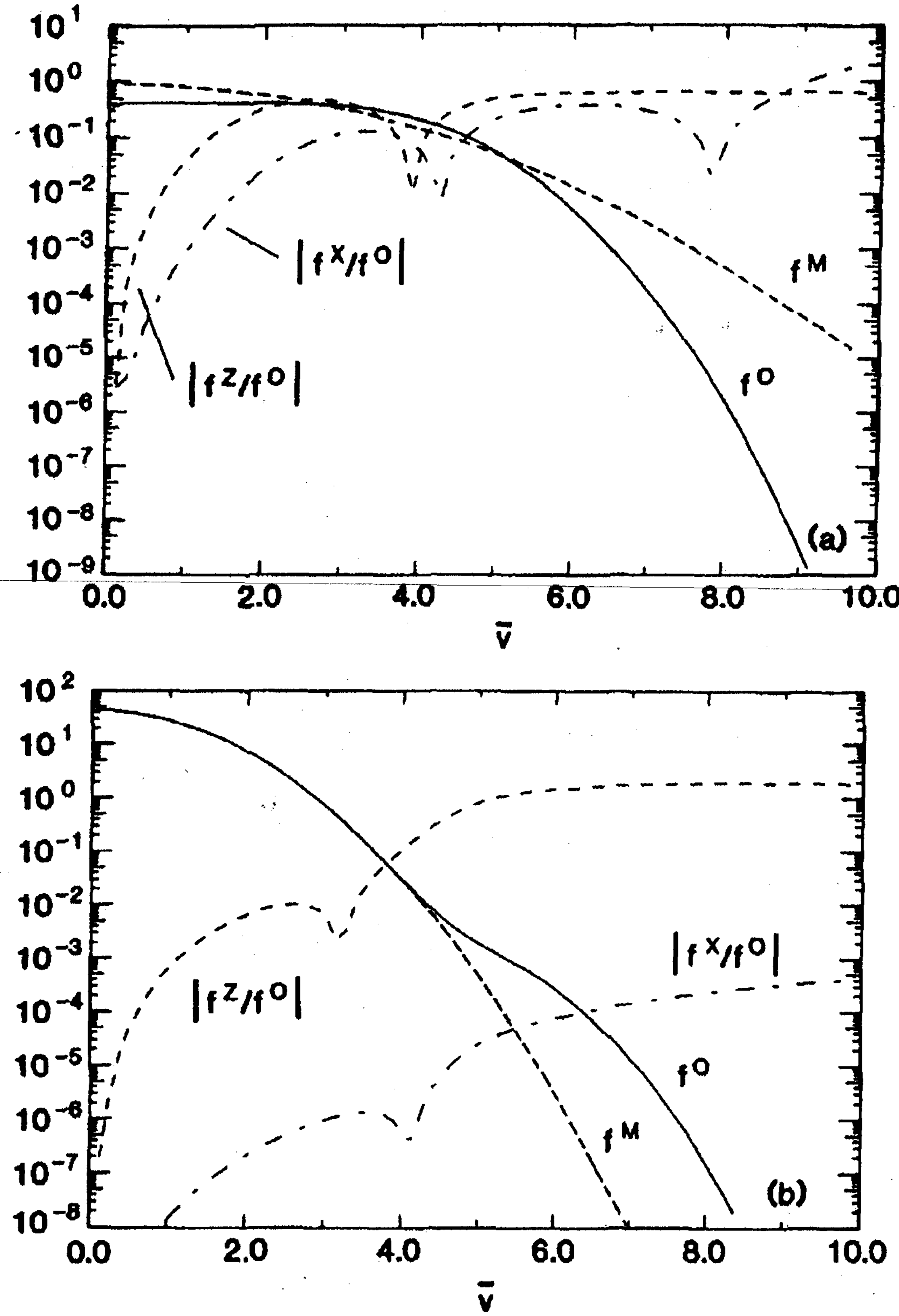

FIG. 4. The distribution functions at positions X and Y as indicated in Fig. 1, at 5 psec. Here f^m is the local Maxwellian and $\bar{v} = 10$ corresponds to a 10 keV electron.

TABLE I. Kinetic values of transport coefficients, normalized by their corresponding terms evaluated from linear transport theory, at various positions in the plasma at $t = 115$ psec.

z ($\times 1.3\,\mu$m)	λ_t/L_t ($\times 10^{-1}$)	$\omega\tau_t$ ($\times 10^{-1}$)	$\beta_\perp^{Tu}$	$\beta_\wedge^{Tu}$	$\alpha_\perp$	$\alpha_\wedge$	$\beta_\perp^{uT}$	$\beta_\wedge^{uT}$	$\chi_\perp$	$\chi_\wedge$
1	1.2	2.2	0.7	0.8	1.0	0.7	0.7	0.2	0.3	0.03
2	0.5	1.6	0.9	0.8	1.0	1.0	0.8	0.3	0.4	0.08
5	0.1	0.7	1.1	0.9	1.0	1.0	1.0	0.5	0.6	0.3
10	0.03	0.3	1.0	0.9	1.0	1.0	1.0	0.8	0.8	0.8
20	0.005	0.03	1.0	1.0	1.0	1.0	1.0	1.0	1.0	1.0

Results and conclusions

1. Nernst convection and amplification of B
2. Nernst velocity $\simeq \dfrac{q}{5/2\,p} \simeq V_T$ (see $\nu \propto \frac{1}{v^2}$ model)
3. Righi-Leduc heat flux severely limit (3%) close to critical surface due to depleted tail and $\omega\tau \sim 0.2 < 1$
   This is partly a result of the Langdon $f_0 \to e^{-v^5}$ tendancy

The collision frequency $\propto v^{-2}$ model

$$\frac{\partial \underline{f}_1}{\partial t} + v\nabla f_0 - \frac{e\underline{E}}{m}\partial_v f_0 - \frac{e\underline{B}}{m_e c}\times \underline{f}_1 = -\nu \underline{f}_1$$

Moments : $\underline{j} = -\frac{4\pi}{3} e \int_0^\infty dv\, v^3 \underline{f}_1$ current density

$\underline{q}_T = \frac{2\pi}{3} m_e \int_0^\infty dv\, v^5 \underline{f}_1$ total heat flux

For $\nu = \nu_T \frac{v_T^2}{v^2}$, $\times \frac{4\pi}{3} v^5$ and integrate

$$\frac{2m_e}{5ep_e}\frac{\partial \underline{q}_T}{\partial t} + \frac{m_e}{ep_e}\nabla R + \underline{E} + \frac{2}{5}\frac{\underline{q}_T \times \underline{B}}{p_e c} = \frac{2\nu_T m_e}{5e^2 n_e}\underline{j}$$

At $t=0$, $-\nabla\times\underline{E} = \frac{\partial \underline{B}}{\partial t} = \nabla\times\left[\frac{m_e \nabla R}{e p_e}\right]$

similar to Kingham and Bell , but here

$R = \frac{4\pi m_e}{15}\int_0^\infty f_0 v^6 dv$ and $p_e = \frac{4\pi}{3} m_e \int f_0 v^4 dv$

Note the Nernst convection of $\underline{B}$ by $\frac{q_{T\perp}}{5/2\, p_e}$

and the equation is true for any f_0.

If ν = constant

$$-\frac{m_e}{ne^2}\frac{\partial \underline{j}}{\partial t} + \frac{1}{ne}\nabla p_e + \underline{E} - \frac{\underline{j}\times\underline{B}}{n_e e c} = \frac{\underline{j}}{\sigma}$$

Compare term by term.

For a Maxwellian $\quad R = \dfrac{p_e^2}{n m_e}$

Also $\quad \underline{q}_T = \underline{q}_e + \dfrac{5}{4} \dfrac{m v_T^2}{e} \underline{j}$

$\dfrac{m_e}{e p_0} \nabla R$ term $\rightarrow \dfrac{\nabla p_e}{ne} + \dfrac{\nabla T}{e}$ $\qquad$ Note scalar β + η.

Comparison with Epperlein and Haines, $\nu \propto \frac{1}{v^3}$ and e-e collisions shows that new Ohm's law is good, especially for $Z = 3$

M.G. Haines, Plasma Phys. Controll. Fusion 28 (1986) 1705

Thomson Scattering Measurements of Heat Flow in a Laser-Produced Plasma

J. Hawreliak

Department of Physics, Clarendon Laboratory

Univerisity of Oxford

Oxford, OX1 3PU, UK

j.hawreliak@physics.ox.ac.uk

D.M. Chambers‡[2], S.H. Glenzer[3], A. Gouveia[1], R.J. Kingham[4], R.S. Marjoribanks[5], P.A. Pinto[2], O. Renner[6], P. Sondhauss[1], S. Topping[7], E. Wolfrum[1]†, P.E. Young[3], and J.S. Wark[1]

1. Department of Physics, Clarendon Laboratory, University of Oxford, Parks Road, Oxford, OX1 3PU, UK
2. Steward Observatory, University of Arizona, Tucson, AZ 85721, USA
3. Lawrence Livermore National Laboratory, Livermore, CA 94550, USA
4. Department of Physics, Blackett Laboratory, Imperial College of Science Technology and Medicine, London SW7 2BZ, UK
5. Department of Physics, McLennan Physical Laboratories, University of Toronto, Toronto, Ontario, M5S 1A7, Canada
6. Institute of Physics, Czech Academy of Sciences, 18221 Prague, Czech Republic
7. School of Mathematics and Physics, Queens University Belfast, Belfast, BT7 1NN, UK

Current Addreses : †Institut fuer Plasmaphysik, Max-Planck-Gesellschaft, D-85748, Garching, Munich,DE
‡Department of Physics, University of York, Heslington, york, YO10 5DD, UK

Outline of Talk

- Background
- Brief introduction to Thomson scattering
- Outline of experiment
- Experimental measurements
- Interpretation of results

History of thermal transport

(in three lines or less)

- Spitzer-Harm / Diffusive theory used to predict thermal transport - fails to model mass ablation rate experiments - introduction of a flux limiter†
- Fokker-Planck modeling shows that non-local effects are important in steep temperature gradients *
- **No *direct* experimental confirmation of FP techniques**

†D.R. Gray and J.D. Kilkenny, Plasma Phys. **22**, 81 (1980)

*A.R. Bell, R.G. Evans, and D.J. Nicholas, Phys. Rev. Let. **51**, 1664 (1983)

Thomson Scattering

- The scattering of electromagnetic radiation from free electrons

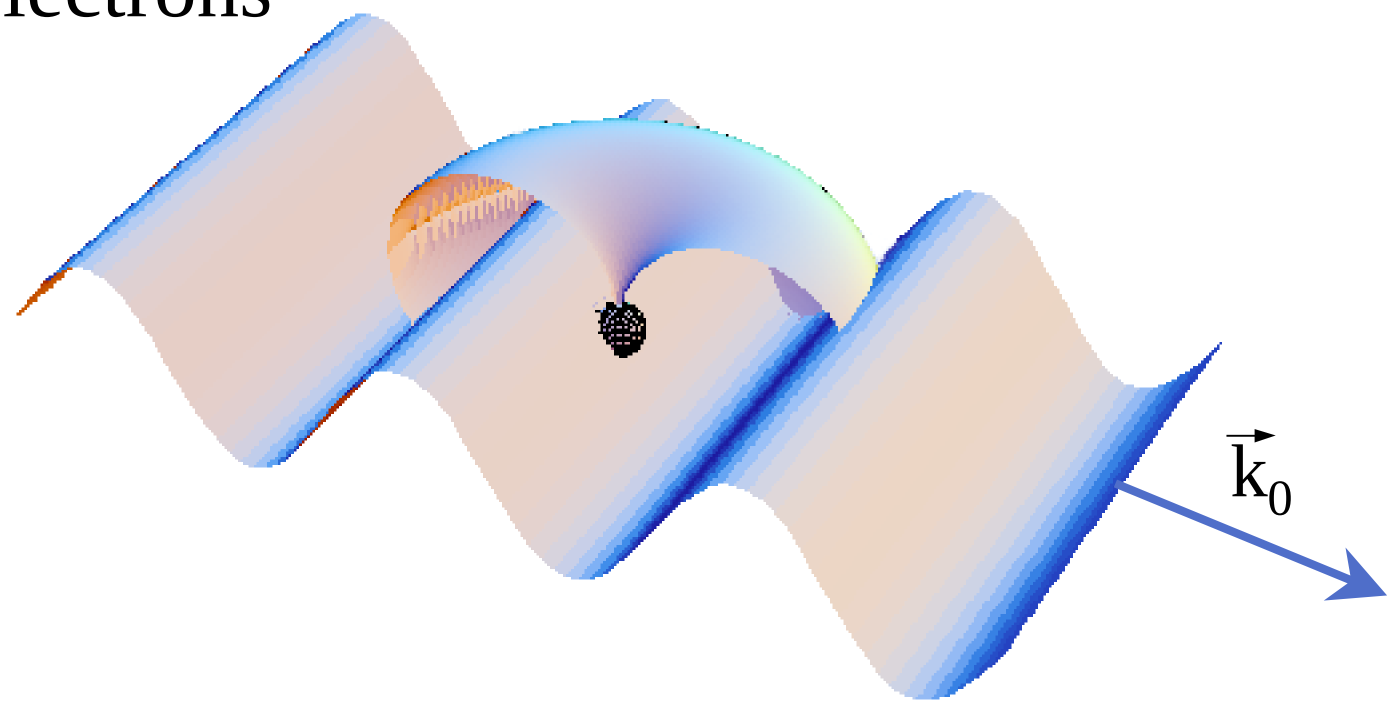

Thomson Scattering from Plasmas (Non-Collective)

- If the plasma density is low or the wavelength is short ($\lambda_0 < \lambda_D$) the scattering will be the sum of the Doppler shifted frequencies of the electrons

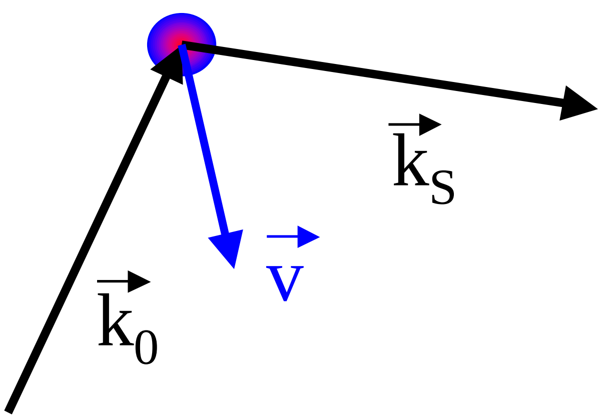

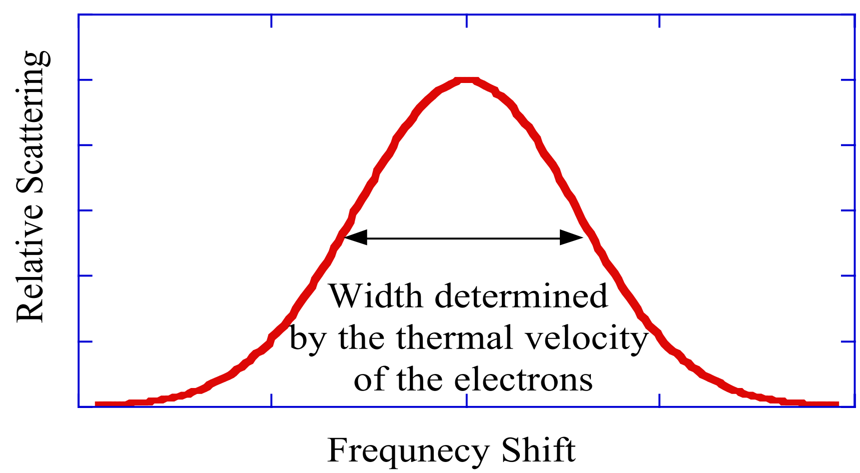

Thomson Scattering from a Laser-Produced Plasma (Collective scattering)

- For long wavelength probes and higher densities plasmas the correlation of the electron motion will cause enhanced scattering from plasma wave fluctuations

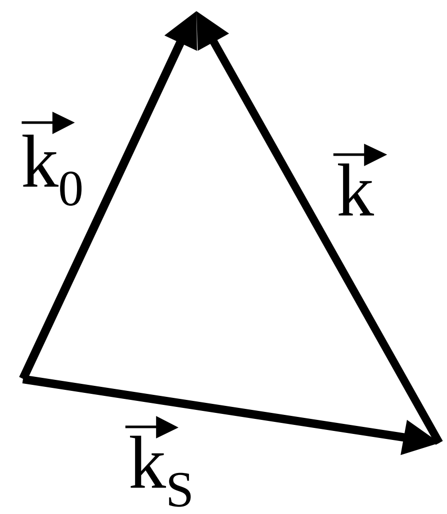

$$\vec{k} = \vec{k}_0 - \vec{k}_S$$

Thomson Scattering from Plasma Wave Fluctuations

Electron Feature:

Scattering from Langmir waves

$$\left(\frac{\omega}{k}\right)^2 = \left(\frac{\omega_e}{k}\right)^2 + 3v_e^2$$

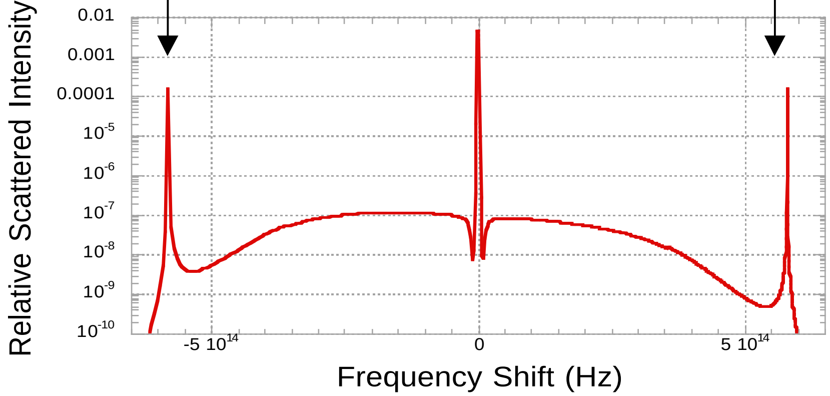

Ion Feature:

Scattering from Ion acoustic waves

$$\left(\frac{\omega}{k}\right)^2 = \frac{Z\,T_e/m_i}{1+k^2\lambda_D} + \frac{3T_i}{m_i}$$

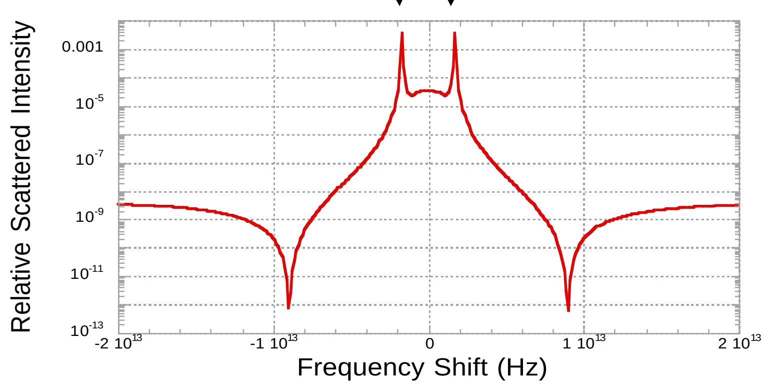

NOTE: We scattered from the ion feature

Experimental Setup

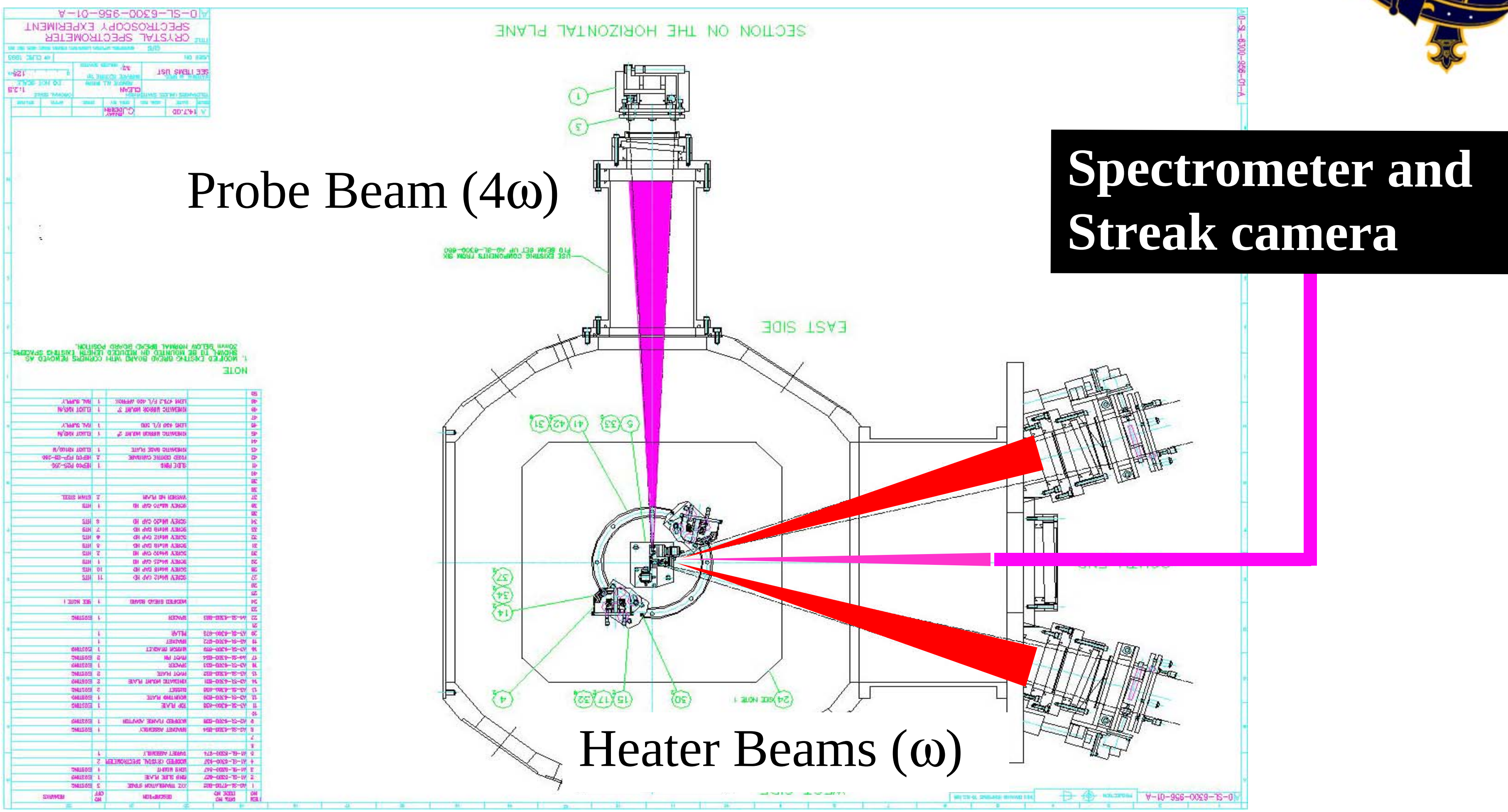

Target Geometry

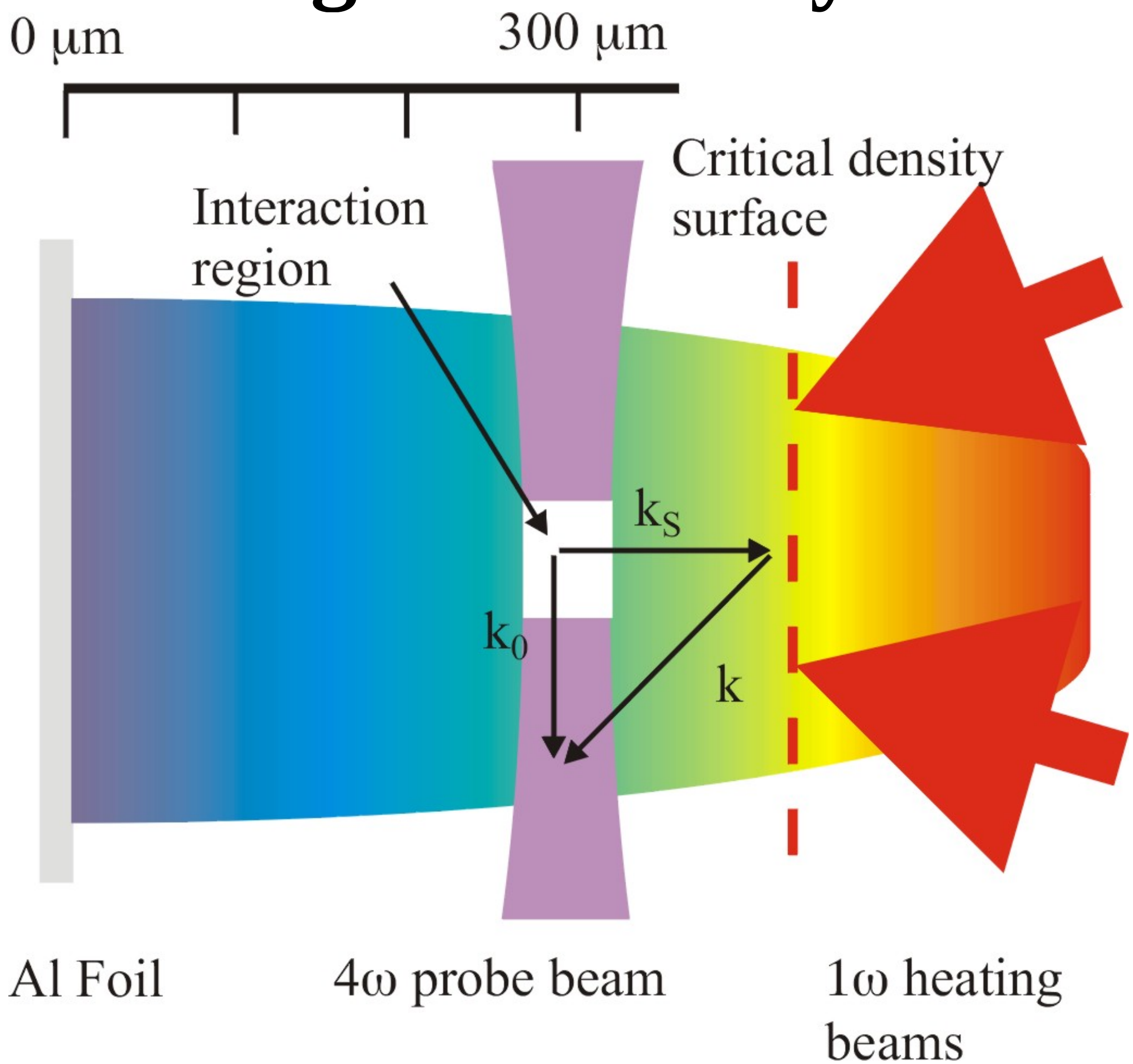

Why 4ω Probe Beam?

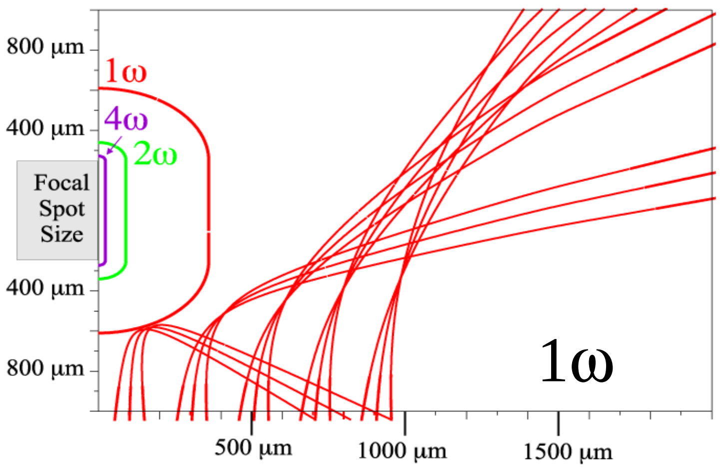

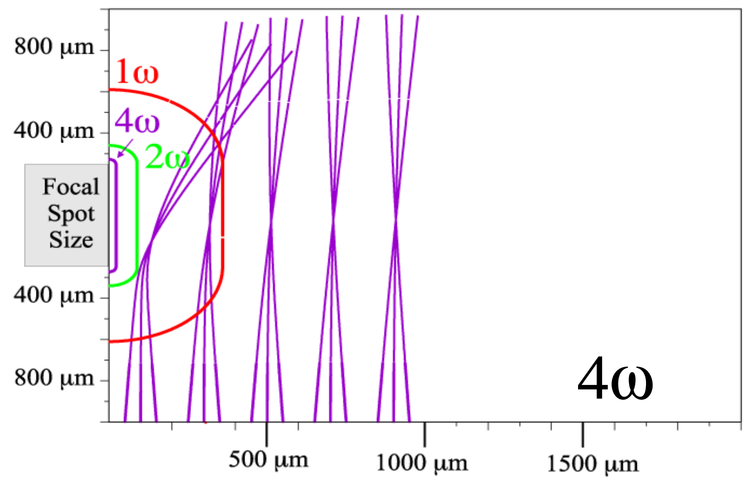

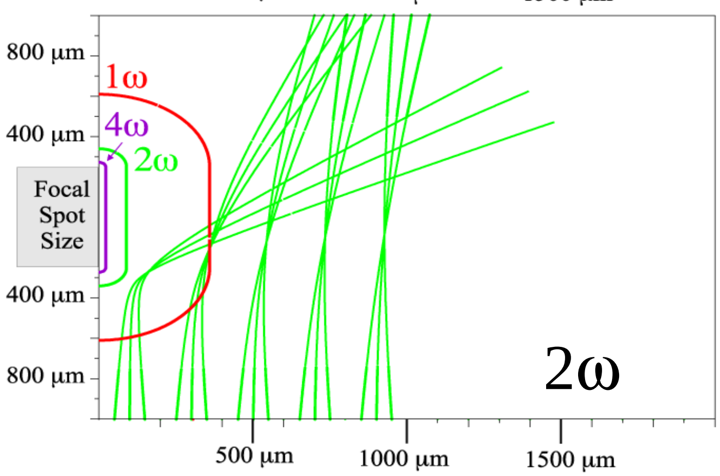

Using a 4 probe beam allows reliable probing behind the critical surface (at 300μm) but not closer then 200μm

Experimental Measurement

Separation of peaks give electron temperature

Doppler shifted centre of the peaks give velocity

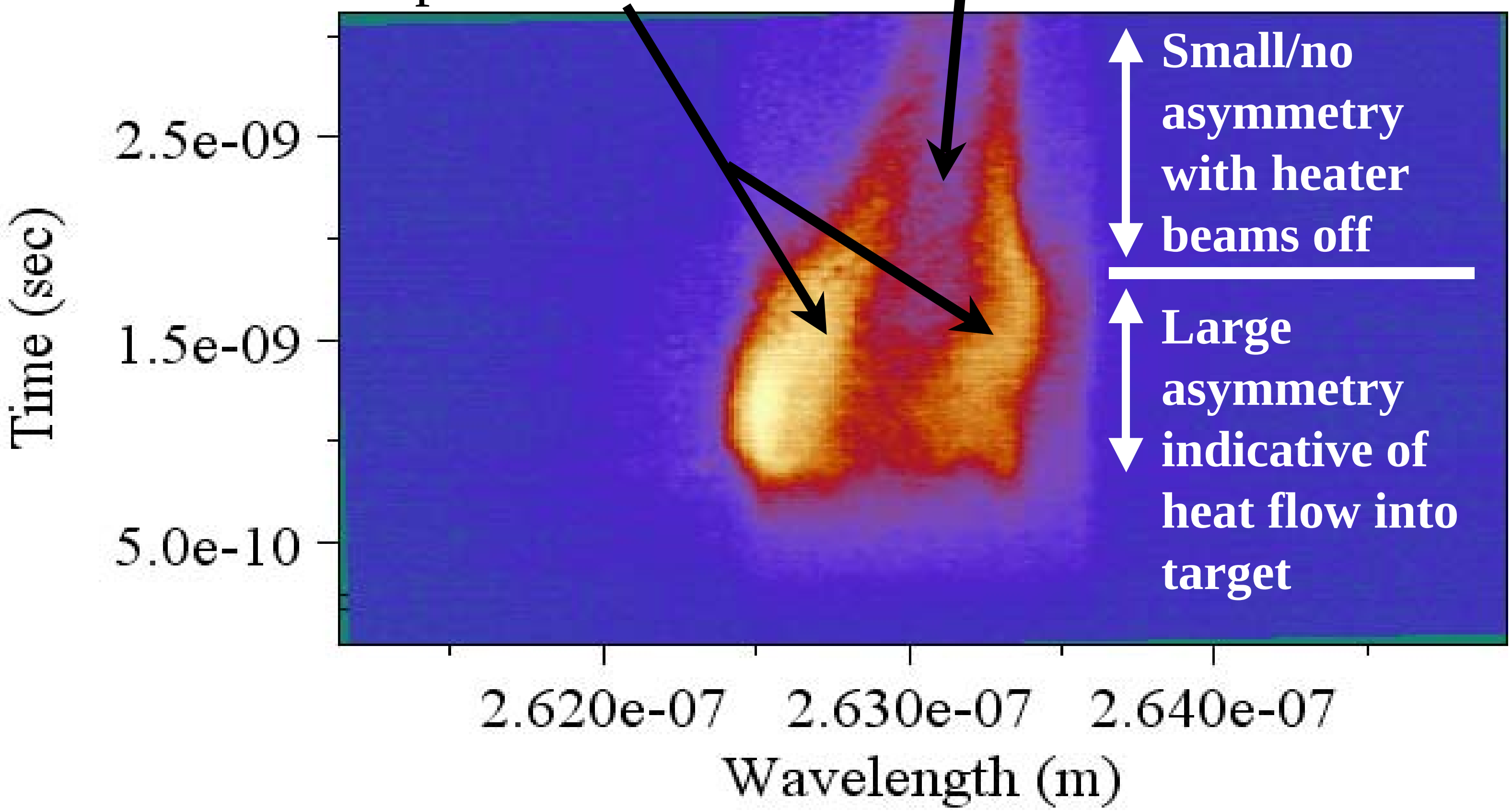

Density Measurement

- Without measuring the electron feature the mass ablation rate will give a measurement of density

$$\rho_M v = (0.87 \pm 0.06) \times 10^5 \left(\frac{I_0}{10^{13} \frac{W}{cm^2}} \right)^{0.21 \pm 0.02} \quad \frac{g}{cm^2 \sec} \qquad *$$

- With a velocity measurement of ±4%, a beam intensity of ±10%, using the above equation at 300μm we get a density of $10^{21} cm^{-3}$ ±20%

* M.H. Key, W.T. Toner, T.J. Goldsack, J.D. Kilkenny, S.A. Veats, P.F. Cunningham, and C.L.S.Lewis, Phys. Fluids **26**,2011,(1983)

Heat Flux Measurement

- Heat flux can be measured behind the critical density surface by using a basic energy balance, energy can only be carried through thermal transport to the target surface.

$$Q = \rho v \left[\frac{5}{2} \left(\frac{Z+1}{A_{mp}} \right) kT + \frac{1}{2} v^2 \right] \qquad *$$

- Where the temperature and velocity are taken from the Thomson scattering data. Using the above equation at 300μm (which has been determined to be behind the critical density surface) we get a heat flux of $6 \times 10^{13} \pm 20\%$ W/cm^2
- Good agreement with energy balance equations (~ 40% absorbed 1/2 which is transported to target, 1/2 needed to maintain plasma corona)

*R. Fabbro, C. Max, and E. Fabre, Phys. Fluids 28,1463 (1985)

Thomson Scattering Cross Section

- The scattering cross section for an electron in a plasma $\sigma(k,\omega) = \sigma_T S(k,\omega)$

$$S(\vec{k},\omega) = \left| \frac{1 - G_i(\omega/k)}{1 - G_e(\omega/k) - G_i(\omega/k)} \right|^2 f_{0e}(\omega/k) \qquad *$$

$$+ Z \left| \frac{G_e(\omega/k)}{1 - G_e(\omega/k) - G_i(\omega/k)} \right|^2 f_{0i}(\omega/k)$$

- $S(k,\omega)$ is the dynamic form factor, which incorporates the motion and collective affects of the plasma

* D.E. Evans and J. Katzenstein, Reports On Progress Phys. **32**, 207 (1969)

Asymmetric Scattering Peaks

$$G_s(\vec{v}_0) = \frac{4\pi Z_s^2 e^2}{m_s k^2} \int \frac{\vec{k} \cdot \vec{\nabla}_v f_{0s}(\vec{v})}{\vec{k} \cdot (\vec{v} - \vec{v}_0)} d\vec{v} \qquad *$$

- $G_s(v_0)$ is the screening integral in the plasma
- Scattering resonances when $\Re\{1\text{-}G_e\text{-}G_i\}=0$, so S(k,) will depend on the velocity gradient of the distribution function along the direction of the scattering vector, k, at the phase velocity of the wave.

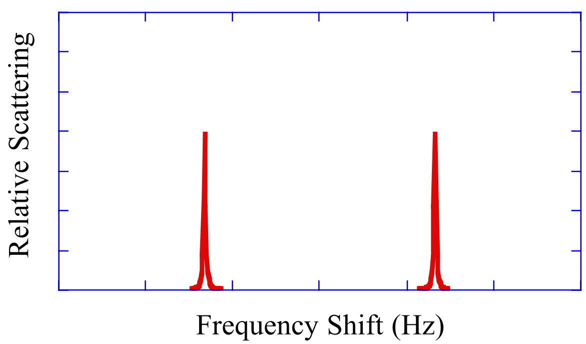

Symmetric distribution

Asymmetric distribution

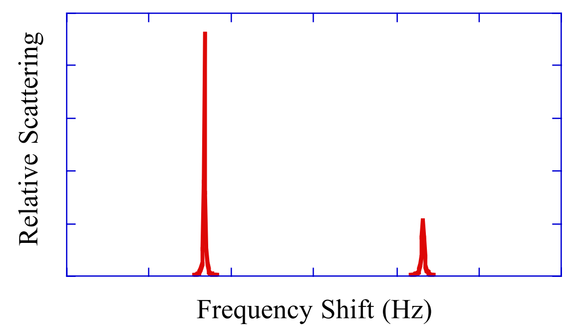

* D.E. Evans and J. Katzenstein, Reports On Progress Phys. **32**, 207 (1969)

A measurement of the distribution function

- The asymmetry in the Thomson scattering peaks gives information about the difference in the reduced distribution function* at the phase velocity of the ion acoustic waves

$$^{*} \quad f(v) = \int f(\vec{v})\,d\vec{v}_{\perp}$$

Generating simulated Thomson scattering images

- Developed Thomson scattering program that numerically solves the screening integrals
- To model experimental geometry where the probe is 45° to the direction of heat flow transform cylindrically symmetric results

$$f(v_z) = \int_0^{\pi/2+\psi} d\theta \left\{ 2 \int_0^{\cos^{-1}(\cot\psi\cot\theta)} d\phi \left[f(v_r,\theta,\phi) \frac{v_z^{\,2}\sin(\theta)}{(\cos\psi\cos\theta+\sin\psi\sin\theta\cos\phi)^3} \right] \right\}$$

$$v_r = \frac{v_z}{\cos\psi\cos\theta+\sin\psi\sin\theta\cos\phi}$$

where ψ is the angle between the direction of heat flow and the scattering vector **k**

Heat Transport Models

- “Classical” Spitzer-Harm heat transport model
  - Transport depends on local quantities
  - Conductivity $\propto (kT)^{5/2}$
  - Distribution taken from numerical results in

    L.J. Spitzer and R. Harm, Phys. Rev. **89**, 977 (1953)
- Fokker-Planck
  - IMPACT as outlined in

    R.J. Kingham and A.R. Bell, Phys. Rev. Let. **88,** 045004/1 (2002)

Using experimentally measured parameters to generate simulated scattered spectrum

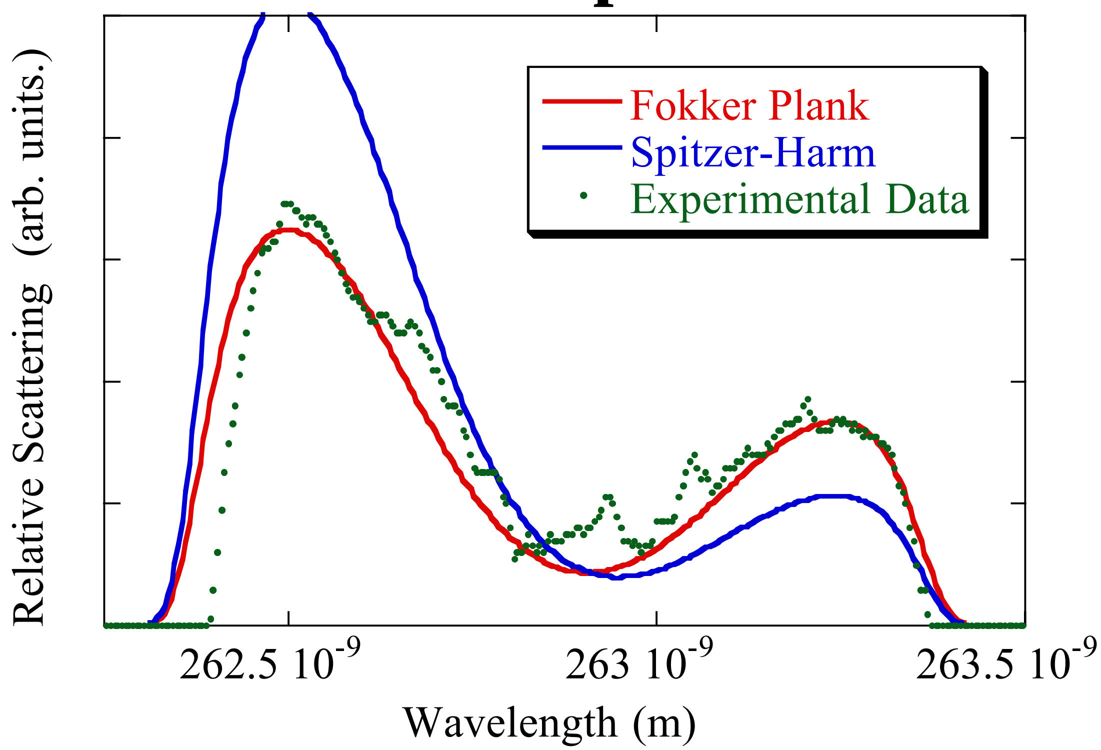

From experimentally measured parameters

$$\frac{L}{\lambda_e} = \frac{T}{\lambda_e}\left(\frac{dT}{dx}\right)^{-1} = 10 \rightarrow 100$$

Within the error bars of the measured temperature gradient

Fokker Plank

- T_e = 1850 eV
- T_i = 960 eV
- n_e = 1 x10^{21}cm^{-3}
- Z = 13.0
- Q = 5.5 x10^{17} W/m^2

☺ ∇T_e = 7 eV/μm
☺ L/λ_e = 17
☺ Asymmetry = 2

Spitzer-Harm

- T_e = 1850 eV
- T_i = 960 eV
- n_e = 1 x10^{21}cm^{-3}
- Z = 13.0
- Q = 5.5 x10^{17} W/m^2

☺ ∇T_e = 3 eV/μm
☺ L/λ_e = 40
☹ Asymmetry = 4

Can Spitzer-Harm fit?

- All the of parameters used to derive the distribution function for both thermal transport models are consistent with experimental measurements (the temperature gradient was calculated from the models for the experimentally measured heat flux).
- To get a SH spectrum to match the experiment requires a temperature gradient of less then **2 eV/μm** and **Q = 3 x10^{17} W/m^2** which **cannot** maintain the energy balance.

Difference between Fokker-Plank and Spitzer-Harm Distributions for experimental conditions at 300 μm both carrying the same heat flux

f_{total} - showing why non-collective scattering would not resolve difference

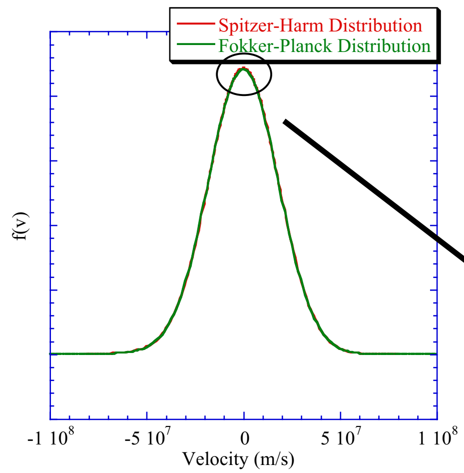

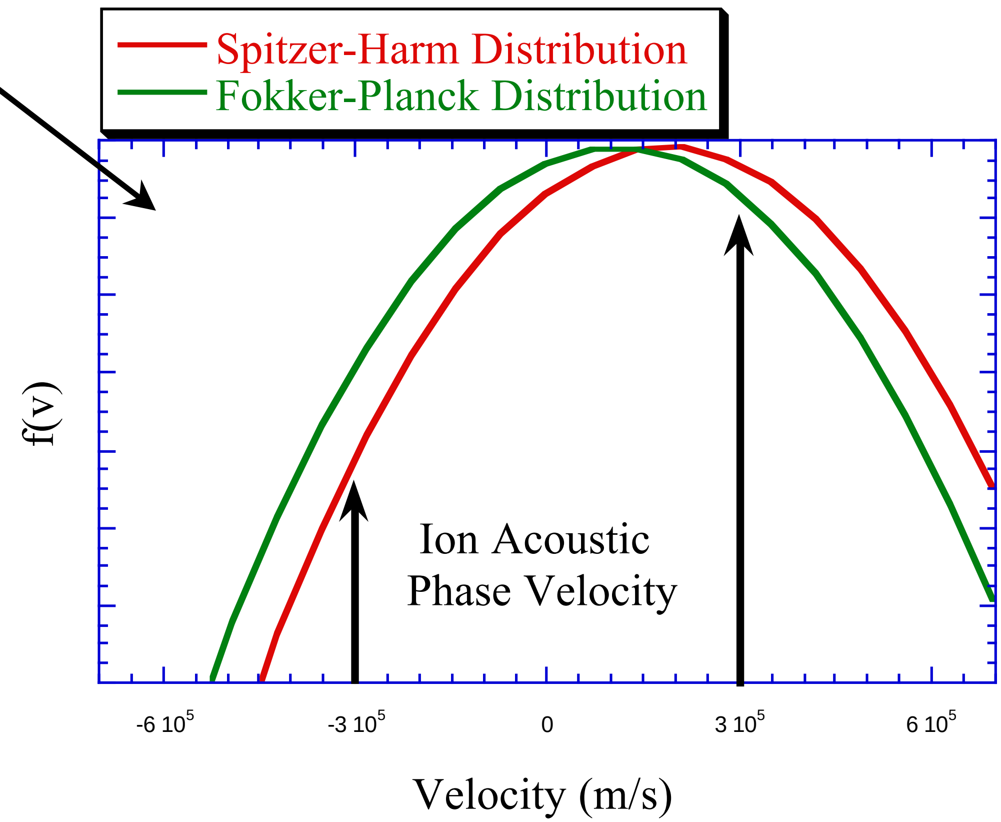

f_1 terms of the reduced distribution functions

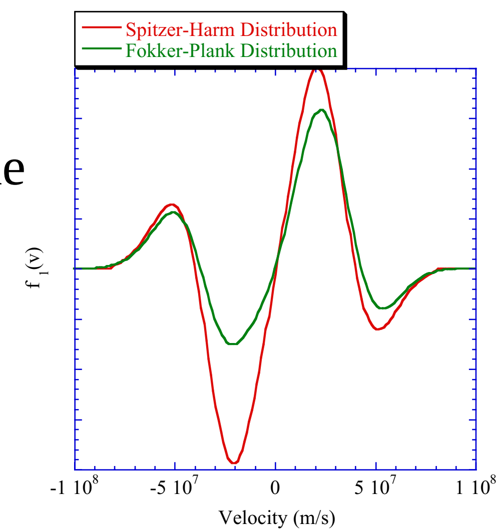

Definition: Asymmetry Measurement

- The asymmetry in the ion features give us a tool for studying the distribution function

$$Asymmetry = \frac{\int_{Blue} Scattering}{\int_{Red} Scattering}$$

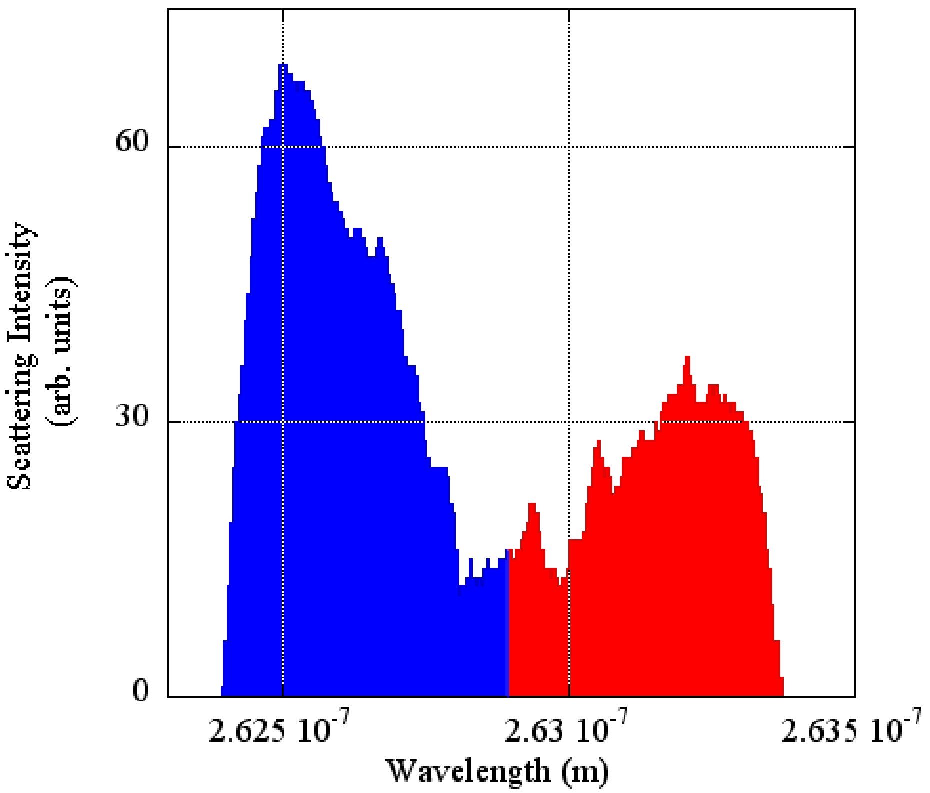

Asymmetry as a function of distance from target surface

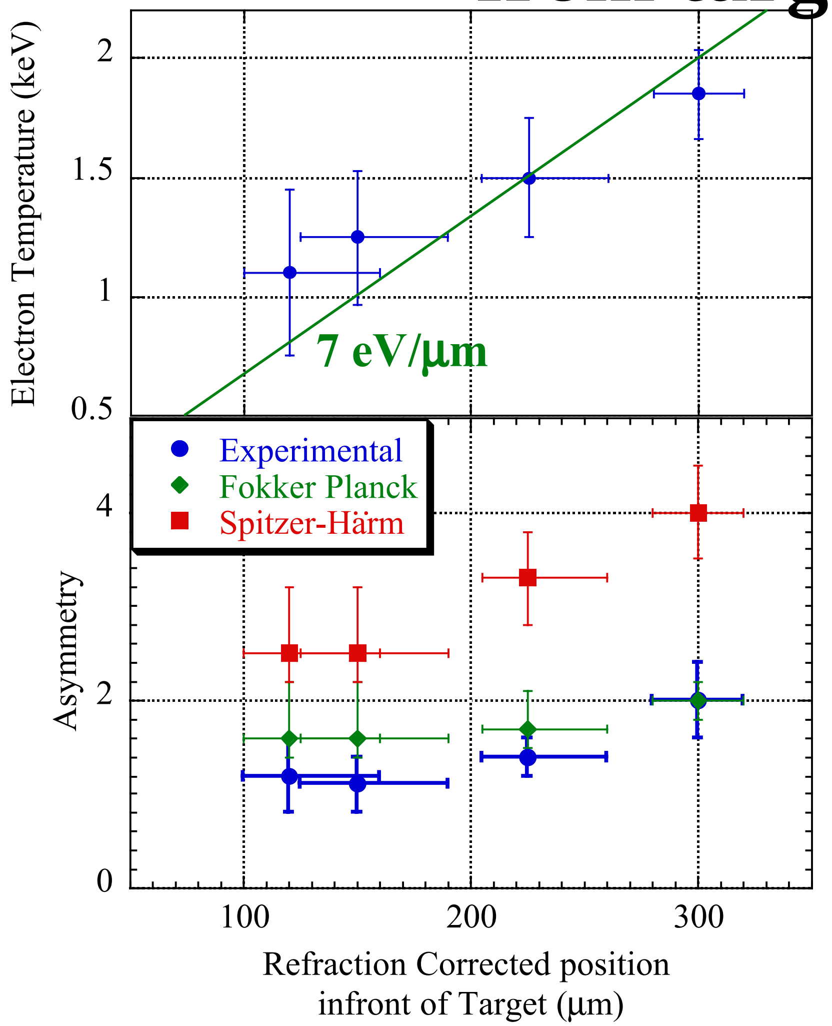

- The Fokker-Planck matches experimental measurement of the asymmetry in the Thomson scattering peaks and is consistent with the measured temperature gradient.
- Spitzer-Harm does not

Conclusions

- ✓The first direct measurement of heat flux behind the critical density surface
- ✓Confirmation of Fokker-Planck modeling techniques
- ✓Diagnostic tool for looking at the changes in the electron distribution function due to heat flux

Fokker-Planck Modelling of Non-local Magnetic Field Generation in Collisional Plasmas

R. J. Kingham and A. R. Bell

Plasma Physics Group, Imperial College, London

LLNL Electron Transport Workshop, Purple Orchid Inn,
Livermore 9th – 11th September 2002

Outline of Talk

- Goal:
  - Know importance of non-local effects for heat flow…
  - What role do non-local effects play in **B**-field generation?
  - B-field generation in regime where Braginskii & Spitzer not valid

- Overview of B-field gen. in collisional plasmas
- Description of IMPACT: 2D electron Fokker-Planck code with self-consistent B-field
- FP sim. $\rightarrow$ non-local B-field generation when $\nabla n_e = 0$ & non-uniform heating
- Basic explanation of non-local B-field mechanism
- FP sim. $\rightarrow$ non-local B-field generation when $\nabla Z \neq 0$ & uniform heating
- Analytical formula for non-local, seed B-field from T_e perturbation
- FP sim. $\rightarrow$ heating in a density gradient & comparison with classical case

Blackett Laboratory
Imperial College

Standard B-field Sources Need $\nabla n \neq 0$ or $\Pi \neq 0$

- Standard collisional B-field source…

$$\boxed{\dot{B} = -\frac{1}{n}\{\nabla n \times \nabla T\}}$$

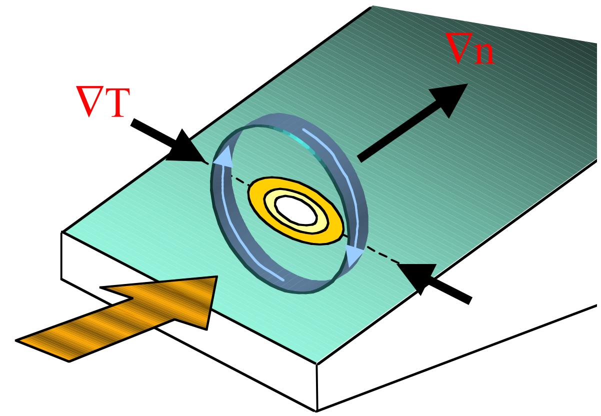

- Originates from "generalized Ohms law" and "Faradays law"

$$\boxed{\nabla \times \boldsymbol{E} = -\dot{\boldsymbol{B}}} \quad \text{and} \quad \boxed{|e| n_e \boldsymbol{E} = -\nabla P_e} - \nabla \cdot \underline{\underline{\boldsymbol{D}}}_e + \boldsymbol{j} \times \boldsymbol{B} + |e| n_e \underline{\underline{\boldsymbol{\alpha}}} \cdot \boldsymbol{j} - n_e \underline{\underline{\boldsymbol{\beta}}}$$

Scalar pressure — Stress tensor — Hall — resistivity — thermoelec

- Ohms' Law, itself, is obtained from the Fokker-Planck equation…

$$\left[\frac{\partial}{\partial t} + \mathrm{v} \cdot \nabla_r + \frac{q}{m_e}(\boldsymbol{E} + \mathrm{v} \times \boldsymbol{B}) \cdot \nabla_{\mathrm{v}}\right] f(\boldsymbol{r}, \mathrm{v}, t) = -\nabla_{\mathrm{v}} \cdot \{f \langle \Delta \mathrm{v} \rangle\} + \nabla_{\mathrm{v}} \nabla_{\mathrm{v}} : \{f \langle \Delta \mathrm{v} \Delta \mathrm{v} \rangle\}$$

Collisional drag — Collisional diffusion

Ohm's Law $\leftarrow$ Moment of FP Equation

- Collisions smooth out fine detail in velocity space…

$$f(\underline{r},\underline{v},t) = \underset{\substack{\text{scalar}\\ n,\,T}}{f_0(\underline{r},v,t)} + \underset{\substack{\text{vector}\\ j,\,q}}{\hat{\underline{v}}\cdot \underline{f}_1(\underline{r},v,t)} + \underset{\substack{\text{tensor (2}^{nd}\text{ order)}\\ \underline{\underline{P}},\text{ viscosity}}}{\hat{\underline{v}}\hat{\underline{v}} : \underline{\underline{f}}_2(\underline{r},v,t)} + \ldots$$

- **Ohm's law:** moment of $\underline{f}_1$ eqn. + Say $f_0 = f_m$ (local transport theory)

- **Local transport theory:** valid $\lambda_{ei} \ll L$, $\tau_{ee} \ll \tau$ (also $r_g \ll L_\perp$ if $\omega\tau \gg 1$)

- The $\int d^3v$ moment of the FP equation…

$$\frac{\partial f_0}{\partial t} + \underset{\nabla.q}{\frac{v}{3}\nabla\cdot \boldsymbol{f}_1} - \underset{\text{Ohmic heating}}{\frac{e}{m_e}\frac{1}{3v^2}\frac{\partial\left(v^2 \boldsymbol{E}\cdot \boldsymbol{f}_1\right)}{\partial v}} = \underset{\substack{\text{e-e collisions}\\ \text{relax. to Maxwellian}}}{\frac{\nu_{ee}}{v^2}\frac{\partial}{\partial v}\left[C f_0 + D\frac{\partial f_0}{\partial v}\right]}$$

- The $\int \underline{v} d^3v$ moment of the FP equation… (momentum balance)

$$\underset{\text{elec. inertia}}{\frac{\partial f_1}{\partial t}} + \underset{\nabla P}{v\nabla f_0} + \underset{\text{stress}}{\frac{2}{5}\nabla\cdot \underline{\underline{f_2}}} - \underset{\text{accn. by E}}{\frac{eE}{m_e}\frac{\partial f_0}{\partial v} - \frac{2e}{5m_e v^3}\frac{\partial}{\partial v}\left(E\cdot \underline{\underline{f_2}}\right)} - \underset{\text{rotation by B}}{\frac{e}{m_e}B\times f_1} = \underset{\substack{\text{e-i collisions}\\ \text{angular scatter}}}{-\nu_{ei} f_1} + \left(\frac{\delta f_1}{\delta t}\right)_{ee}$$

- **IMPACT** $\rightarrow$ **Implicit Magnetised Plasma And Collisional Transport**
- **Solves f_o & f_1 FP equations for e^- self consistently with Maxwell's equations in 2D**
- **Obtain evolution of . . .**
  - $\rightarrow$ $f_o(x, y, v)$ *Isotropic part of e^- dist. (defines T,n, scalar p)*
  - $\rightarrow$ $f_x(x, y, v)$, $f_y(x, y, v)$ *vector part of e^- dist. (defines* **j**,**q***)*
  - $\rightarrow$ $E_x(x, y)$, $E_y(x, y)$, $B_z(x, y)$ *macroscopic fields*
- **Geometry: 2D Cartesian grid (x & y)**
- **Periodic, reflective and fixed BC's independently in x and y**
- **e-e collisions $\rightarrow$ relax. of f_o to Maxwellian**
- **e-i collisions $\rightarrow$ angular scattering of e^-**
- **Ignore e-e collisions in f_1 eqn. $\rightarrow$ Lorentz approx. (valid at high Z)**
- **Keep $\partial \mathrm{f}_1/\partial t$ term in f_1 eqn. (electron inertia term)**
- **Configurable ion and Z profiles (non-evolving)**
- **No displacement current $\rightarrow$ $\nabla \times \mathbf{B} = \mu_o \mathbf{j}$**
  - $\rightarrow$ *Valid for overdense plasmas*
  - $\rightarrow$ *Plasma can maintain quasineutrality*
- **E, f_o, f_1 are solved implicitly**
  - $\rightarrow$ *numerical stability + large "dt" possible*
- **Change-Cooper differencing scheme used for e-e collision term**
  - $\rightarrow$ *Ensures exact relaxation to a Maxwellian*

The f_1 equation

- **Finite difference form for the r^{th} component of the $\mathbf{f}_1$ equation at location $\mathbf{r}^b_{i,j}$, where $b = \{X, Y\}$ denotes the cell boundary**

$$(f^b_r)^{n+1}_{i,j,k} = \left[\chi^n_k \sum_{q=\{x,y\}} \left(\delta_{rq} + \epsilon_{rzq}\, \omega^{b,n}_{i,j}\, \tau'_k \right) \left\{ -v_k\, (\nabla_q\, f_o)^{n+1}_k + E^{n+1}_q\, (\partial_v\, f_o)^{n*}_k + (f_q)^n_k / \Delta t \right\} \right]^b_{i,j} \quad , \tag{1}$$

$$\chi^{b,n}_{i,j,k} = \frac{\tau'_k}{1 + (\omega^{b,n}_{i,j}\, \tau'_k)^2} \quad , \quad \tau'_k = \left[\frac{1}{\Delta t} + \frac{1}{\tau(v_k)} \right]^{-1} \quad , \tag{2}$$

$$\begin{aligned} \omega^X_{i,j} &= \omega_{i+1/2,j} = (1 - \mu_{i+1/2})\, \omega_{i+1,j} + \mu_{i+1/2}\, \omega_{i,j} \quad , \\ \omega^Y_{i,j} &= \omega_{i,j+1/2} = (1 - \mu_{j+1/2})\, \omega_{i,j+1} + \mu_{j+1/2}\, \omega_{i,j} \end{aligned} \tag{3}$$

2D-FP Simulations With Heating and $\nabla n=0$

- System & heating profile…

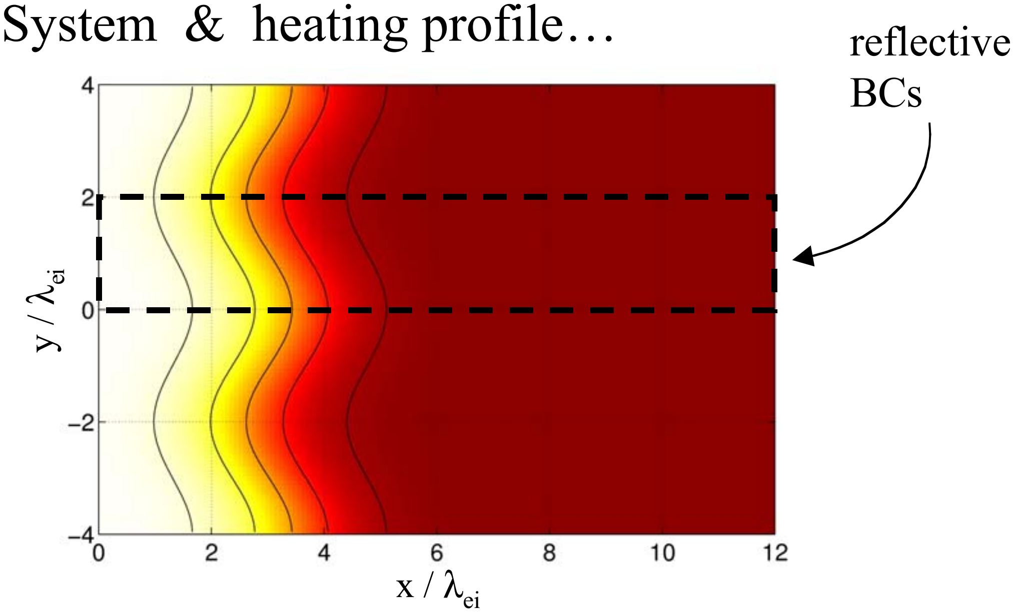

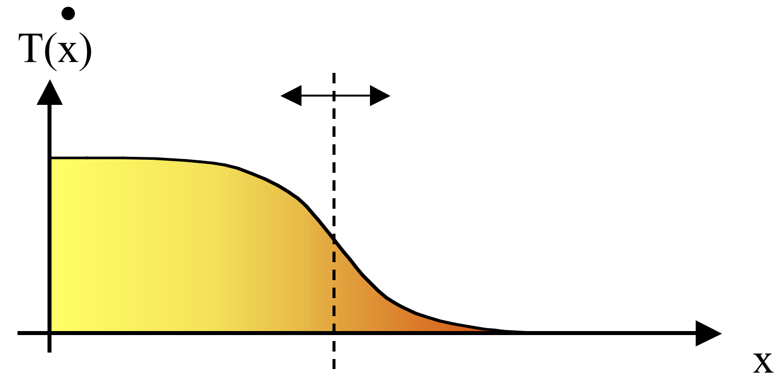

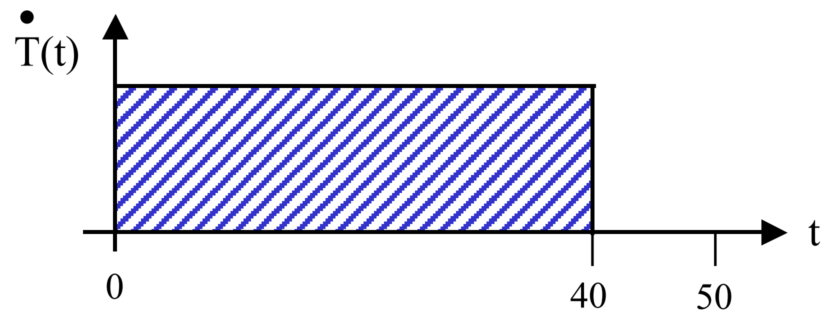

- Parameters…

$Z = 10$

$\dfrac{\lambda_{ie}}{\delta_c} = 100$

Solid: $T_{eo} = 11$ keV, $n_{eo} = 3 \times 10^{23}$ cm^{-3} } $\lambda_{ei} = 1\mu$m, $\tau_{ei} = 16$ fs, $\ln \Lambda_{ei} = 6.3$

$10 \times n_{cr}$: $T_{eo} = 5$ keV, $n_{eo} = 11 \times 10^{21}$ cm^{-3} } $\lambda_{ei} = 5\mu$m, $\tau_{ei} = 0.12$ ps, $\ln \Lambda_{ei} = 7.2$

B-field grows to $\omega\tau>1$ even though $\nabla n=0$

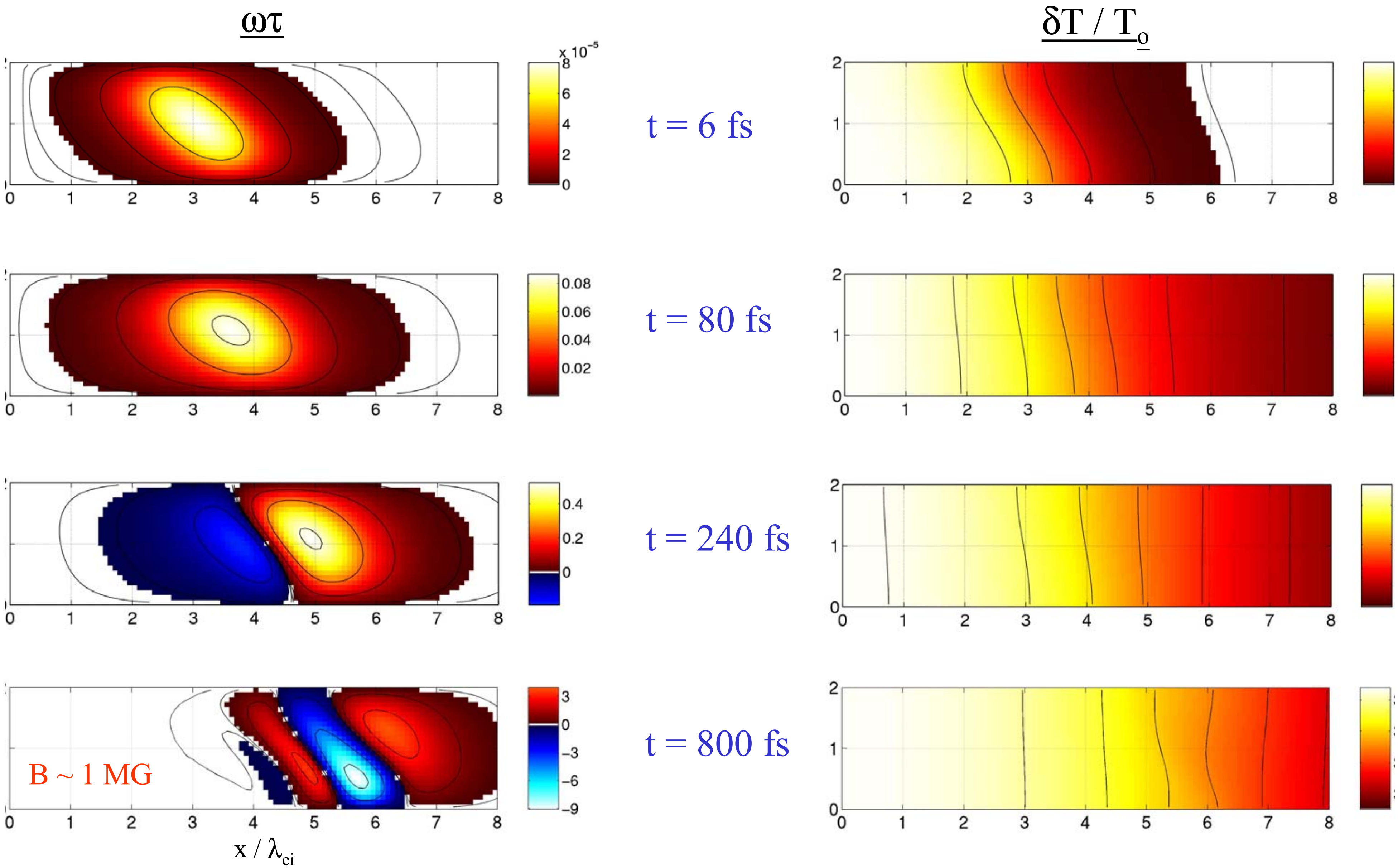

Heat Flow Direction Affected by B-field

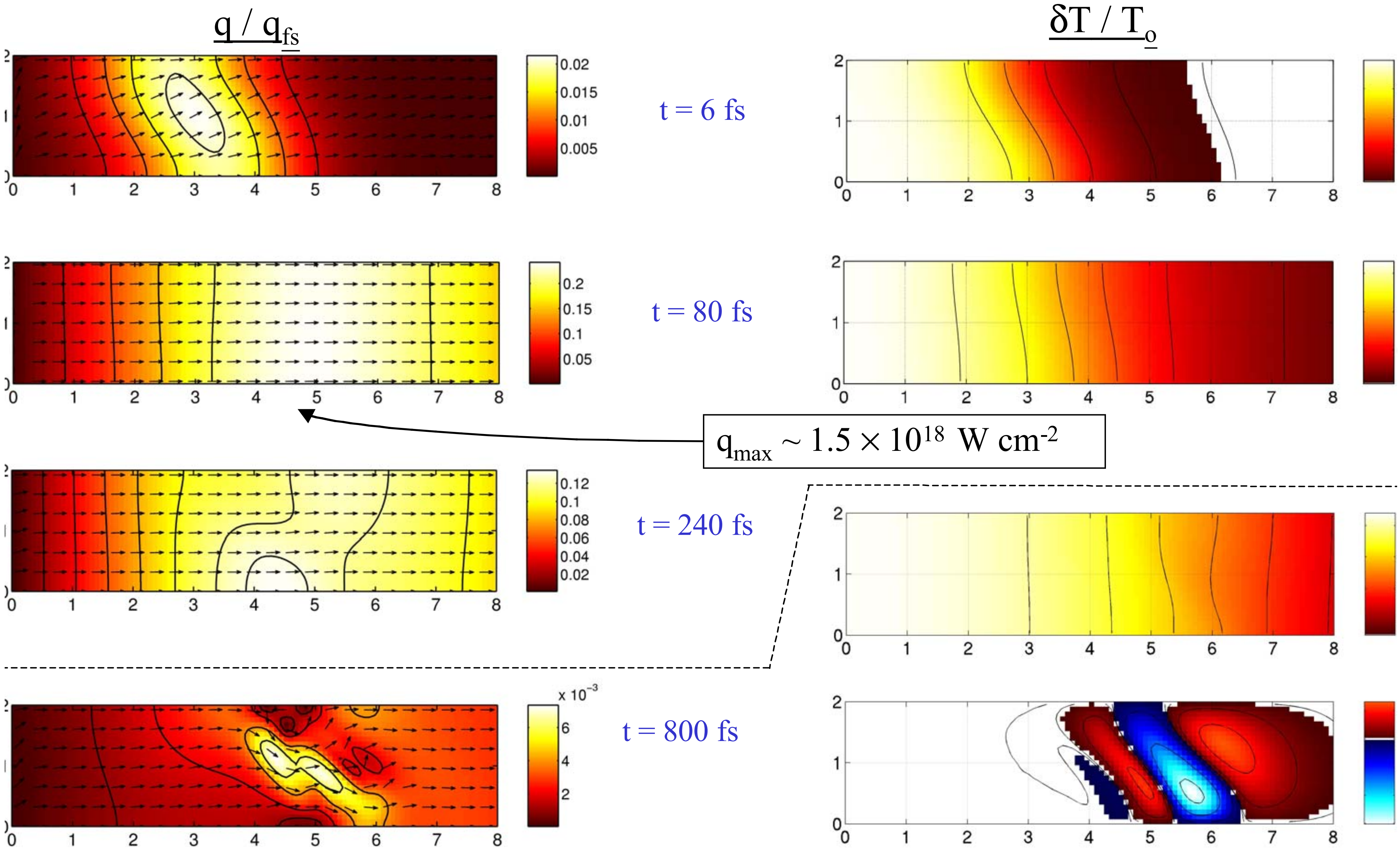

Zoom of Heat Flow After 800fs

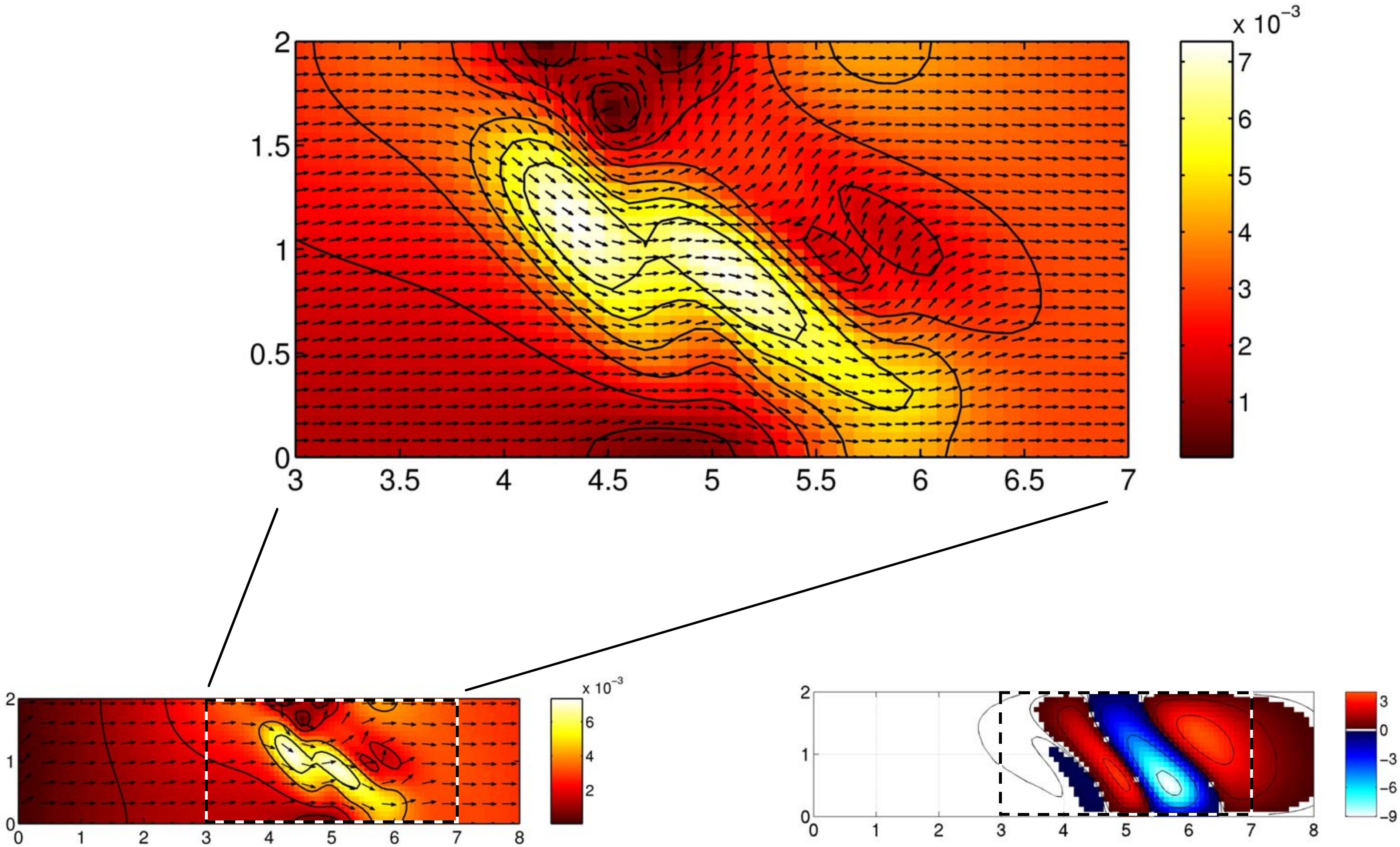

Sign of B-field Alternates Along Ripple

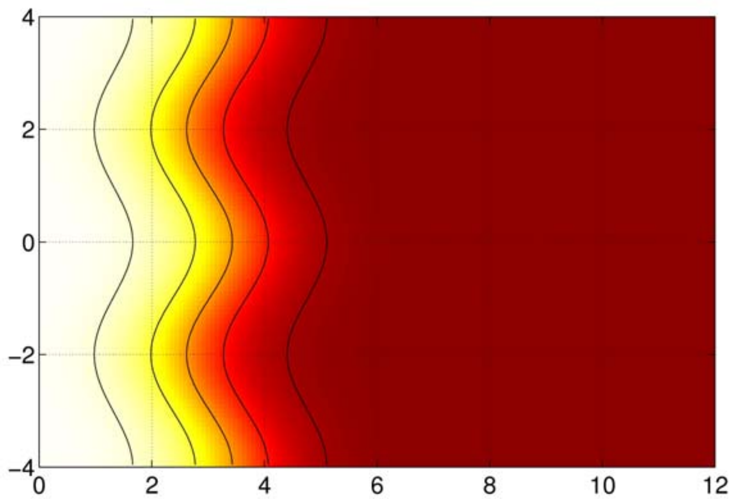

t = 240 fs

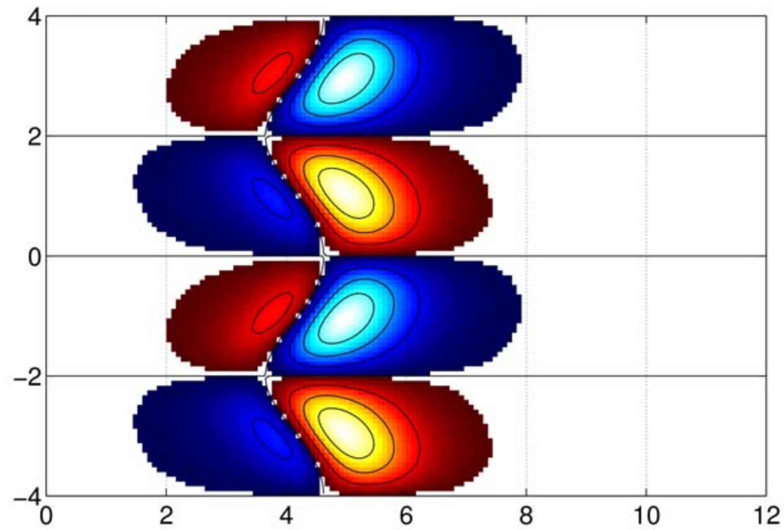

General Expression for $\nabla\times E$

- Object: derive an expression for $\nabla\times\underline{E}$ when B and j are zero

- General expression for E, valid arbitrary f_o …

$$\boxed{\boldsymbol{E} = -\frac{\nabla\left(n\langle \mathrm{v}^5\rangle\right)}{6n\langle \mathrm{v}^3\rangle}} \qquad \text{where} \qquad \langle \mathrm{v}^m\rangle = \frac{4\pi}{n_e}\int f_0 \mathrm{v}^{m+2} d\mathrm{v} \qquad \begin{array}{l}\langle \mathrm{v}^0\rangle = 1 \\ \langle \mathrm{v}^2\rangle = T\end{array}$$

- This originates from the $\int \mathrm{v}^6 d\mathrm{v}$ moment of the $\underline{f}_1$ equation

$$\mathrm{v}\nabla f_0 - \boldsymbol{E}\frac{\partial f_0}{\partial \mathrm{v}} = -\nu'_{ei}\frac{Z^2 n_i}{\mathrm{v}^3}\boldsymbol{f}_1 \qquad \text{where} \qquad \boldsymbol{j} \propto -\int \boldsymbol{f}_1 \mathrm{v}^3 d\mathrm{v} \rightarrow 0$$

Hence in general…

$$\boxed{\dot{\boldsymbol{B}} = -\nabla\times\boldsymbol{E} = \frac{-1}{6n^2\langle \mathrm{v}^3\rangle^2}\nabla\left(n\langle \mathrm{v}^3\rangle\right)\times\nabla\left(n\langle \mathrm{v}^5\rangle\right)}$$

Non-local B Caused by Non-parallel Moments

$$\dot{\boldsymbol{B}} = -\frac{1}{6n^2\langle \mathrm{v}^3\rangle^2} \nabla\left(n\langle \mathrm{v}^3\rangle\right)\times\nabla\left(n\langle \mathrm{v}^5\rangle\right)$$

For a Maxwellian (local approximation) … $\boxed{\langle \mathrm{v}^m\rangle \propto \mathrm{T}^{m/2}}$ $\quad \nabla\langle \mathrm{v}^m\rangle \propto \mathrm{T}^{\frac{m}{2}-1}\nabla\mathrm{T}$

Local B …

$f_0 = f_m$

$$\dot{\boldsymbol{B}}_L \propto \frac{-1}{n^2T^3}\nabla\left(nT^{3/2}\right)\times\nabla\left(nT^{5/2}\right) \quad \Rightarrow -\frac{1}{n}\nabla n\times\nabla T \qquad \nabla n \neq 0$$

$$\boxed{\Rightarrow \quad \nabla T\times\nabla T = 0 \qquad \nabla n = 0}$$

Non-local …

$f_0 \neq f_m$

$$\boxed{\dot{\boldsymbol{B}}_{NL} \propto \frac{-1}{\langle \mathrm{v}^3\rangle^2}\nabla\langle \mathrm{v}^3\rangle\times\nabla\langle \mathrm{v}^5\rangle \qquad \nabla n = 0}$$

- Local approximation forces parallel moments when ∇n=0 .

Non-local Heat Flow Generates "Angle"

- Hot electrons diffuse faster than cold electrons
  - Diffusion coefficient; $D \propto v^5$
  - ϒ Ripples in $\langle v^5 \rangle$ smooth out faster than in $\langle v^3 \rangle$

<u>Conceptual illustration</u>: 2-temp. elec. dist.

$$f_0 = (f_0)_h + (f_0)_c$$

$$\dot{\boldsymbol{B}}_{NL} \propto -\nabla\langle v^3\rangle \times \nabla\langle v^5\rangle$$

$$\nabla\langle v^m\rangle \propto n_c T_c^{m/2-1}\,\nabla T_c + n_h T_h^{m/2-1}\,\nabla T_h$$

$$\boxed{\dot{\boldsymbol{B}}_{NL} \propto \frac{n_h n_c (T_h T_c)^{1/2}}{n_t^2\, T^3}\,[\,T_h - T_c\,]\,(\nabla T_h \times \nabla T_c)}$$

$$\dot{T}_s \propto \kappa_s \nabla^2 T_s \propto T_s^{5/2} \nabla^2 T_s$$

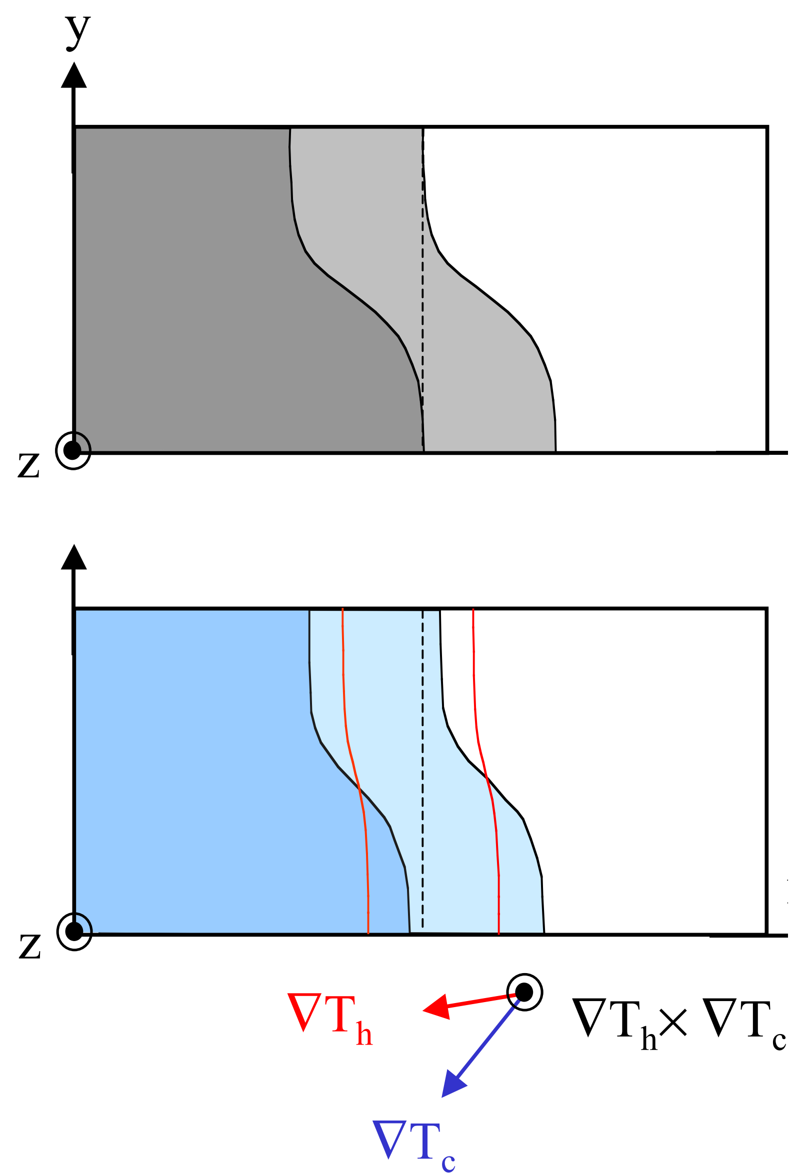

Demonstration of Evolving "Angle"

- Initial ripple, simulation
- "Injection", simulation

$t = 5\ \tau_{ei}$

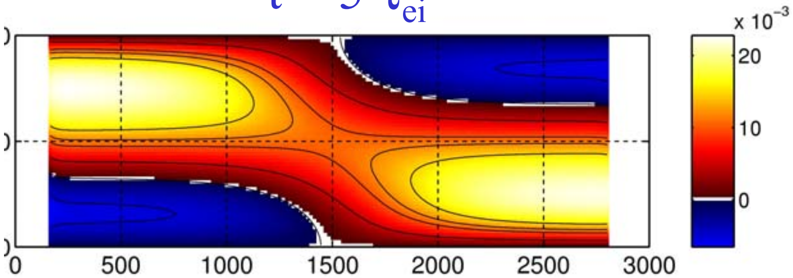

$t = 50\ \tau_{ei}$

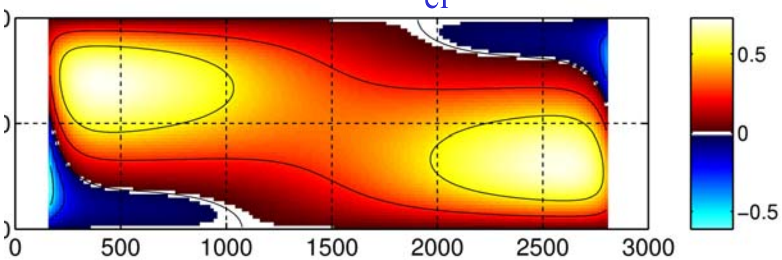

$t = 500\ \tau_{ei}$

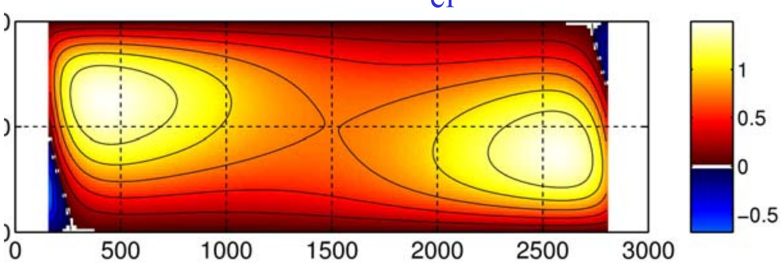

θ in degrees

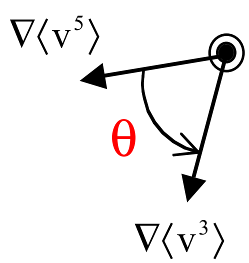

$t = 6$ fs

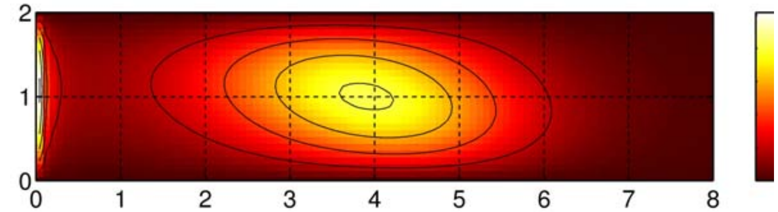

$t = 320$ fs

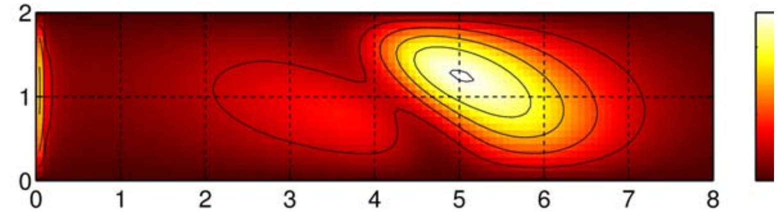

$t = 390$ fs

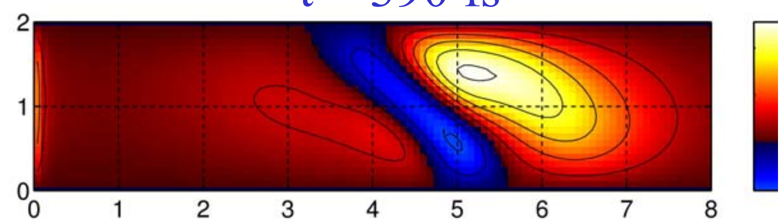

Analytic Formula for B_{NL} Agrees With Sims.

- Tractable analysis of FP eqn possible when…
  - e-e collisions neglected
  - electron inertia neglected ($\partial f_1/\partial t=0$)
  - effect of B on evolution negligible; <u>early time</u>

- B_{NL} from an <u>initial Maxwellian hot spot source</u>…

$$\ddot{\boldsymbol{B}}_{NL} = C_{NL}\nabla T\times\nabla\left(\nabla^2 T\right)$$

$$\boxed{\left|\frac{\ddot{B}_{NL}}{\bar{\nu}_{ei}^{3}}\right| = C'_{NL}G\left(\frac{\delta T}{T}\right)^2\left(\frac{L}{\bar{\lambda}_{ei}}\right)^{-4}}$$

…for $\delta T < T_o$

- Compare with $\nabla n\times\nabla T$ mechanism…

$$\left|\frac{\dot{B}_{n\times T}}{\bar{\nu}_{ei}^{2}}\right| = C_{n\times T}\left|\sin\theta_{n\times T}\right|\left(\frac{\delta T}{T}\right)\left(\frac{\delta n}{n}\right)\left(\frac{L}{\bar{\lambda}_{ei}}\right)^{-2}$$

<u>$\delta T/T_0$ at t=0</u>

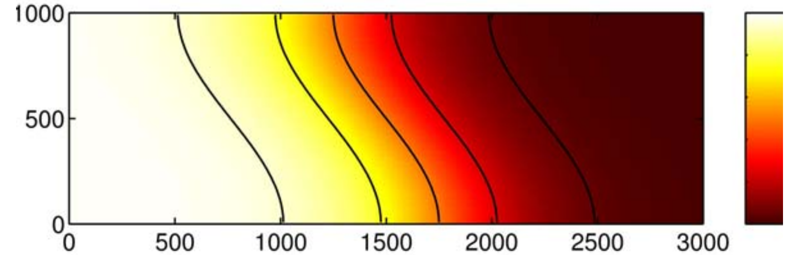

<u>Theory</u>

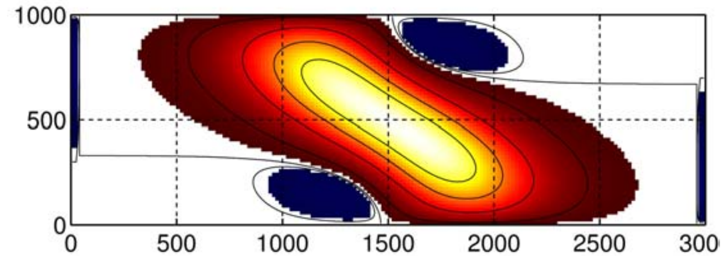

<u>FP simulation</u>

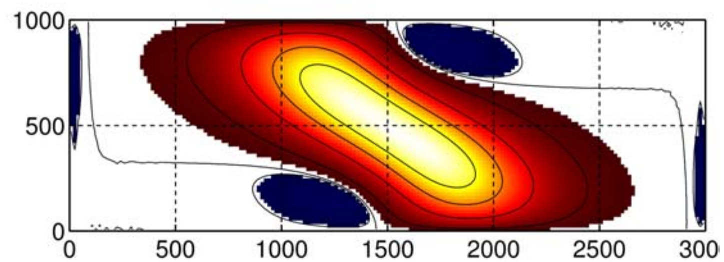

2D-FP Sims. With Heating and ∇Z but $\nabla n=0$

- System & Z, heating profiles…

Z - profile (static) reflective BCs

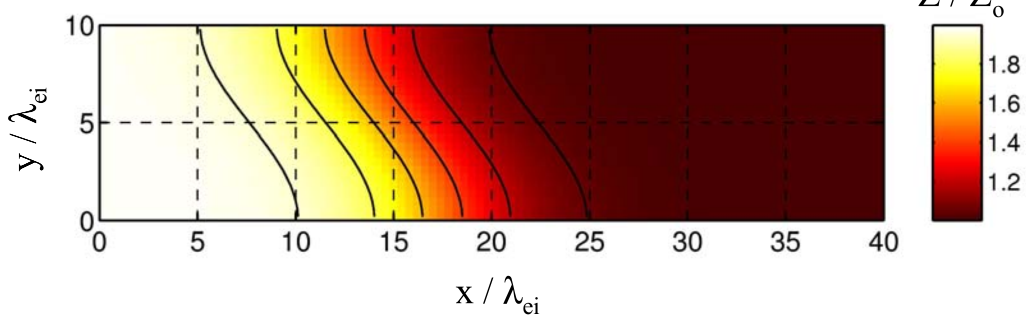

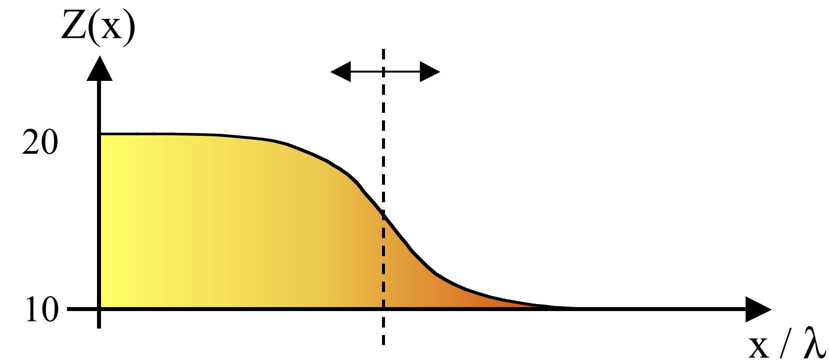

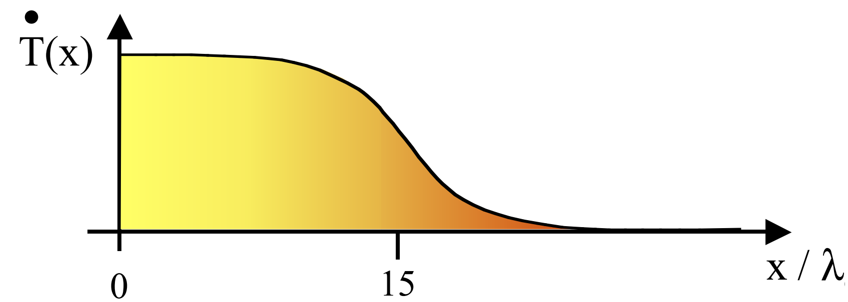

- 1D heating profile

- Parameters…

$Z_o = 10$

$\dfrac{\lambda_{eio}}{\delta_c} = 32$

Solid	$T_{eo} = 6$ keV $n_{eo} = 3 \times 10^{23}$ cm^{-3}	$\lambda_{ei} = 0.3\mu$m $\quad \tau_{ei} = 7$ fs	$\ln \Lambda_{ei} \sim 6$
$n_e = n_{cr}$	$T_{eo} = 1.5$ keV $n_{eo} = 10^{21}$ cm^{-3}	$\lambda_{ei} = 5\mu$m $\quad \tau_{ei} = 70$ fs	$\ln \Lambda_{ei} \sim 7$

B-field grows to $\omega\tau>1$ even though $\nabla n=0$

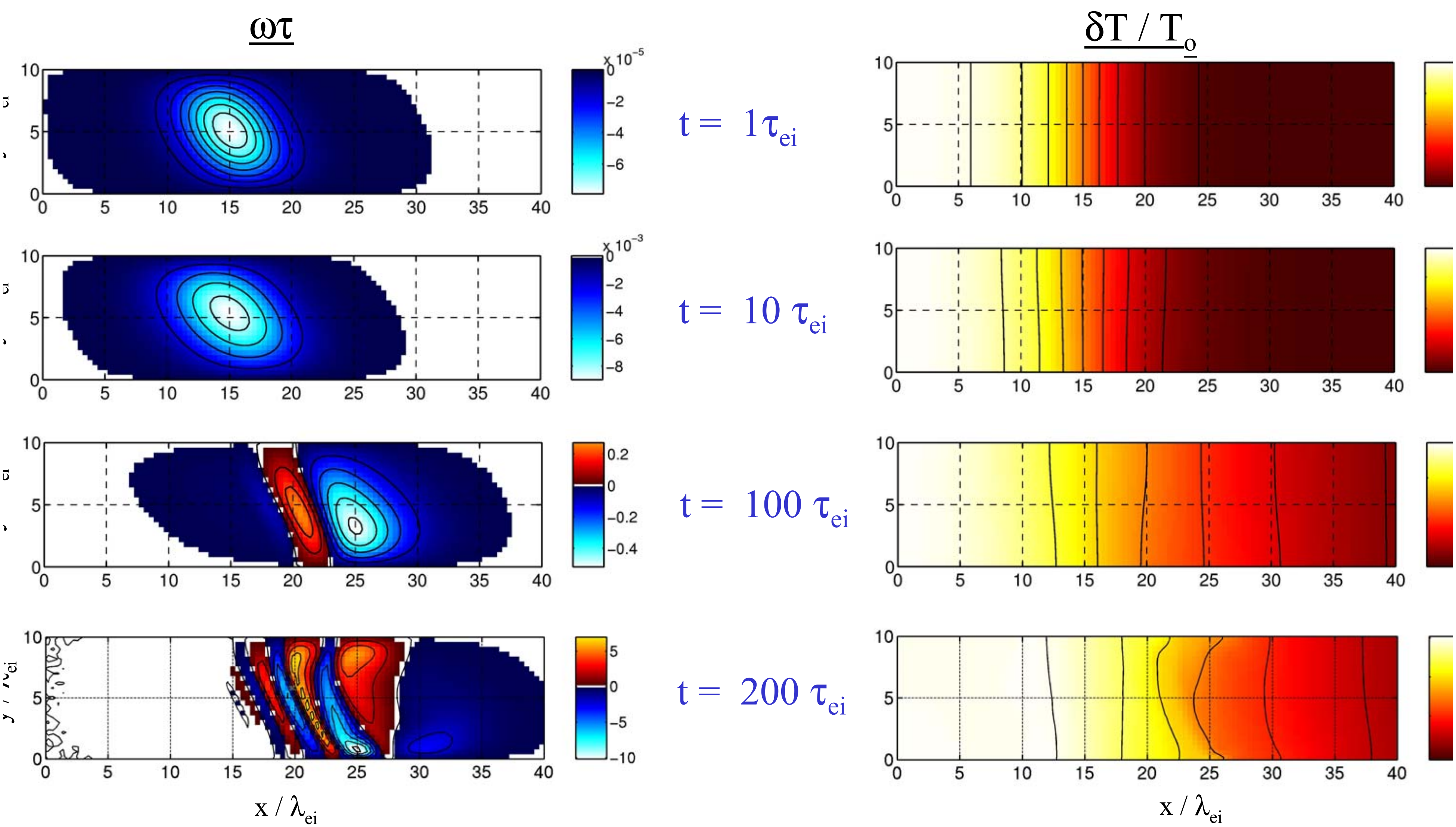

Classical, local theory → B=0 ! (for Lorentz approx.)

Heat flow direction affected by B-field

q / q_{fs}

$t = 1\tau_{ei}$

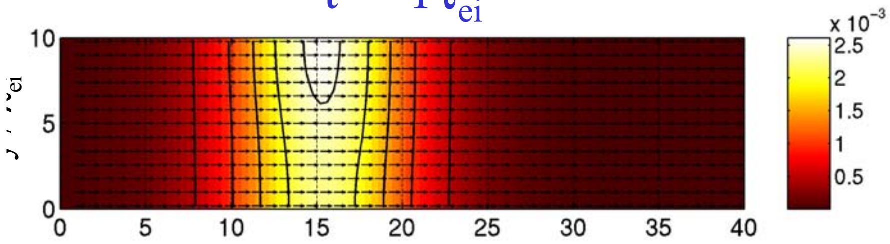

$t = 10\ \tau_{ei}$

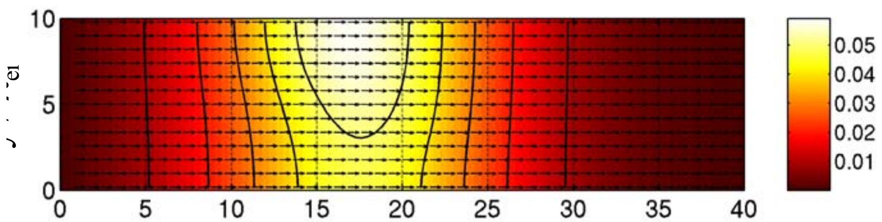

$t = 100\ \tau_{ei}$

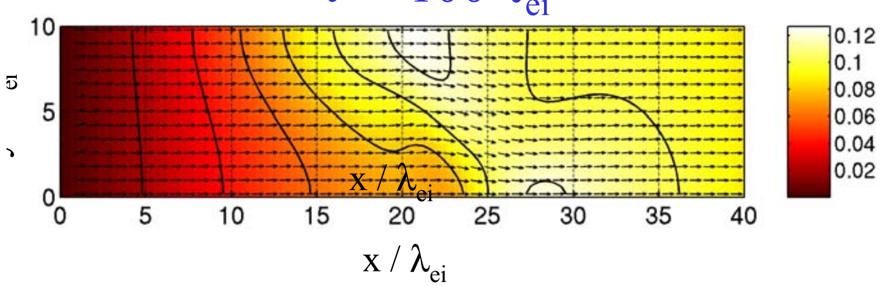

$t = 200\ \tau_{ei}$

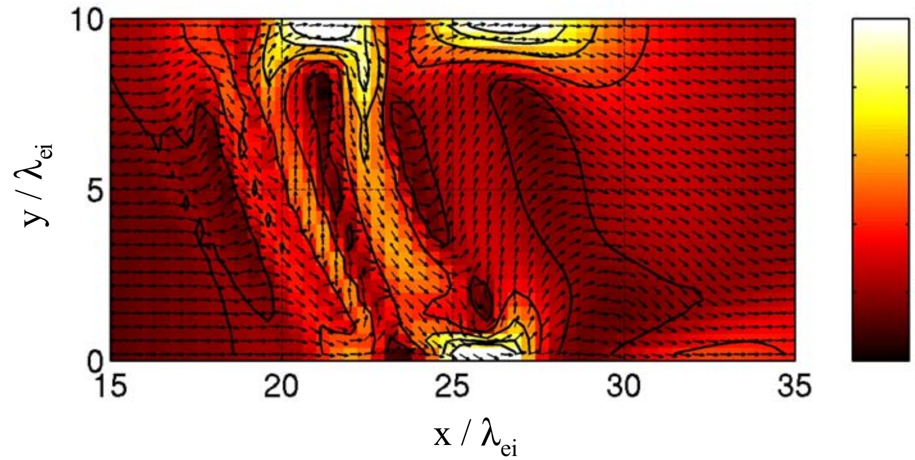

$\omega\tau$

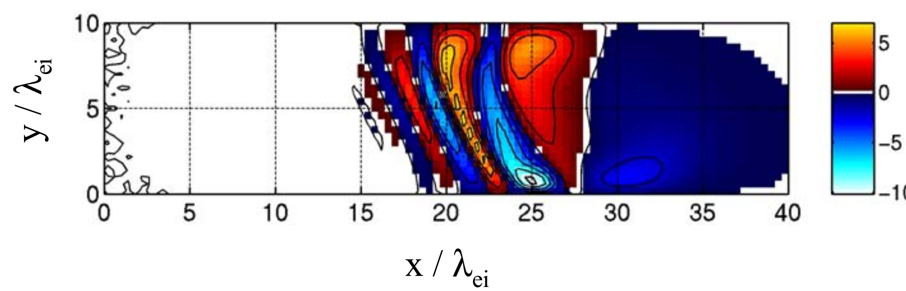

Non-local seed field for $\nabla Z \neq 0$

$\delta T/T_{ave}(x,y)$ (t=0)

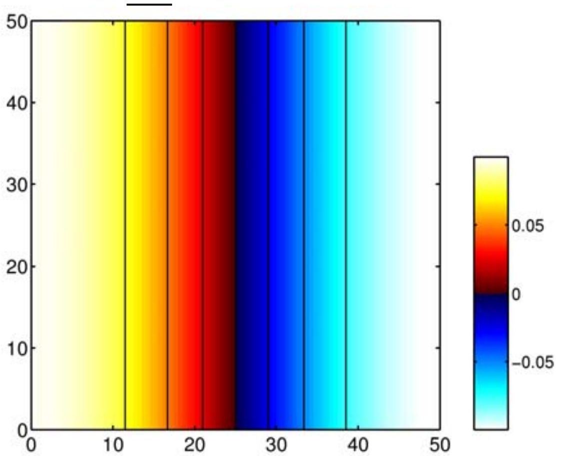

$\delta Z/Z_o(x,y)$

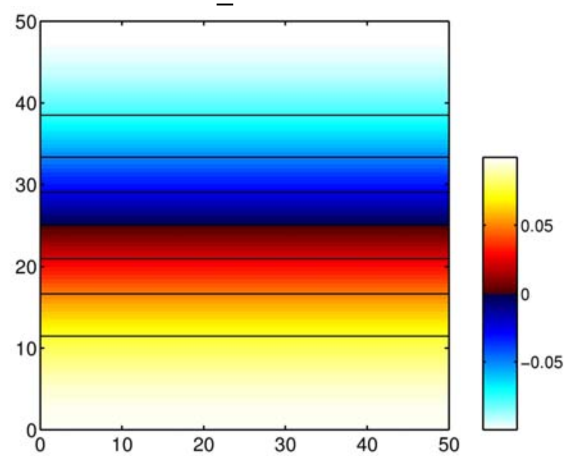

- B at $t = \tau_{ei}$
- $\nabla n = 0$

$$B(t) = -t \frac{\nabla n \times \nabla T_0}{n} + \frac{t^2}{2}\ddot{B}$$

B(x,y) - Local formula

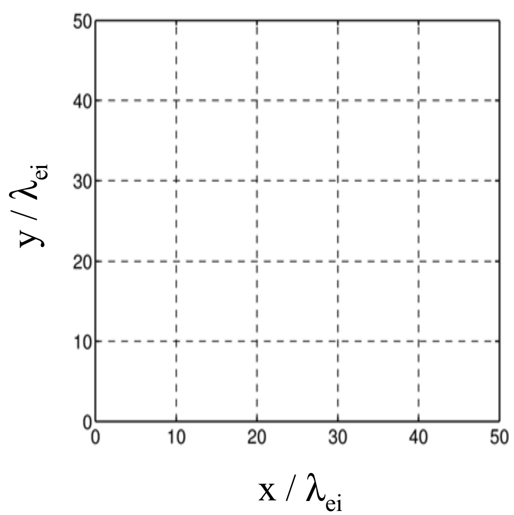

B(x,y) - Non-Local formula

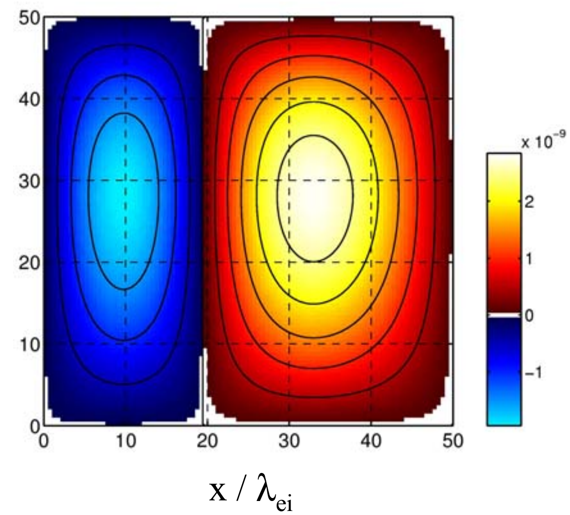

B(x,y) - FP code

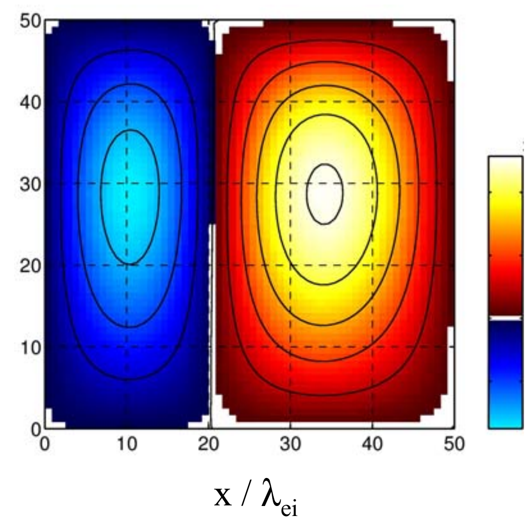

Non-local seed field for $\nabla n \neq 0$

- B at $t = \tau_{ei}$
- $\nabla Z = 0$

$$B(t) = -t \frac{\nabla n \times \nabla T_0}{n} + \frac{t^2}{2} \dot{B}$$

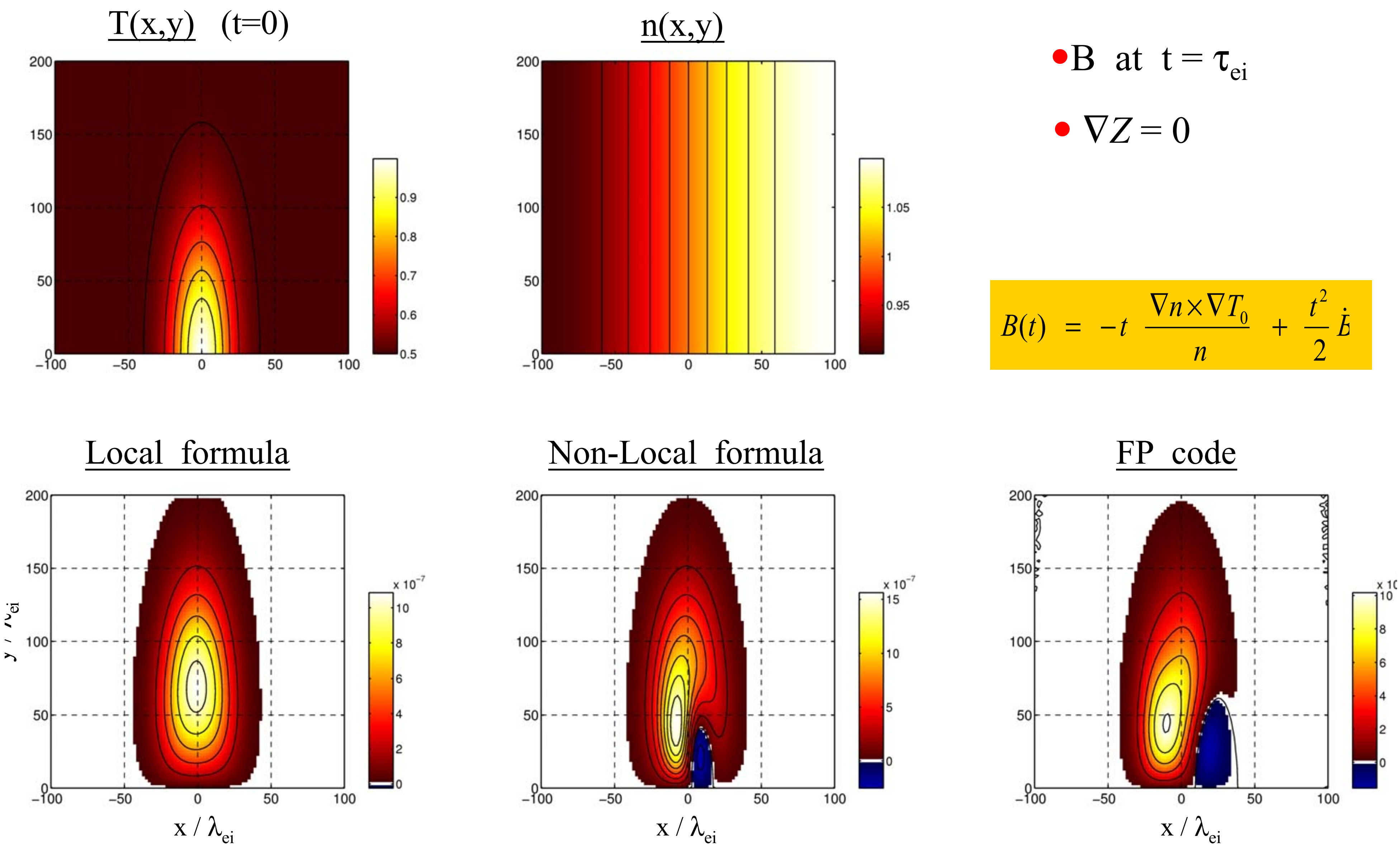

FP sim: heating in a density ramp

B-field

Classical transport | Fokker-Planck code

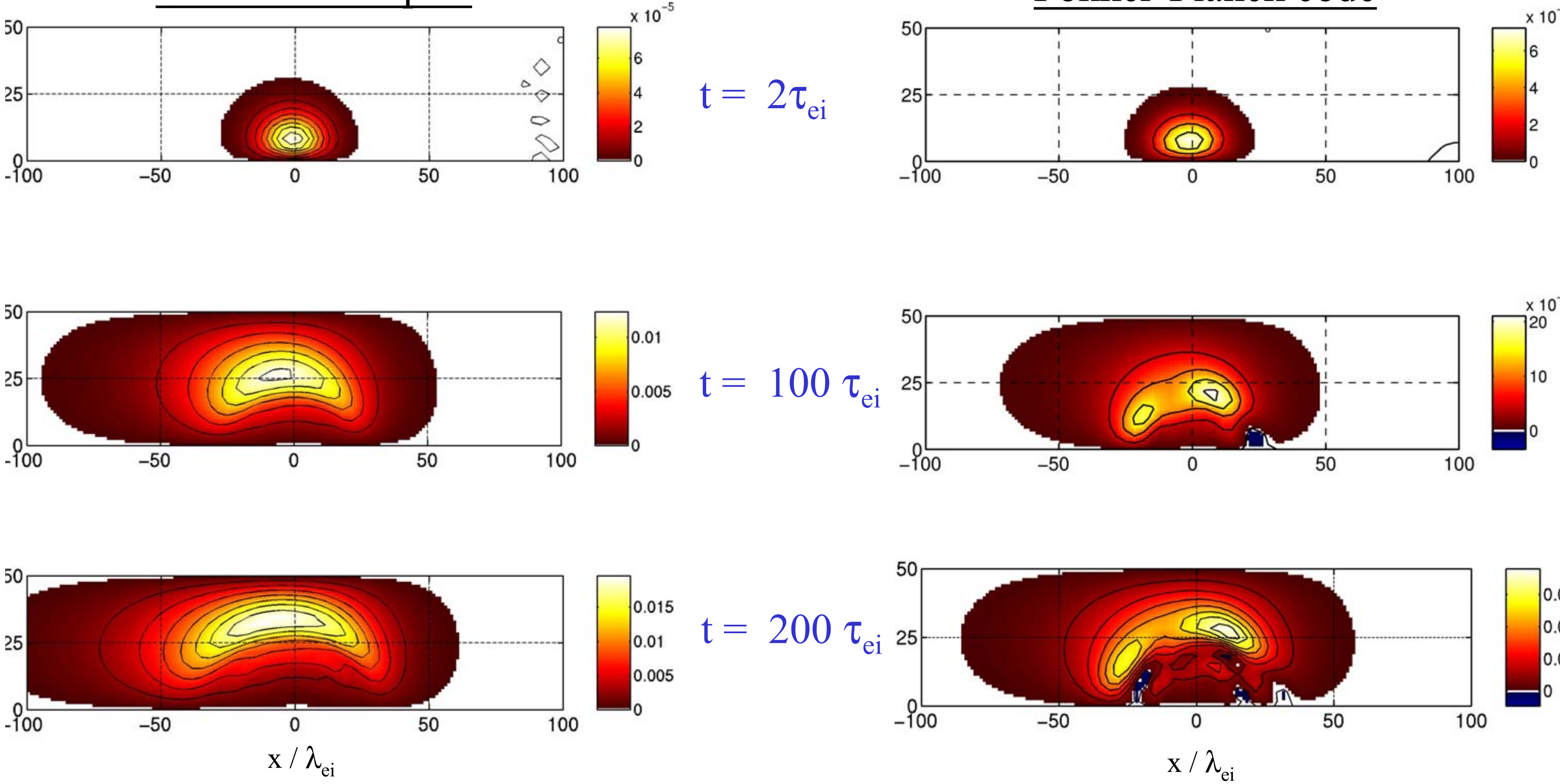

$$n(x) = 1 + 0.95\ \tanh(x/60)$$

$$\frac{\lambda_{eio}}{\delta_c} \sim 1000$$

FP sim: heating in a density ramp

δTe

Classical transport

Fokker-Planck code

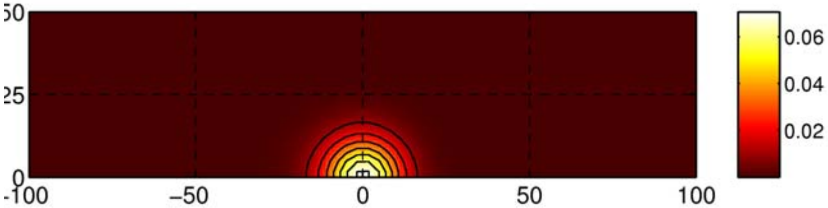

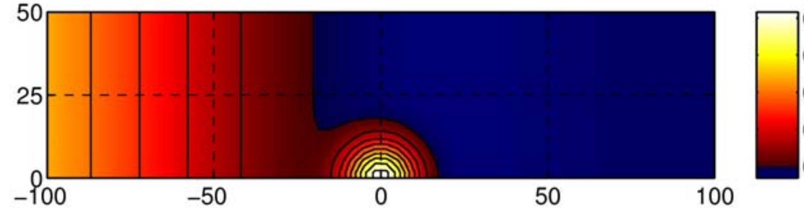

$t = 2\tau_{ei}$

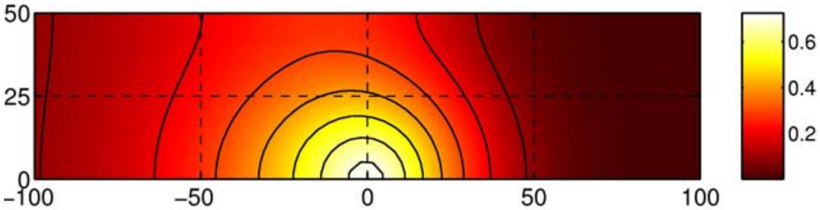

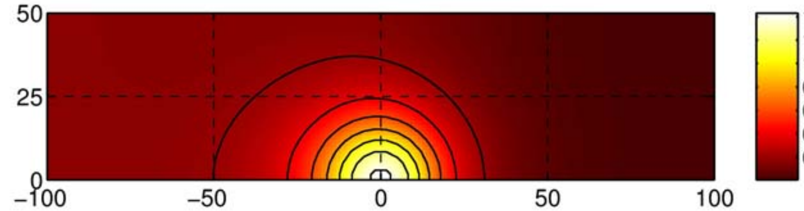

$t = 100\ \tau_{ei}$

q / q_{fs}

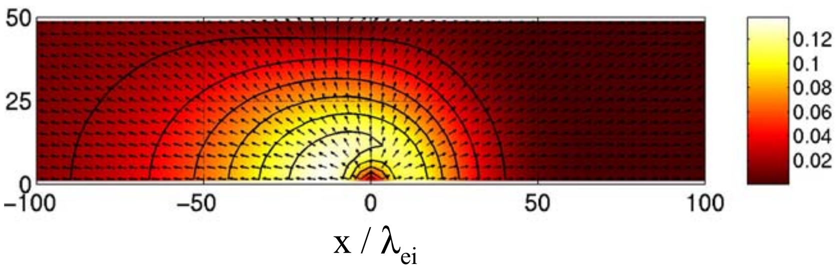

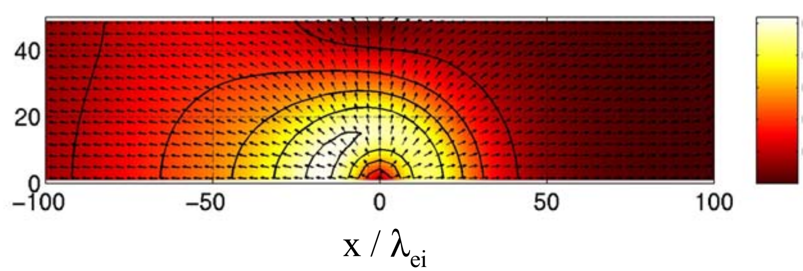

$t = 50\ \tau_{ei}$

FP sim: heating in a density ramp

Classical transport $\quad t = 50\ \tau_{ei} \quad$ Fokker-Planck code

$\dot{B} = -\nabla\times E$

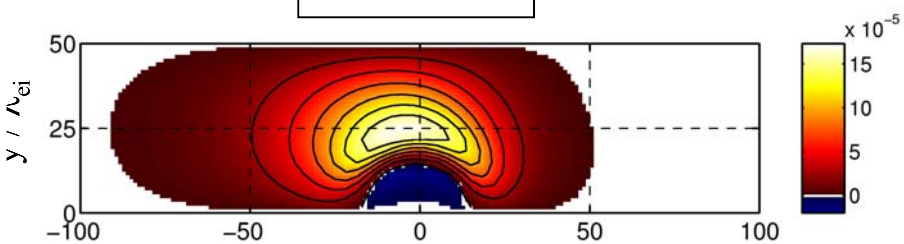

$\dot{B} = -\nabla\times E$

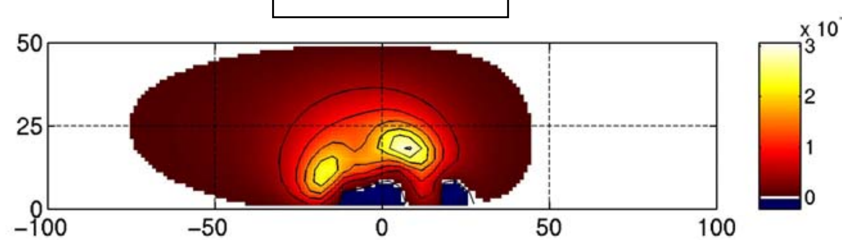

$-(\nabla n \times \nabla T)/n \;+\; \nabla \times (\boldsymbol{\beta} \,.\, \nabla T)$

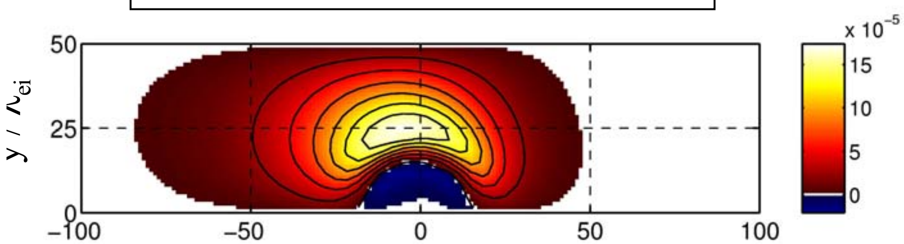

x / λ_{ei}

$-(\nabla n \times \nabla T)/n \;+\; \nabla \times (\boldsymbol{\beta} \,.\, \nabla T)$

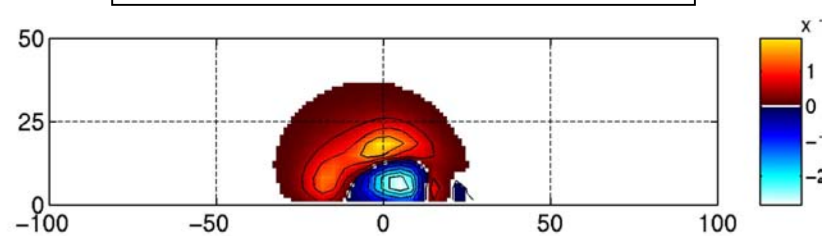

x / λ_{ei}

Conclusions

- New B-field generation mechanism - a non-local effect
  - Driven by non-parallel gradients in moments of f_o $\longrightarrow$ $\dot{B} \propto -\nabla\langle v^3\rangle \times \nabla\langle v^5\rangle$
  - *Kingham & Bell, PRL **88**, 045004 (2002)*

- Works under conditions where local theory says B=0
  - Isotropic electron pressure (c.f. anisotropic pressure in PIC & hybrid code)
  - Growth even when $\nabla n = 0$ which isn't allowed by $\nabla n \times \nabla T$
  - Growth for $\nabla Z \neq 0$ and uniform heating in Lorentz approximation

- FP sims: Get growth of B-field to ùô > 1 and see its effect on transport

- Anayltical formula for seed B-field from initial Maxwellian f_0
  - Arbitrary Z, n_e and initial T_e profile
  - New terms for $\ddot{B}$ $\longrightarrow$ e.g. $\ddot{B} \propto -\nabla T \times \nabla(\nabla^2 T)$
  - "Local-like" terms bigger in non-local case

- FP simulation: Density gradient + heating …
  - 2x larger B-field than local equivalent & less Nerst advection + more structure

- Future: go to $\mathbf{f}_2$ (and beyond) + couple to hydro

3D models for non-local electron heat flux

Sergei Krasheninnikov

University California San Diego

Workshop on Electron Transport

Livermore, September 9-11, 2002

Outline

I. 3D heat transport in “high Z” approximation

Ia. Conclusions

II. 3D self-similar solution of electron kinetic equation

IIa. Conclusions

III. Alternatives

I. 3D heat transport in "high Z" approximation

- Consider kinetic equation for the electron distribution function $f(\mathbf{v},\mathbf{r})$ neglecting electron-ion energy exchange and assuming zero averaged ion velocity:

$$\mathbf{v}\cdot\nabla_{\mathbf{r}} f(\mathbf{v},\mathbf{r}) - e\nabla_{\mathbf{r}}\varphi(\mathbf{r})\nabla_{\mathbf{v}} f(\mathbf{v},\mathbf{r})$$

$$= \frac{2\pi e^4}{m^2}\Lambda\left\{C_{ee}(\mathbf{v},f) + Z_{eff}\, n(\mathbf{r})\frac{\partial}{\partial v_\alpha}\left(V_{\alpha\beta}\frac{\partial f}{\partial v_\beta}\right)\right\}, \quad (I.1)$$

where Λ is the Coulomb logarithm, e, m, and n are the electron charge, mass, and density, Z_{eff} is the effective ion charge

$$C_{ee}(\mathbf{v},f) = \frac{\partial}{\partial v_\alpha}\int\left(f(\mathbf{v},\mathbf{r})\frac{\partial f(\mathbf{v}',\mathbf{r})}{\partial v'_\alpha} - f(\mathbf{v}',\mathbf{r})\frac{\partial f(\mathbf{v},\mathbf{r})}{\partial v_\alpha}\right)U_{\alpha\beta}\,d\mathbf{v}',$$

$$U_{\alpha\beta} = \left(u^2\delta_{\alpha\beta} - u_\alpha u_\beta\right)/u^3, \ \mathbf{u} = \mathbf{v} - \mathbf{v}', \text{ and } V_{\alpha\beta} = \left(v^2\delta_{\alpha\beta} - v_\alpha v_\beta\right)/v^3$$

- Introducing total energy $\varepsilon = mv^2/2 + e\varphi(\mathbf{r})$, from (1) we have

$$\mathbf{v}\cdot\nabla_{\mathbf{r}} f(\varepsilon,\mathbf{r}) = \frac{2\pi e^4}{m^2}\Lambda\left\{C_{ee}(\mathbf{v},f) + Z_{eff}\, n(\mathbf{r})\frac{\partial}{\partial v_\alpha}\left(V_{\alpha\beta}\frac{\partial f}{\partial v_\beta}\right)\right\}. \qquad \text{(I.2)}$$

- Next we assume that the distribution function $f(\mathbf{v},\mathbf{r})$ can be represented by the sum of the symmetric function, $f_0(v,\mathbf{r})$, and the small asymmetric part, $f_1(\mathbf{v},\mathbf{r})$. With this approximation for $Z_{eff} >> 1$ we find

$$f_1(\mathbf{v},\mathbf{r}) = -\frac{v^3 m^2}{4\pi e^4 Z_{eff}\, n(\mathbf{r})}\mathbf{v}\cdot\nabla_{\mathbf{r}} f_0(\varepsilon,\mathbf{r}). \qquad \text{(I.3)}$$

- Averaging Eq. (2) and using (3) we find

$$\nabla_{\mathbf{r}}\cdot\left(\frac{v^5 m^2}{12\pi e^4 Z_{eff}\, n(\mathbf{r})}\nabla_{\mathbf{r}} f_0\right) + \frac{2\pi e^4}{m^2}\Lambda C_{ee}(v,f_0) = 0. \qquad \text{(I.4)}$$

- Since the electrons with the energies higher than thermal, T_e, contribute most to the heat flux, we can use superthermal approximation for e-e collision term

$$\nabla_{\mathbf{r}} \cdot \left(\frac{m^2}{12\pi e^4 Z_{eff} n_e(\mathbf{r})} \nabla_{\mathbf{r}} f_0 \right) + \frac{4\pi e^4 \Lambda n_e(\mathbf{r})}{m^2} \frac{\partial}{v^7 \partial v} \left(f_0 + \frac{T(\mathbf{r})}{mv} \frac{\partial f_0}{\partial v} \right) = 0. \qquad \text{(I.5)}$$

- Following Albritton et al. PRL, 1986 with the modifications from Krasheninnikov Phys. Fluids B, 1993

$$f_0 \approx f_M + A(\varepsilon / T_e)\Psi, \qquad \text{(I.6)}$$

where $\Psi = f_0 + T_e(\partial f_0 / \partial \varepsilon)$, we find

$$\begin{pmatrix} \mathbf{q}(\mathbf{r}) \\ \mathbf{j}(\mathbf{r}) \end{pmatrix} = -\frac{1}{\pi^2} \left(\frac{5T}{2mZ_{eff}} \right)^{1/2} \int d\mathbf{r}' n'(T')^5 \begin{pmatrix} 1 \\ 1/T' \end{pmatrix}$$

$$\times \left\{ \begin{pmatrix} P_{0,-3/2} \\ P_{-1/5,-5/2} \end{pmatrix} \nabla T' - \begin{pmatrix} P_{0,-5/2} \\ P_{-1/5,-7/2} \end{pmatrix} \nabla e\varphi' \right\}, \qquad \text{(I.7)}$$

where

$$P_{\alpha,\beta} \equiv P_{\alpha,\beta}(g) = \int_0^1 d\tau\, \tau^{\alpha} (1-\tau)^{-3/2} \int_0^{\infty} d\sigma\, \sigma^{\beta} \exp\left(-\sigma - \frac{g^2}{\sigma^5 (1-\tau)} \right),$$

$$g^2 = \frac{5}{4} \frac{\left(\mathbf{s}(\mathbf{r}) - \mathbf{s}(\mathbf{r}')\right)^2}{(T')^5}, \text{ and } \quad d\mathbf{s} = 6\pi e^4 \Lambda n(\mathbf{r}) \left[\left(Z_{\mathrm{eff}} + 1 \right) T(\mathbf{r}) \right]^{1/2} d\mathbf{r} \qquad \text{(I.8)}$$

Ia. Conclusions

- The expression for electron heat flux, $\mathbf{q}(\mathbf{r})$, for 3D case is derived
- However, it contains 3D integral and, therefore, it might be rather time consuming to use it. Differential form of $\mathbf{q}(\mathbf{r})$ might be more preferable
- Benchmarking can be an issue. 3D self-similar solutions can be used for benchmarking

II. 3D self-similar solution of electron kinetic equation

- Self-similar solutions of electron kinetic equation in 1D2V (azimuthal symmetry) case were introduced in [Krasheninnikov, JETP 1988] (see also numerical solutions in [Krasheninnikov et al, Contr. Plasma Phys., 1992] and high Z_{eff} in [Bakunin and Krasheninnikov, Plasma Phys. Reports, 1995])

- In 1D2V case electron kinetic equation written in spherical coordinates $(v, \mu = \cos\vartheta)$ in velocity space (ϑ is the angle between the $\mathbf{x}$ and $\mathbf{v}$) has the form

$$v\mu \frac{\partial f(v,\mu,x)}{\partial x} - eE(x)\left(\mu \frac{\partial f(v,\mu,x)}{\partial v} + \frac{1-\mu^2}{v}\frac{\partial f(v,\mu,x)}{\partial \mu}\right)$$

$$= \frac{2\pi e^4}{m^2}\Lambda\left\{C_{ee}(\mathbf{v},f) + Z_{eff}\, n \frac{\partial}{\partial v_\alpha}\left(V_{\alpha\beta}\frac{\partial f}{\partial v_\beta}\right)\right\}, \qquad \text{(II.1)}$$

- The trick here is to use self-similar variable $\mathbf{w} = \mathbf{v}\sqrt{m/2T(x)}$ and apply the anzatz for electron distribution function

$$f(\mathbf{v},x) = F(w,\mu)\big/(T(x))^{\alpha} \qquad \text{(II.2)}$$

- As a result, rather to deal with 1D2V equation (II.1) for $f(\mathbf{v}, x)$ we have 2W kunetic equation for $F(w, \mu)$

$$\gamma w \mu \left(\alpha F + \frac{w}{2} \frac{\partial F}{\partial w} \right) - \frac{\gamma_E}{2} \left(\mu \frac{\partial F}{\partial w} + \frac{1-\mu^2}{w} \frac{\partial F}{\partial \mu} \right)$$

$$= \frac{1}{4} \left\{ C_{ee}(\mathbf{w}, F) + \frac{Z_{eff}}{w^3} \frac{\partial}{\partial \mu} \left(\left(1-\mu^2 \right) \frac{\partial F}{\partial \mu} \right) \right\}. \qquad \text{(II.3)}$$

where $\gamma = -T^2 (d \ln T / dx) \big/ \left(2\pi e^4 \Lambda n \right) \equiv (\lambda / L) = \text{const.}$, and

$$\gamma_E = eET \big/ \left(2\pi e^4 \Lambda n \right) = \text{const.} \qquad \text{(II.4)}$$

- From (II.2) and (II.4) we have $n \propto T^{3/2-\alpha}$ and $T^{\alpha+1/2}(d \ln T / dx) = \text{const.}$, which gives

$$T(x) \propto x^{1/(\alpha+1/2)}. \qquad \text{(II.5)}$$

- Conservation of heat flux, q, along x coordinate with anzatz (II.2) results in

$$q = \int f\mathbf{v}(mv^2/2)d\mathbf{v} \propto (T(x))^{3-\alpha} \int Fw^2\mathbf{w}d\mathbf{w} = \text{const.} \quad \rightarrow \quad \alpha = 3. \qquad \text{(II.6)}$$

- Solution of nonlinear self-similar kinetic equation (II.3) gives the following asymptotic expression for $F(w,\mu)$ at $\xi \equiv w^2 \rightarrow \infty$

$$F(\xi,\mu) = \frac{\Phi(\mu)}{\xi^\alpha}, \qquad \text{(II.7)}$$

where $\Phi(\mu)$ is asymmetric function which magnitude and asymmetry depends on Z_{eff}

- As one can see, with (II.7) the expression (II.6) for $\alpha = 3$ logarithmically diverges at high ξ at any (even arbitrary small) $\gamma \equiv (\lambda/L)$

$$q = \int f\mathbf{v}(mv^2/2)d\mathbf{v} \propto e^{-A/\gamma^{1/3}} \int \Phi(\mu)\mu d\mu \int \xi^{2-\alpha} d\xi. \qquad \text{(II.8)}$$

- It demonstrates effects of non-expandable terms and importance of ENTIRE density and temperature profiles for the problem of non-local heat conduction

- Here we show that self-similar technique can be extended in a way which allows to study the effects of 3D geometry on non-local electron heat conduction

- We assume spherical symmetry of the problem in $\mathbf{r}$ space and introduce local spherical coordinates $(v, \mu = \cos\vartheta)$ in velocity space, ϑ is the angle between the $\mathbf{r}$ and $\mathbf{v}$

$$v\left(\mu\frac{\partial f(v,\mu,r)}{\partial r}+\frac{1-\mu^2}{r}\frac{\partial f(v,\mu,r)}{\partial \mu}\right)-eE(r)\left(\mu\frac{\partial f(v,\mu,r)}{\partial v}+\frac{1-\mu^2}{v}\frac{\partial f(v,\mu,r)}{\partial \mu}\right)$$

$$=\frac{2\pi e^4}{m^2}\Lambda\left\{C_{ee}(\mathbf{v},f)+Z_{eff}\,n\frac{\partial}{\partial v_\alpha}\left(V_{\alpha\beta}\frac{\partial f}{\partial v_\beta}\right)\right\}, \qquad \text{(II.9)}$$

$$v\left(\mu\frac{\partial f(v,\mu,r)}{\partial r}+\frac{1-\mu^2}{r}\frac{\partial f(v,\mu,r)}{\partial \mu}\right)-eE(r)\left(\mu\frac{\partial f(v,\mu,r)}{\partial v}+\frac{1-\mu^2}{2v}\frac{\partial f(v,\mu,r)}{\partial \mu}\right)$$

- Following [Krasheninnikov JETP 1988] we introduce self-similar variable $\mathbf{w}=\mathbf{v}\sqrt{m/2T(r)}$ and use the anzatz for electron distribution function

$$f(\mathbf{v},\mathbf{r})=F(w,\mu)\big/(T(r))^{\alpha} \qquad \text{(II.10)}$$

- Then from (II.9) we find

$$\gamma w\left\{\mu\left(\alpha F+\frac{w}{2}\frac{\partial F}{\partial w}\right)-\frac{1-\mu^2}{(d\ln T/d\ln r)}\frac{\partial F}{\partial \mu}\right\}-\frac{\gamma_E}{2}\left(\mu\frac{\partial F}{\partial w}+\frac{1-\mu^2}{w}\frac{\partial F}{\partial \mu}\right)$$

$$=\frac{1}{4}\left\{C_{ee}(\mathbf{w},F)+\frac{Z_{eff}}{w^3}\frac{\partial}{\partial \mu}\left(\left(1-\mu^2\right)\frac{\partial F}{\partial \mu}\right)\right\}. \qquad \text{(II.11)}$$

where $\quad \gamma=-T^2(d\ln T/dr)\Big/\left(2\pi e^4\Lambda n\right)\equiv(\lambda/L)=\text{const.},$ and

$$\gamma_E=eET\Big/\left(2\pi e^4\Lambda n\right)=\text{const.} \qquad \text{(II.12)}$$

- From (II.10) and (II.12) we have $n\propto T^{3/2-\alpha}$ and $T^{\alpha-1/2}(dT/dr)=\text{const.}$, which gives

$$T(r)\propto r^{1/(\alpha+1/2)} \qquad \text{(II.13)}$$

- As a result Eq. (II.11) can be written as follows

$$\gamma w\left\{\mu\left(\alpha F+\frac{w}{2}\frac{\partial F}{\partial w}\right)-(\alpha+1/2)\left(1-\mu^2\right)\frac{\partial F}{\partial \mu}\right\}-\frac{\gamma_E}{2}\left(\mu\frac{\partial F}{\partial w}+\frac{1-\mu^2}{w}\frac{\partial F}{\partial \mu}\right)$$

$$=\frac{1}{4}\left\{C_{ee}(\mathbf{w},F)+\frac{Z_{eff}}{w^3}\frac{\partial}{\partial \mu}\left(\left(1-\mu^2\right)\frac{\partial F}{\partial \mu}\right)\right\}. \qquad \text{(II.14)}$$

- Notice an extra (in comparison with 1D2V case considered before) term $(\alpha+1/2)\left(1-\mu^2\right)(\partial F/\partial\mu)$ causing, as we will see, picking of F around $\mu=1$

- Conservation of heat flux for spherically symmetric case with anzatz (II.10) results in

$$4\pi r^2 q \propto r^2\int f v^2 \mathbf{v} d\mathbf{v} \propto r^2 T^{3-\alpha}\int F w^2 \mathbf{w} d\mathbf{w} \propto r^2 T^{3-\alpha} = \text{const.}, \qquad \text{(II.15)}$$

which is compatible with the self-similar temperature profile (II.13) for

$$\alpha=-4. \qquad \text{(II.16)}$$

- 2D Eq. (II.14) can be treated either numerically or, at small γ, analytically

- Here we analyze (II.14) for large energies. If only convective term would be important, i. e.

$$\mu\left(\alpha F + \frac{w}{2}\frac{\partial F}{\partial w}\right) - (\alpha + 1/2)\left(1-\mu^2\right)\frac{\partial F}{\partial \mu} = 0, \tag{II.17}$$

then the solution of (II.17) can be written as follows

$$F(\xi,\mu) = \frac{H\left((1-\mu^2)\xi^{-(2\alpha+1)}\right)}{\xi^{\alpha}}, \tag{II.18}$$

where $\xi = w^2$ and H(x) is an arbitrary function

- From (II.18) we find that with increasing ξ the function $F(\xi,\mu)$ becomes more and more picked around $\mu = 1$ caused by divergence of electron flux due to simple geometrical effects

- As a result, unlike 1D case, to analyze energetic tail of the distribution function we need to keep Coulomb scattering term

$$\mu\left(\alpha F+\xi\frac{\partial F}{\partial\xi}\right)-(\alpha+1/2)\left(1-\mu^2\right)\frac{\partial F}{\partial\mu}=\frac{1+Z_{\mathrm{eff}}}{4\gamma\xi^2}\frac{\partial}{\partial\mu}\left(\left(1-\mu^2\right)\frac{\partial F}{\partial\mu}\right)\qquad\text{(II.19)}$$

- Introducing $\eta=(1-\mu)/\xi^{2\alpha+1}$ and $F=\tilde{F}/\xi^{\alpha}$, and considering (II.19) at $\mu\approx 1$ we have

$$\xi^{2\alpha+4}\frac{\partial\tilde{F}}{\partial\xi}=\frac{1+Z_{\mathrm{eff}}}{2\gamma}\frac{\partial}{\partial\eta}\left(\eta\frac{\partial\tilde{F}}{\partial\eta}\right)\qquad\text{(II.20)}$$

- Solution of (II.20) can be found easily and as a result in

$$F(\xi,\mu)=C\xi^{\alpha+3}\exp\left(-\frac{(1-\mu)\xi^2}{D}\right)\qquad\text{(II.21)}$$

where $D=-\left(1+Z_{\mathrm{eff}}\right)/(2\alpha+3)2\gamma$

- For $\alpha = -4$, the expression for electron flux

$$j \propto \int F(\xi,\mu)\xi d\xi d\mu \propto \int \frac{\exp(-(1-\mu)\xi^2 / D)}{\xi^{-(\alpha+3)}} \xi d\xi d\mu \propto \int \xi^{\alpha+2} d\xi,$$

converges at $\xi \to \infty$, while the heat flux

$$q \propto \int F(\xi,\mu)\xi^2 d\xi d\mu \propto \int \frac{\exp(-(1-\mu)\xi^2 / D)}{\xi^{-(\alpha+3)}} \xi^2 d\xi d\mu \propto \int \xi^{\alpha+3} d\xi,$$

diverges logarithmically at $\xi \to \infty$

IIa. Conclusions

- Geometry can indeed play an important role in non-local electron heat transport
- 3D self-similar solutions of electron kinetic equation are available and can be used for benchmarking of both reduced models and codes

III. Alternatives

- Finally it does not matter where we are taking our non-local heat flux expressions from
- We may "guess" about the heat flux expression and benchmark it against some "exact" expressions (e. g. Spitzer-Harm and self-similar solutions) and numerics
- "Conventional" wisdom suggests that non-locality of electron heat flux can be written as follows

$$q(x) = \int q_{SH}(x')K(x,x')dx', \qquad \text{(III.1)}$$

where $q_{SH}(x)$ is the Spitzer-Harm heat flux and the kernel $K(x,x')$, describing non-local effects, obeys the normalization

$$\int K(x,x')dx' = 1. \qquad \text{(III.2)}$$

- However, 1D2V self-similar solution with $\alpha = 3$ corresponds to $q_{SH}(x) = \text{const.}$ (recall $\gamma = (\lambda/L) \propto T^{\alpha-1/2}(dT/dx) = \text{const.}$). As a result, logarithmic divergence of self similar heat flux, $q = \int f\mathbf{v}(mv^2/2)d\mathbf{v} \propto \int \Phi(\mu)\mu d\mu \int \xi^{2-\alpha}d\xi \propto \ln \xi$, at high energies (= large x) CANNOT be recovered with Eq. (III.1)

- Should we alter normalization/asymptotic of $K(x,x')$ at $|x'| \to \infty$?! E. g.

$$K(x,|x'| \to \infty) \propto \exp(-A/(\gamma_{\pm\infty})^p), \qquad \text{with} \quad \gamma = \lambda/L. \tag{III.3}$$

- Differential models for non-local heat flux can also be considered. E. g. diffusive model

$$\lambda(x)\frac{d}{dx}\left(\lambda(x)\frac{dq(x)}{dx}\right) + q_{SH}(x) - q(x) = 0. \tag{III.4}$$

- However, "standard" solution of the equation (III.4) is equivalent to the integral form like (III.1) with the kernel

$$K(x,x') = \exp\left(-\left|\int_x^{x'} dx''/\lambda(x'')\right|\right)\Big/2\lambda(x). \tag{III.5}$$

- Could it be that "nonstandard" solution of the equation (III.4) with nonzero boundary conditions at $|x| \to \infty$ or mixed diffusion/convection model, e. g.

$$\lambda(x)\frac{d}{dx}\left(\lambda(x)\frac{dq}{dx} + \sigma(x)q\right) + q_{SH}(x) - q = 0 \qquad \text{with} \quad \sigma(x) \propto (\lambda/L)^p. \tag{III.6}$$

will work?!

Magnetic Fields In Laser Light Speckles.

B. F. Lasinski, C. H. Still, A. B. Langdon,

D. E. Hinkel, and E. A. Williams

for the

Electron Transport Workshop

September 9-11, 2002.

X-Division

Lawrence Livermore National Laboratory

University of California

Work performed under the auspices of the US DoE by the Lawrence Livermore National Laboratory under contract W-7405-ENG-48

Static magnetic field structures due to Raman scatter have been identified in MPP 3D and 2D PIC simulations – a preliminary report.

- In laser light speckles, Raman scatter, both forward and back, generates localized currents of forward going electrons.
- These currents (J_z) result in surrounding magnetic fields (B_θ).
- We have identified these magnetic fields in our MPP 3D and 2D PIC simulations with **Z3** for parameters associated with NIF high temperature hohlraums and NIF ignition hohlraums.
  - Large 2D and 3D PIC simulations with dedicated diagnostics are required for this effort.
- These magnetic fields are ~ MG and are large enough to confine the background electrons and hence affect electron transport in these plasmas.

λ Studies are underway to elucidate the complex spatial and time dependence of these magnetic fields.

These B-fields were initially seen in Z3 simulations of conditions expected in small, high temperature hohlraums.

HTH parameters: flat density profile at $0.2n_c$, $ZT_e/T_i = 13$, Te = 14 keV;
Gaussian beams or $(\sin)^4$ spatial profile
$I = 7 \times 10^{16}$ W/cm^2 for blue (1/3 μm) light; intense speckle

Raman scatter is the decay of the incident light wave into an electron plasma wave and a lower frequency light wave.

At these parameters, find vigorous back and forward scatter (A. B. Langdon and D. E. Hinkel, Phys. Rev. Lett. **89**, 2002 (015003)).

Will also describe our preliminary findings on B-fields from SRS for parameters relevant to NIF ignition hohlraums.

Current Z3 simulation volumes are on the order of an f/4 to f/8 speckle.

Simulation geometry:

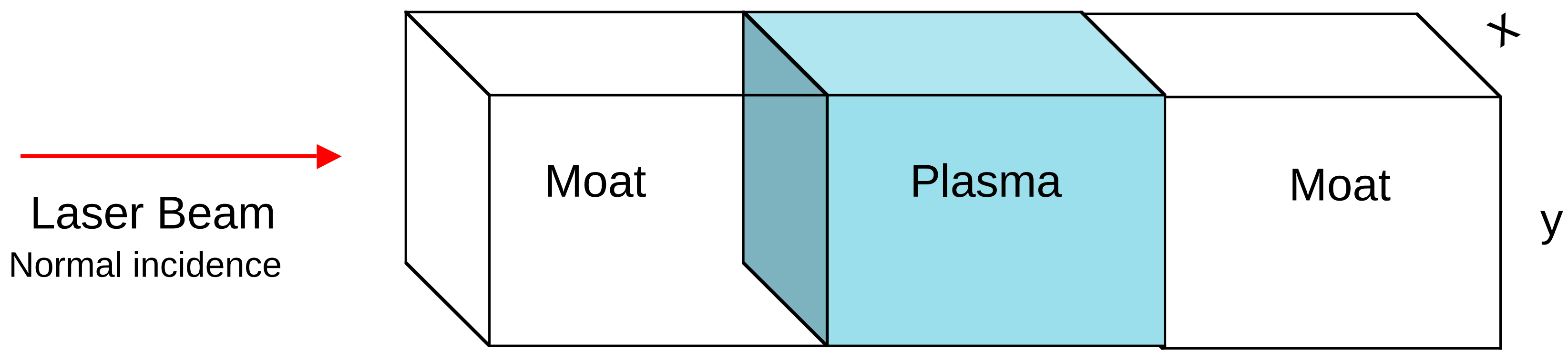

Z = laser propagation direction

- In these 3D simulations the plasma slab is $24\lambda_0$ x $24\lambda_0$ x ($61\lambda_0$ or $138\lambda_0$). The smaller simulation system has 1.4 x 10^8 cells and 3.4 x 10^9 particles (electrons and ions).

- 2D simulations are as wide as $98\lambda_0$ in the transverse direction and as long as $300\lambda_0$ in the propagation direction.

2D slices of the Poynting vector, P_z, show the propagation of this linearly polarized laser (E_y, B_x).

At an early time (0.14 ps), light has not yet penetrated the entire slab.

Plot of P_z vs (x, z) in the y/2 plane.

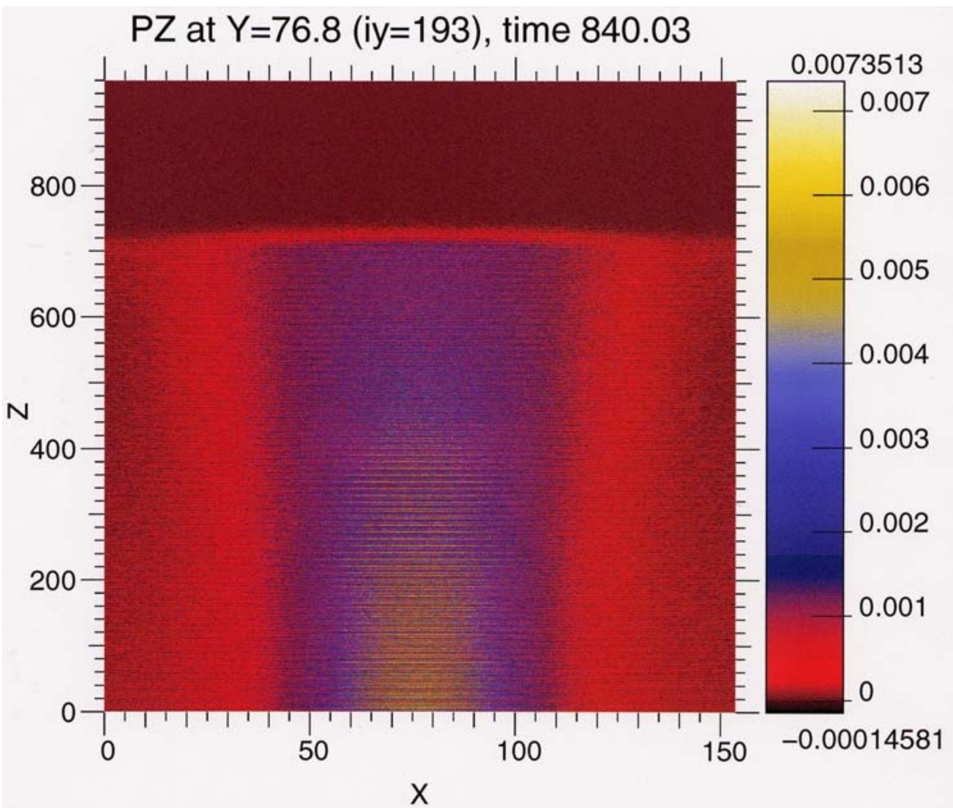

Peak laser in Gaussian beam has B_0 = 0.08 which corresponds to 7 x 10^{16} W/cm^2 for blue light.

Note different aspect ratios for the two axes.

Spatial scales are in units of c/ω_0.

Readily identify $\lambda_0/2$, as expected for snapshot in time of P_z

At later times, we identify forward and back Raman scatter in the 2D slice of the Poynting vector.

As part of the Z3 diagnostics suite, we apply a low pass temporal filter, $[\sin(\pi\omega/\omega_0)/(\pi\omega/\omega_0)]^2$, to fields and fluxes to separate the laser and the low frequency fields and fluxes. We identify these quantities with the subscript s

Plot of $(P_z)_s$ vs (x,z) in the y/2 plane at 0.27 ps

3D; 0.2nc; 14 keV; 7×10^{16} W/cm^2

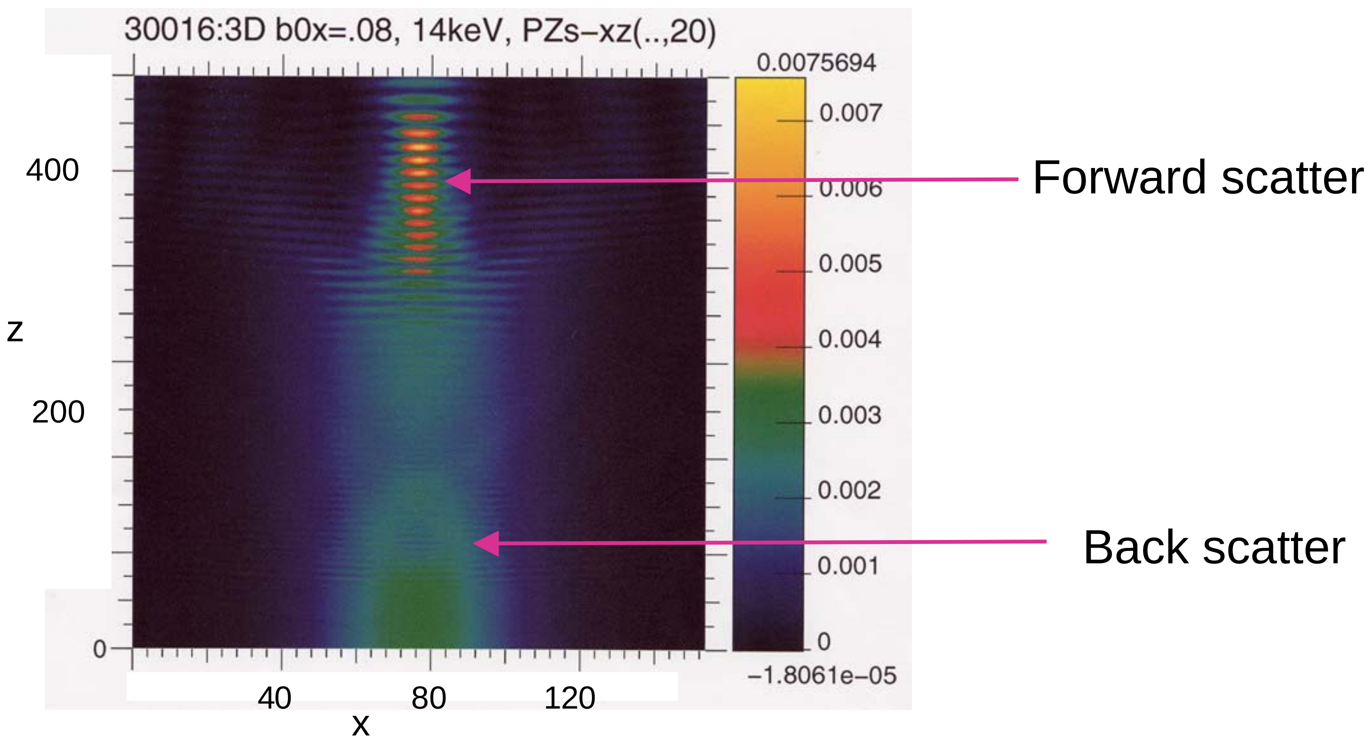

Static magnetic fields associated with back and forward scatter are readily apparent in the 2D slice of B_y vs x and z

3D, 0.2 nc, 14 keV, 7 x 10^{16} W/cm^2, linearly polarized (B_x, E_y)

Plot of B_y vs (x, z) in the y/2 plane at 0.27 ps.

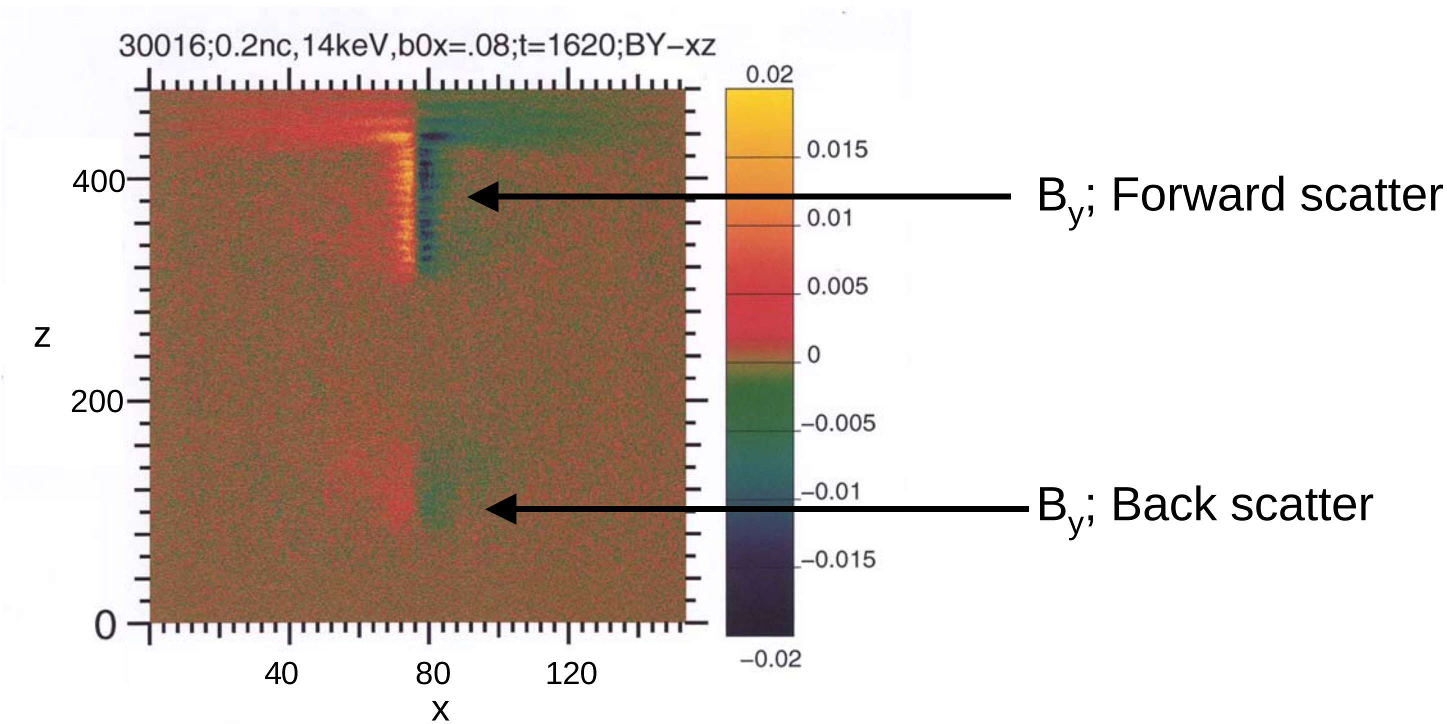

Raman back and forward scatter, as well as their associated magnetic fields, are readily visible in this 2D slice of (Bx)s.

3D, 0.2 nc, 14 keV, 7 x 10^{16} W/cm^2, linearly polarized (B_x, E_y)

Plot of B_x vs (y, z) in the x/2 plane at 0.27 ps.

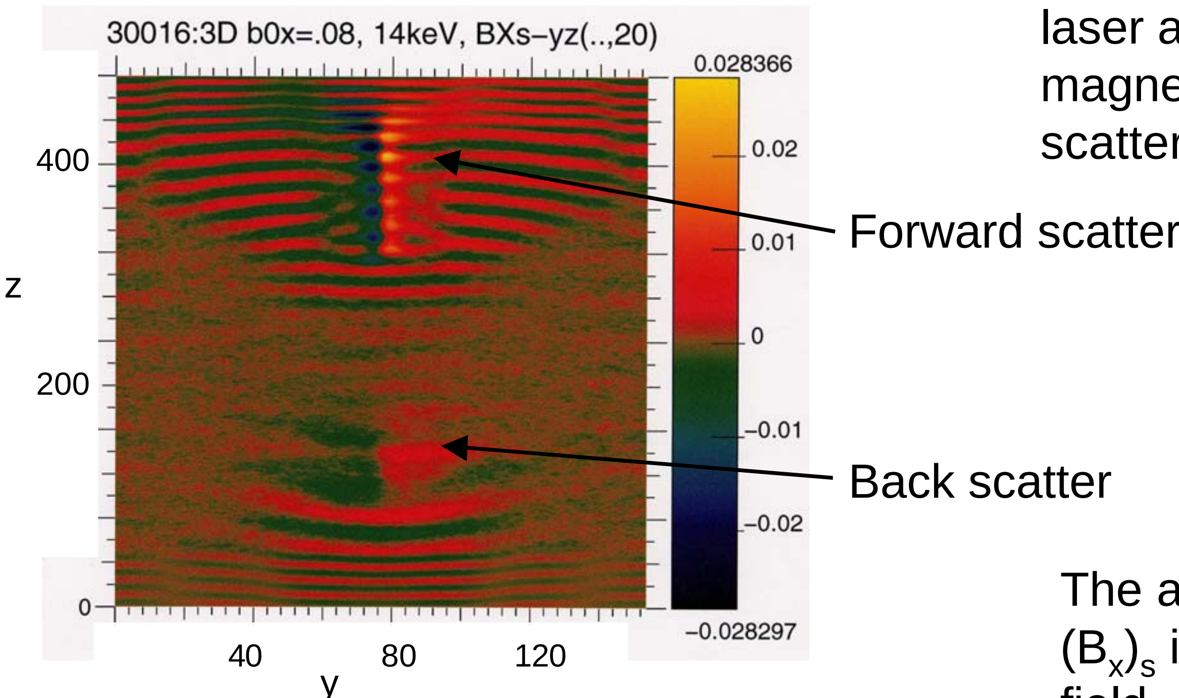

Filtering removes the incident laser and brings out the static magnetic fields and the Raman scatter.

The long wavelengths of the SRS forward and back scattered light are readily apparent.

The antisymmetric component of $(B_x)_s$ isolates the static magnetic field.

In 3D, find the B_x and B_y components of B_θ consistent with net $J_z < 0$.

3D, 0.2 nc, 14 keV, 7 x 10^{16} W/cm^2, linearly polarized (B_x, E_y)

Components of B_θ at 0.27 ps.

Antisymmetric component of $(B_x)_s$ vs (y,z) in the x/2 plane

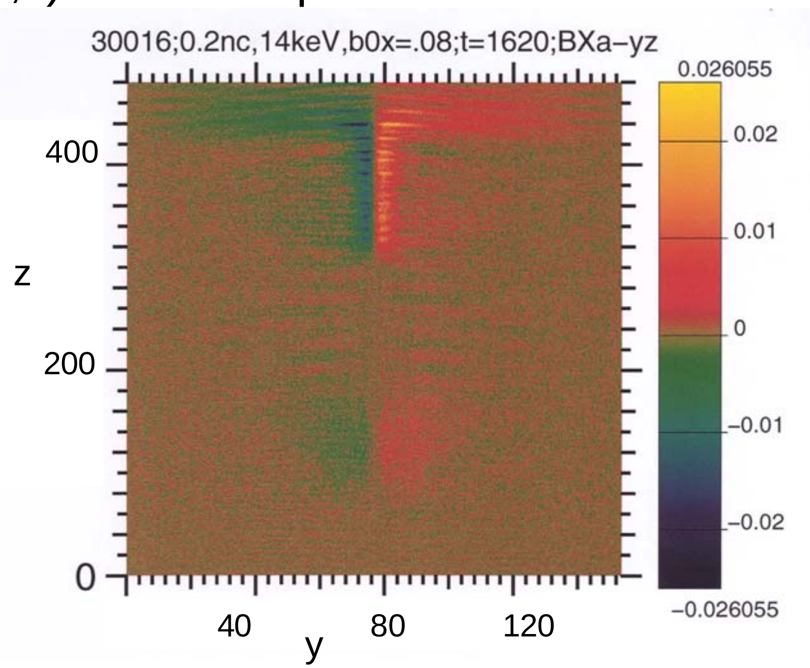

$(B_y)_s$ vs (x,z) in the y/2 plane.

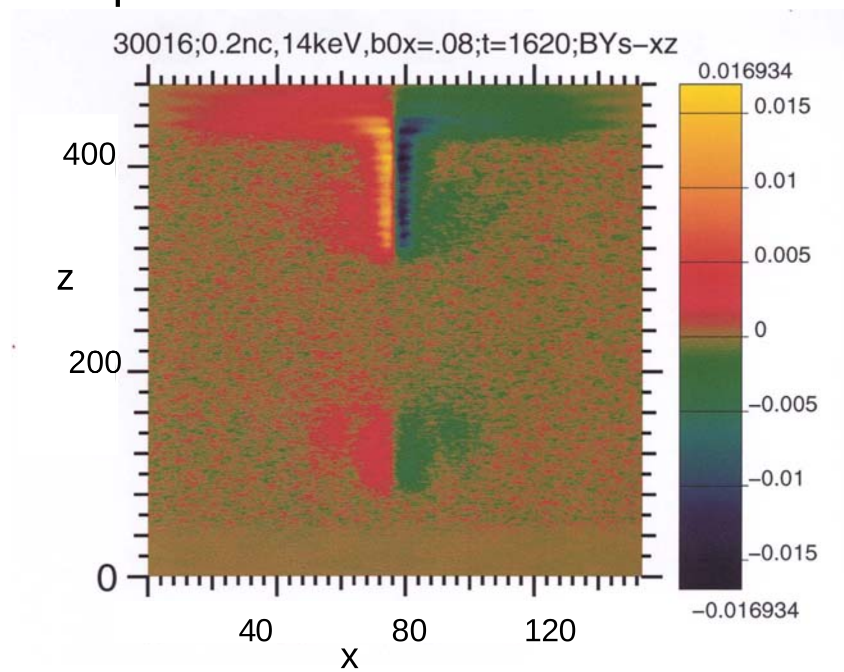

In these units, B = 0.02 corresponds to 6 MG.

We also have preliminary results on B-field generation in 2D simulations.

2D, 0.2 n_c, 14 keV, 7 x 10^{16} W/cm^2, linearly polarized (B_y, E_x); at 0.4 ps

$(B_y)_s$ vs (x,z)

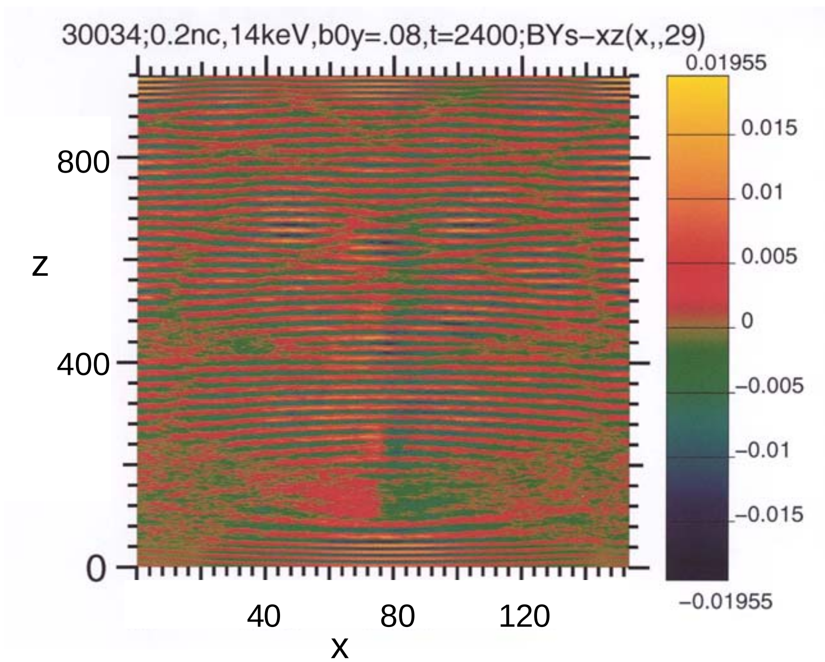

$(B_y)_a$ vs (x,z)

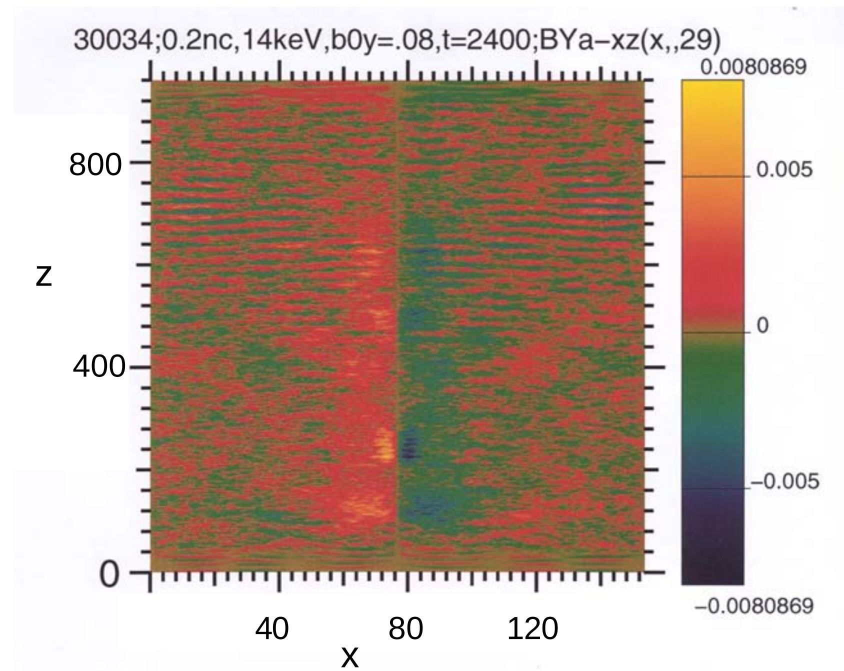

- Find the expected back and forward Raman scatter as well as the $(B)_s$
- In 2D, we can readily simulate bigger systems for longer times.

We find the B-field due to Raman Backscatter in simulations for parameters relevant to NIF ignition hohlraums.

Parameters; 2D; $0.2n_c$, 5 keV, 1 x 10^{16} W/cm^2 for blue light; an intense speckle

Filtered B_y vs (x, z) at y/2 shows Raman backscatter with static B-field superimposed; t=0.37ps

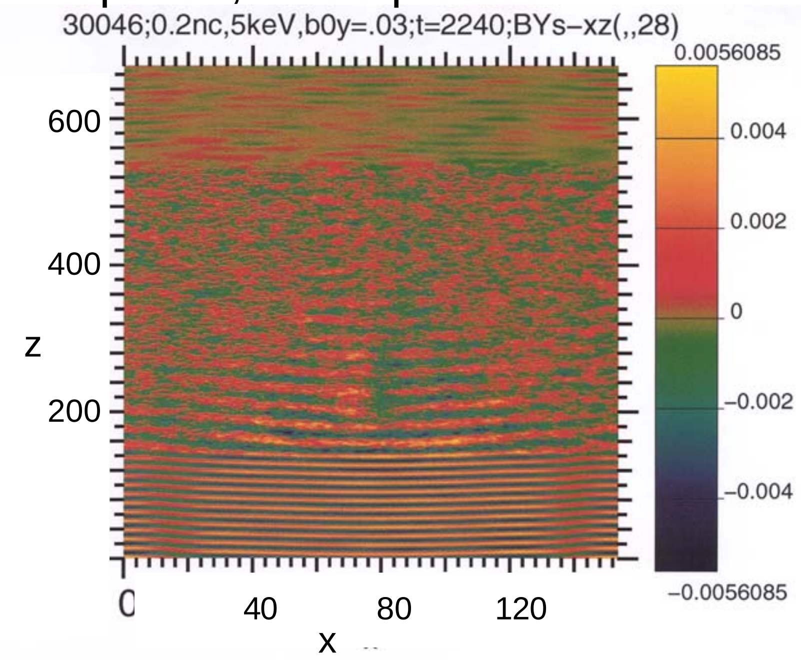

Antisymmetric part of filtered B_y emphasizes static B-field with peak ~ 1 MG.

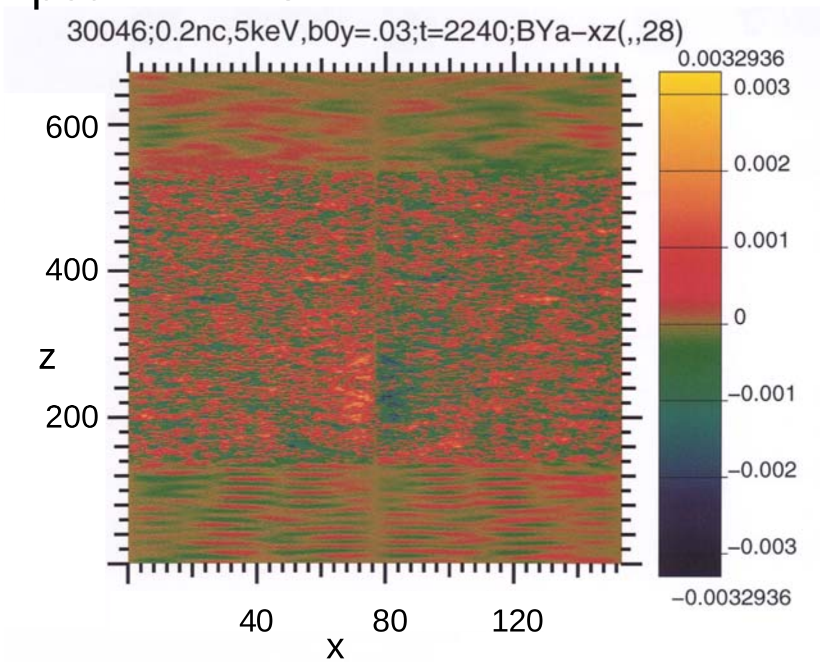

• 3D simulation with these parameters and 2D modeling at lower densities are underway.

Raman electrons are highly magnetized.

- The Larmor radius of electrons in MG field is smaller than an f/8 speckle width. Assume B_θ = .02 or 6 MG. Then an 80 keV hot electron has a Larmor radius of ~ $3\lambda_0$.
- This is less than a speckle width and in rough agreement with the narrow spatial extent of B_θ seen in the simulations.
- We estimate that the net current associated with B_θ is ~ Alfven current for the Raman forward scatter in the small hohlraum with laser-interactions parameters: 0.2 n_c, 14 keV, and I = 7 x 10^{16} W/cm^2 for blue light.

λ For NIF ignition hohlraum conditions, we expect mainly Raman backscatter and less energetic hot electrons. Extremely preliminary results indicate B_θ ~ 1 MG.

Static magnetic field structures due to Raman scatter have been identified in MPP 3D and 2D PIC simulations – a preliminary report.

- In laser light speckles, Raman Scatter, both forward and back, generate localized currents of forward going electrons.
- These currents (J_z) result in surrounding magnetic fields (B_θ).
- We have identified these magnetic fields in our MPP 3D and 2D PIC simulations with **Z3** for parameters associated with NIF high temperature hohlraums and NIF ignition hohlraums.
  - Large 2D and 3D PIC simulations with dedicated diagnostics are required for this effort.
- These magnetic fields are ~ MG and are large enough to confine the background electrons and hence affect electron transport in these plasmas.

λ Studies are underway to elucidate the complex spatial and time dependence of these magnetic fields.

If numbers of energetic electrons are the same from forward and back, expect more energetic currents and B-fields of greater magnitude from forward scatter since higher phase velocity of plasma waves leads to more energetic electrons.{rewrite}

Electron Transport Workshop

Purple Orchid Inn, Livermore, Ca

September 9-11, 2002

AN IMPROVED MODEL OF NONLOCAL HEAT FLOW IN LASER HEATED PLASMAS

Fathallah Alouani Bibi and Jean-Pierre Matte

INRS-Énergie, Matériaux et Télécommunications, Varennes, Québec, Canada J3X-1S2

OUTLINE

2 Talks for the price of 1

I) Nonlocal heat flow in plasmas heated by inverse bremsstrhalung.

Work of F. Alouani, Ph. D. student.

How the super-Gaussian deformation of the distribution function by the heating affects nonlocal heat flow.

II) Simulation of high intensity, long pulse, planar experiments.

Collaboration with D. Braun, J. Edwards and L. Suter of LLNL.

Preliminary comparison of an electron kinetic (FPI) simulation to LASNEX.

I) Nonlocal heat flow in plasmas heated by inverse bremsstrhalung

Work of F. Alouani, Ph. D. student.

How the super-Gaussian deformation of the distribution function by the heating affects nonlocal heat flow.

INTRODUCTION

- **Plasma heating by collisional absorption (IB) leads to super-Gaussian electron distributions.**

- Absorption preferably by slow electrons (because $\_{e\text{-}i} \propto v^{-3}$) => very superGaussian EVDF: $\exp[-(v/u(t))^5]$ (Langdon, Phys. Rev. Lett. **44**, 2717 (1980)).

- Collisional relaxation (e-e) tends to establish a Gaussian (Maxwellian) EVDF: $\exp[-(v/u(t))^2]$

- For finite _ ($\_=Z(V_{osc}/V_{th})^2$ = IB heating/e-e relaxation rate), the EVDF has shape $\exp[-(v/u(t))^m]$, where 2<m<5, m is an increasing function of _. (Matte, Lamoureux et al., P.P.C.F. **30**, 1665 (1988)).

This causes:

- Reduced absorption (Langdon, Phys. Rev. Lett. **44**, 2717 (1980)).

  Correction factor to IB absorption R, decrease from 1 to 0.45 as _ increases (*ibid*).
- Reduced thermal conductivity **(**Mora and Yahi, Phys. Rev. A **26**, 2259 (1982)).
- Increased sound speed (Afeyan *et al.,* Phys. Rev. Lett. **80**, 2322 (1998)).
- Reduced Landau damping for Langmuir waves (*ibid*).
- Reduced ionization and excitation rates (Alaterre *et al.*, Phys. Rev. A **26**, 2259 (1986)).

- **Needed:** accurate study of the resulting non-local effects, and their influence on the plasma macroscopic characteristics (temperature profiles, heat flux, etc…).

THE FOKKER-PLANCK SIMULATION CODE ("FPI")

- The "FPI" kinetic code is:

  1-D in space; slab geometry.

  2-D in V-space ($V,\mu=V_x/V$), Legendre expansion for μ.

- Included physical processes:

  - Advection (transport term: $V_x\, \partial F/\partial x$)
  - Space charge field for quasi-neutrality, and acceleration ($-eE/m\, \partial F/\partial V_x$)
  - Fokker-Planck term for e-i and e-e collisions
  - Heating by Collisional absorption (IB).

    Prescribed laser intensity, Gaussian in x and t.

PARAMETERS OF THE RUNS AND DIAGNOSTICS

- Laser heated plasma: N_e=2x10^{20} cm^{-3} (N_c/20), T_e=500 eV. (Initially uniform)

- Atomic number: Z= 4, 11, 20.

- Laser wavelength 0.53 _m, intensities from 10^{15} to 8x10^{15} W/cm^2 , with FWHM's from 38 to 4.75 _m. Temporal FWHM was 200 psec in all cases.(I_0*FWHM=10^{15} W/cm^2*38 _m)

- The Legendre polynomial expansion was to order 3.

COMPARED MODELS

The FPI results are compared with those obtained by using:

- Flux-limited diffusion with *f* equal to 0.03, 0.05, 0.1 and 0.5.
- Nonlocal models from literature:

1) Luciani-Mora (LMV) nonlocal heat flow (PRL **51**, 1664 (1983))

2) Bendib, Luciani *et al.* nonlocal heat flow with propagator correction due to the electric field (Phys. Fl. **31**, 711 (1987))

3) Epperlein-Short (ES) nonlocal heat flow (Phys.Fl. B **4**, 2211 (1992))

4) Our new delocalization model including non-Maxwellian heating effects.

RESULTS AND DISCUSSION

• Temperature and heat flux profiles:

- Neither of the earlier fluid models correctly reproduces FPI's $T_e(X,t)$.
- LMV: Delocalization kernel far too small for high $k\lambda_e$.
- Even taking into account the effect of the electric field as in Bendib *et al.*, the differences with FPI are still considerable.
- ES: Closer to FPI, but lower near x=0 (center of laser beam).
- Flux limiters: All flat near x=0, sudden drop some distance away. (higher f: lower T_e maximum but wider). At x=0: f=0.10 matches ES and f=0.05 matches FPI.
- AM: The newly developed model gave a good fit of the temperature profiles for the three cases: immobile ions, mobile ions, mobile ions with the ponderomotive force.

Reason: Our new nonlocal model takes into account the variation of $k\lambda_e$ **AND** of _ = $Z (V_{osc}/V_{th})^2$.

- **Nonlocal kernel:**

The non-local heat flux can be expressed as a convolution over the Spitzer-Harm flux with a non-local kernel:

$$q(x) = \beta^{-1}(x) \int_{-\infty}^{+\infty} q_{SH}(x') \frac{w(\xi(x,x'))}{\lambda_e(x')} dx'$$

By making a small laser intensity perturbation (~1%), we obtained a new propagator:

$$\tilde{w}(k\lambda_e, \alpha(k\lambda_e)) = \frac{\tilde{q}(k\lambda_e, \alpha(k\lambda_e))}{\tilde{q}_{SH}(k\lambda_e, \alpha(k\lambda_e))}$$

Approach pioneered by Epperlein and Short (Phys. Rev. E, 1994)

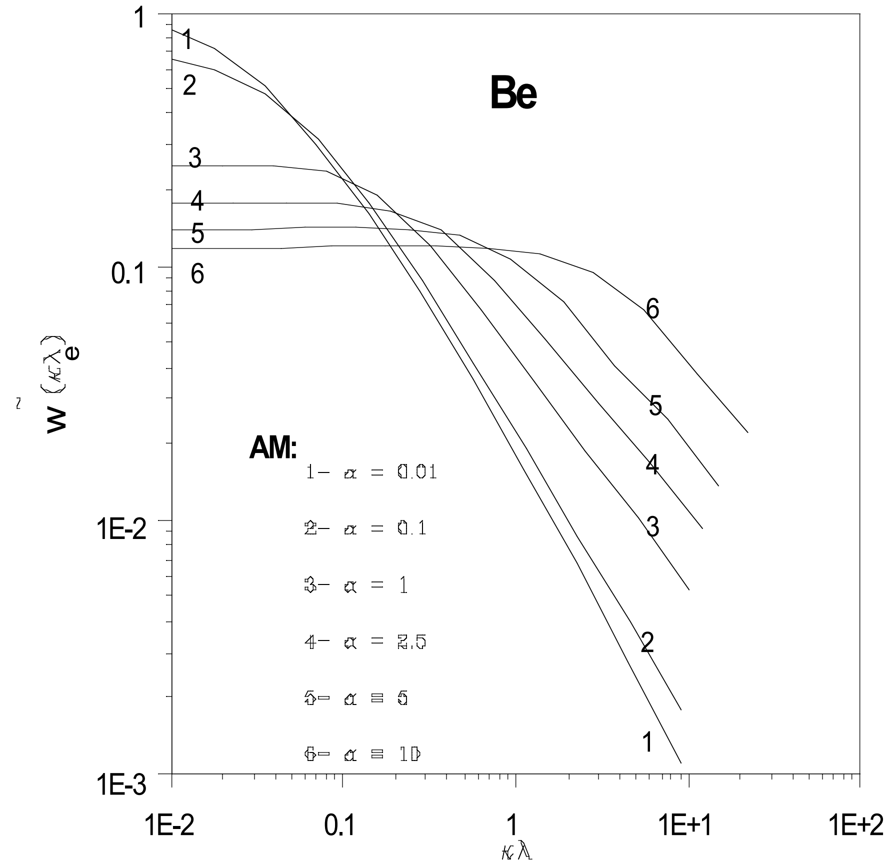

Heath flux propagators for different electron velocity distribution functions, i.e. different _.

Comparison of FPI and flux limiting for T_e profiles.

$T_e(x,t_0)$ temerature profile at the peak of the pulse:

FPI; Flux limiters , in Al for $T_e(x,0)$=0.5 keV, N_e=0.2x10^{21} cm^{-3}.

Laser intensity = 10^{15} W/cm^2, at pulse maximum (t_0=200 ps), FWHM = 38 _m.

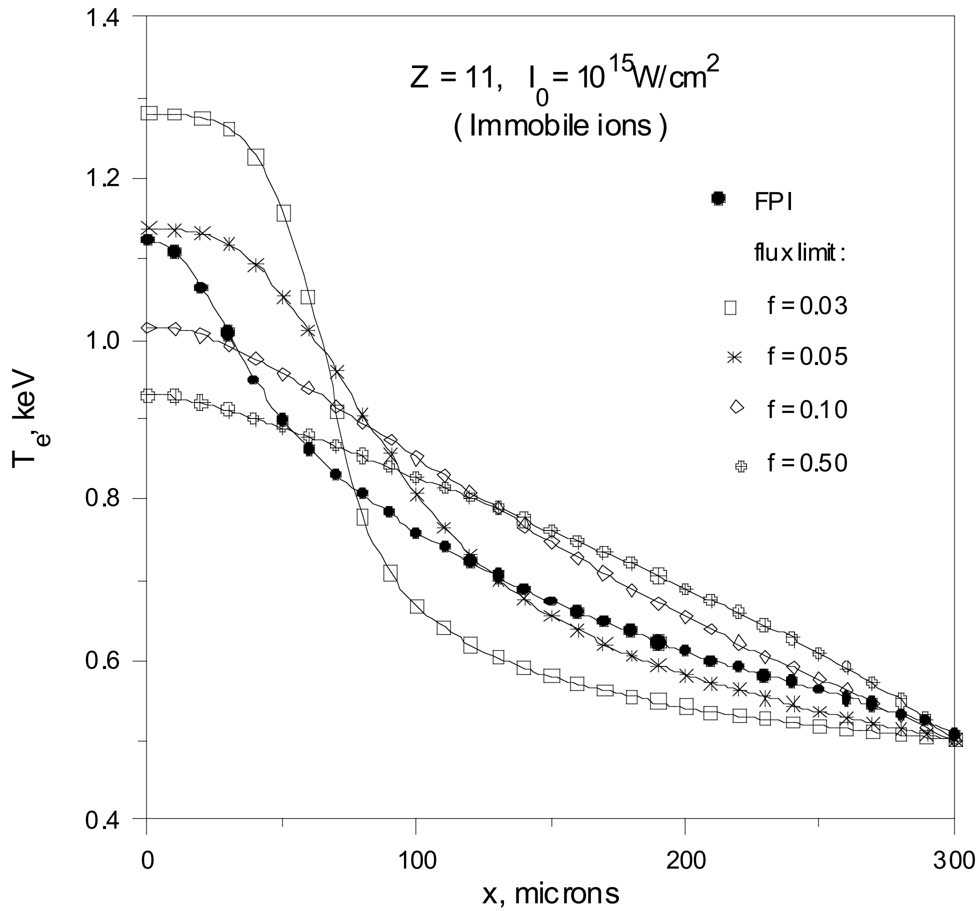

Temperature and heat flux profiles in plasma irradiated by 10^{15} W/cm^2 laser beam, at the pulse maximum (200ps) and with FWHM equal to 38 _m, the ions are considered immobile:

Comparison of FPI, the our model and some other nonlocal models.

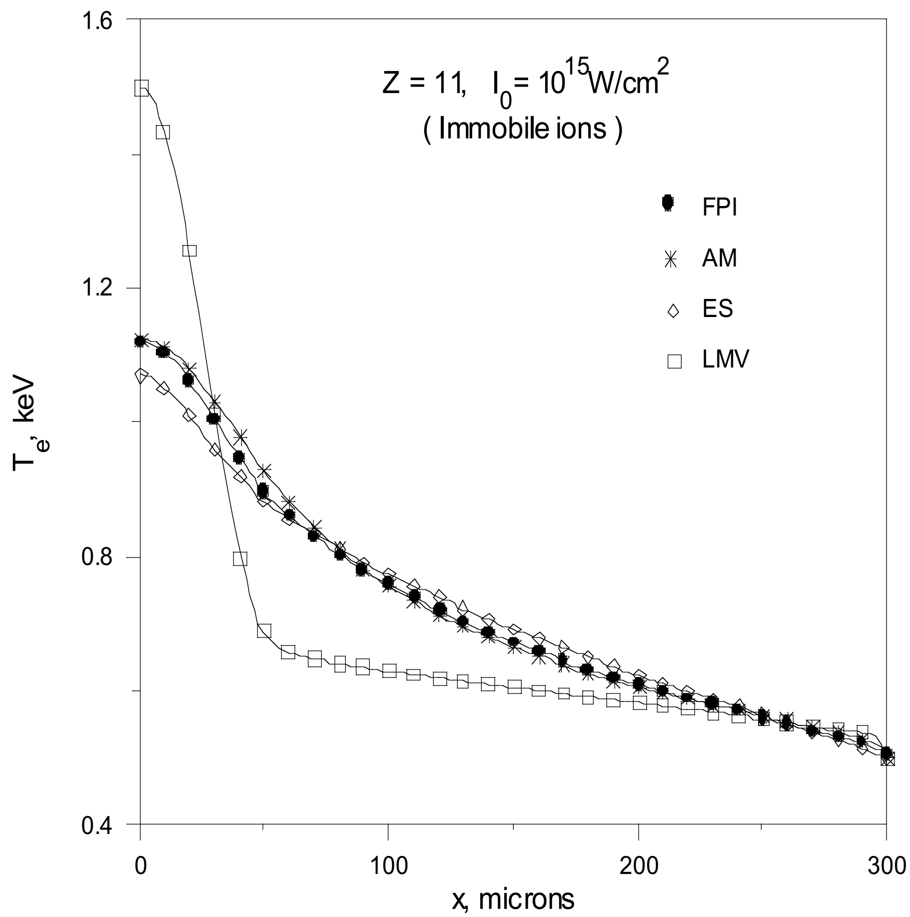

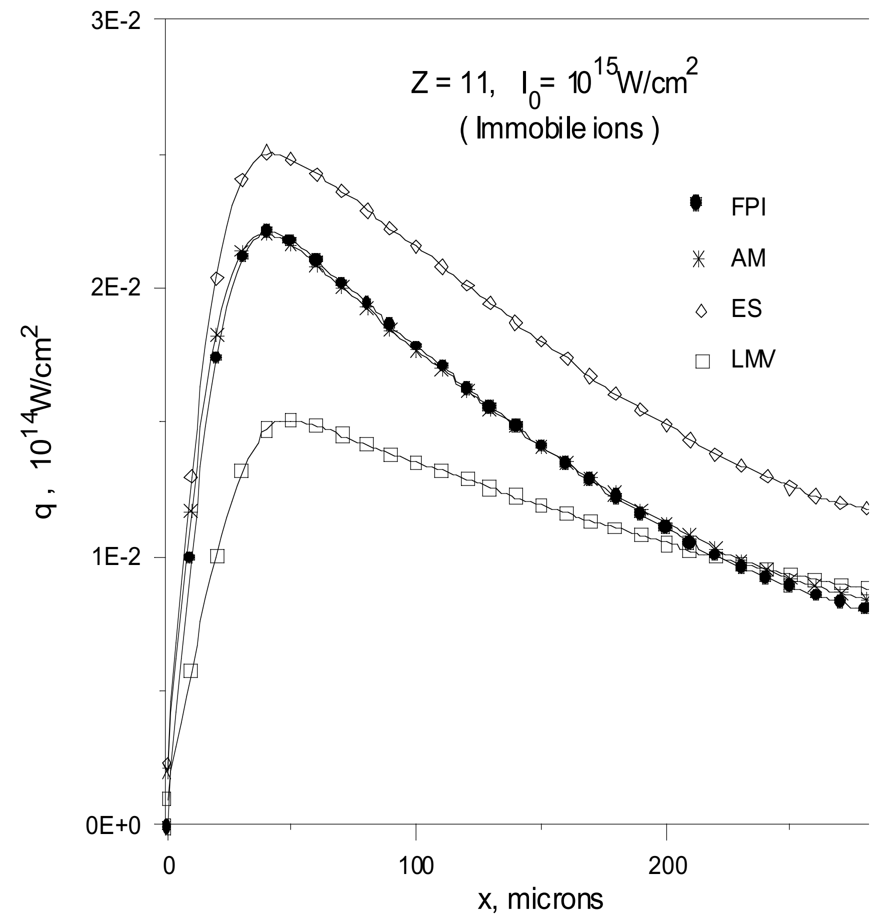

Temperature and heat flux profiles in plasma heated by 10^{15} W/cm^2 laser beam, at the pulse maximum (200ps) and with FWHM equal to 38 _m, the ions are mobile:

Comparison of FPI, the our model and some other nonlocal models.

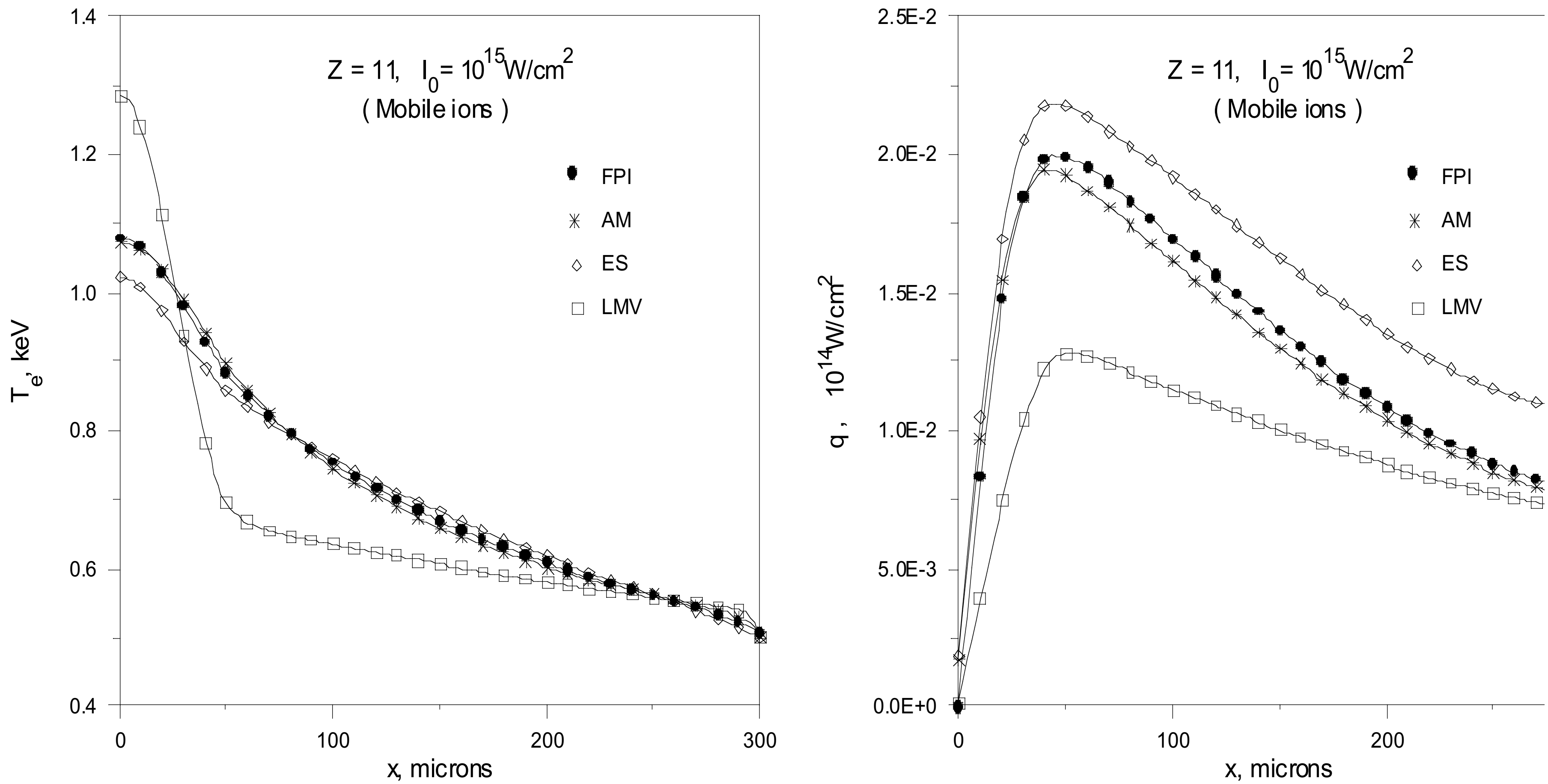

Temperature and heat flux profiles in plasma irradiated by 10^{15} W/cm^2 laser beam; at the pulse maximum (200ps) and with FWHM equal to 38 _m, the ions are mobile and the ponderomotive force is taken into acount: Comparison of FPI, the our model and some other models.

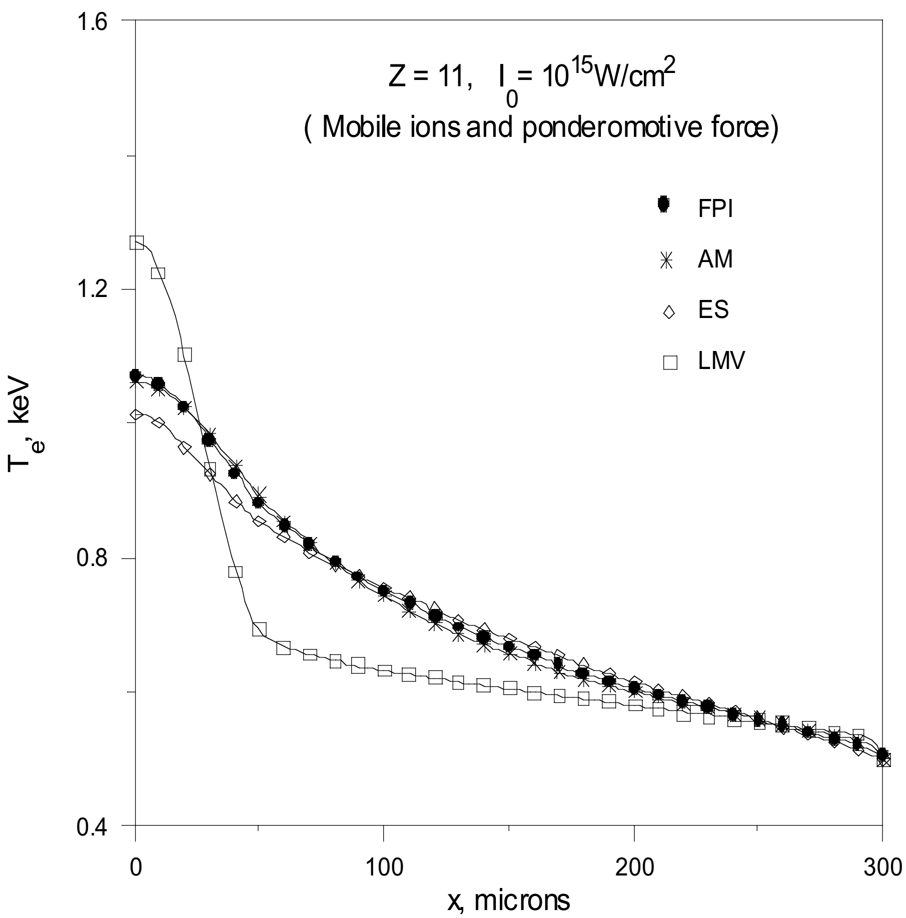

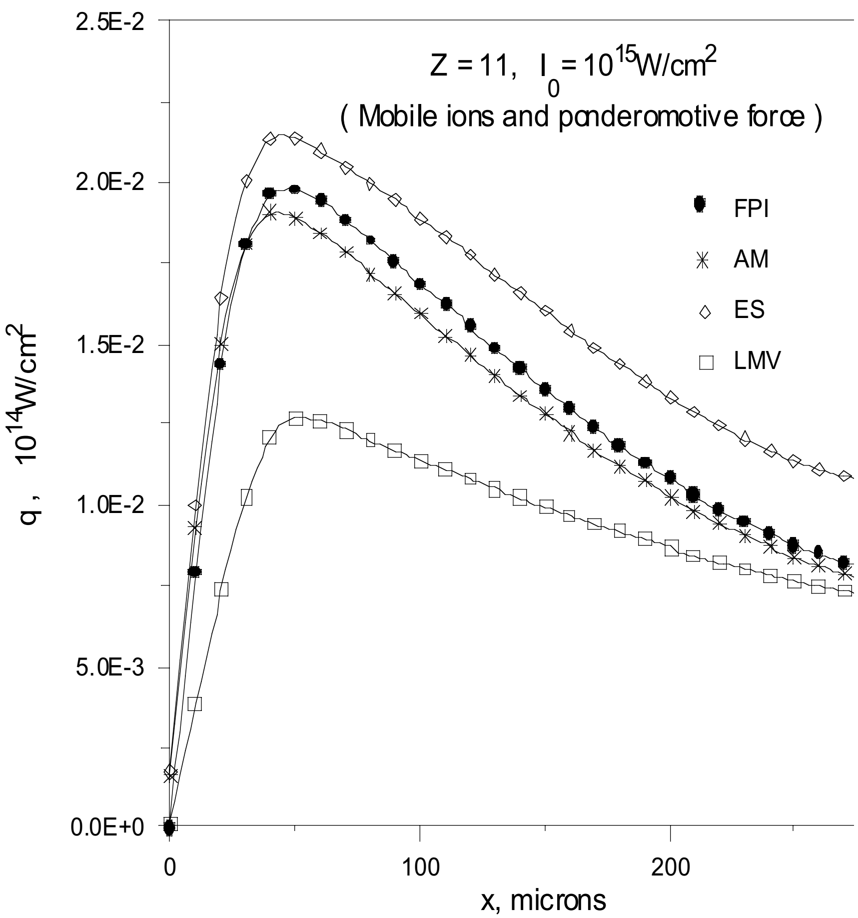

Filamentation growth rate in laser heated plasmas

Ponderomotive + Thermal

Spatial growth rate = $$K=\frac{k_\perp}{2\sqrt{\varepsilon}}\left\{2\frac{n}{n_c}\left[\gamma_P+\gamma_T\left(\frac{\kappa_{SH}}{\kappa}\right)\frac{\omega^2}{k_\perp^2c^2}\right]-\frac{k_\perp^2c^2}{\omega^2}\right\}$$

$k_\perp$: perturbation wave number perpendicular to the beam

_ : the laser frequency, _=1-n/n_c,

Ponderomotive filamatation: $\gamma_P=\frac{ponderomotive\ \ pressure}{plasma\ thermal\ \ pressure}$,

Thermal filamentation: $\gamma_T=\frac{inverse\ bremsstrahlung\ \ heating\ rate}{thermal\ \ conduction\ rate\ across\,(c/\omega)}$

Compare effects of two nonlocal conductivities:

Epperlein-Short (_ = _ES)

Our new model (_ = _AM)

Results

1- Low intensity (case 1), i.e. when the EVDF is Maxwellian:

Both models agree and agree with experiments (P.E. Young, Phys. Plasmas (1995))

2- High intensity (case 2), i.e. . when the EVDF is non-Maxwellian, due to I.B.

High k: E-S model predicts large enhancement above ponderomotive growth.

Our model: No enhancement, due higher _ at high k.

Case 1: I_0=10^{13}W/cm^2, λ_0=1.06μm, T_e=0.8keV, n/n_c=0.1, Z=5.3.

Case 2: I_0=2.5×10^{15}W/cm^2, λ_0=1.06μm, T_e=2 keV, n/n_c=0.1, Z=20.

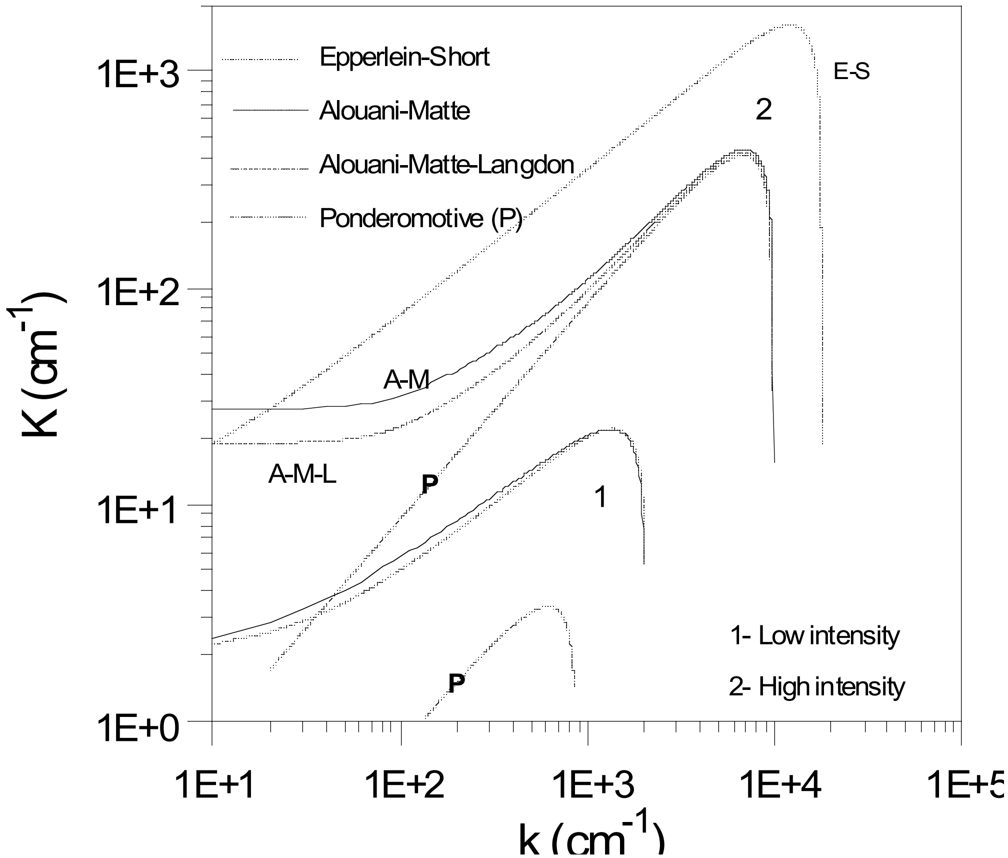

INRS- Énergie, Matériaux et Télécommunications

Distribution functions at maximum laser intensity (in x and t)

F_0 in He-like Al for $T_e(x,0)$=0.5 keV, N_e=0.2·10^{21} cm^{-3} (N_c/20) , FWHM = 200 ps

A- I_0 = 10^{15} W/cm^2 ,FWHM = 38 _m;   **B-** 8·10^{15} W/cm^2 , 4.75 _m;.

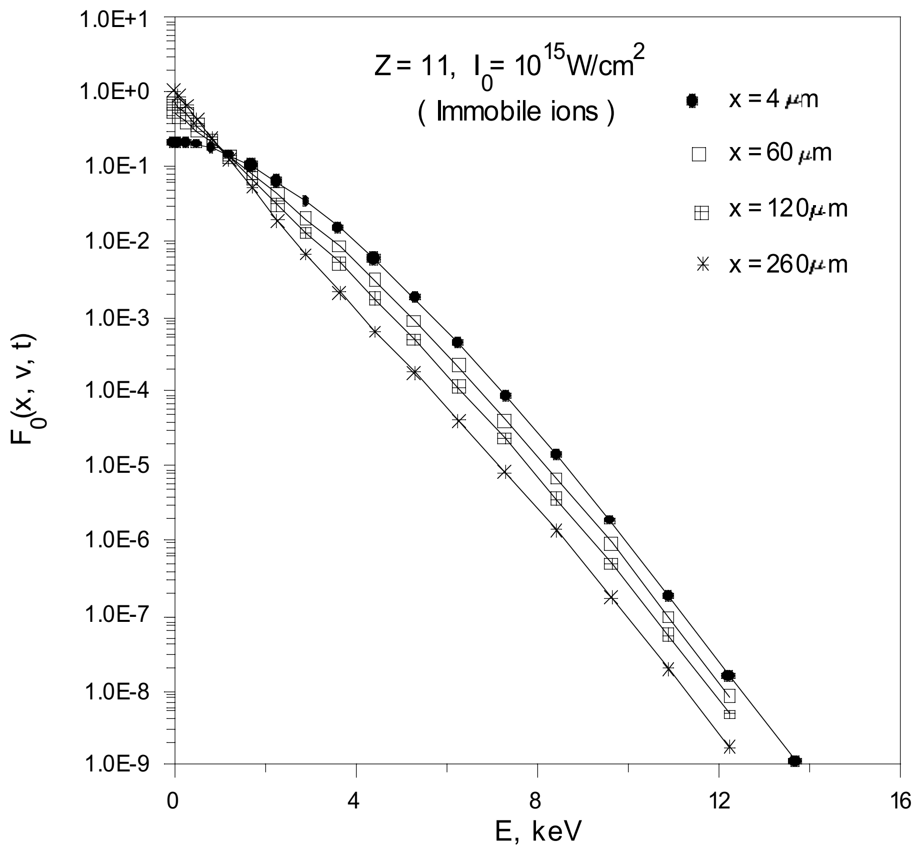

A

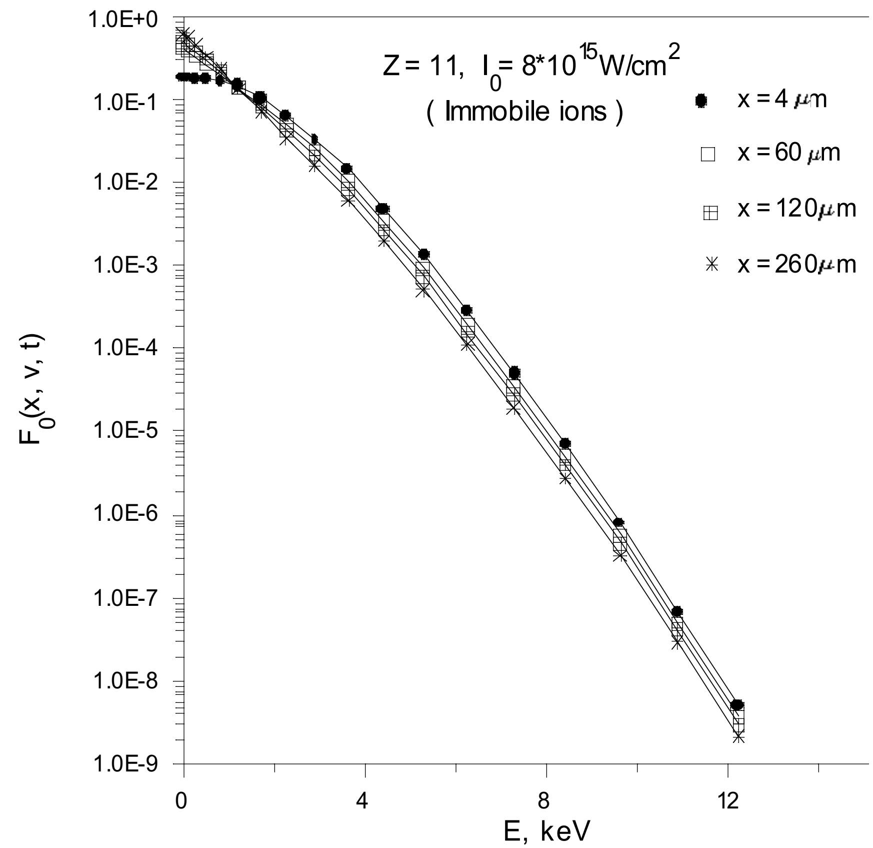

B

Estimating the EVDF deformation

Method analogous to that for heat flux :

f_0(x,v,t): Convolution of local Maxwellians.

$$f_0(x,v)=\int_{-\infty}^{+\infty} g(\xi(x,x'),\alpha(x'),v)\, f_M(x',v)\, dx$$

Kernel *g(_,_,v)* depends on _ **and** *v*

Obtained from FPI perturbation runs

$$\tilde{g}(k,\alpha,v)=\tilde{f}_0(k,\alpha,v)/\tilde{f}_M(k,v)$$

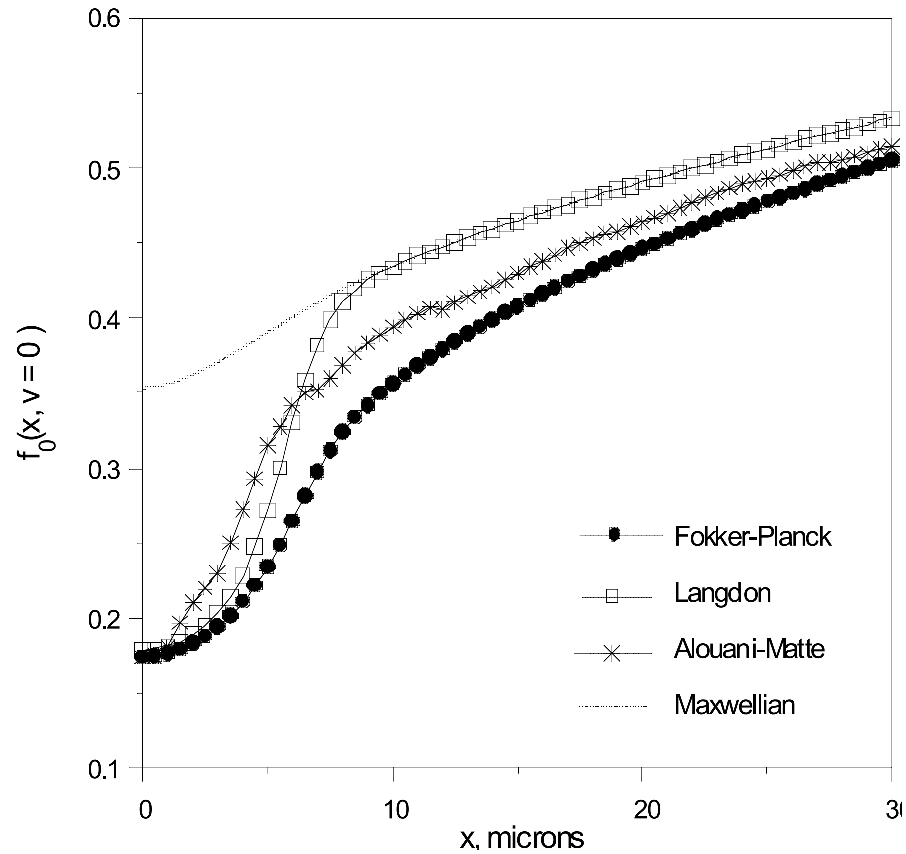

F_0 *(x=0,v=0),* in Al for $T_e(x,0)$=0.5 keV, N_e=0.2x10^{21} cm^{-3}, I_0 = 10^{15} W/cm^2 , at pulse peak,

FWHM's: 38 _m; 200 ps.

Needs further improvement

Super-Gaussian indices *m* from fits to FPI $F_0(x=0,v, t=t_0)$ (at pulse peak)

(Fits weighted for thermal electrons)

A- $I_0 = 10^{15}$ W/cm^2, t_0 = 200 ps, FWHM's: 38 _m; 200 ps. **B**- 8x10^{15} W/cm^2; 4.75 _m.

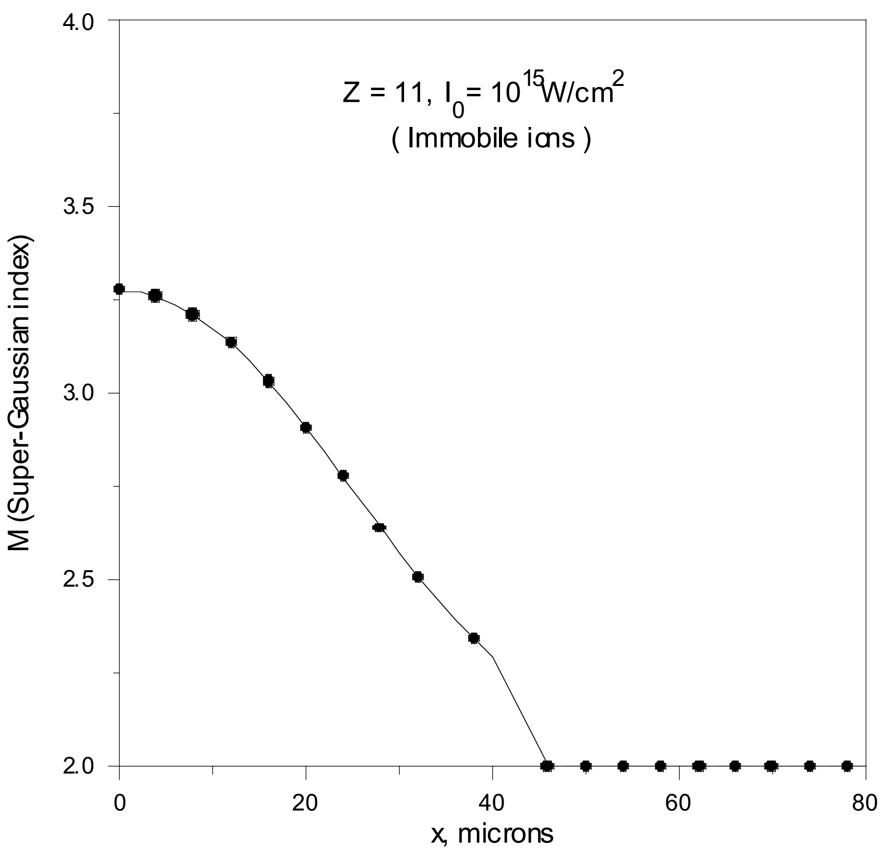

A

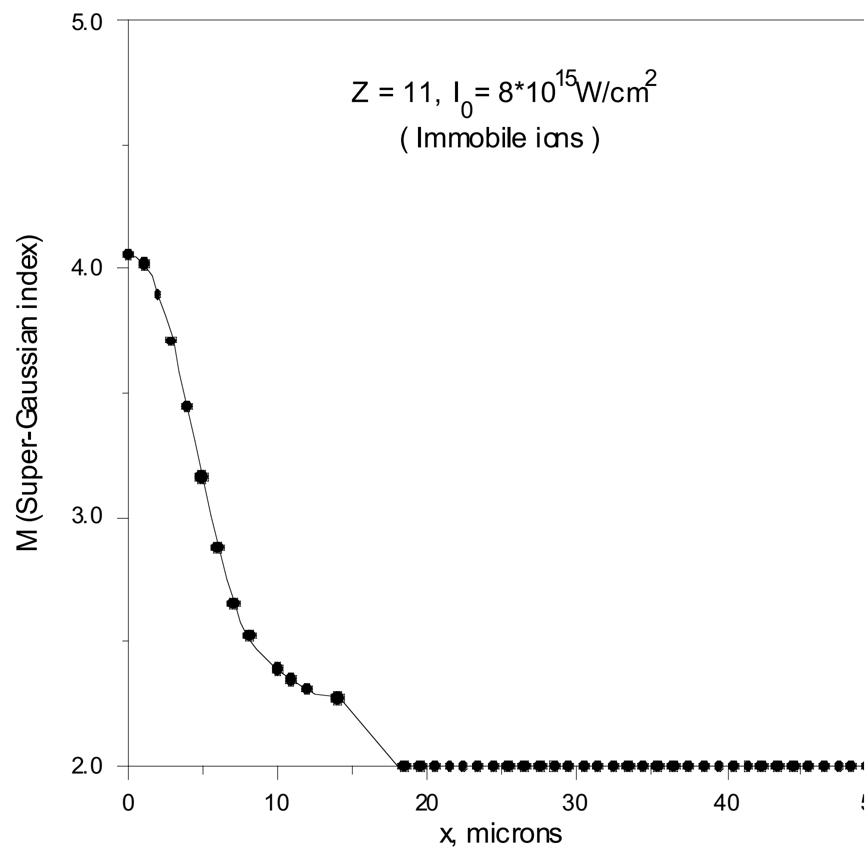

B

$F_1\ V^5$ in Al At pulse peak for $T_e(x,0)$=0.5 keV, N_e=0.2x10^{21} cm^{-3}, $\frac{n_e}{6}\int_0^\infty F_1(x,v,t)v^5\,dv = Q_e(x,t)$.

A- $I_0 = 10^{15}$ W/cm^2 FWHM's: 38 _m; 200 ps. **B**- 8x10^{15} W/cm^2 ;4.75 _m; 200 ps.

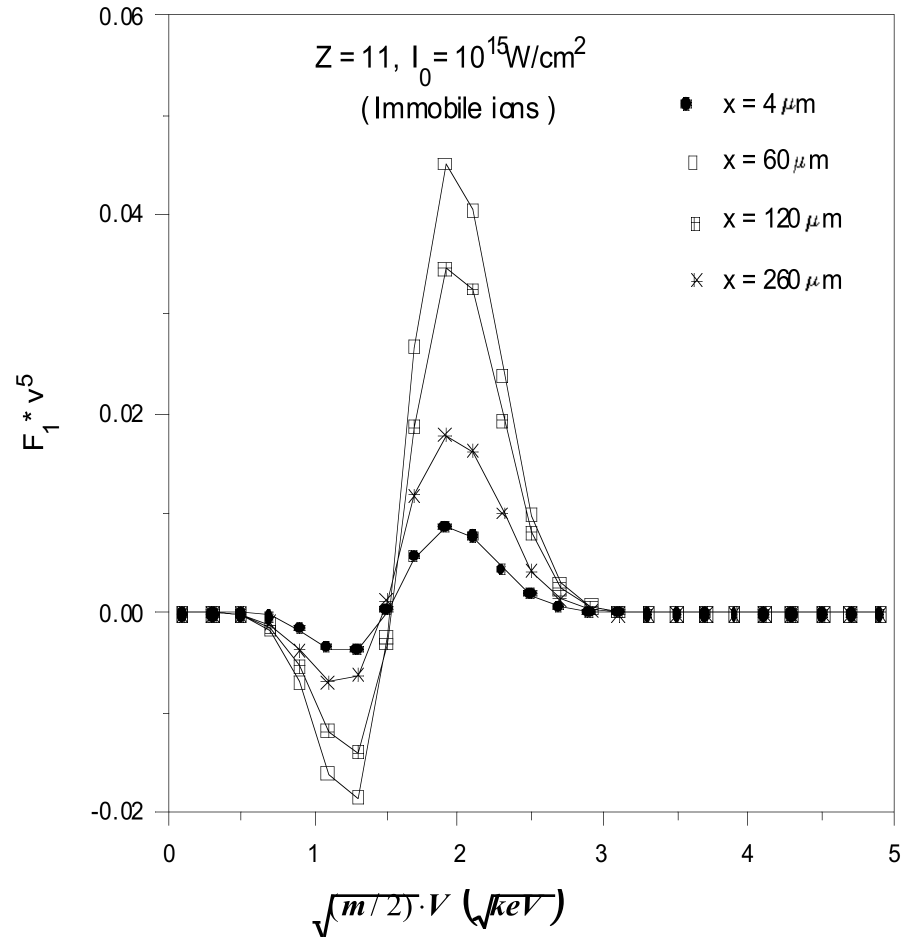

A

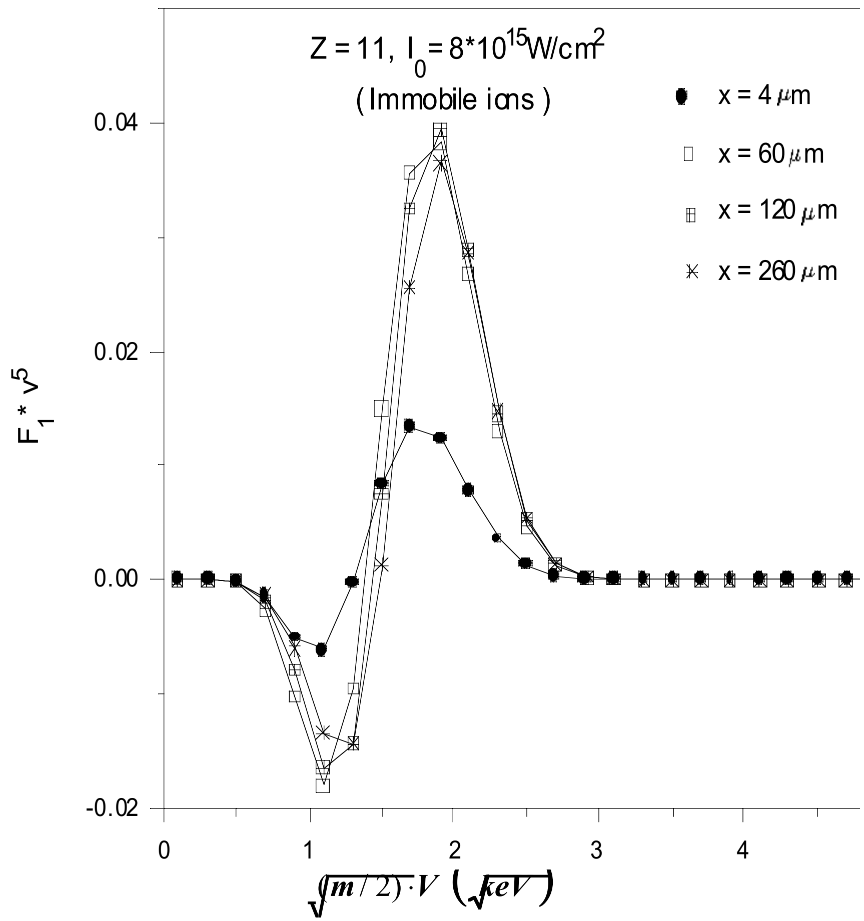

B

CONCLUSIONS TO PART I

- Flux limited diffusion temperature profiles do not match FPI's.
- Neither of the earlier delocalization formula reproduces FPI temperature and heat flux profiles well enough.
    - 1st Luciani-Mora (LMV) formula inhibits heat flux too much at high $k\lambda_e$.
    - Epperlein-Short (ES) formula does not inhibit it quite enough.
    - Thermal filamentation is weaker than calculated by ES.
- Our new nonlocal model shows that in presence of strong collisional heating, i.e. when the electron velocity distribution function super-Gaussian, there are great changes in the filamentation grow rate especially at higher wave vectors *k*, that cannot be predicted by a Maxwellian theory. Another important remark deduced from our model is that the ponderomotive mechanism of filamentation becomes dominant compared to the thermal one.

- The new nonlocal approach reproduces the Fokker-Planck results well in the presence of strong or weak collisional heating in laser created plasma. Our formula for the isotropic component (F_0) at low velocity of the electron distribution function showed a fair agreement with the Fokker-Planck solution (FPI).

  Some improvement still necessary, especially for higher velocities.

II) Simulation of high intensity, long pulse, planar experiments.

Collaboration with D. Braun, J. Edwards and L. Suter of LLNL.

Preliminary comparison of an electron kinetic (FPI) simulation to LASNEX

Physical situation:

Initially: Flat, solid carbon target.
Fully stripped (no atomic physics).
$N_{e0} = 6.8x10^{23}$ cm^{-3} ; T_{e0} = 100 eV.
Normal incidence.
WKB approximation for absorption.
Warm, fluid ions.
Laser beam: $\_{0}$ = 0.35µm, 1 nsec "square" pulse, 10^{16} W/cm^2 .
0.0-0.1 nsec: linear rise
0.1-0.9 nsec: constant at 10^{16} W/cm^2
0.1-1.0 nsec: linear decrease .

LASNEX profiles of N_e, T_e, T_i, and V_{hydro} at t=0.1 nsec read by FPI.
Interpolated onto FPI's Eulerian grid (_x = 0.25µm).
Run FPI for 0.2 nsec, up to t=0.3 nsec.
(Simulation box is increased gradually, on the low density side)
Legendre polynomial expansion carried to order 3.
Compare profiles at t=0.3 nsec.

OBSERVATIONS

Much more ablation in FPI run: (approx. 9µm, vs 5 µm).
Effect of nonlocal heat flow (preheat).
Similar results were obtained at lower intensity by LLE (APS2001) and ILE (PF B, 1992 ; PRL 2002).

T_e profile: About the same near critical (6 keV)
Lesser drop at very low density.
T_i is lower in the corona, for FPI.

Initial state for FPI: 0.1 ns output from LASNEX. (+ V_{hydro}, not shown)

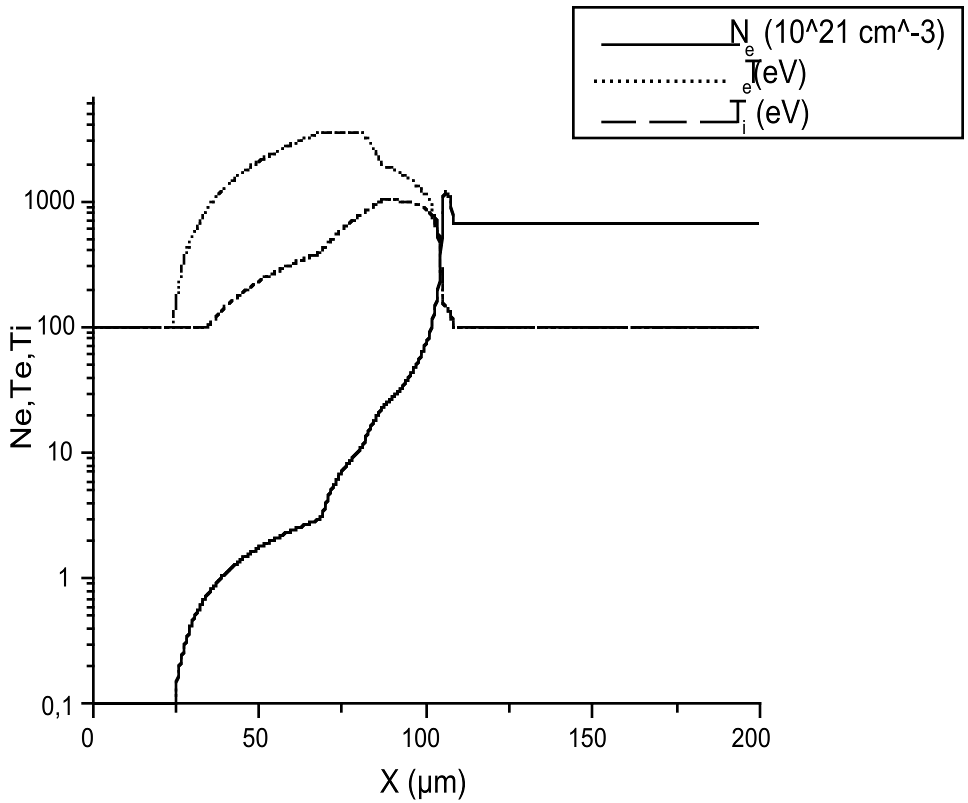

0.3 ns output from LASNEX. (N_e: 10^{21} cm^{-3} ; T_e,T_i: eV)

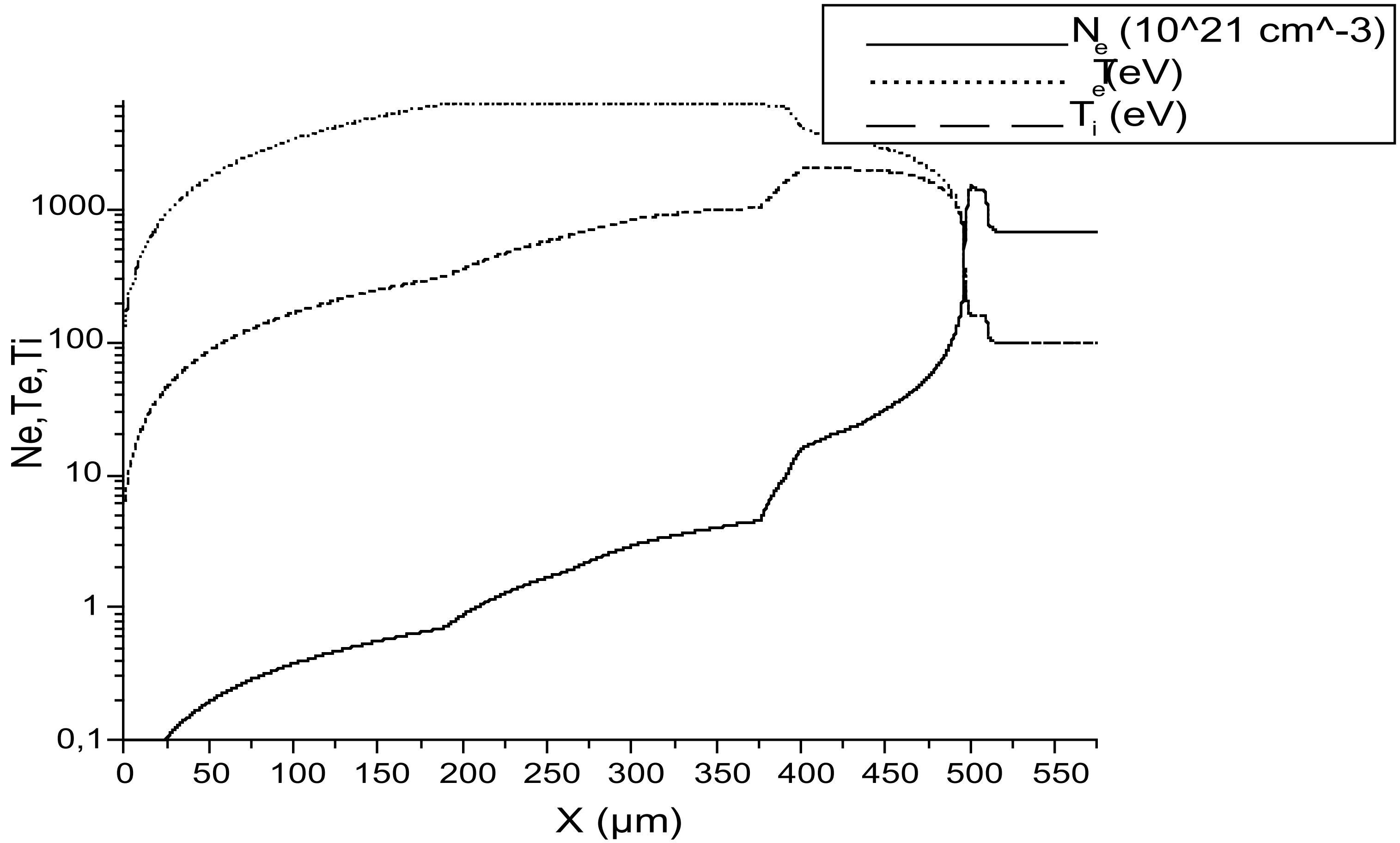

0.3 ns output from FPI. (N_e: 10^{21} cm^{-3} ; T_e,T_i: eV)

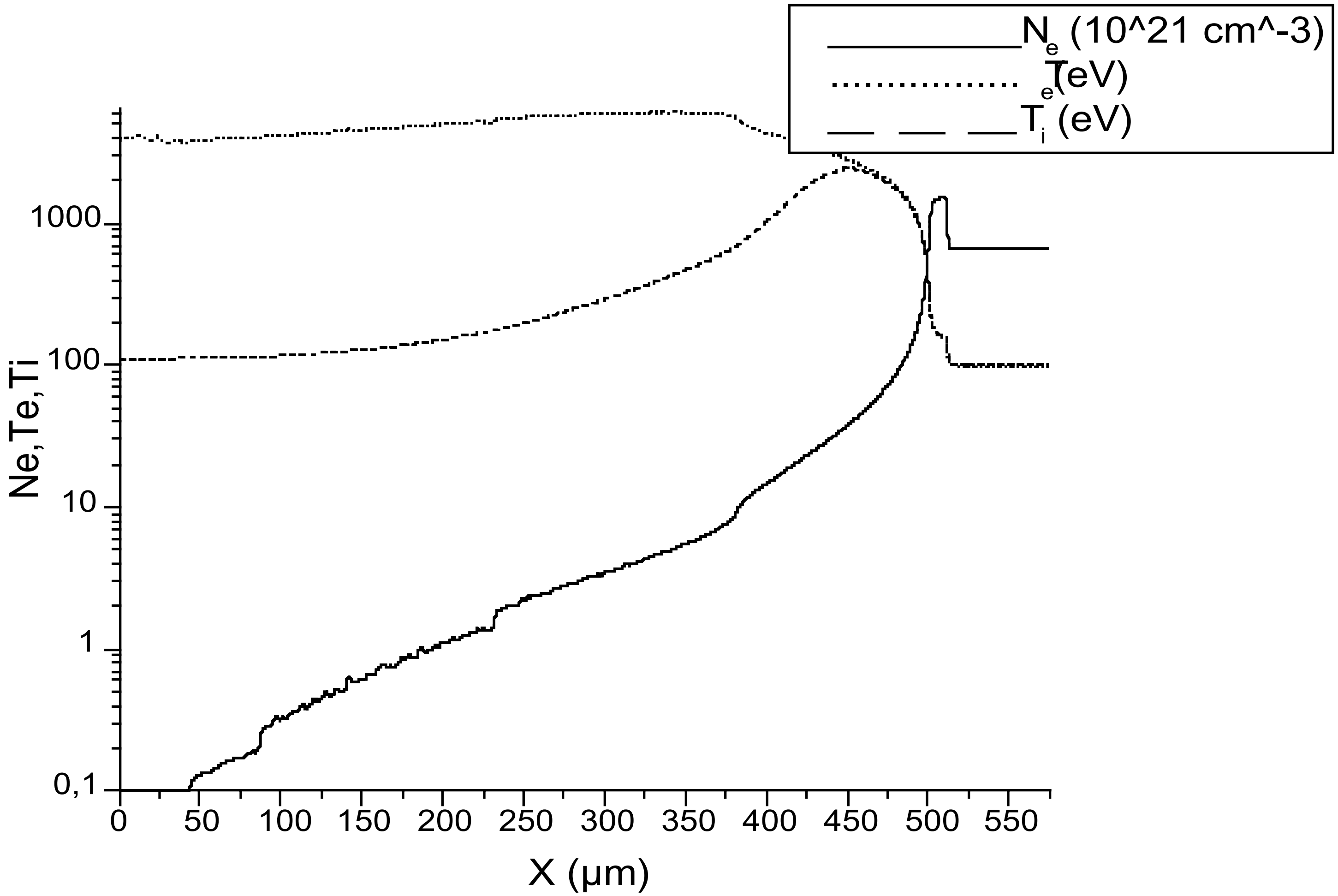

Lagrangian plots: (exclude unperturbed solid) LASNEX , 0.3 nsec

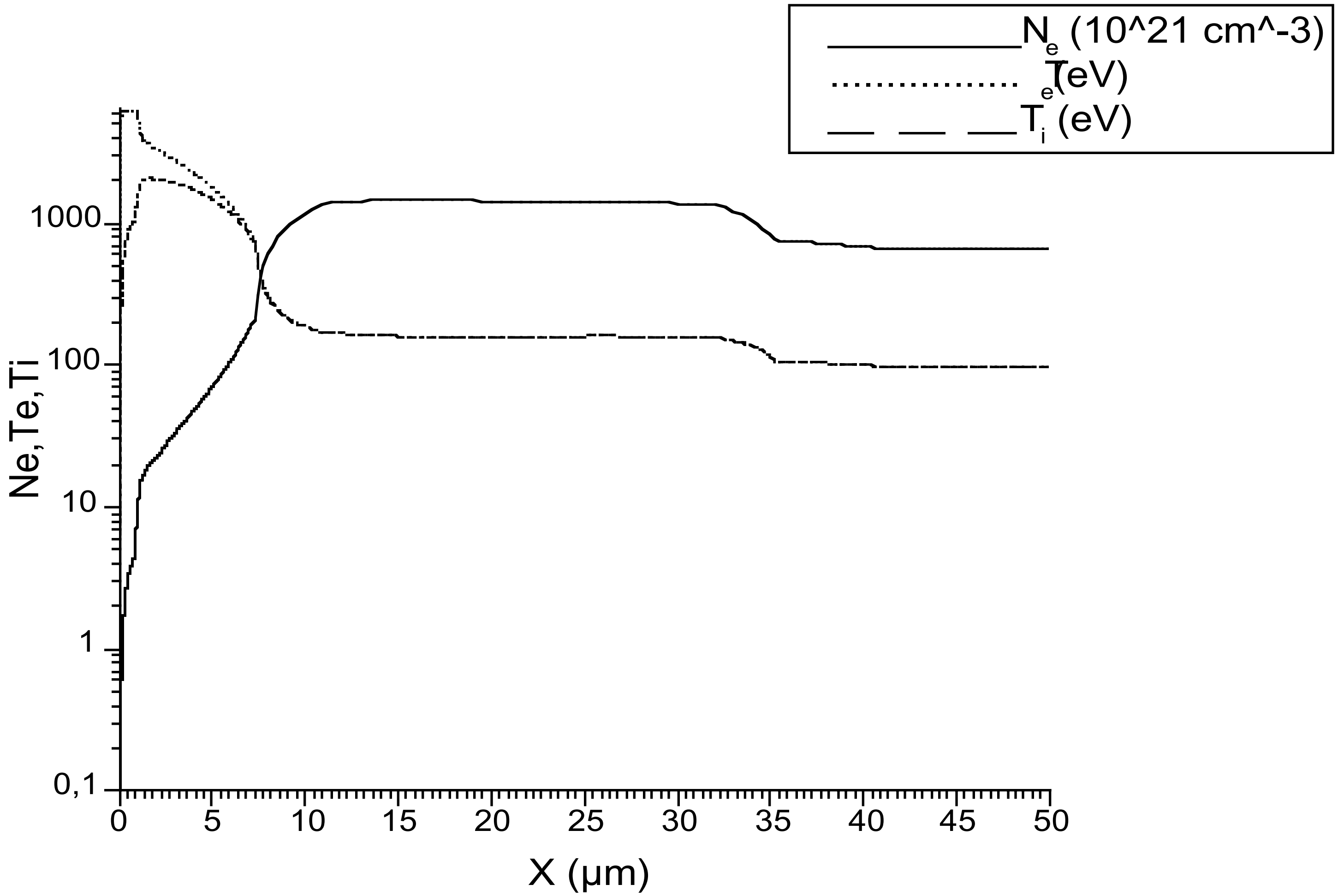

Lagrangian plots: (exclude unperturbed solid) FPI , 0.3 nsec

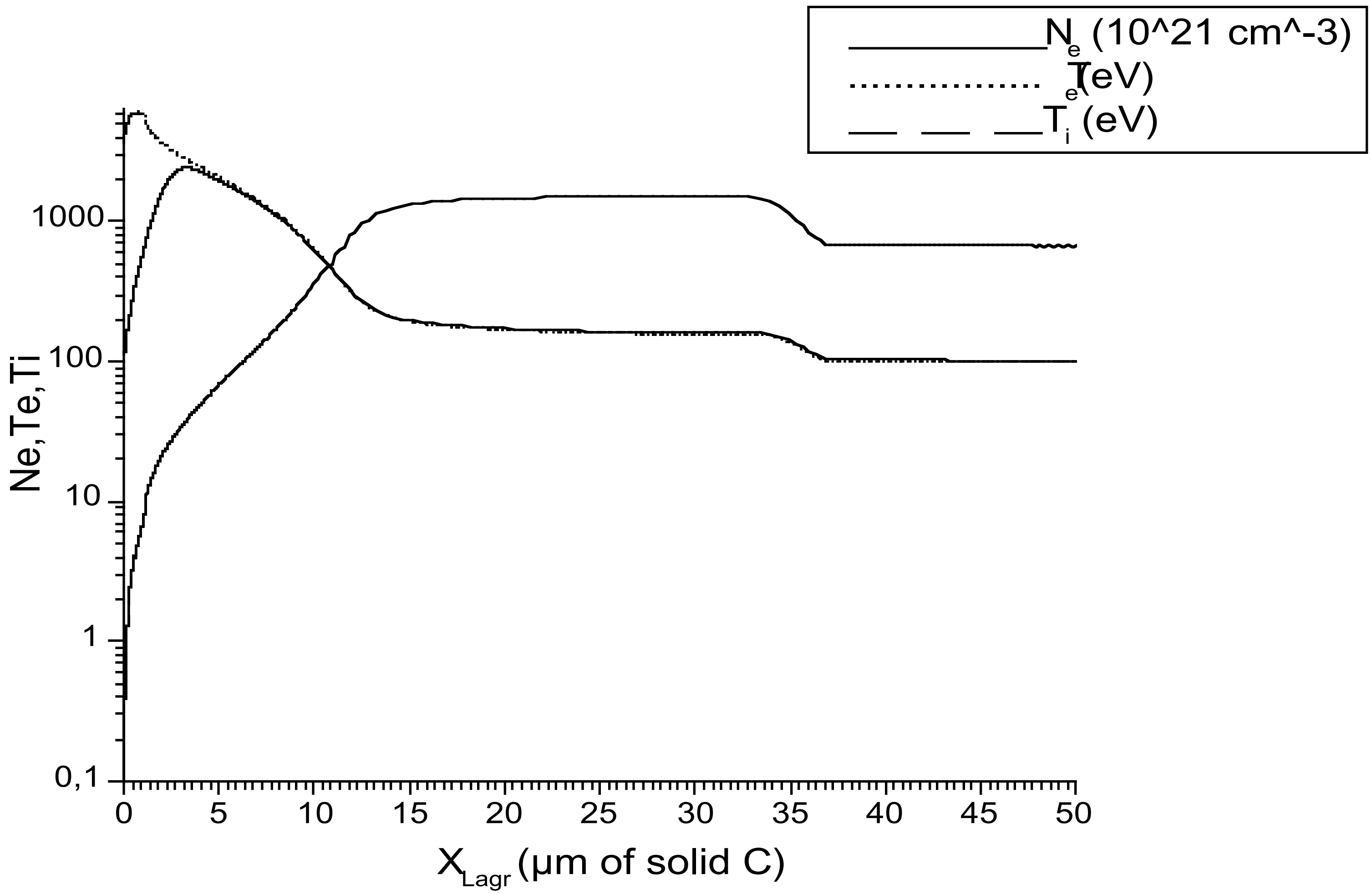

Distribution function plots $F_0(x,v,t)$ vs $m_e v^2/2$

$F_0(x,v,t)$: Angle averaged velocity distribution function

We will compare $F_0(x,v,t)$ to $F_{Maxw}(x,v,t)$

where $F_{Maxw}(x,v,t)$ is a Maxwellian of same N_e and $T_e=2/3\langle v^2\rangle$

Cell IX=1379; N_e=5.3_10^{21} cm^{-3} (0.59 N_c) ; T_e= 6141 ev (maximum T_e)

See a SuperGaussian (DLM) distribution up to 50 keV.

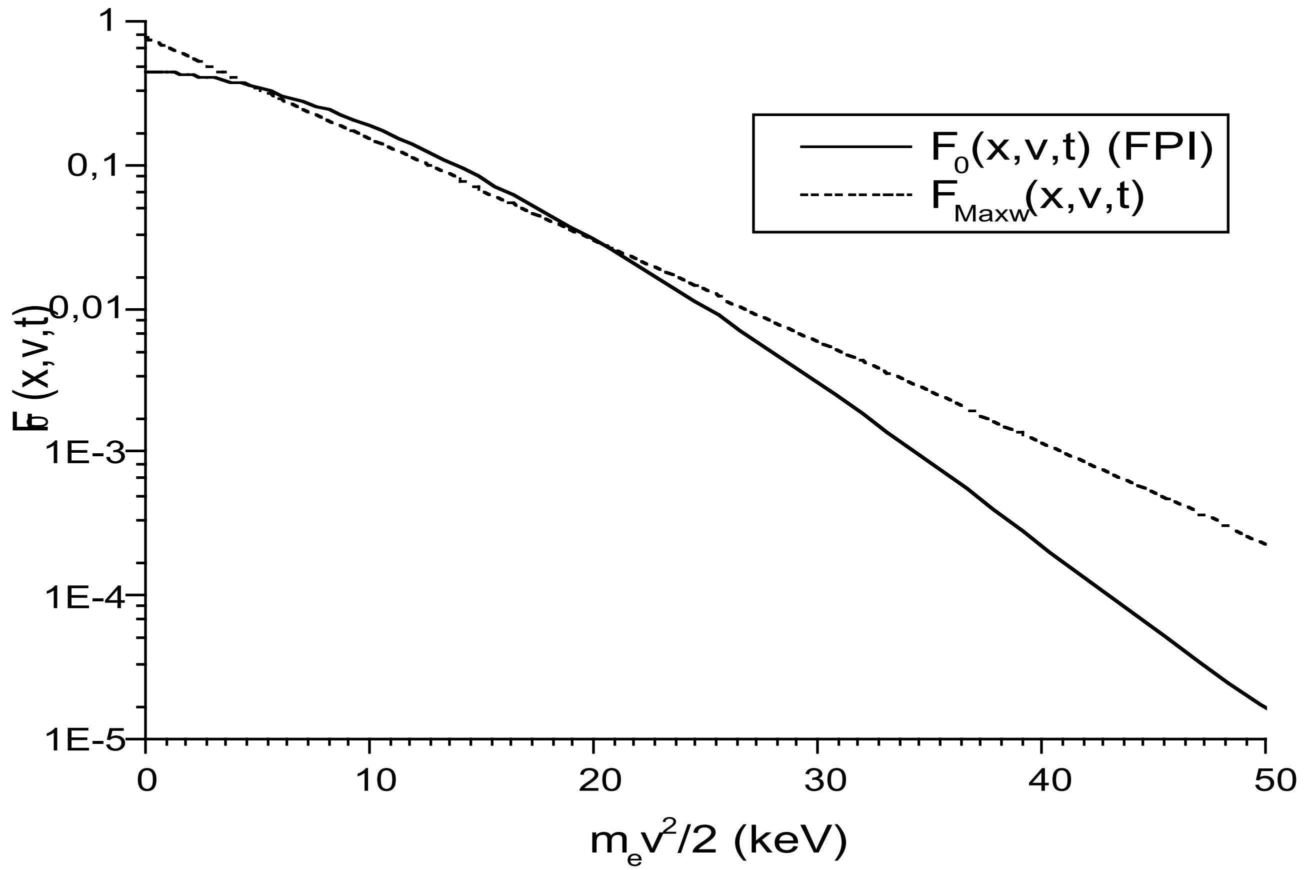

Cell IX=1379; N_e=5.3_10^{21} cm^{-3} (0.59 N_c) ; T_e= 6141 ev (maximum T_e) (cont'd)

Surprise: Beyond 50 keV : Hot tail in the underdense plasma

Reason: _ comparable to L_N, density scale length.

Strong acceleration by ambipolar field, unchecked by collisions.

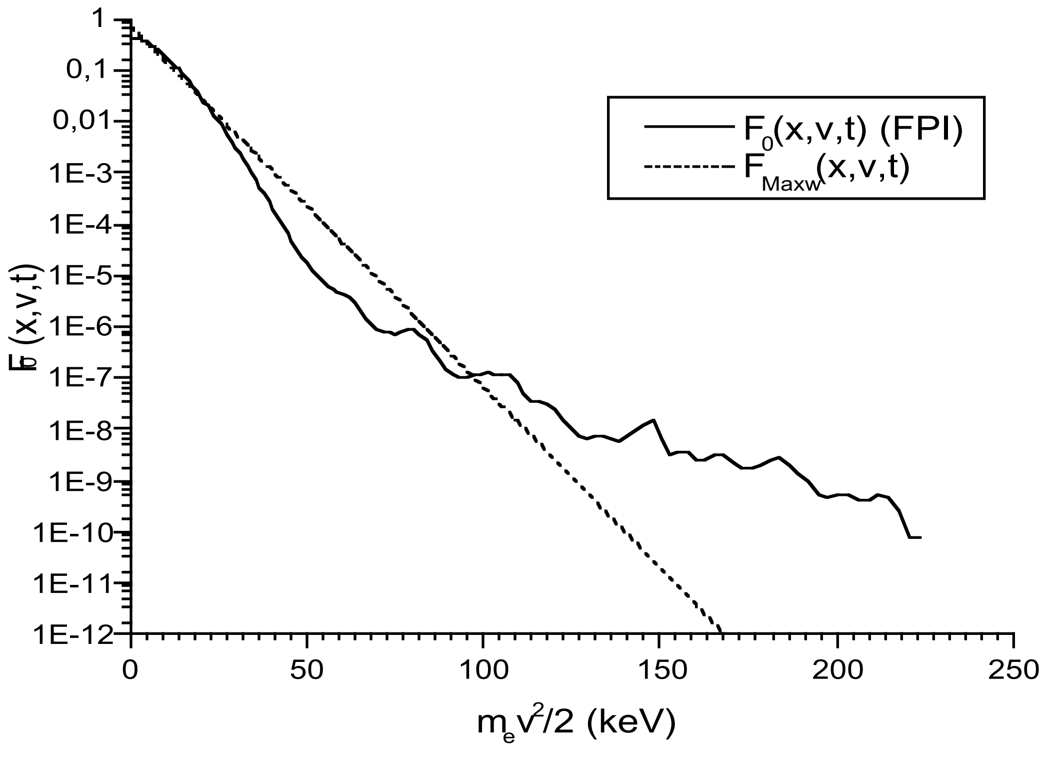

Cell IX=1934; N_e=101_10^{21} cm^{-3} (11 N_c) ; T_e= 1678 ev

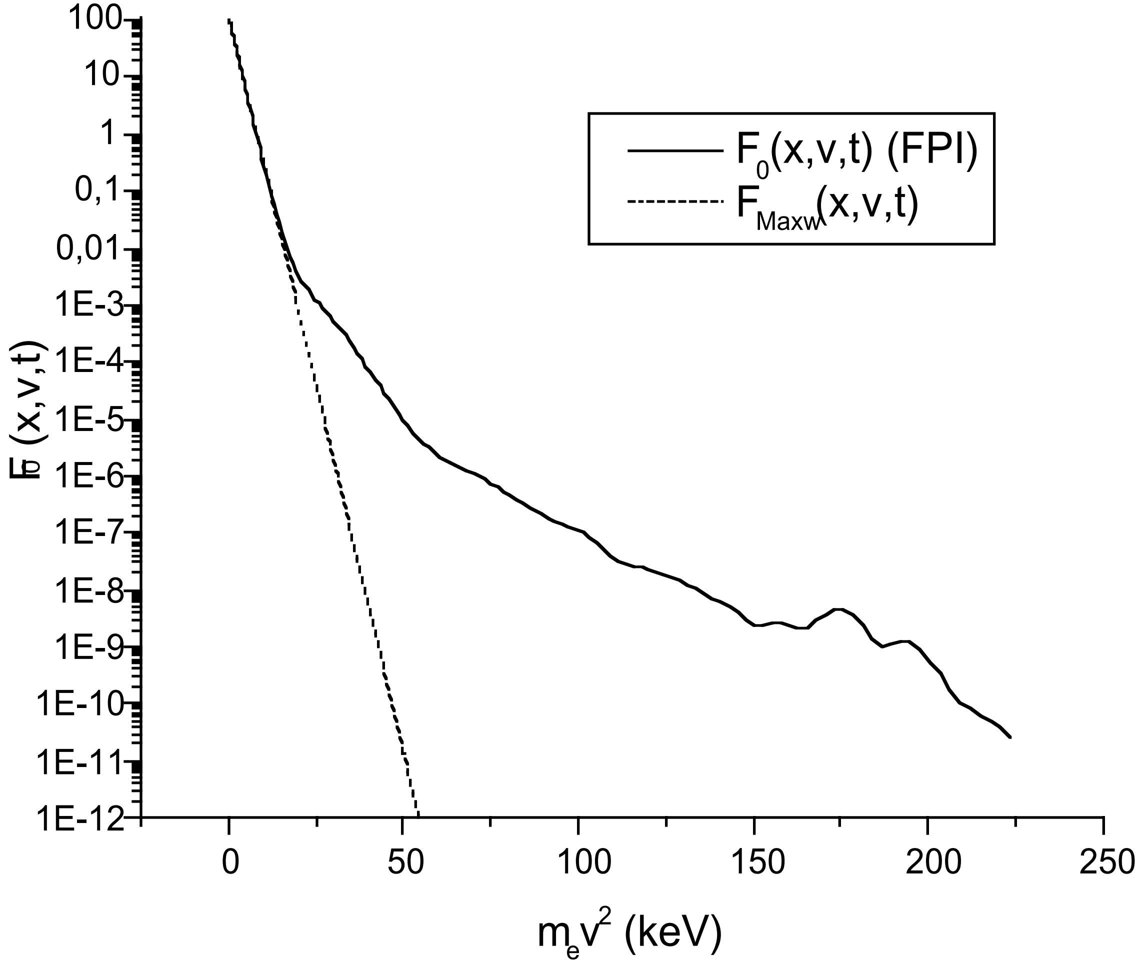

Cell IX=2001; N_e=676_10^{21} cm^{-3} (75 $N_c \approx$ N_{solid}) ; T_e= 362 ev (Ablation surface)

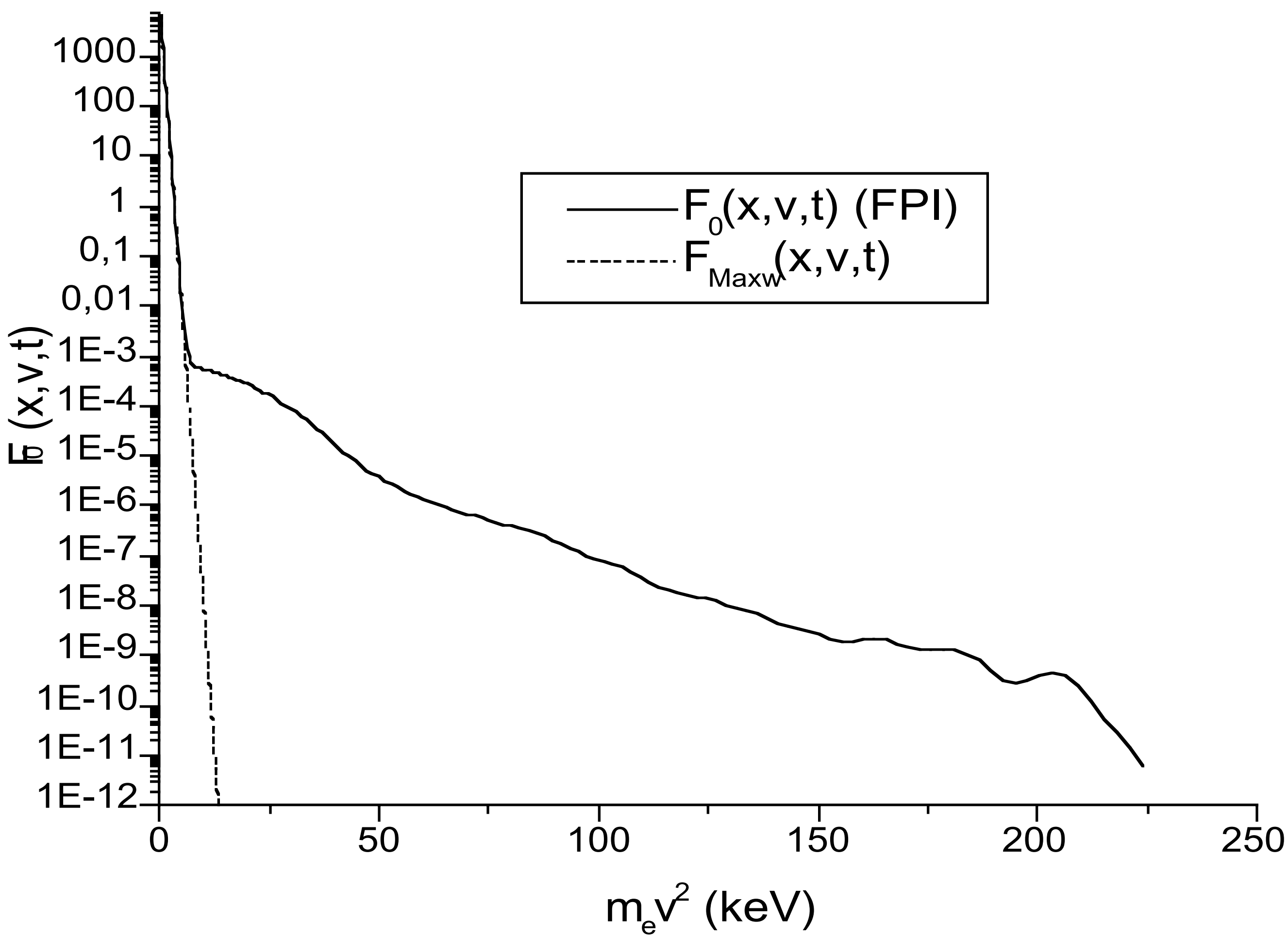

Cell IX=2012; N_e=1400_10^{21} cm^{-3} (156 $N_c \approx$ 2 N_{solid}); T_e= 186 ev (compressed)

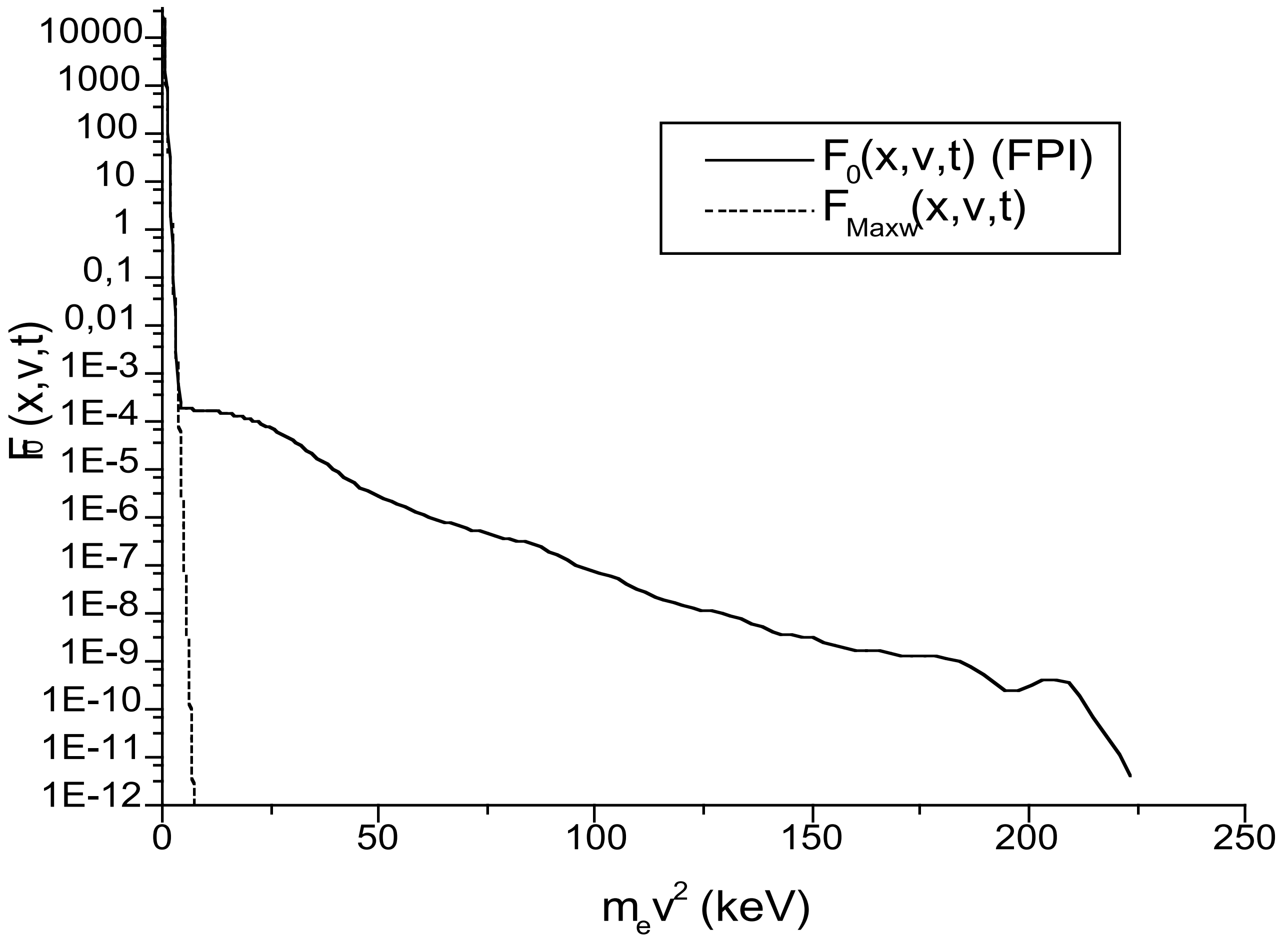

CONCLUSIONS FOR PART 2

- High intensity ablation has been simulated by both a fluid code (LASNEX) and an electron kinetic code (FPI).

- The maximum electron temperature is about the same for both codes. However, the coronal temperature profile is different.

- The ion temperature profile in the corona is also different: lower for FPI.

- Considerably more ablation, due to electron preheat (non local effect).

- "New" non-Maxwellian effect: acceleration by the ambipolar field in the underdense plasma ➔ Hot electron component.

FUTURE WORK

_ Continue the simulation for longer times (1 nsec pulse)

_ Apply our new non-local model to this problem (ongoing).

Laser expériments :
Interpretations and predictions

Ph. NICOLAÏ, D. BABONNEAU, M. BONNEFILLE, B. CANAUD, F. CHAIGNEAU,

E. DATTOLO, C. ESNAULT, J-P. JADAUD, S. LAFFITE, M-C. MONTEIL,

G. SCHURTZ, M. VANDENBOOMGAERDE, B. VILLETTE, F. WAGON.

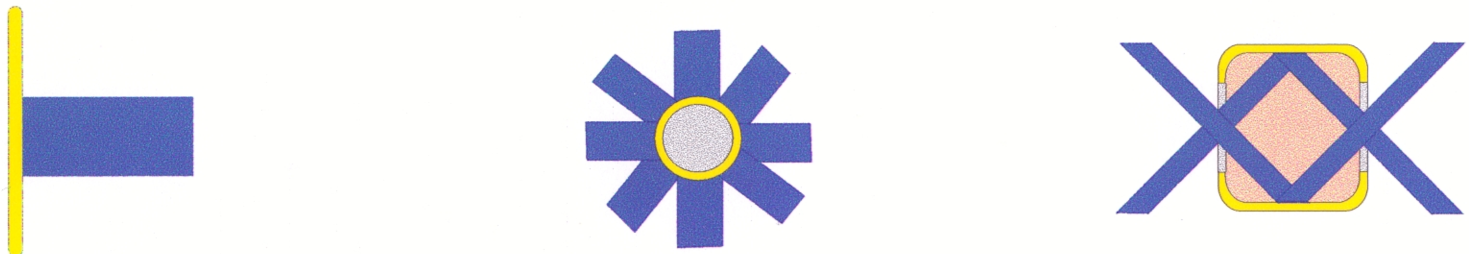

Magnetic fields and nonlocal fluxes

Effects of each process are less or more large following :

- experimental geometry [plane-sphérical]
- observed quantity [Tr, Te, ne, hυ ...]
- plasma zone seen (probed) by diagnostic

The choice of an experiment and diagnostics (can) enables us :

- to test both effect combined or alone
- to check our model
- to improve our understanding of physical processes involved

  (to improve theory)

Planar target (Phebus facility)

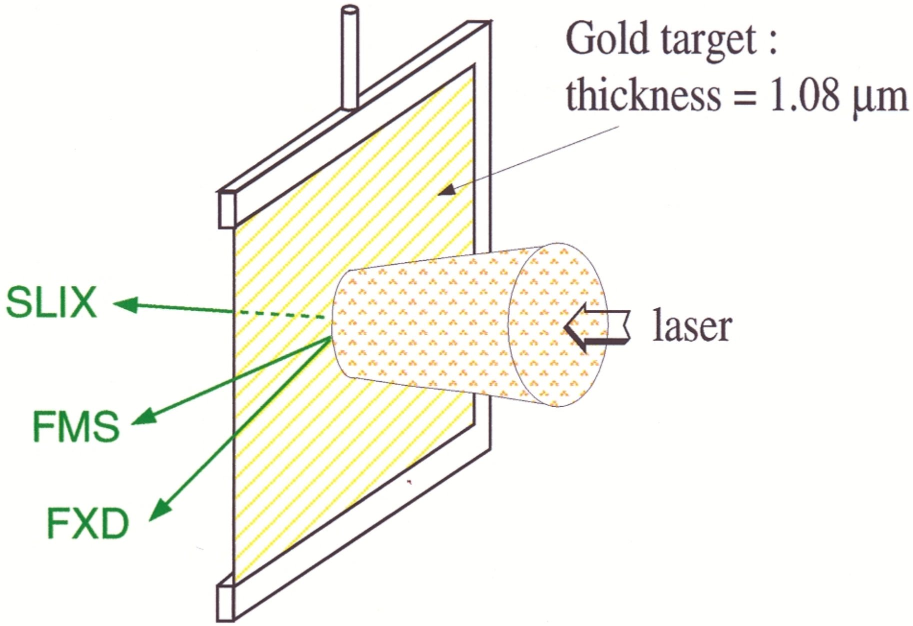

Laser

- smoothed by RPP
- 3ω
- 1.5ns square pulse
- 3kJ
- FWHM=340µm

FMS :streak camera wich images 200 eV X-ray emission perpendicular to laser axis

☛ provides a time-resolved 1D image

FXD : streak camera wich images above 2 KeV X-ray emission perpendicular to laser axis

☛ provides a time-resolved 1D image

SLIX : gated microchannel plate detector images 2.5KeV X-ray (M-shell) from rear side

☛ provides a time-resolved 2D image

2D Simulation of experiment

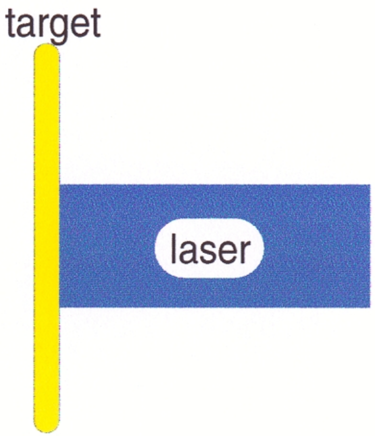

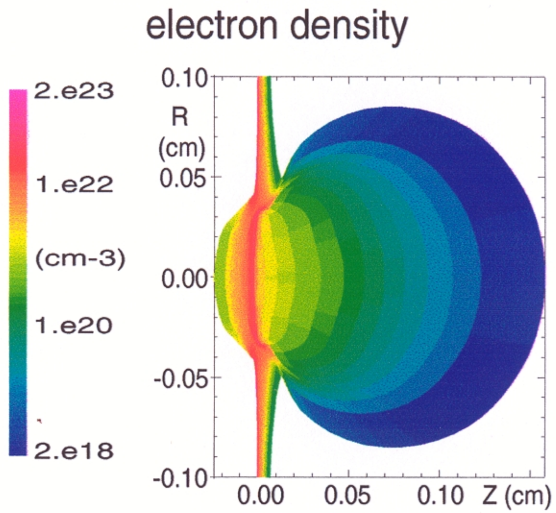

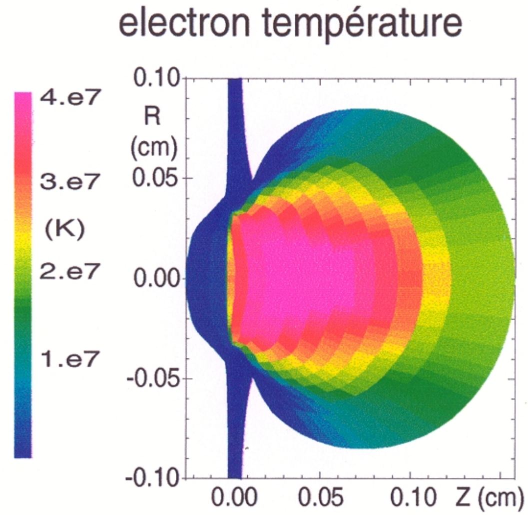

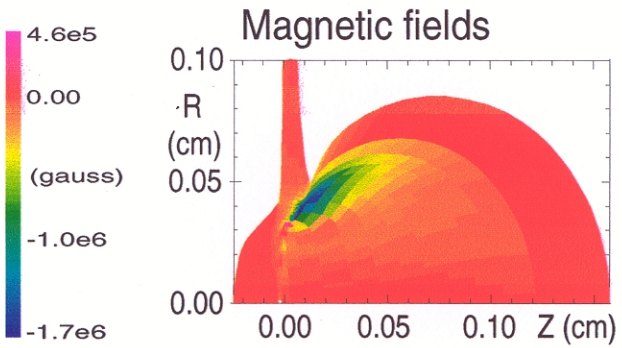

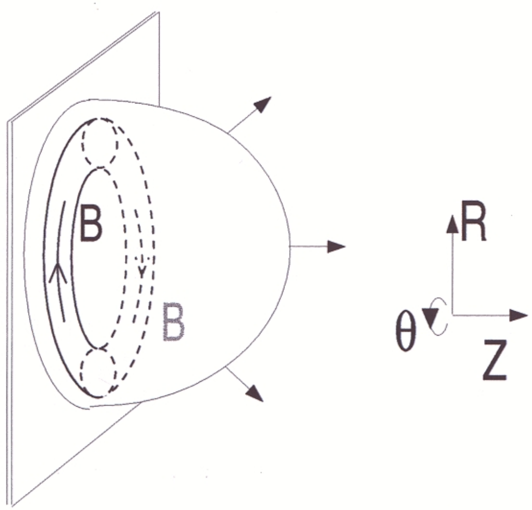

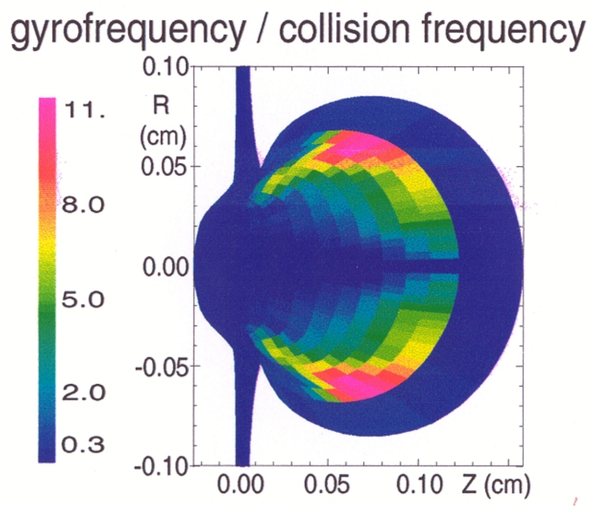

Electron heat fluxes

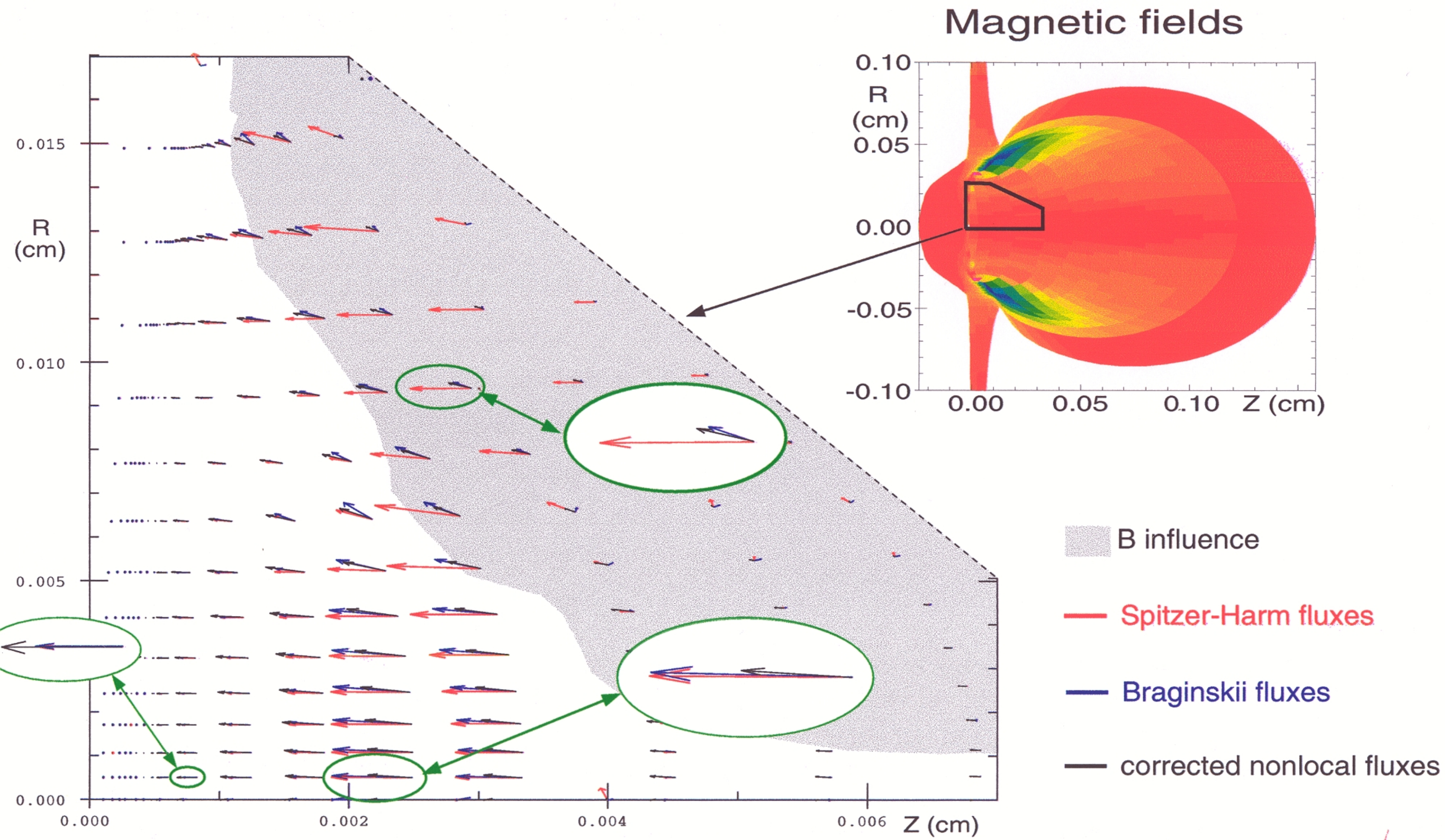

FMS diagnostic

Streak camera which measures 200 eV X-ray emission through a slit

➲ side view, 1D time-resolved image

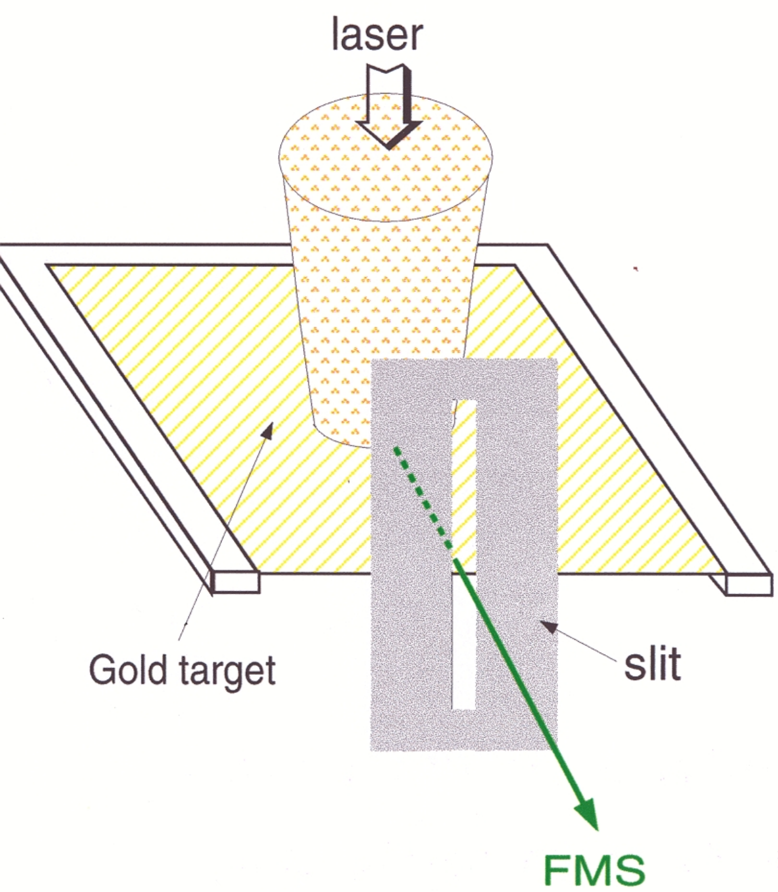

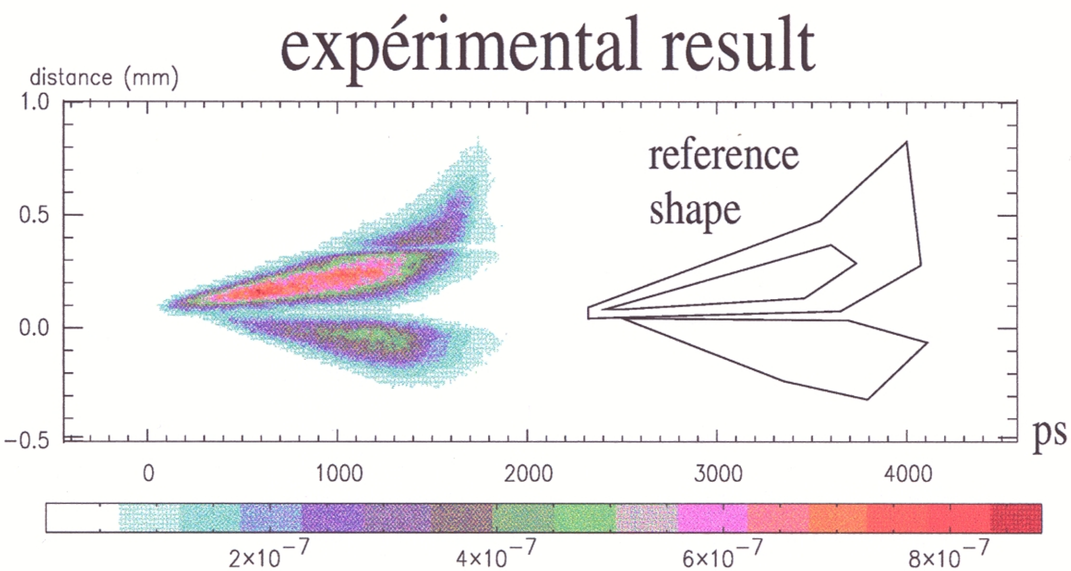

Experiment-simulations comparisons

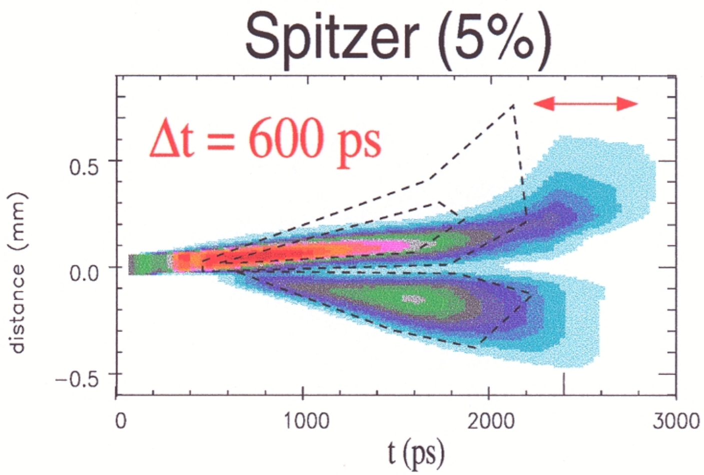

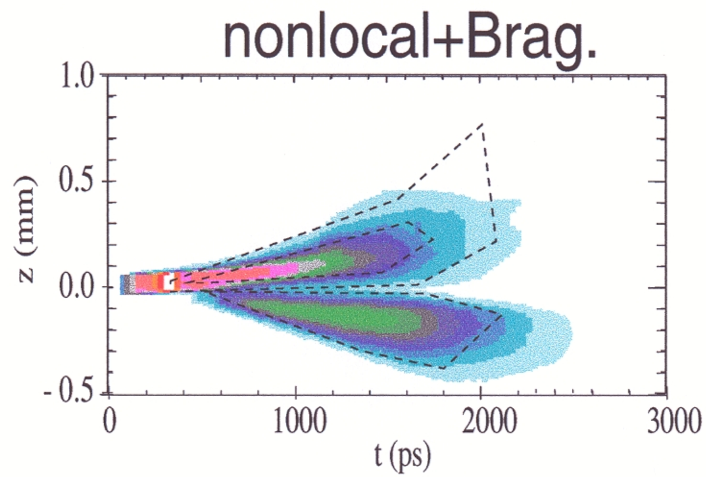

- ✔ Using Spitzer-Harm fluxes, we obtain (front side) an emission too long (600ps). Second, the slope of the upper part is too small (velocity of the emitting zone).

- ✔ We tried to change limiter value, average between SH and free streaming, laser parameters, mesh refinement, etc... But no effect on numerical results.

- ✔ Using B-fields and nonlocal transport, we obtain a emission length shorter and the slope of the upper part is higger and is in good agreement with exp. result .

Individual effects of each process

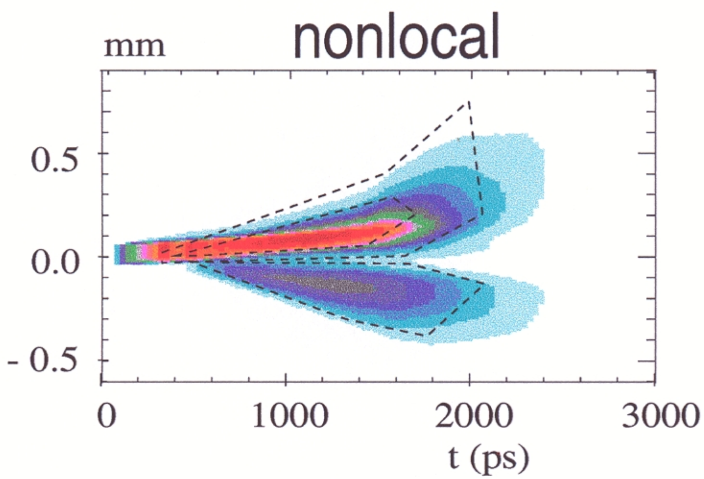

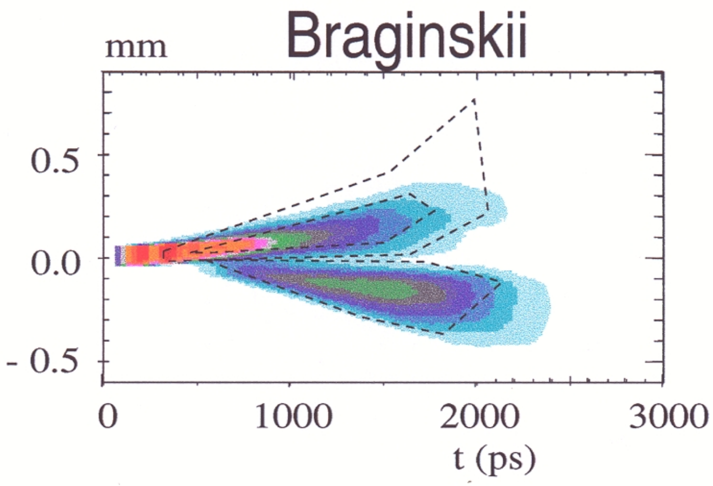

- ✔ Using nonlocal fluxes, we obtain a shortening of emission but not enough to reproduce experiment.The emitting zone shifting (laser side) is correct
- ✔ Using B-fields, we obtain a good length of emision (front side) but the slope of the upper part is too small (slightly)to mach experimental data.
- ✔ So, it seems that combined effects produce the best agreement with experiment

SLIX Diagnostic

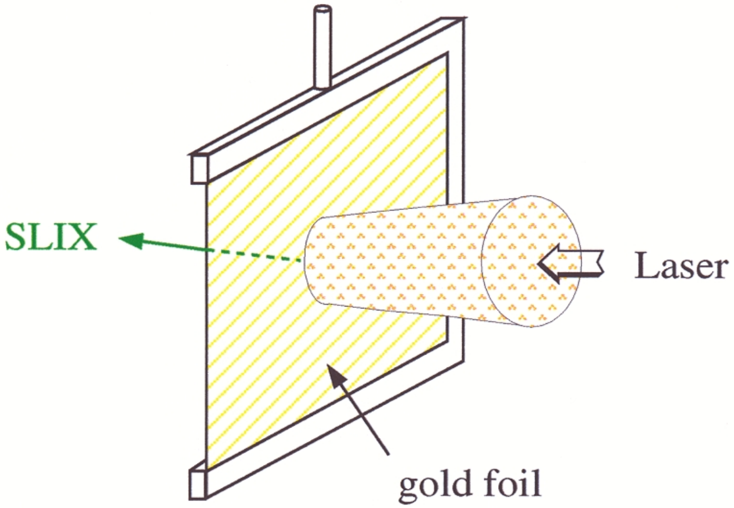

Slix diagnostic takes 'photos' of the rear side in the range about 2.5Kev (M-shell)

Res.=10μm et Δt=100ps

experimental image

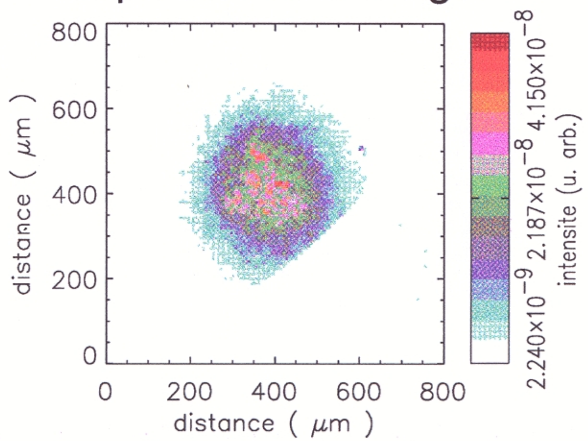

circular average

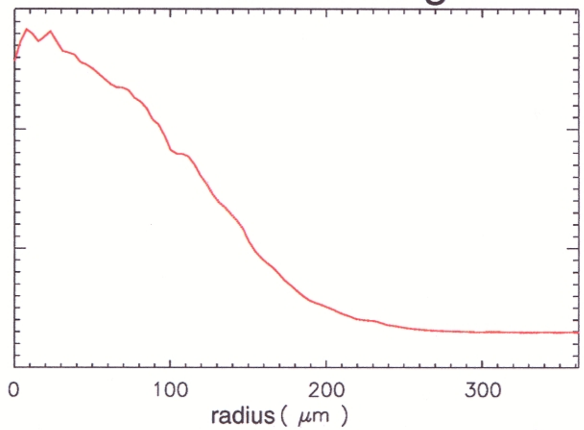

Expériment-simulation comparisons

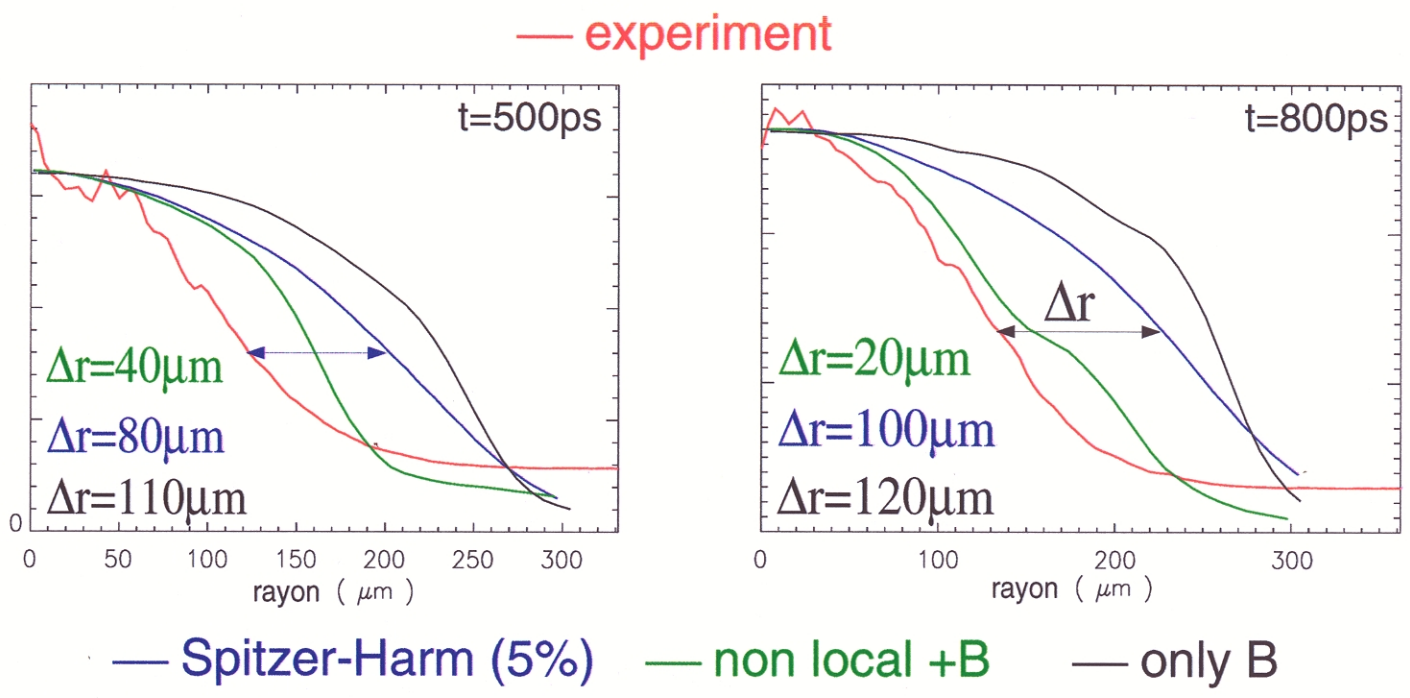

✔ Using Spitzer-Harm , we get images too large by about 80 and 100 μm at half maximum.

✔ B-flieds do not improve results

✔ B-flieds and nonlocal fluxes give the best agreement

FXD Diagnostic

Streak camera which measures X-ray emission above 2KeV

➲ side view, 1D time resolved image

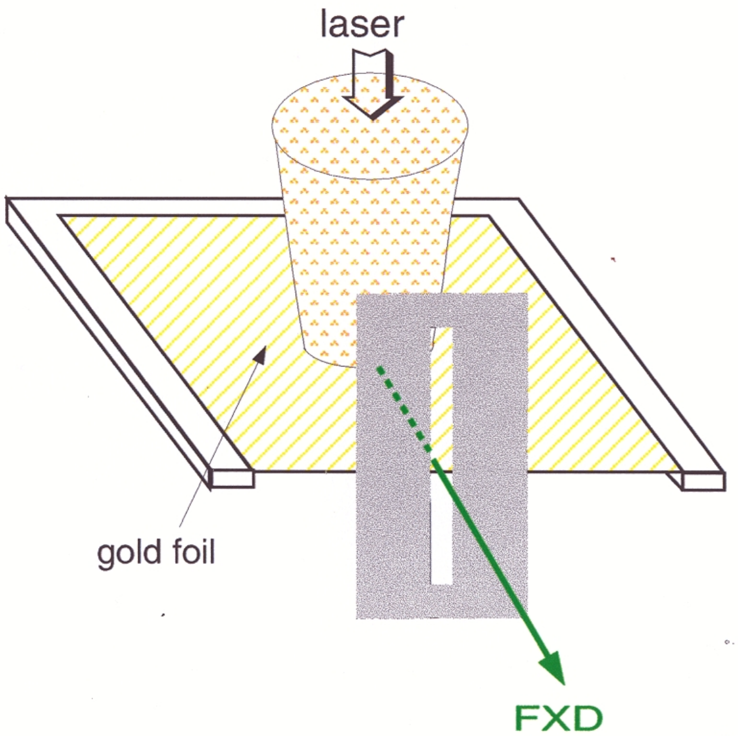

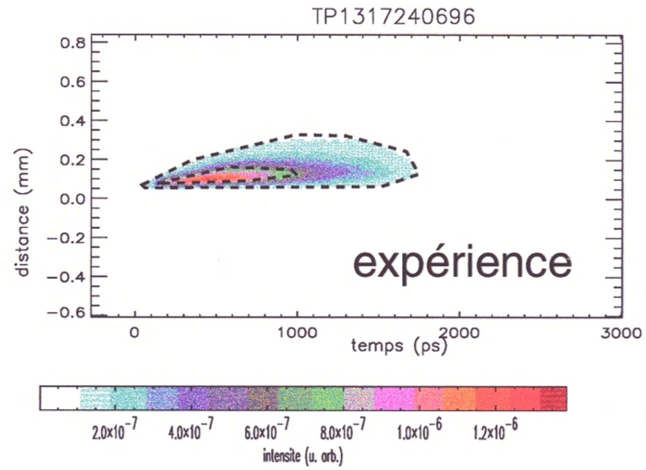

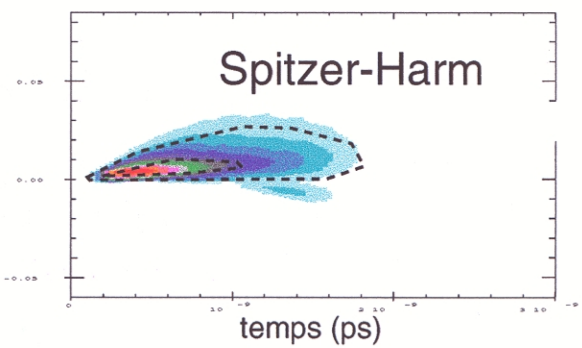

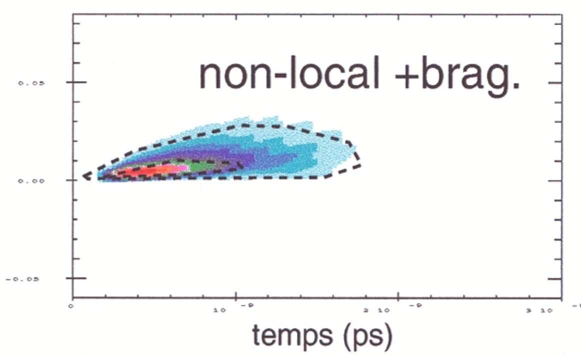

Planar target : summary

- Using Spitzer-Harm fluxes, simulations are unable to reproduce all diagnostics, whatever variations of flux limiter, laser parameters, zoning,...

- Both non local and magnetic effects improve simulation results without arbitrary parameter (flux limiter).

- If we only use one process,we get some improvements but not enough to match experimental data.

Hohlraum experiments
(NOVA / OMEGA facilities)

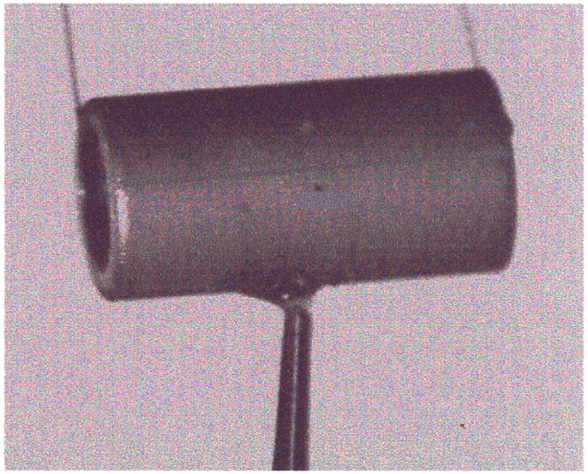

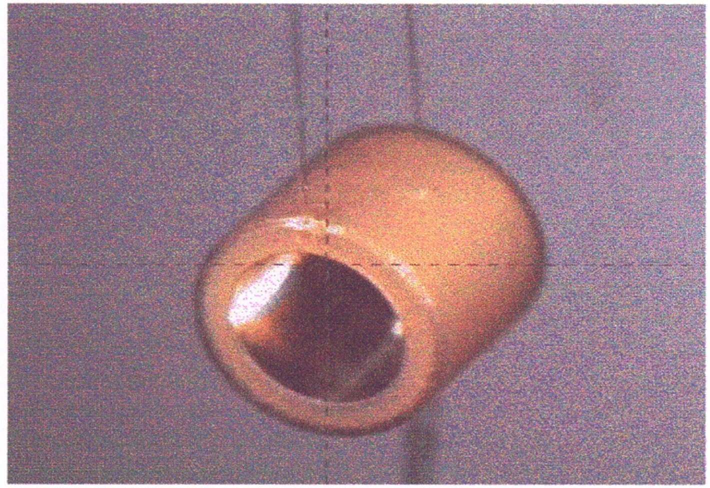

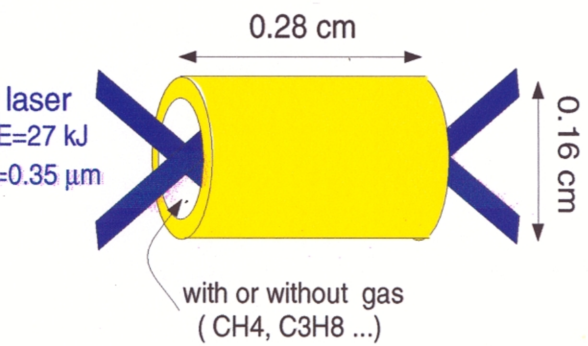

Thomson scatttering

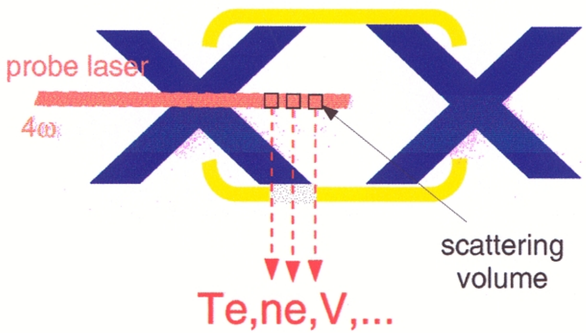

X-ray Spectrum ➠ Tr

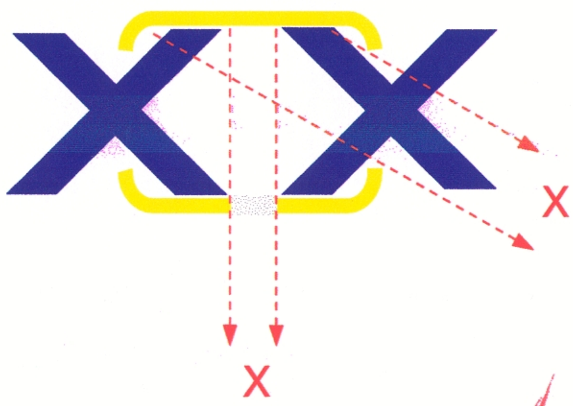

Gas-filled Hohlraum (nova exp.)

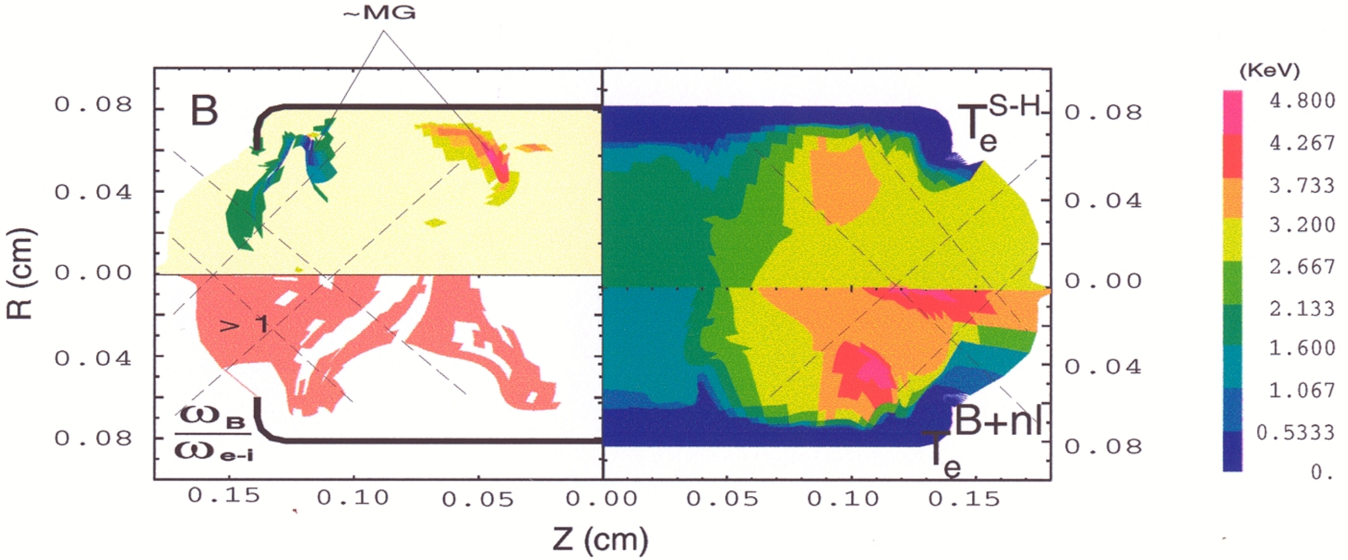

✔ Simulations with radiation-hydrodynamic code (FCI2) predict B fields of order of 1 MG

✔Hall parameter exceeds unity in a large zone of the hohlraum (B effects)

✔Calculations with SH or with our model (w/o flux limiter) lead to differents results :

- higher electron temperature in off-axis region (from 3.5 keV to 4.8 keV)
- larger temperature gradient along the axis (beams crossing)

✔ experimental data of electron temperature from Thomson scattering seem to confirm large gradients along z-axis and temperature in order of 5KeV close to LEH

Hohlraum experiment

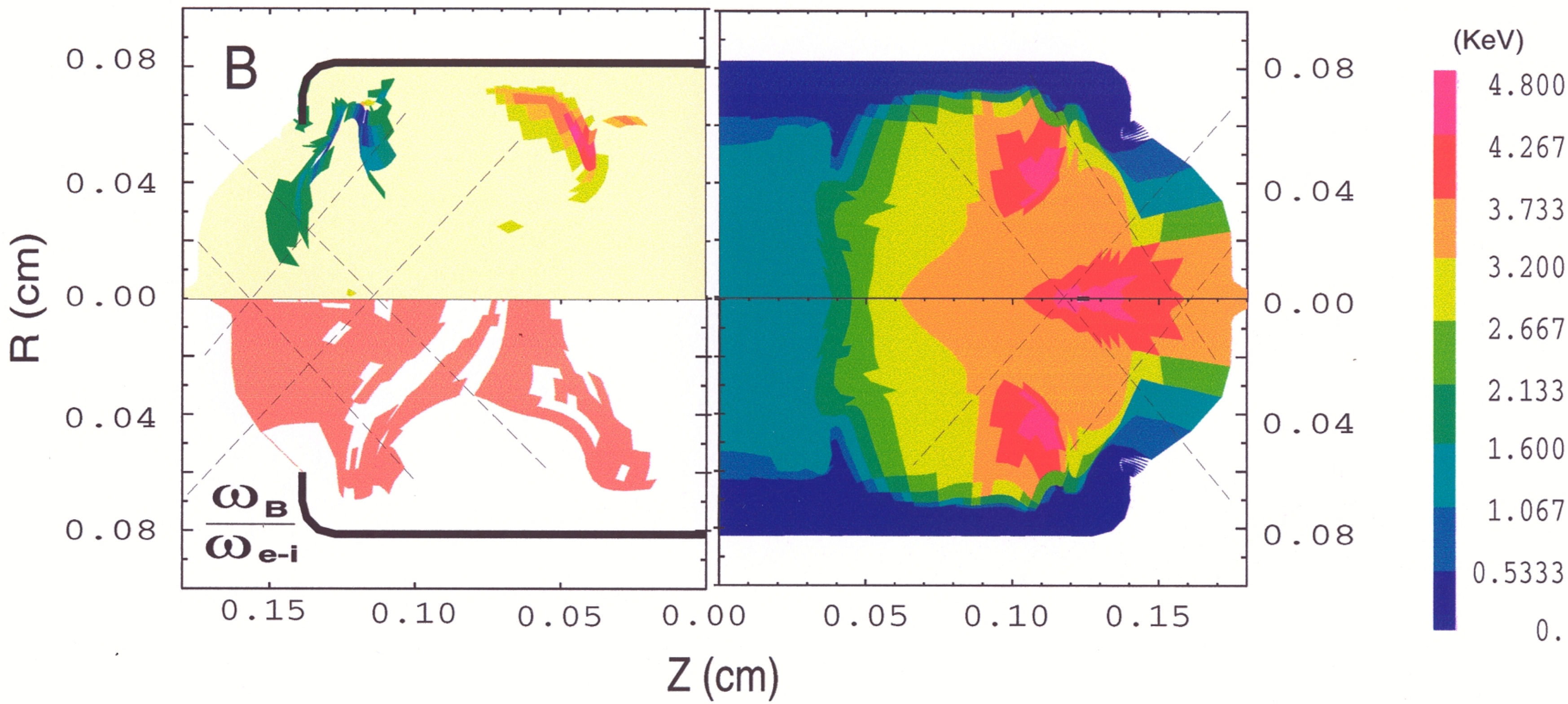

Hohlraum experiments

- In a hohlraum, magnetic fields quickly spread in the whole plasma.

- B-fields reduce or cut nonlocal effects. The deformation of the spherical part of the distribution function due to nonlocal effects may be reduced or cancelled by B-fields.

- Simulations without nonlocal fluxes but with B effects can correctly reproduce, in this case, experimental results.

B-fields (nonlocal effects) can modify density

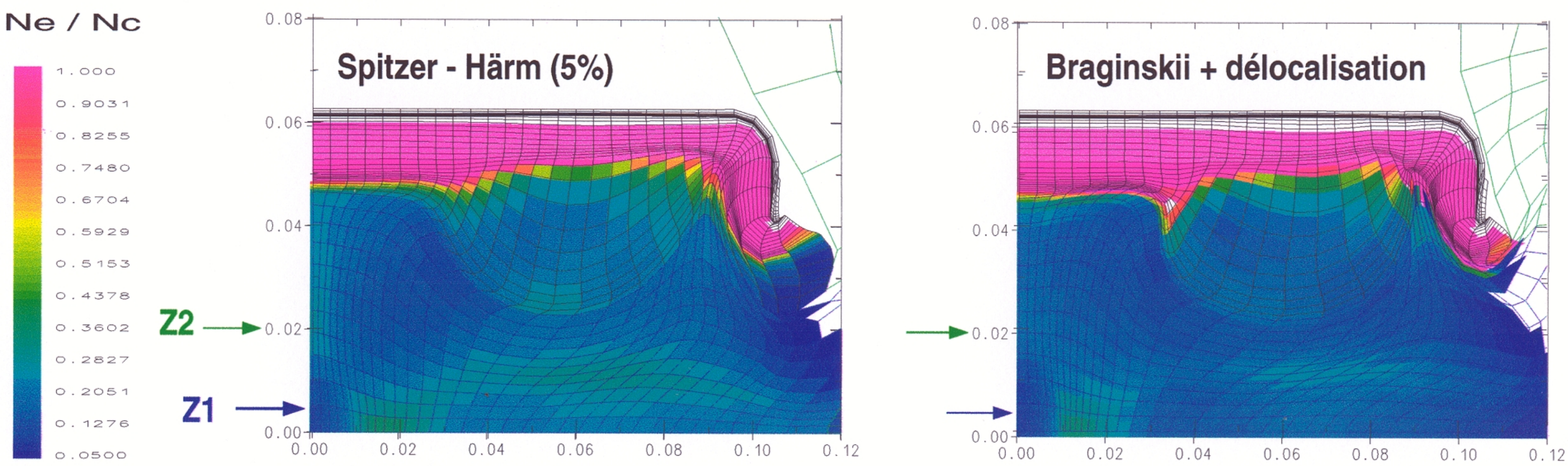

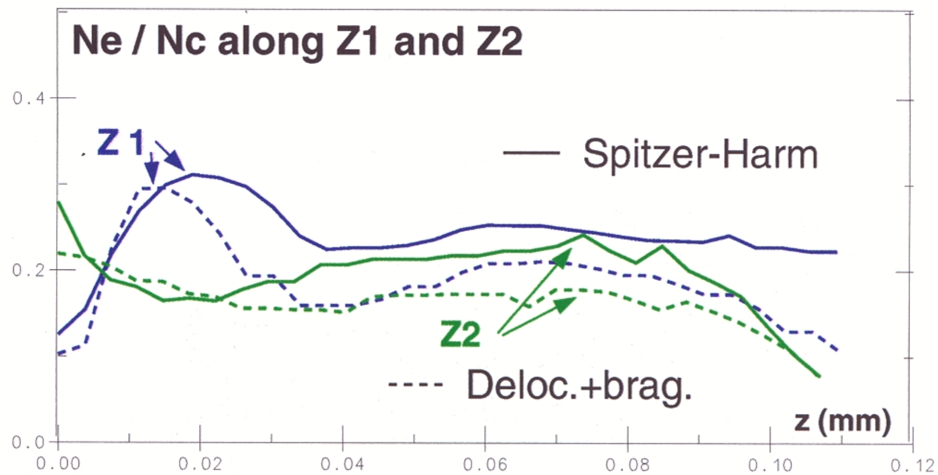

✔ Electron density is lower with Braginskii + deloc model. (about 15%)

Same radiation temperature versus formula

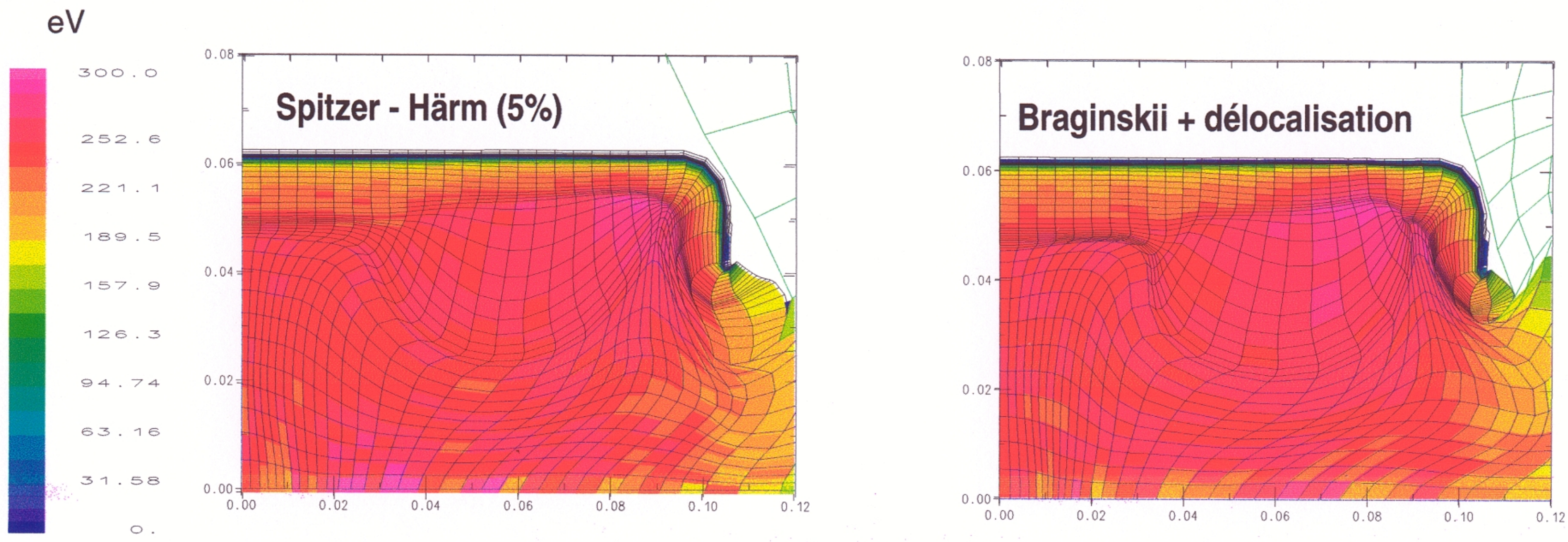

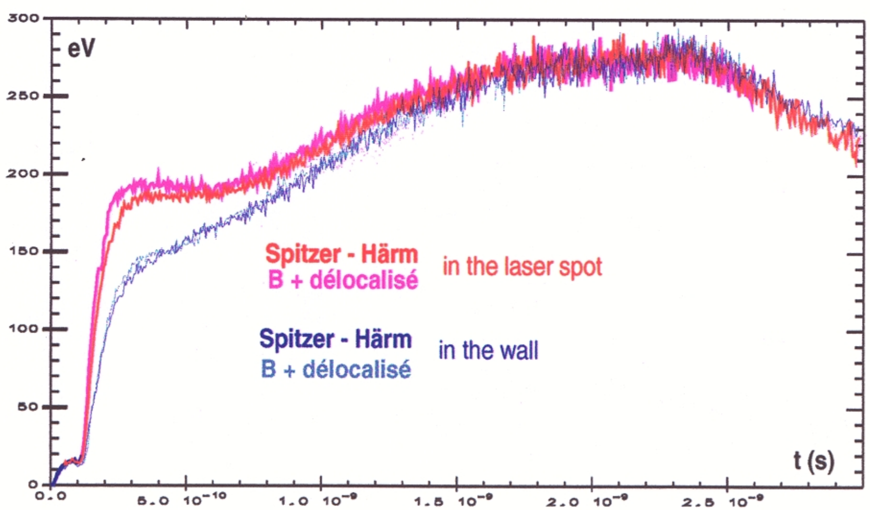

✔ same Tr but w/o flux limiter : (good value)

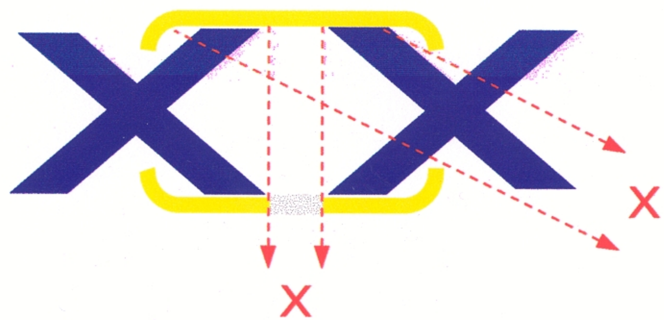

✔So X-ray Diagnostics simulation correct?

Our electron conduction model can modify hydrodynamic motion

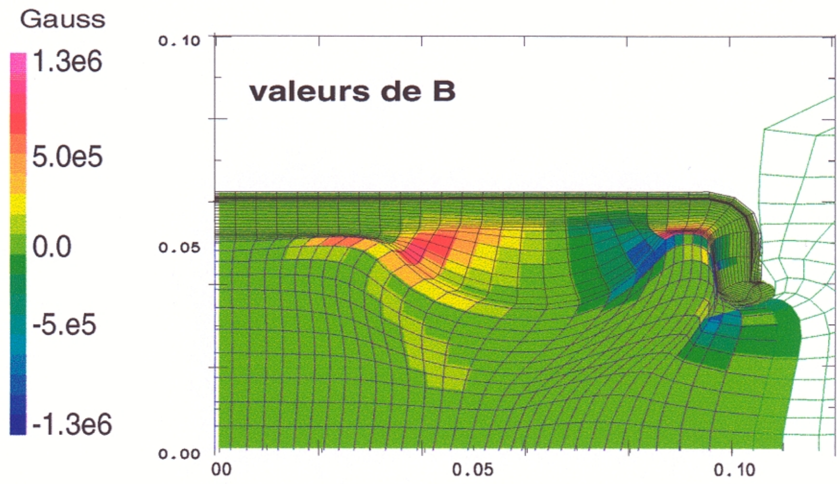

✔heating and expansion of LEH w/o B-fields -> X-ray emission of this zone

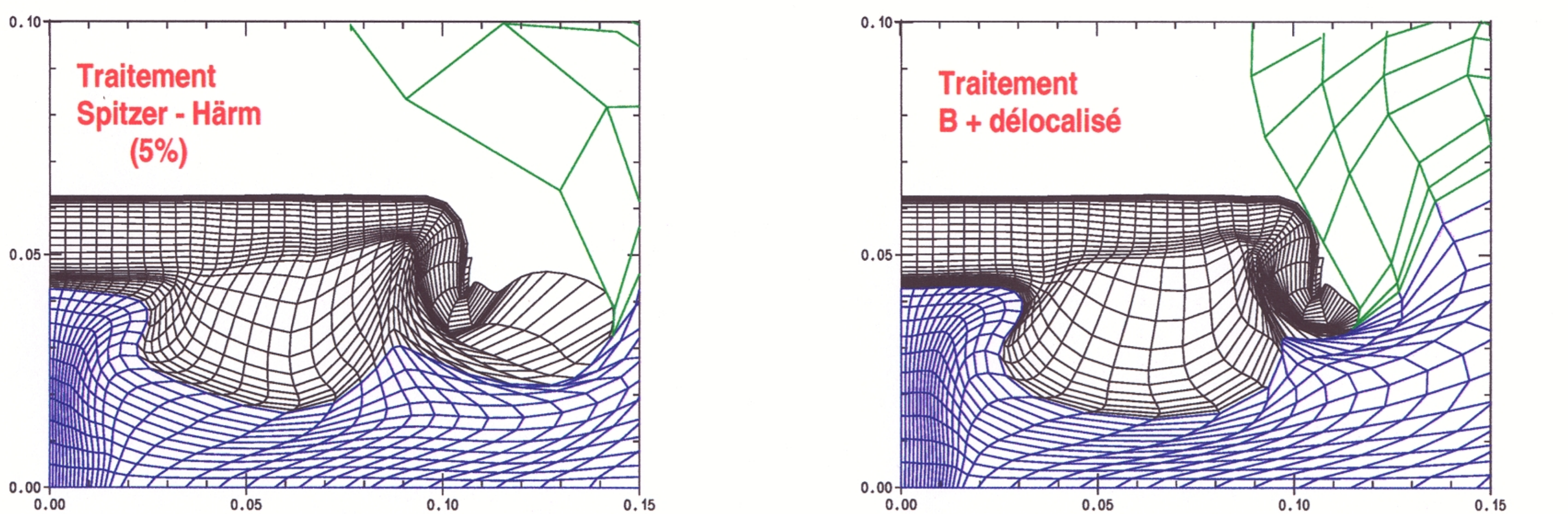

Hydrodynamic effect on X-ray emission

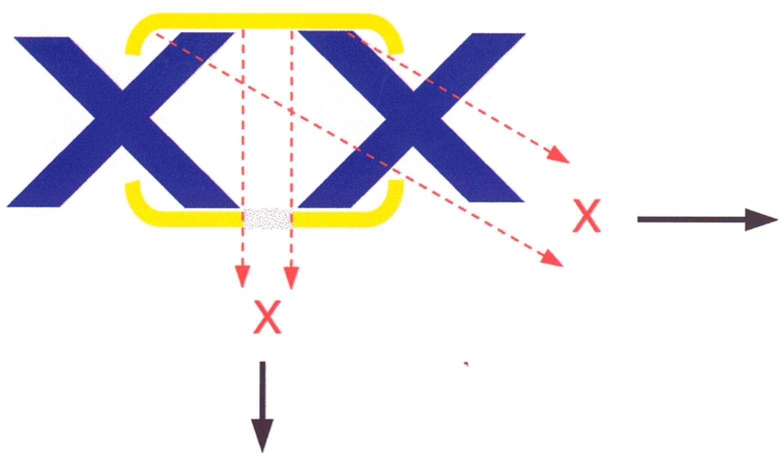

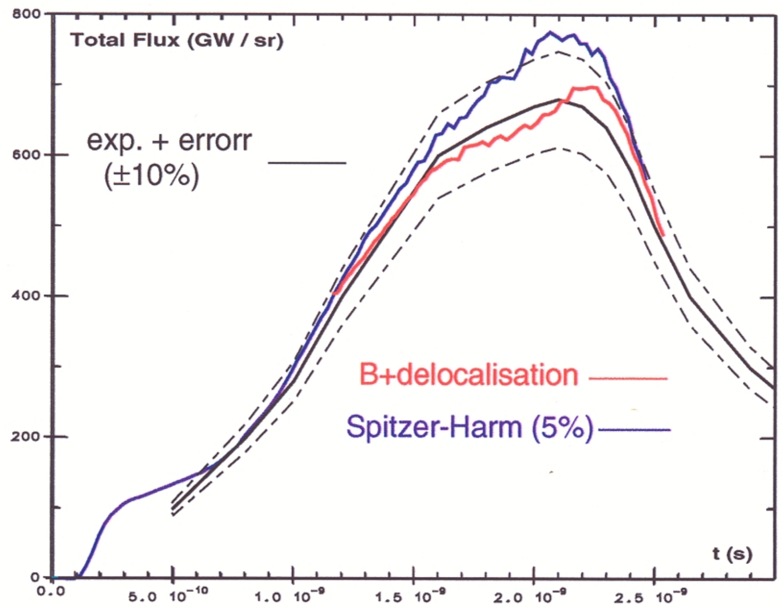

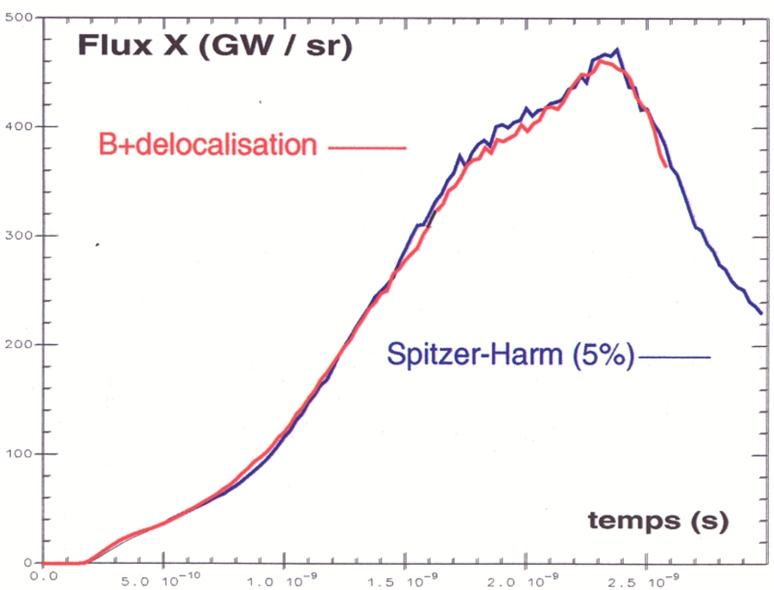

- ✔ For Dante, both heat flux models give similar results
- ✔ B-fields reduce X-ray emission of 'LEH' and enable us to better reproduce exp. data
- ✔ Both simulations are inside error bars

Effects of our model on LMJ cavity

Max. laser power = 400 TW (16 ns) ; Laser energy = 1,4 MJ

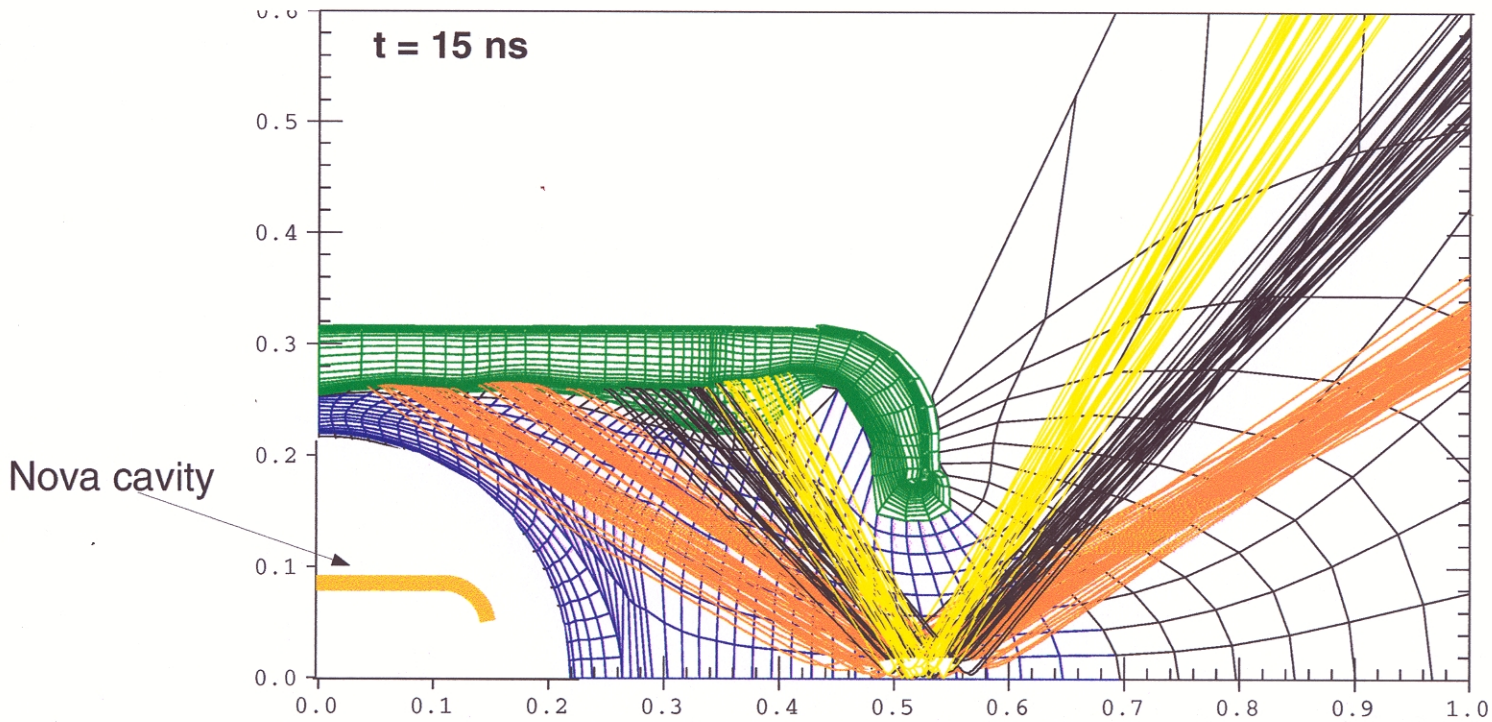

Magnétic fields at 16 ns (max. laser power)

❍ B effects are important in a large part of the cavity

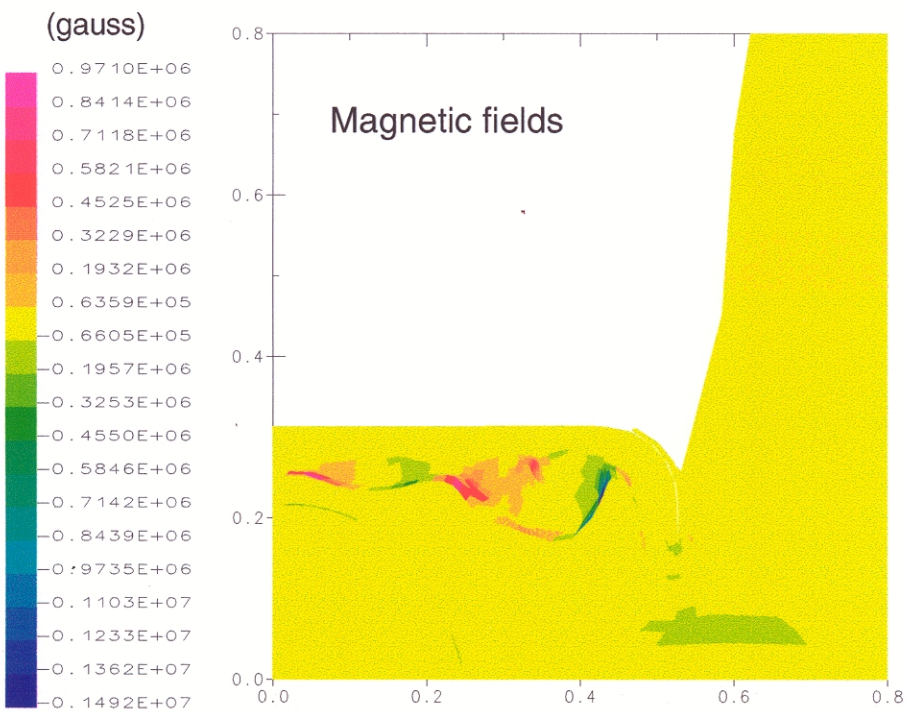

➲ We expect some modifications for

- ✓ electron température
- ✓ ion température
- ✓ density
- ✓ionization
- ✓ hydrodynamic speed
- ✓ ...

Electron temperature color map at t = 16ns

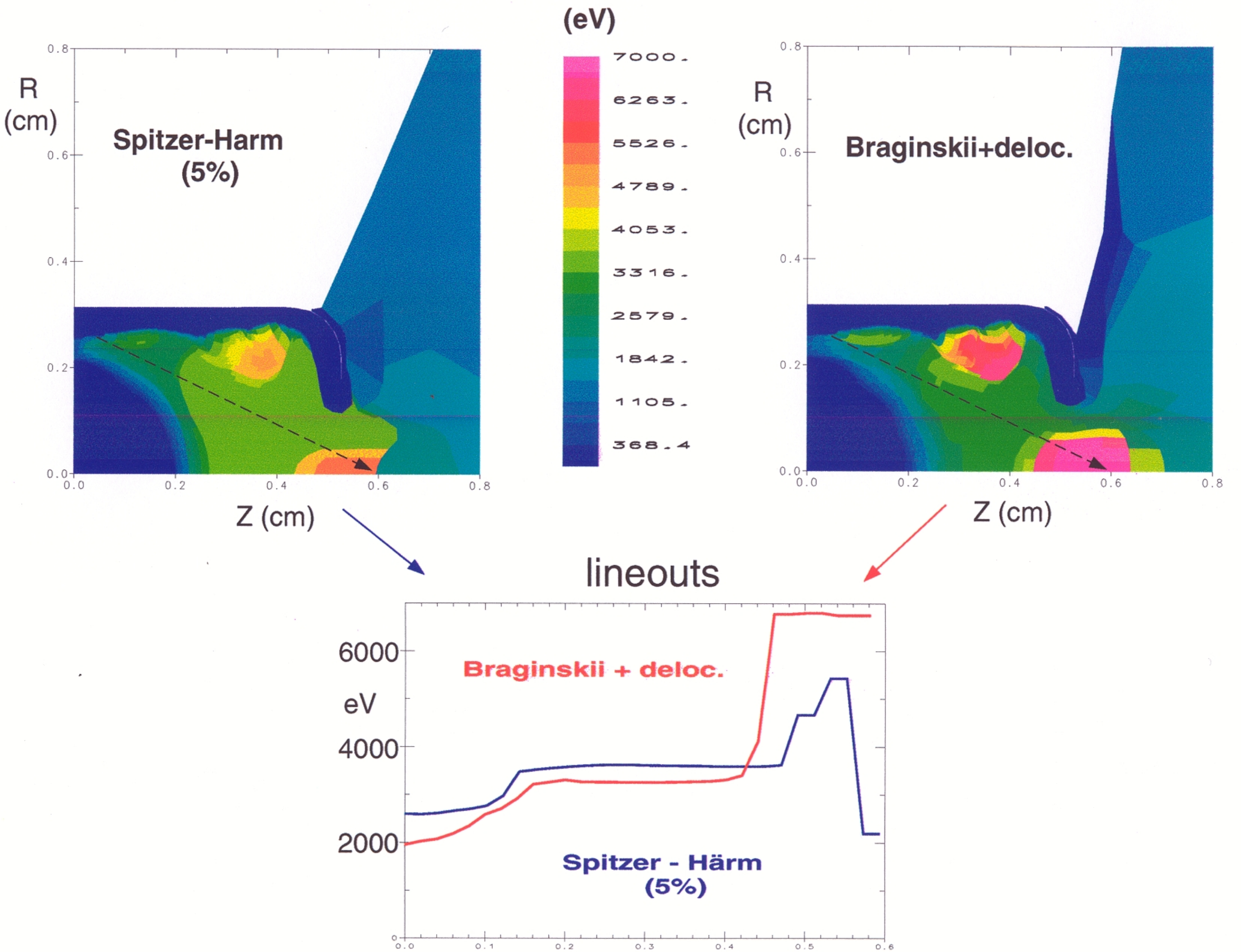

Electron density map at t = 16ns

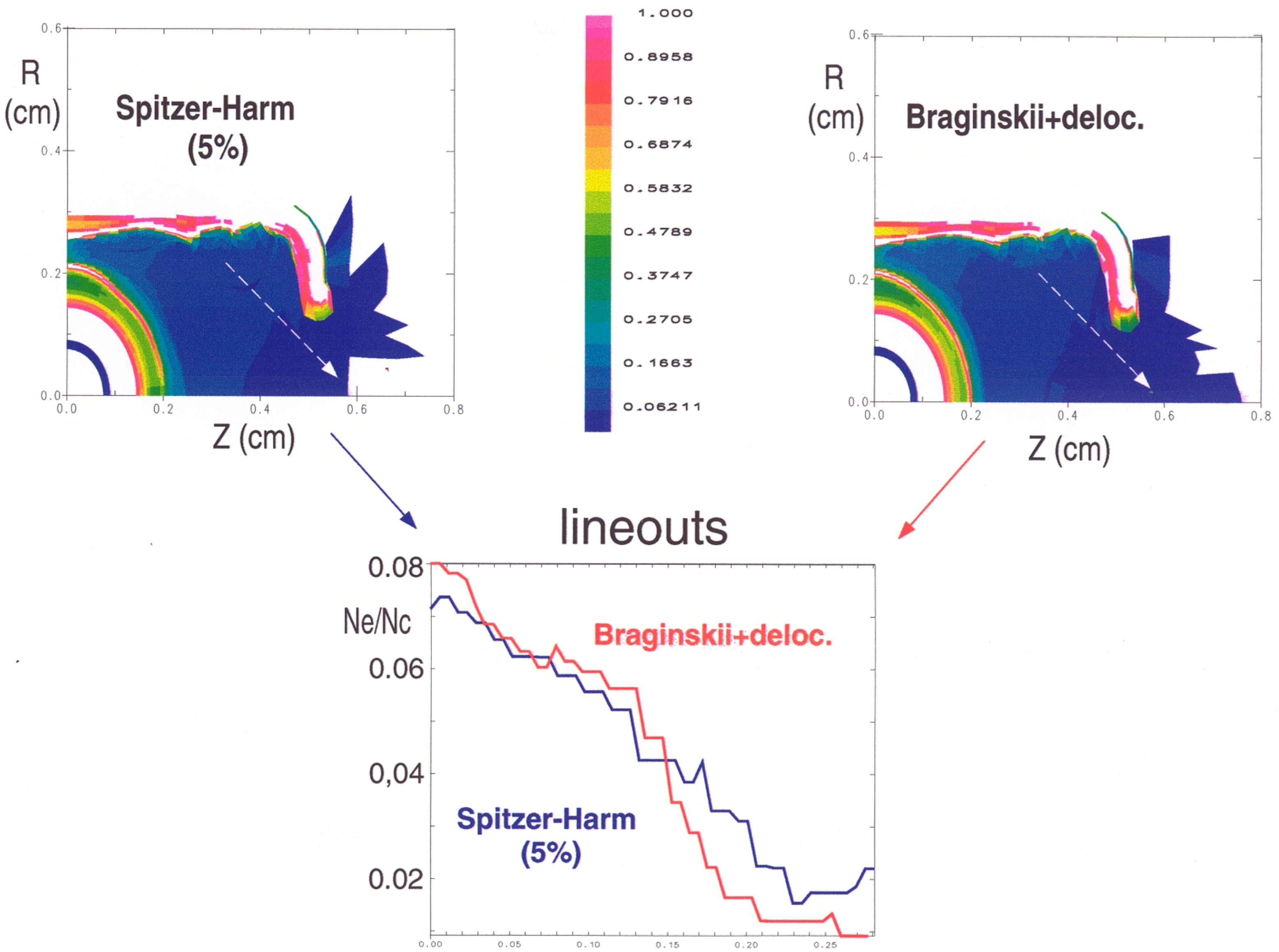

X-rays non uniformities on the ablation front

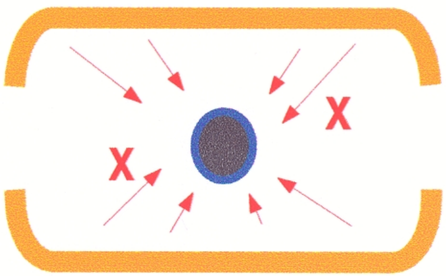

❍ Expansion of the X-ray flux on a Legendre polymomial basis

mode 2 mode 4 mode 6 ...

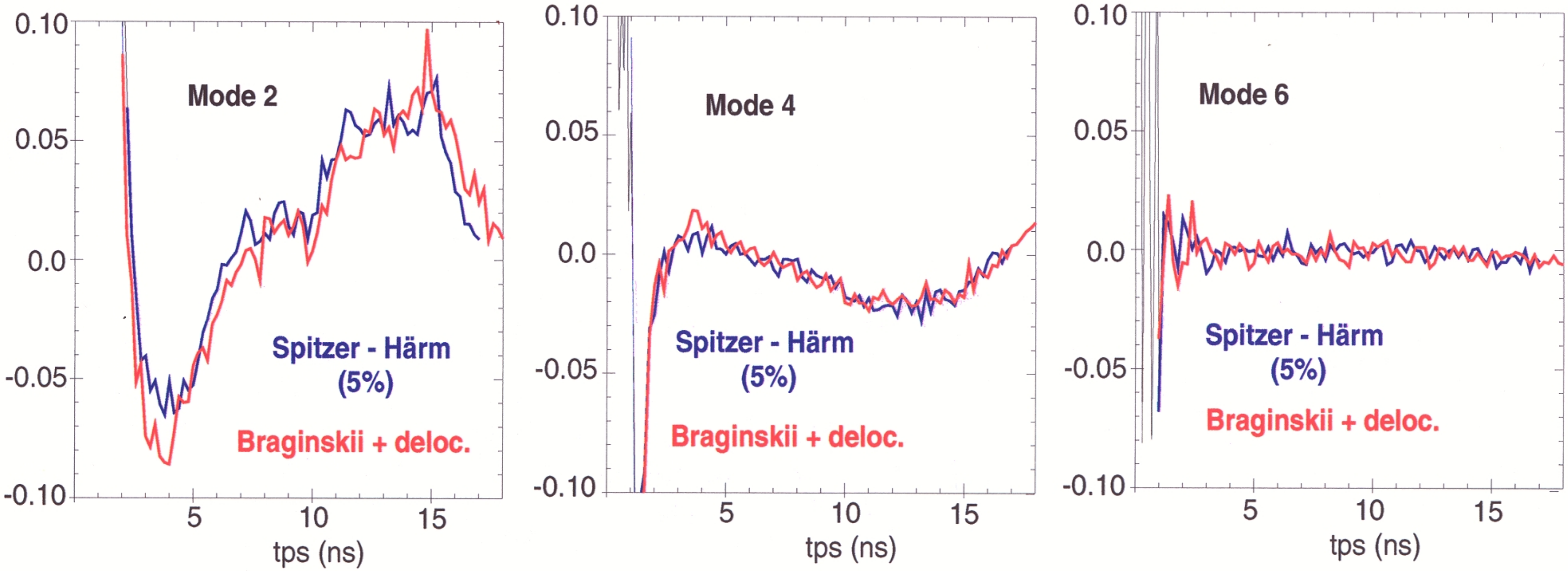

!neither beam-phasing nor pointing optimization !

Cavity : summary

- Simulations using magnetic fields and nonlocal fluxes match Thomson scattering results unlike simulations with S-H fluxes.

- The fields diffusion inside cavity reduce non-local effects.
  - ➡ Using Braginskii fluxes, simulation passes through expérimental error bars

- Hydrodynamics quantities (Te,Ti,Ne,V,...) can be hardly modified by magnétics fields ⇨ effects on others processes (Laser Plasma Interaction)

- The radiation temperature and the irradiation symetry of micro-ballon are not affected by our model ⇔ limited Spitzer-Harm (f~5%)

Spherical target (Omega facility)

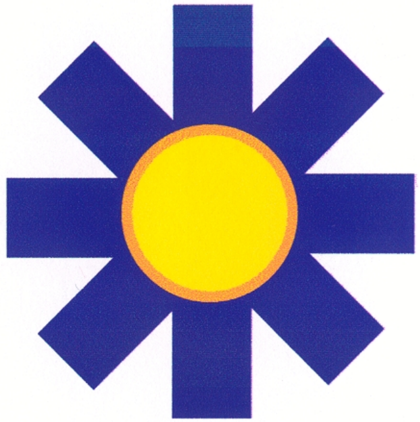

✔ CH targets (950µm) cover with gold (2.5µm)

✔ laser : - 3ω
- intensities from 1e13 to 1e15 W/cm2
- square pulses for from 1 to 4ns
- fwhm ≈ 500µm

simplified expérimental configuration

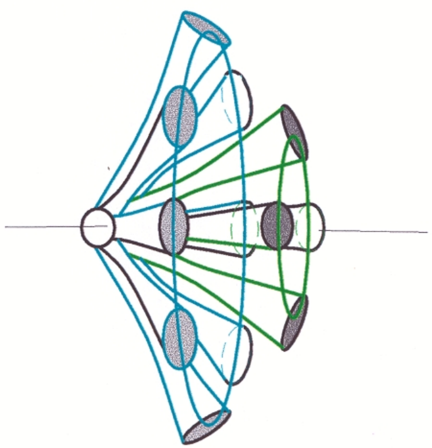

simplified 2D simulation →

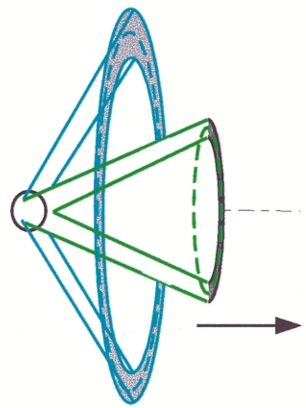

→

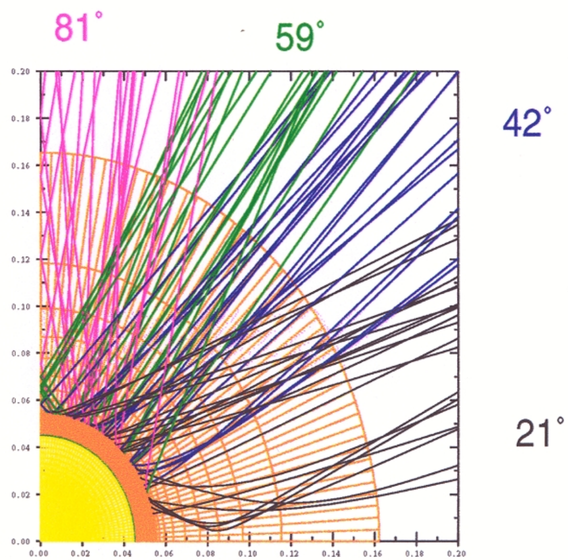

✔ X-ray Diagnostics : spectrum, conversion efficiency, imaging with spectral resolution

Influence of self-generated magnetic fields

✔Crossed gradients Te-Ne can create B-fields

✔ For this geometry, with an isotropic irradiation, gradients are collinear -> no B-fields

✔ In experiment, we can have unbalanced laser power between beams (cones)

I=1.4e14, at 21° (-14%), at 42° (+2%) at 58° (-0.3%) at 81° (+6%) *worst case*

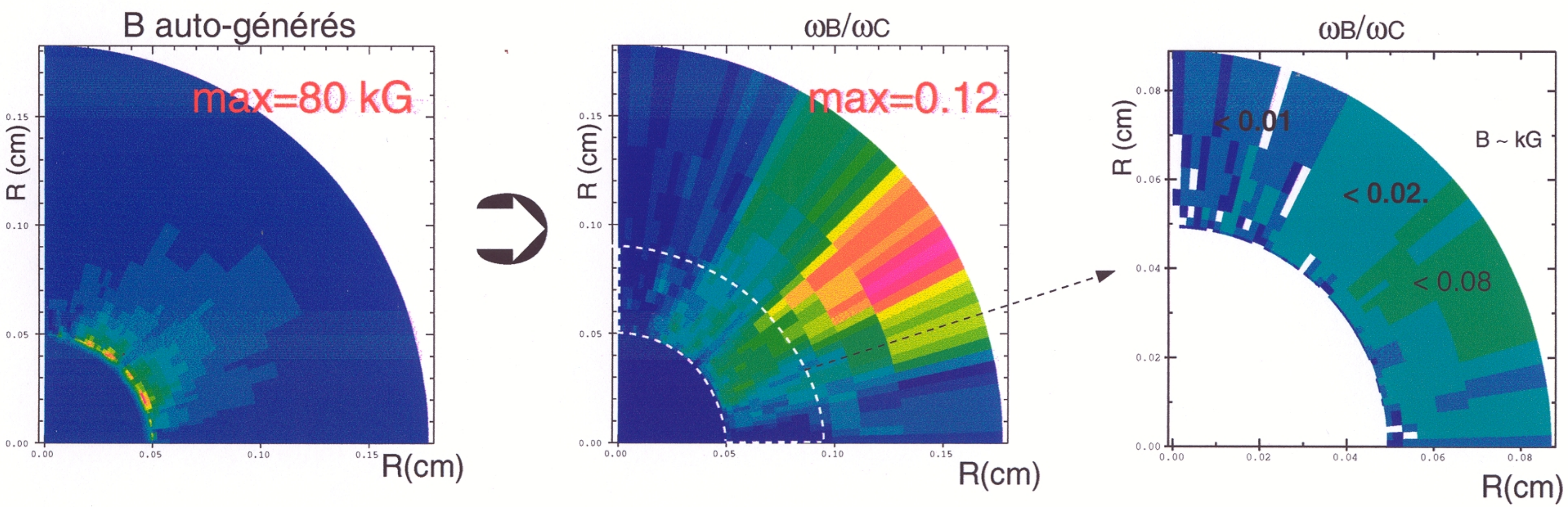

➥ No influence of magnetic fields (same res. w or w/o B)

➥ Only nonlocal flux acts on plasma in these experiments

X-ray Conversion

X-ray Energy / Absorbed laser energy

✔ We test the influence of heat flux on X-ray conversion

✔ Expérimental data come from several experiments

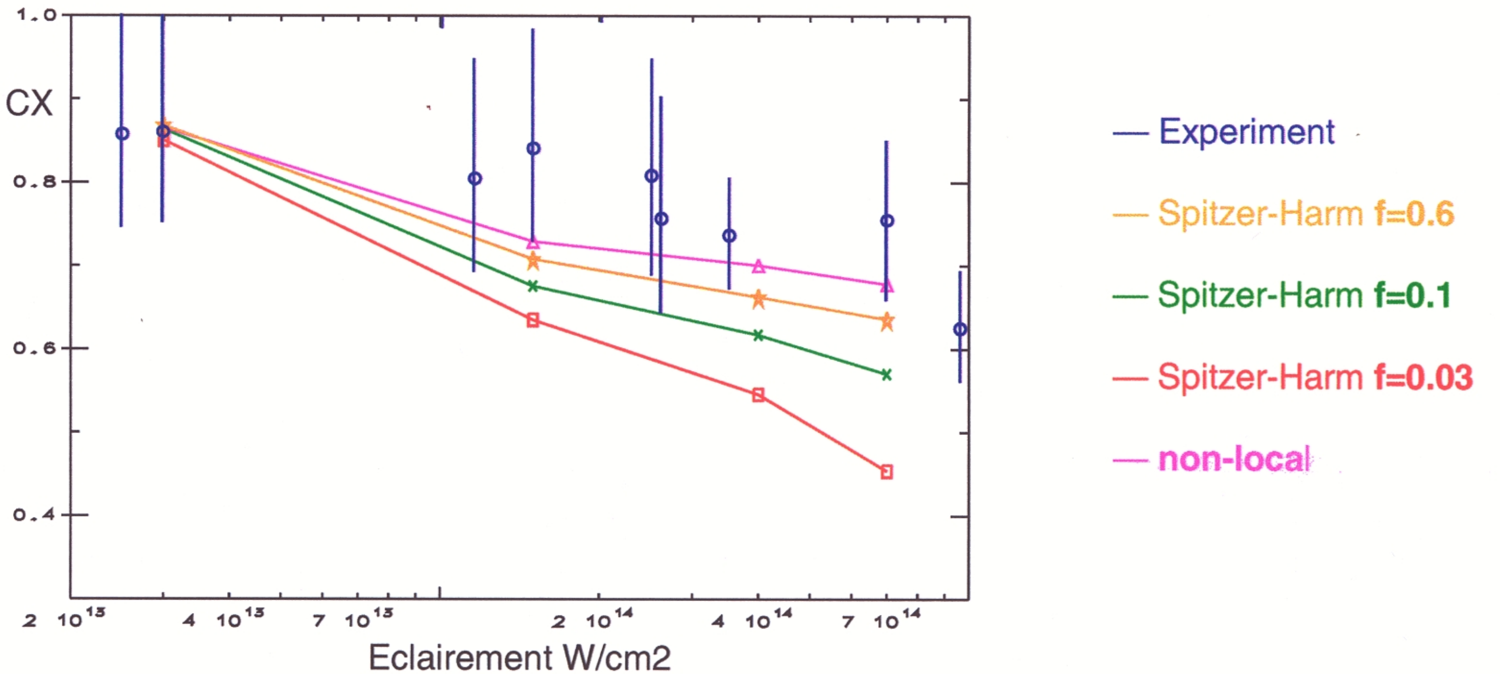

✔ The slightly limited SH flux and the nonlocal flux reproduce experimental data

Heat fluxes for high and low laser intensities

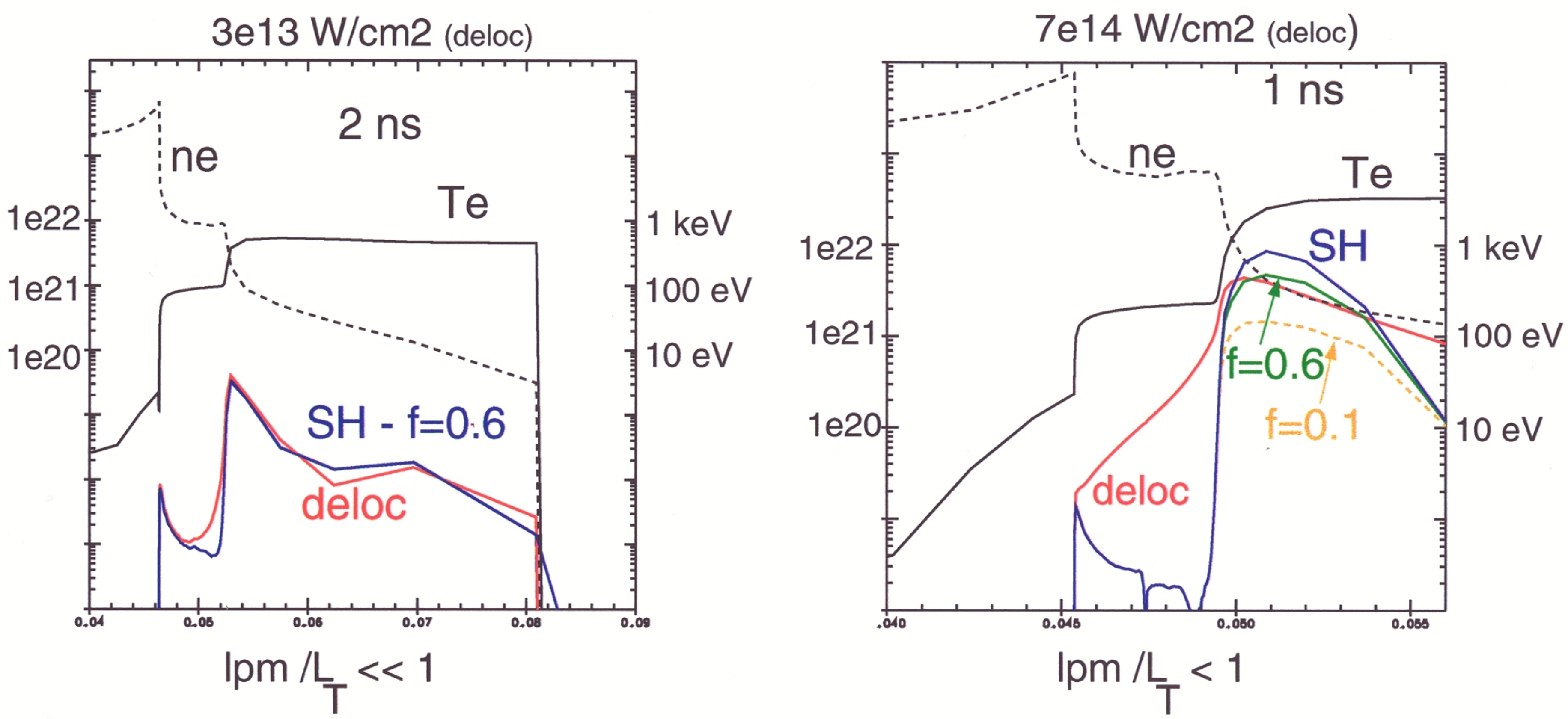

- low temperature, smooth gradient, short e.m.f.p, the nonlocal flux tends towards Spitzer-Harm flux.
- high température, sharp gradient, long e.m.f.p., the flux is nonlocal and different from Spitzer-Harm flux.

Simulation of X-ray imaging

Characterize plasma expansion

- From 2D hydrodynamic computations, we can simulate diagnostic (post-process)

emission at 2 keV

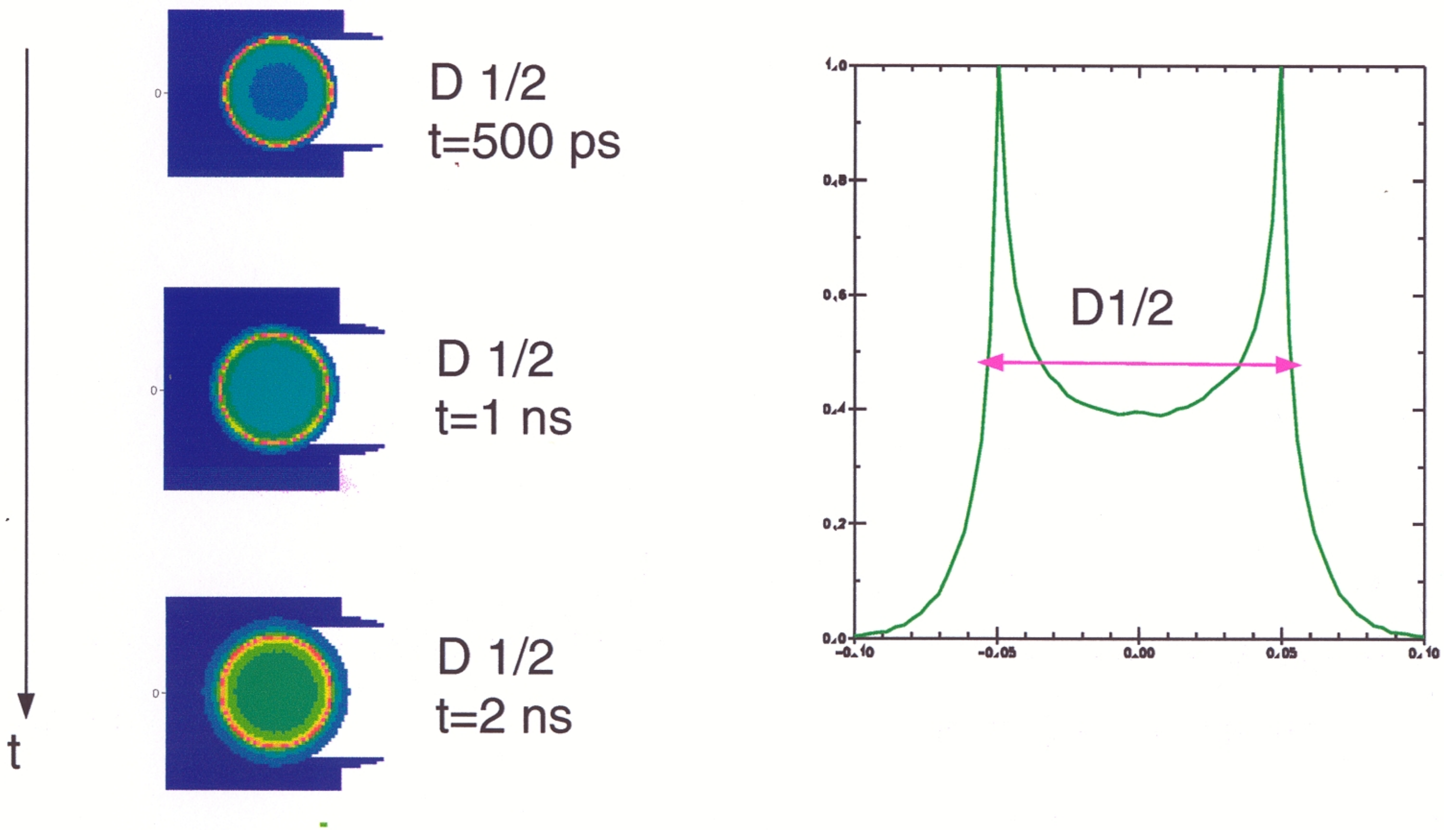

Emitting zones movement for I=7e14W/cm2

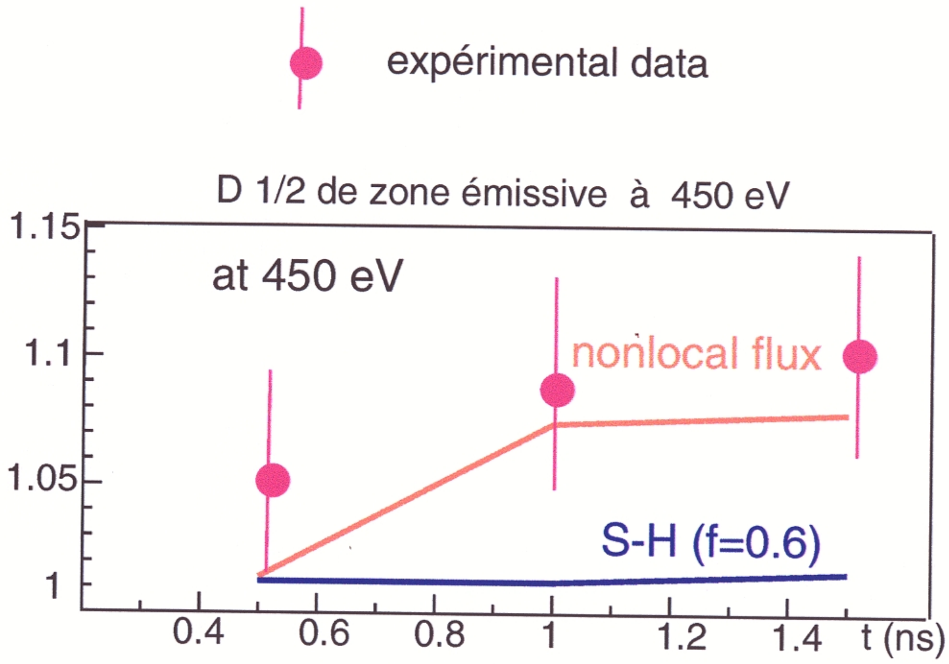

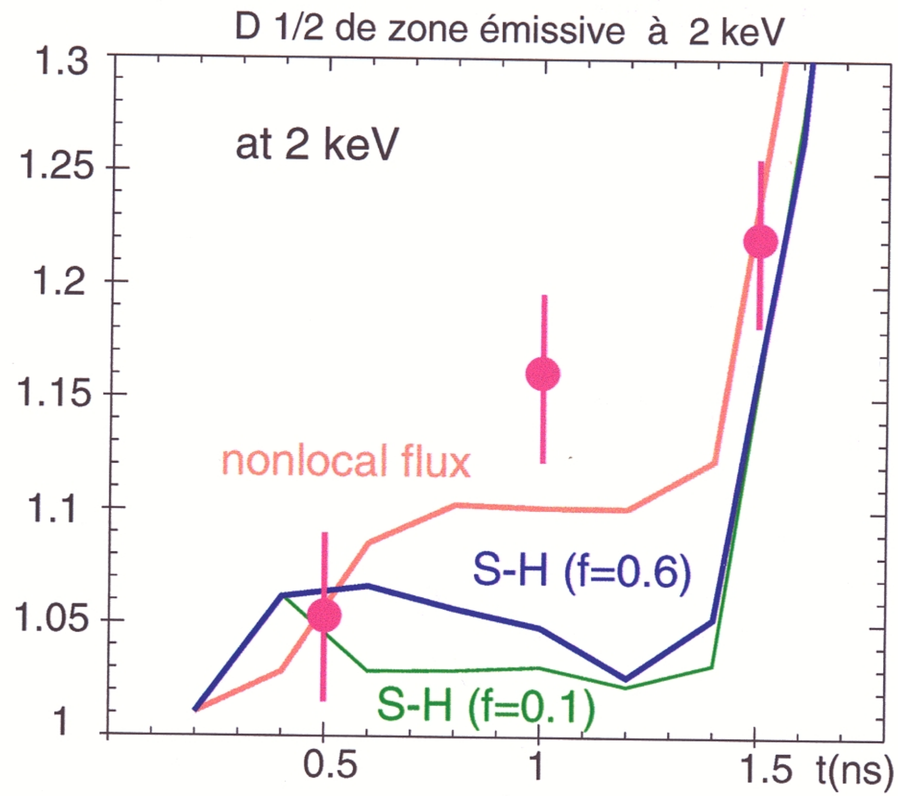

✔Spitzer-Harm fluxes do not be able to reproduce experiment

✔A flux limiter does not improve results

✔Using nonlocal fluxes, we get simuation closer to experimental data

Emitting zones movement for I = 4e14W/cm2

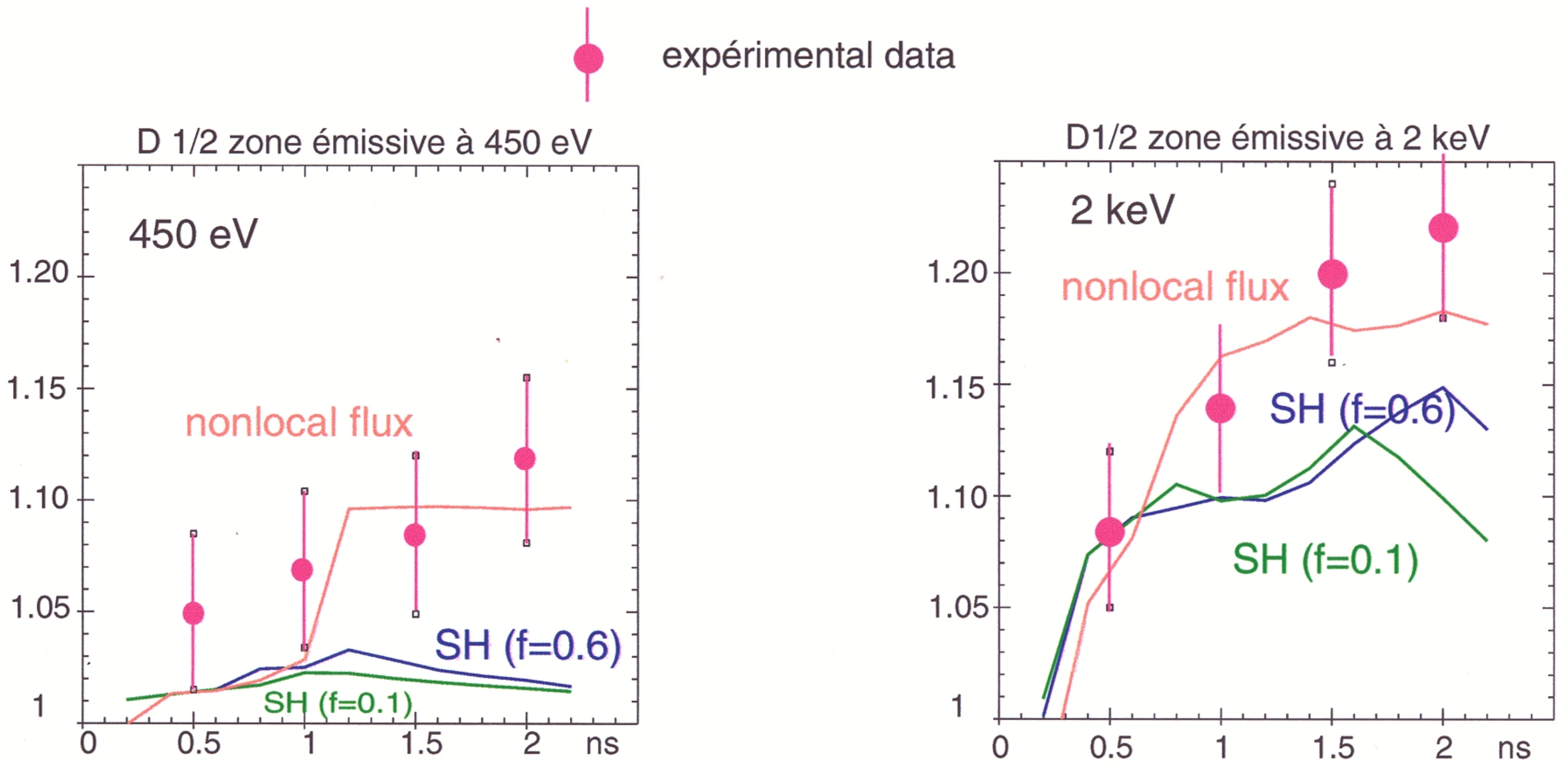

✔ Discrepancies between S-H and nonlocal fluxes are reduced but only nonlocal simulation passes through experimental data.

Emitting zones movement for I = 1e14W/cm2

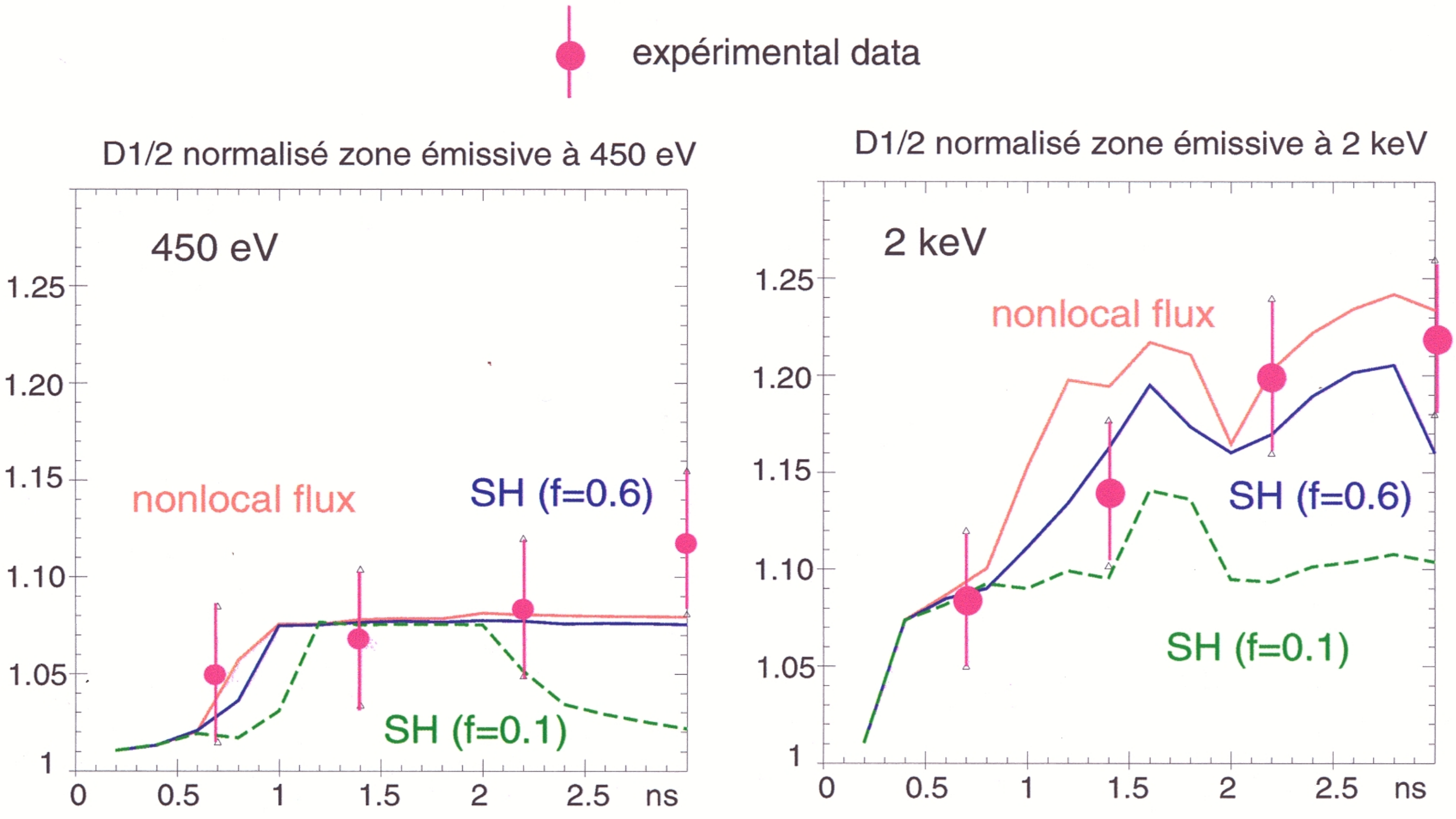

✔Non local flux tends towards SH flux for low intensity

✔ Both models reproduce experiment

Spherical target : summary

- Unlike cavity experiments, only nonlocal effetcs act on heat fluxes

- If some results like X-ray conversion efficiency can be explain by the use of Spitzer-Harm fluxes, only the nonlocal fluxes reproduce the movement of emitting zones.

- The variation of laser intensity in experiment allows us to test the convergence of our model to Spitzer-Harm model (low flux).

Conclusion

- The use of Spitzer-Harm fluxes, limited or not, does not allow us to reproduce some experimental results.

- From one experiment to another, and even from one diagnostic to another, the flux limiter value can be different : interpretation $\Longleftarrow\!\Longrightarrow$ prevision

- Nonlocal fluxes combined with magnetic fields improve simulations and so our understanding of laser plasma experiments

(up to now...)

Laser expériments : Interpretations and predictions

Ph. NICOLAÏ, D. BABONNEAU, M. BONNEFILLE, B. CANAUD, F. CHAIGNEAU,

E. DATTOLO, C. ESNAULT, J-P. JADAUD, S. LAFFITE, M-C. MONTEIL,

G. SCHURTZ, M. VANDENBOOMGAERDE, B. VILLETTE, F. WAGON.

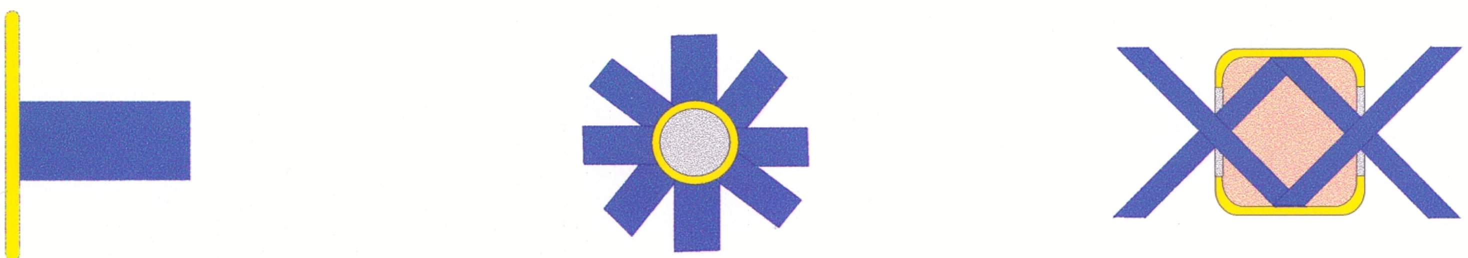

Magnetic fields and nonlocal fluxes

Effects of each process are less or more large following :

- experimental geometry [plane-sphérical]
- observed quantity [Tr, Te, ne, hυ ...]
- plasma zone seen (probed) by diagnostic

The choice of an experiment and diagnostics (can) enables us :

- to test both effect combined or alone
- to check our model
- to improve our understanding of physical processes involved

  (to improve theory)

Planar target (Phebus facility)

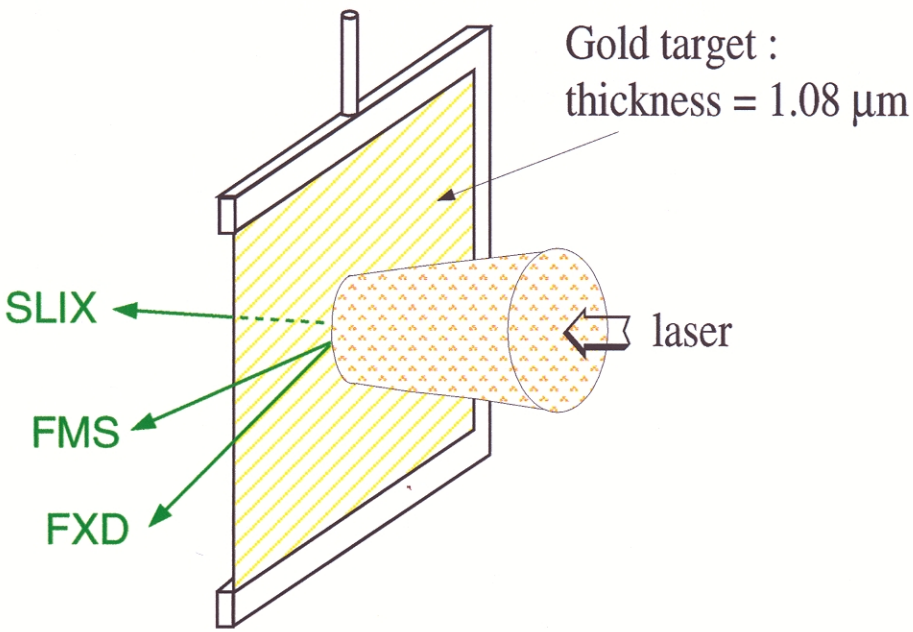

<u>Laser</u>

- smoothed by RPP
- 3ω
- 1.5ns square pulse
- 3kJ
- FWHM=340µm

FMS :streak camera wich images 200 eV X-ray emission perpendicular to laser axis

☛ provides a time-resolved 1D image

FXD : streak camera wich images above 2 KeV X-ray emission perpendicular to laser axis

☛ provides a time-resolved 1D image

SLIX : gated microchannel plate detector images 2.5KeV X-ray (M-shell) from rear side

☛ provides a time-resolved 2D image

2D Simulation of experiment

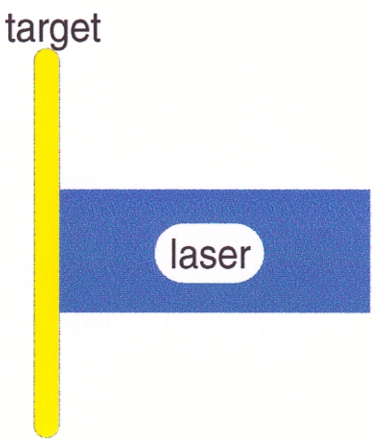

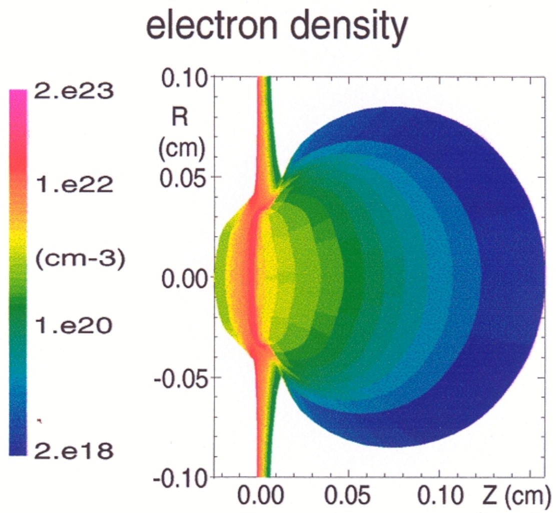

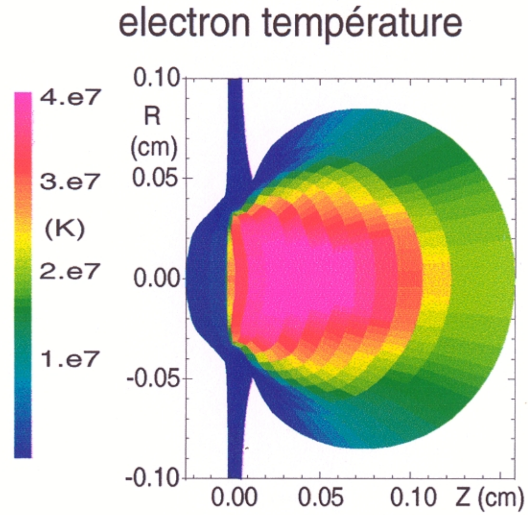

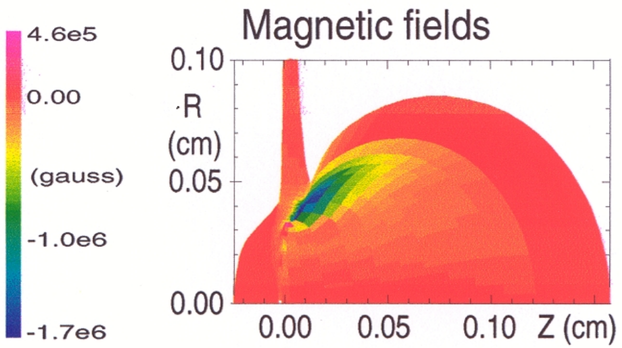

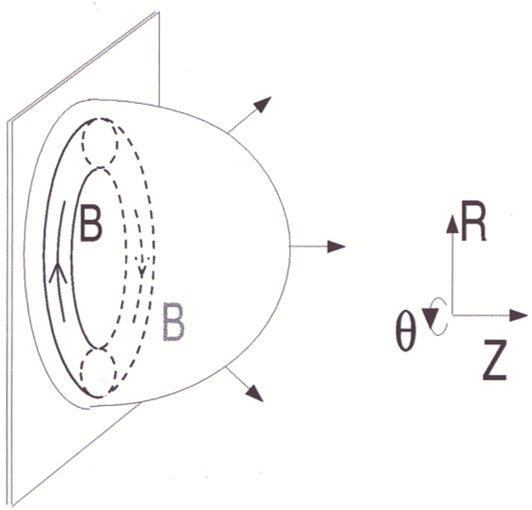

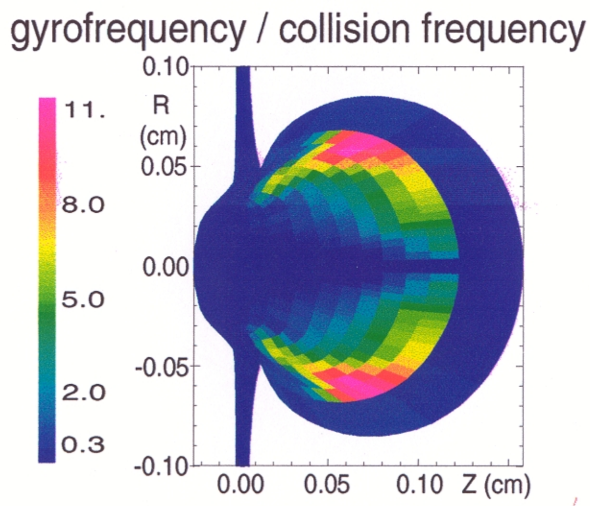

Electron heat fluxes

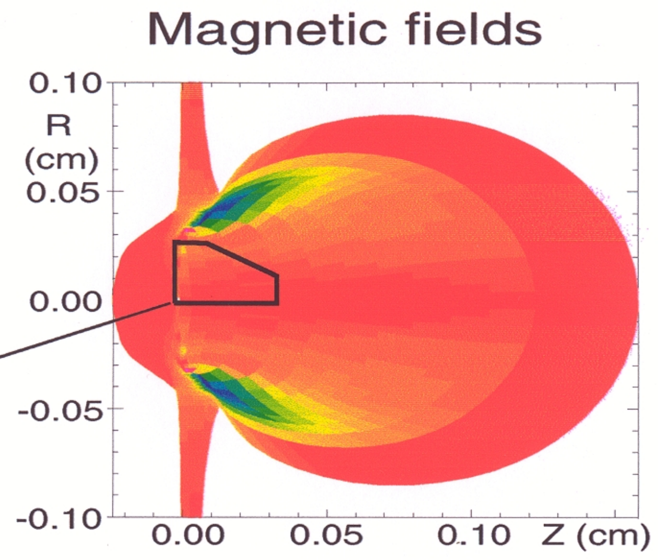

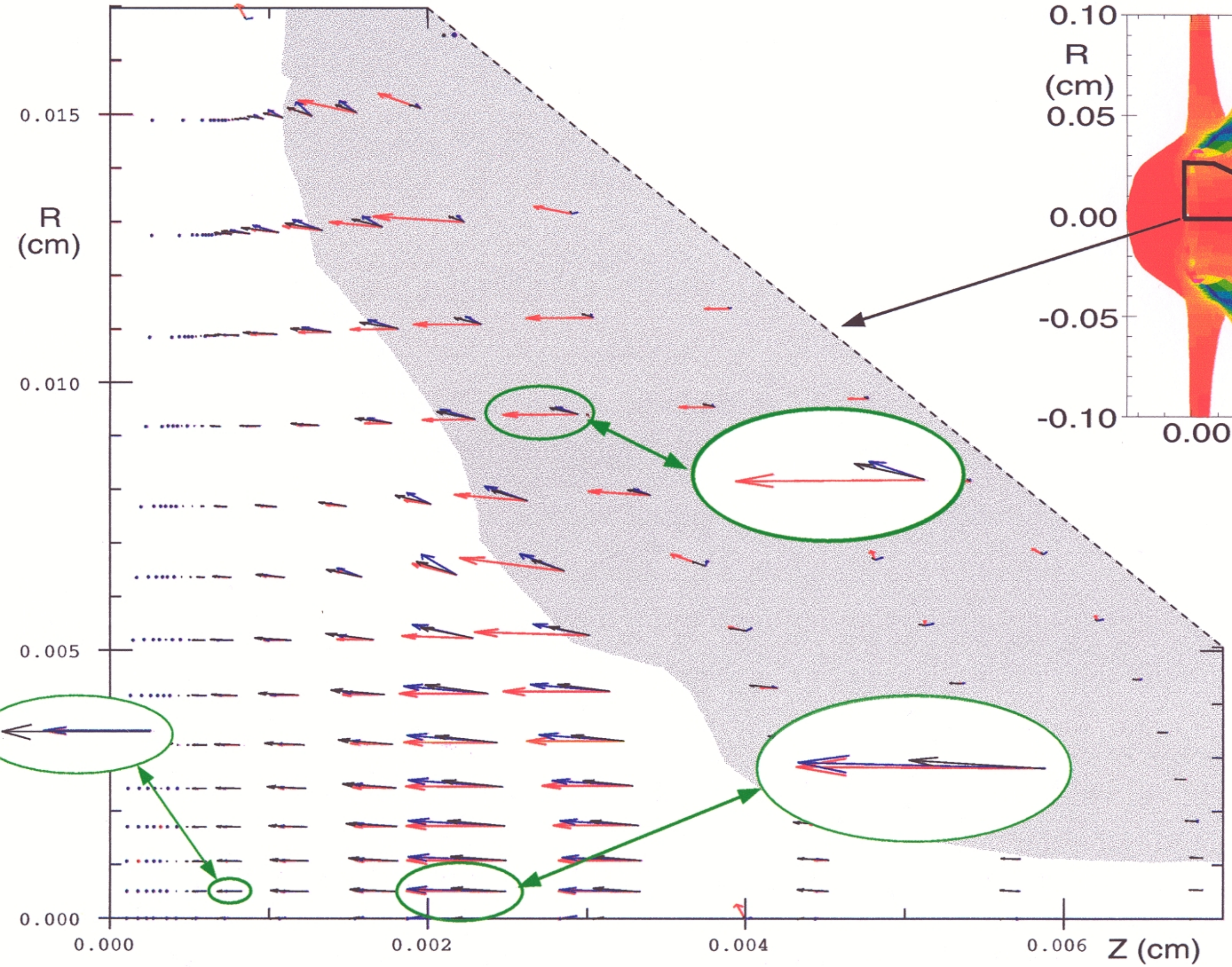

FMS diagnostic

Streak camera which measures 200 eV X-ray emission through a slit

➲ side view, 1D time-resolved image

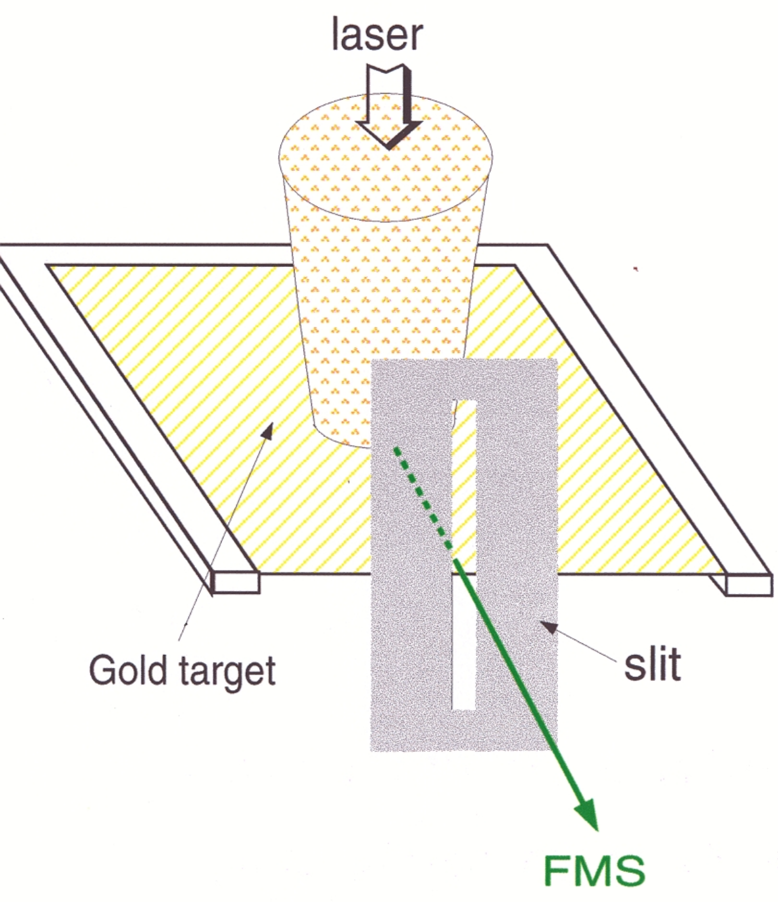

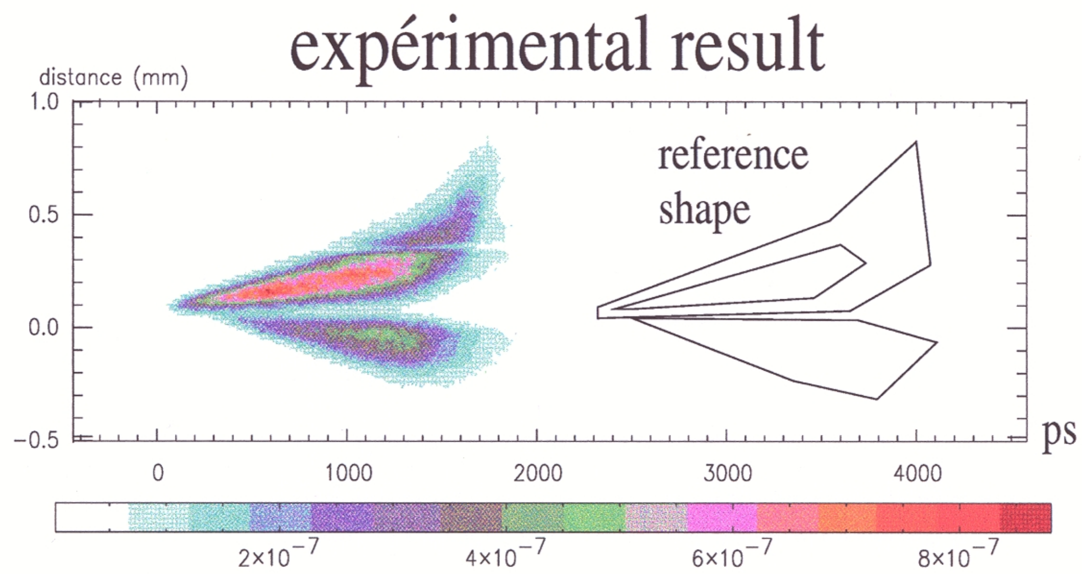

Experiment-simulations comparisons

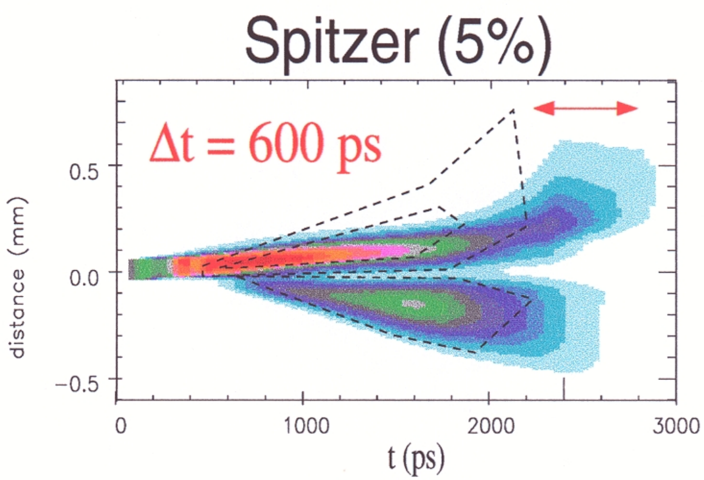

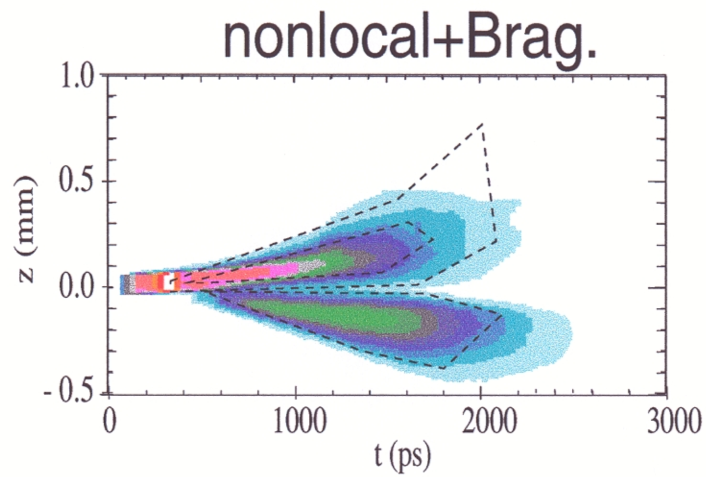

- ✔ Using Spitzer-Harm fluxes, we obtain (front side) an emission too long (600ps). Second, the slope of the upper part is too small (velocity of the emitting zone).

- ✔ We tried to change limiter value, average between SH and free streaming, laser parameters, mesh refinement, etc... But no effect on numerical results.

- ✔ Using B-fields and nonlocal transport, we obtain a emission length shorter and the slope of the upper part is higger and is in good agreement with exp. result .

Individual effects of each process

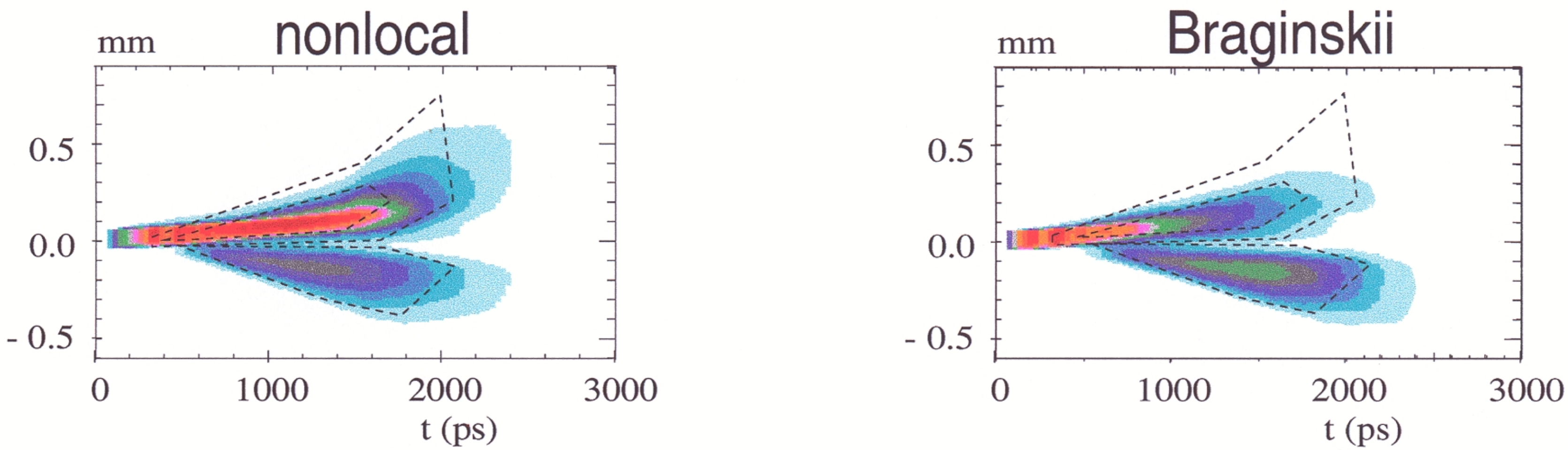

✔ Using nonlocal fluxes, we obtain a shortening of emission but not enough to reproduce experiment.The emitting zone shifting (laser side) is correct

✔ Using B-fields, we obtain a good length of emision (front side) but the slope of the upper part is too small (slightly)to mach experimental data.

✔ So, it seems that combined effects produce the best agreement with experiment

SLIX Diagnostic

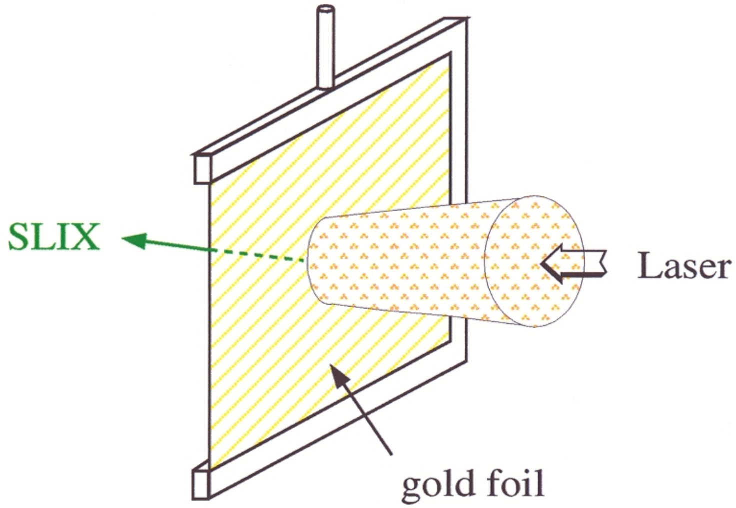

Slix diagnostic takes 'photos' of the rear side in the range about 2.5Kev (M-shell)

Res.=10µm et Δt=100ps

experimental image

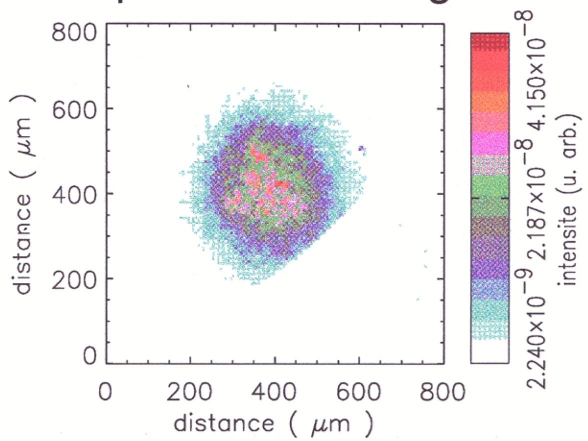

circular average

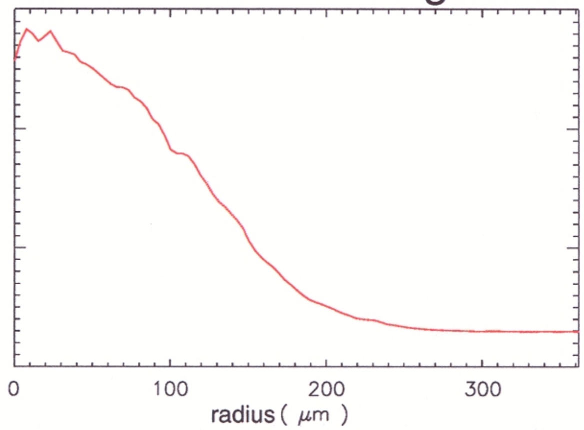

Expériment-simulation comparisons

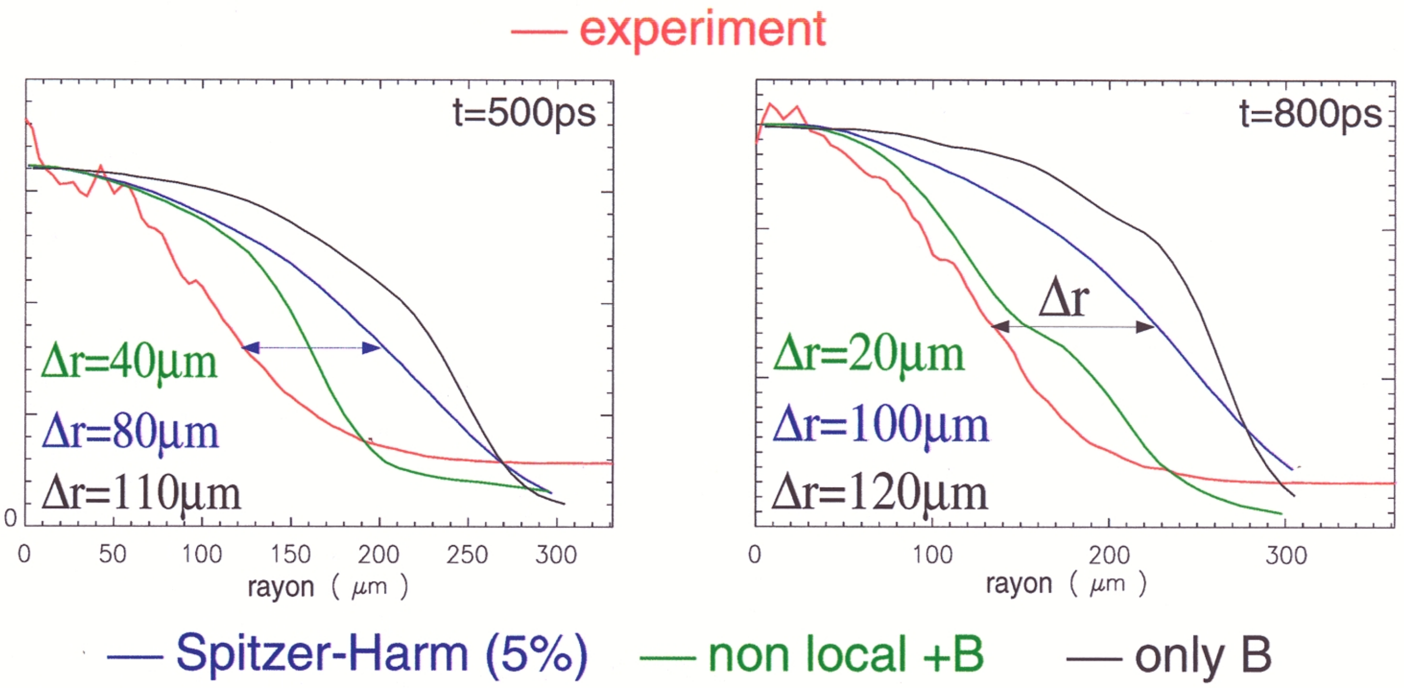

✔ Using Spitzer-Harm , we get images too large by about 80 and 100 µm at half maximum.

✔ B-flieds do not improve results

✔ B-flieds and nonlocal fluxes give the best agreement

FXD Diagnostic

Streak camera which measures X-ray emission above 2KeV

➲ side view, 1D time resolved image

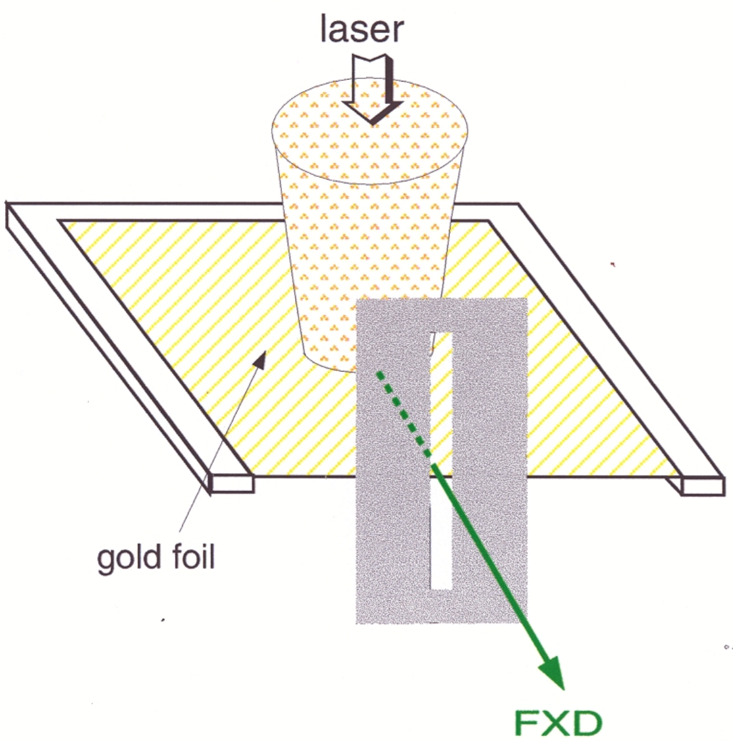

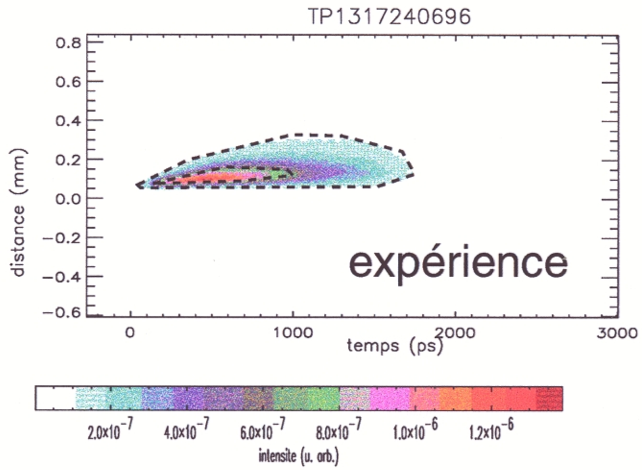

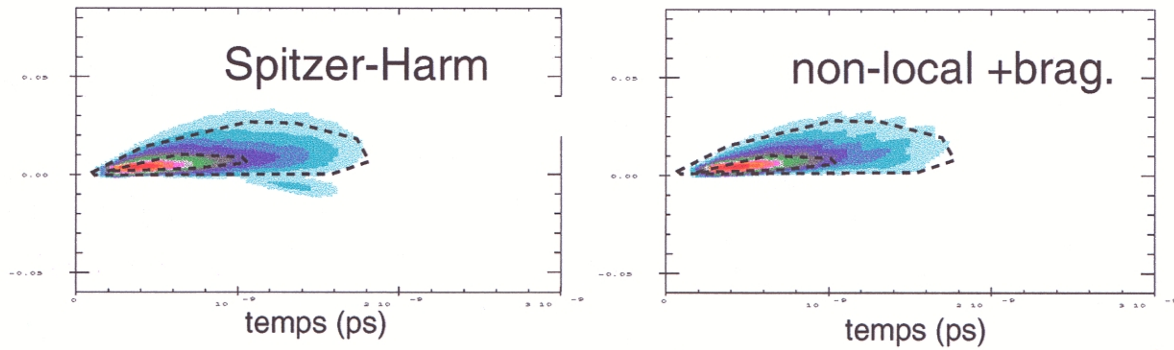

Planar target : summary

- Using Spitzer-Harm fluxes, simulations are unable to reproduce all diagnostics, whatever variations of flux limiter, laser parameters, zoning,...

- Both non local and magnetic effects improve simulation results without arbitrary parameter (flux limiter).

- If we only use one process,we get some improvements but not enough to match experimental data.

Hohlraum experiments
(NOVA / OMEGA facilities)

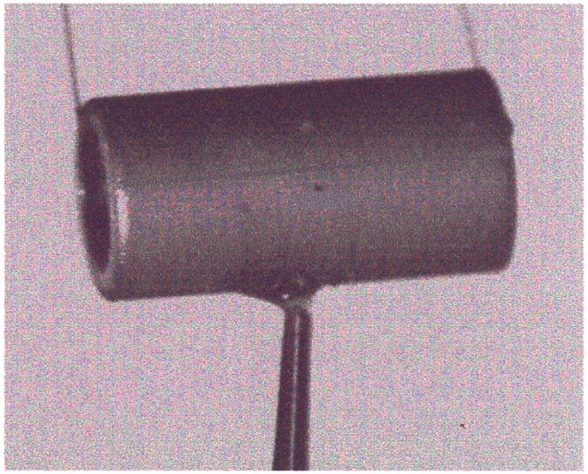

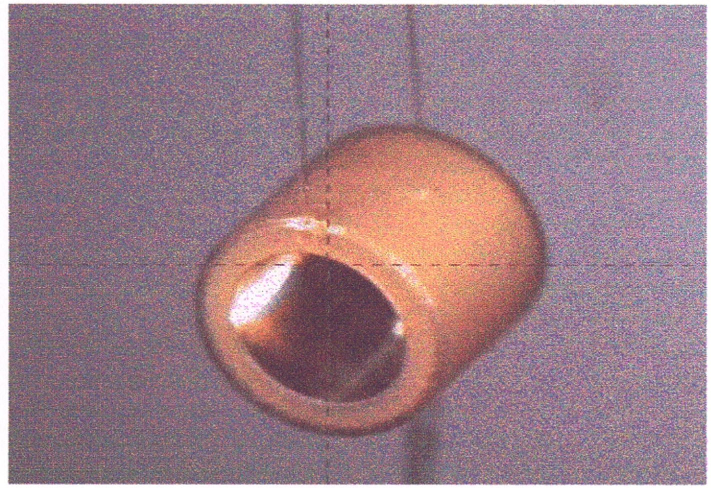

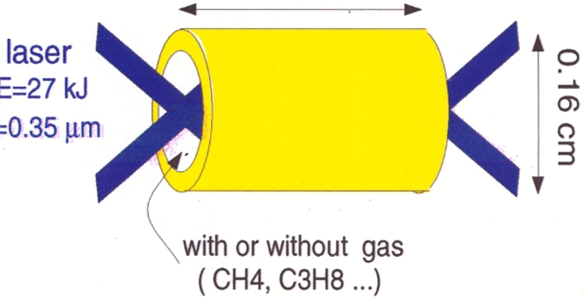

Thomson scatttering

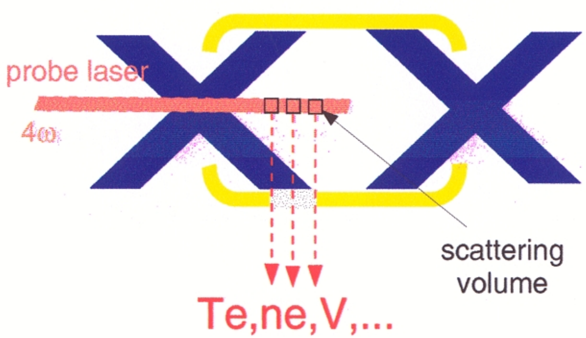

X-ray Spectrum ➠ Tr

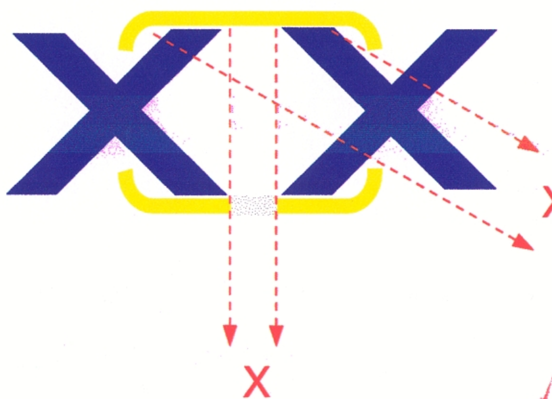

Gas-filled Hohlraum (nova exp.)

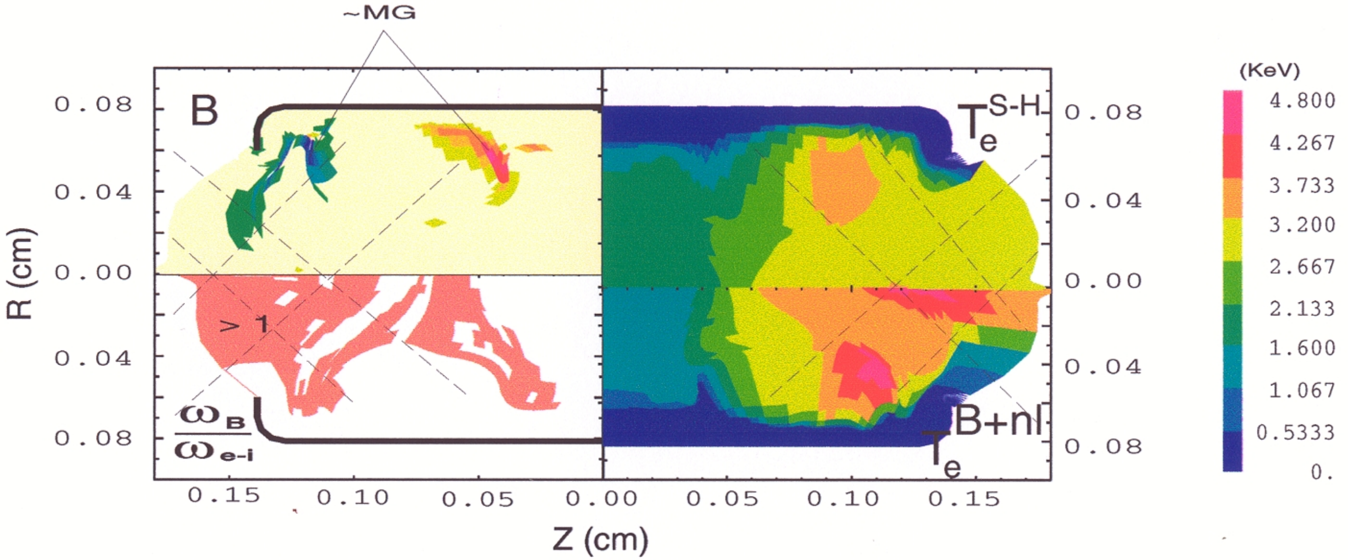

✔ Simulations with radiation-hydrodynamic code (FCI2) predict B fields of order of 1 MG

✔Hall parameter exceeds unity in a large zone of the hohlraum (B effects)

✔Calculations with SH or with our model (w/o flux limiter) lead to differents results :

- ☛ higher electron temperature in off-axis region (from 3.5 keV to 4.8 keV)
- ☛ larger temperature gradient along the axis (beams crossing)

✔ experimental data of electron temperature from Thomson scattering seem to confirm large gradients along z-axis and temperature in order of 5KeV close to LEH

Hohlraum experiment

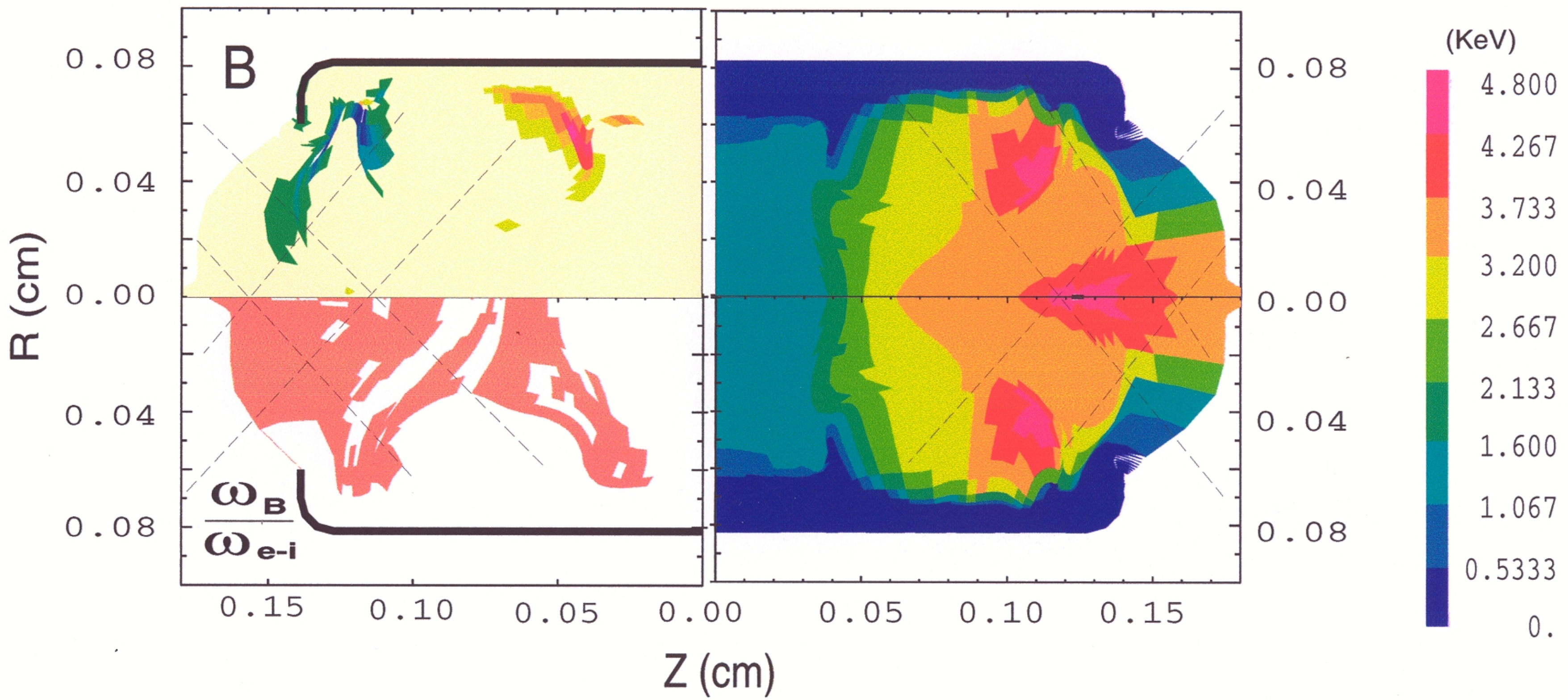

Hohlraum experiments

✔ In a hohlraum, magnetic fields quickly spread in the whole plasma.

✔ B-fields reduce or cut nonlocal effects. The deformation of the spherical part of the distribution function due to nonlocal effects may be reduced or cancelled by B-fields.

✔ Simulations without nonlocal fluxes but with B effects can correctly reproduce, in this case, experimental results.

B-fields (nonlocal effects) can modify density

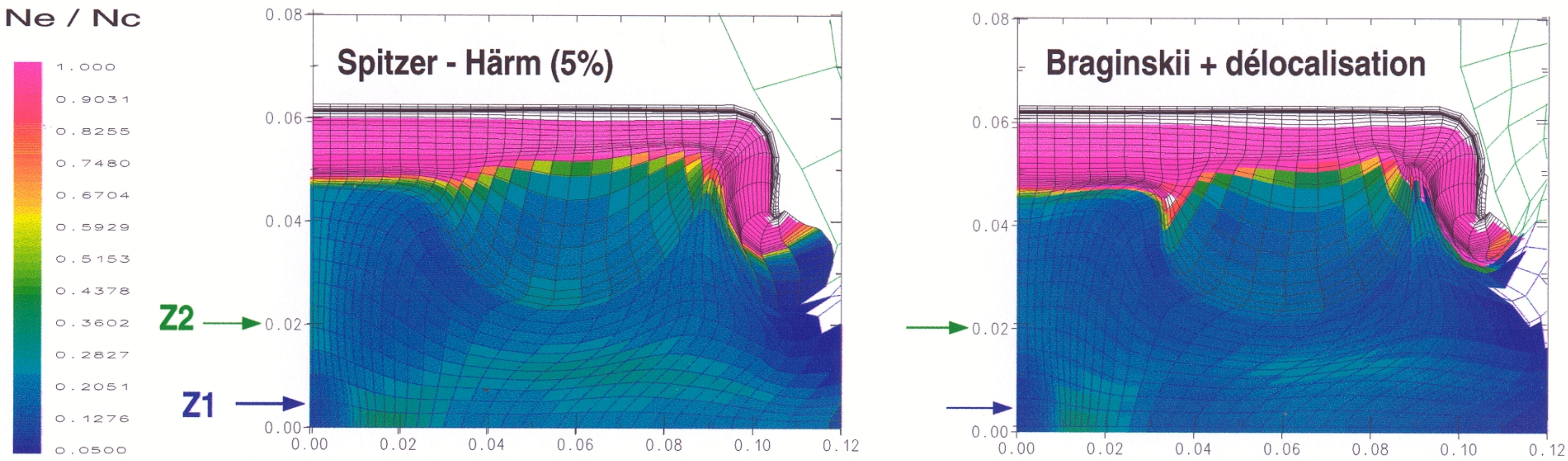

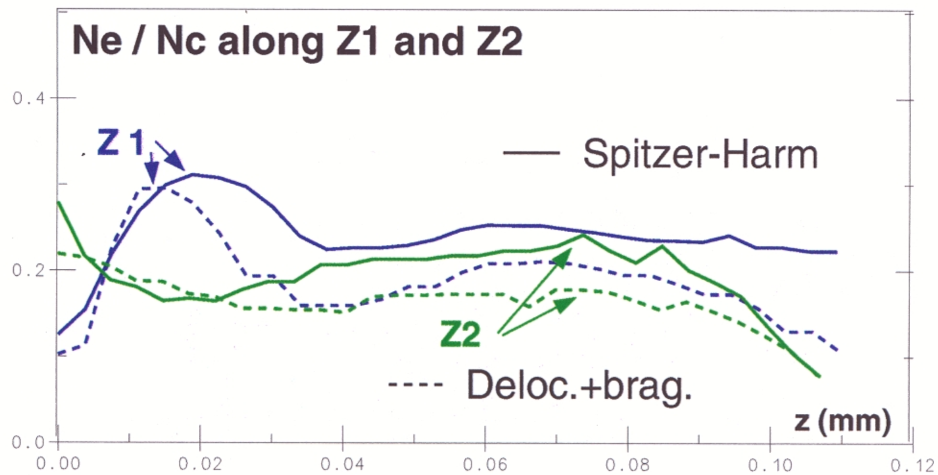

✔ Electron density is lower with Braginskii + deloc model. (about 15%)

Same radiation temperature versus formula

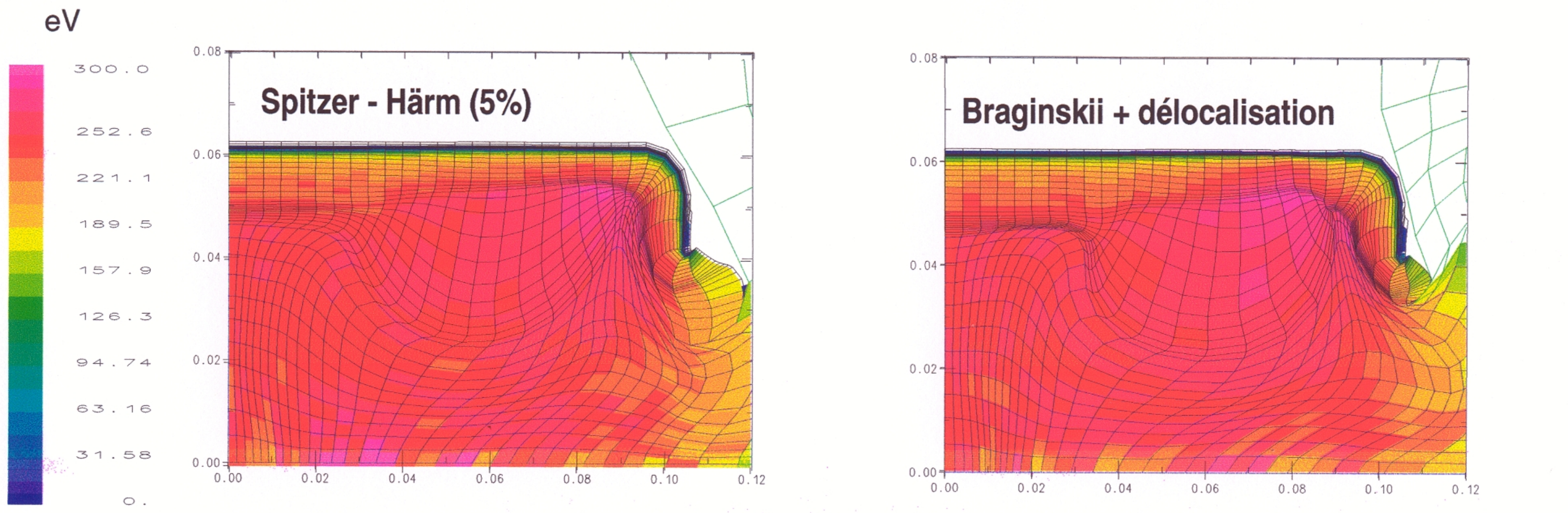

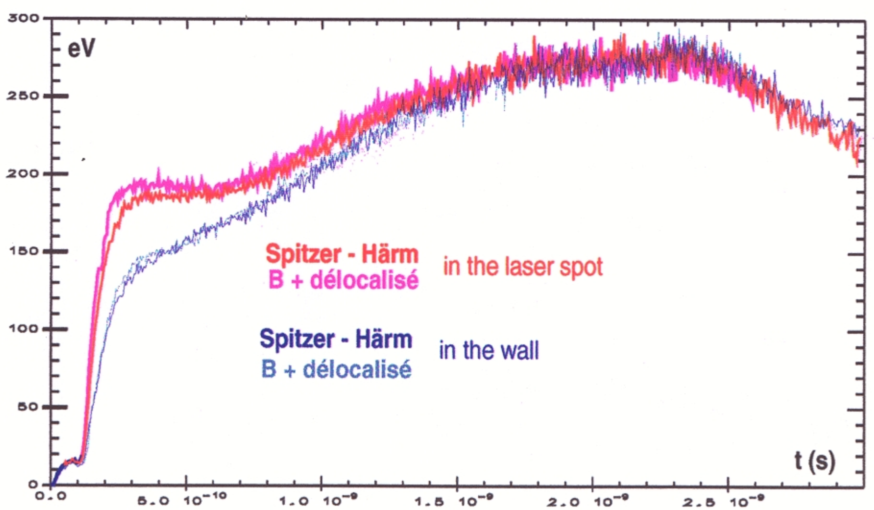

✔ same Tr but w/o flux limiter : (good value)

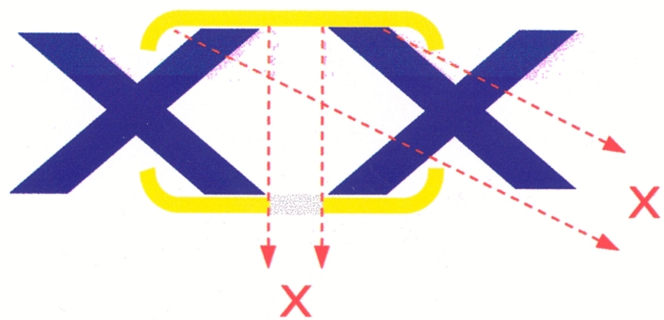

✔So X-ray Diagnostics simulation correct?

Our electron conduction model can modify hydrodynamic motion

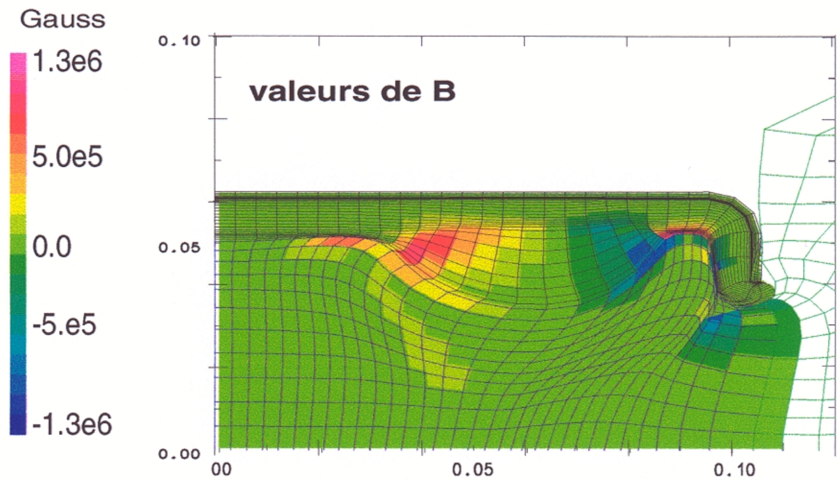

✔heating and expansion of LEH w/o B-fields -> X-ray emission of this zone

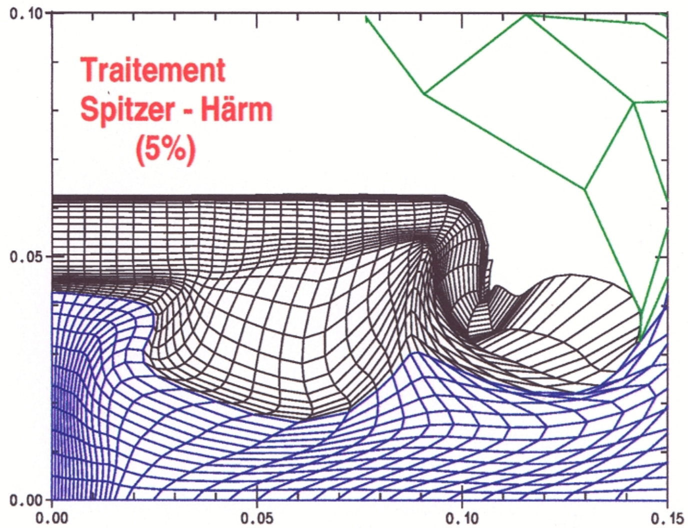

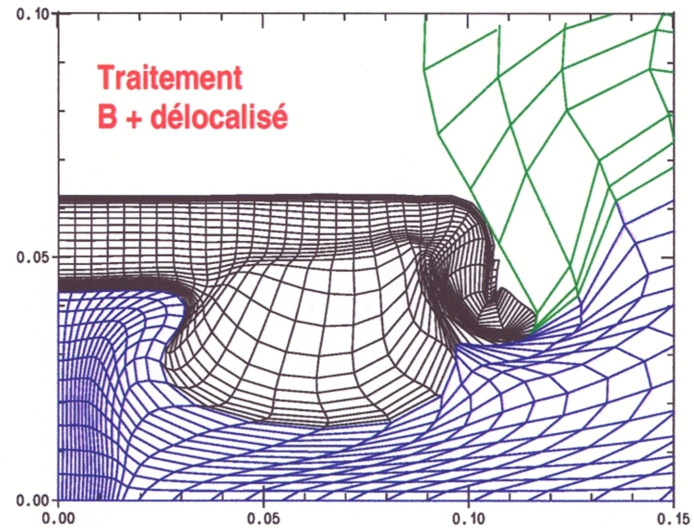

Hydrodynamic effect on X-ray emission

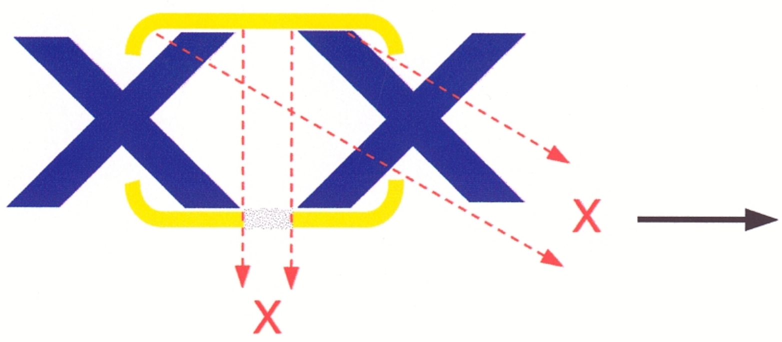

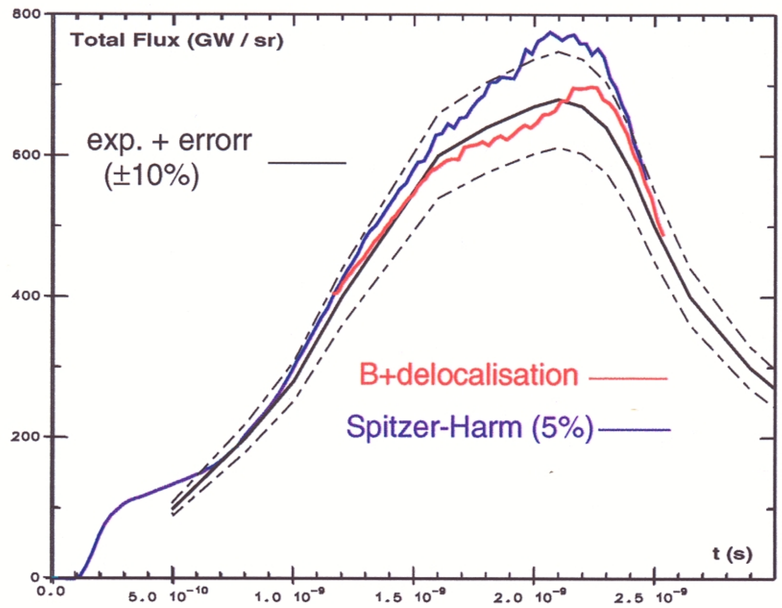

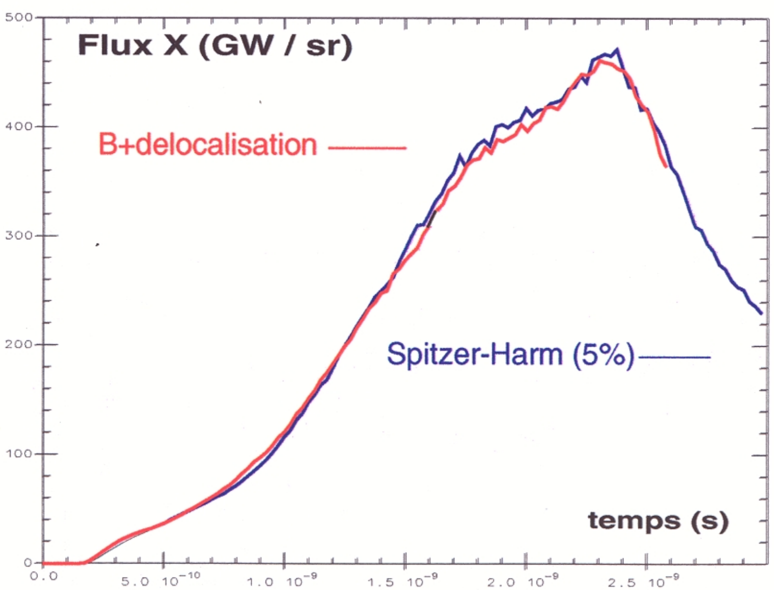

- ✔ For Dante, both heat flux models give similar results
- ✔ B-fields reduce X-ray emission of 'LEH' and enable us to better reproduce exp. data
- ✔ Both simulations are inside error bars

Effects of our model on LMJ cavity

Max. laser power = 400 TW (16 ns) ; Laser energy = 1,4 MJ

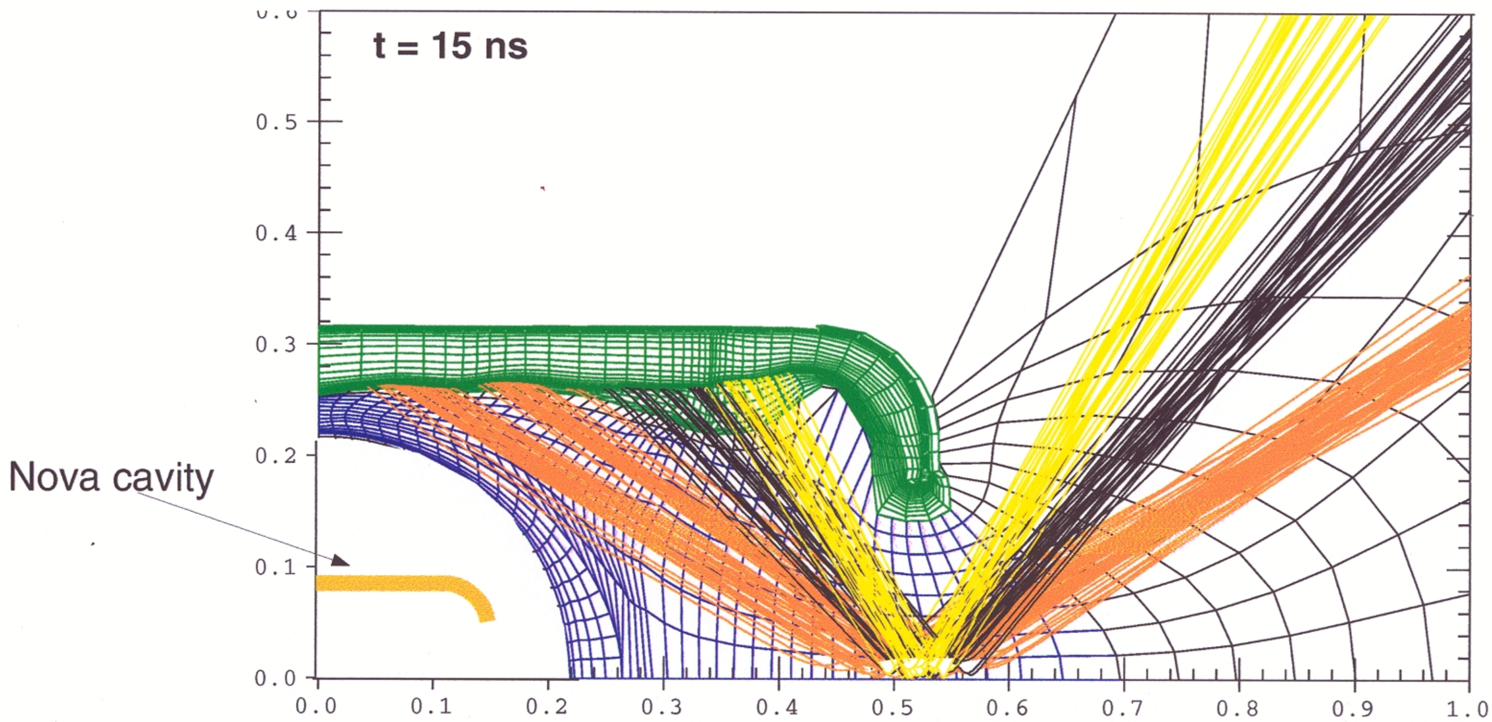

Magnétic fields at 16 ns (max. laser power)

❍ B effects are important in a large part of the cavity

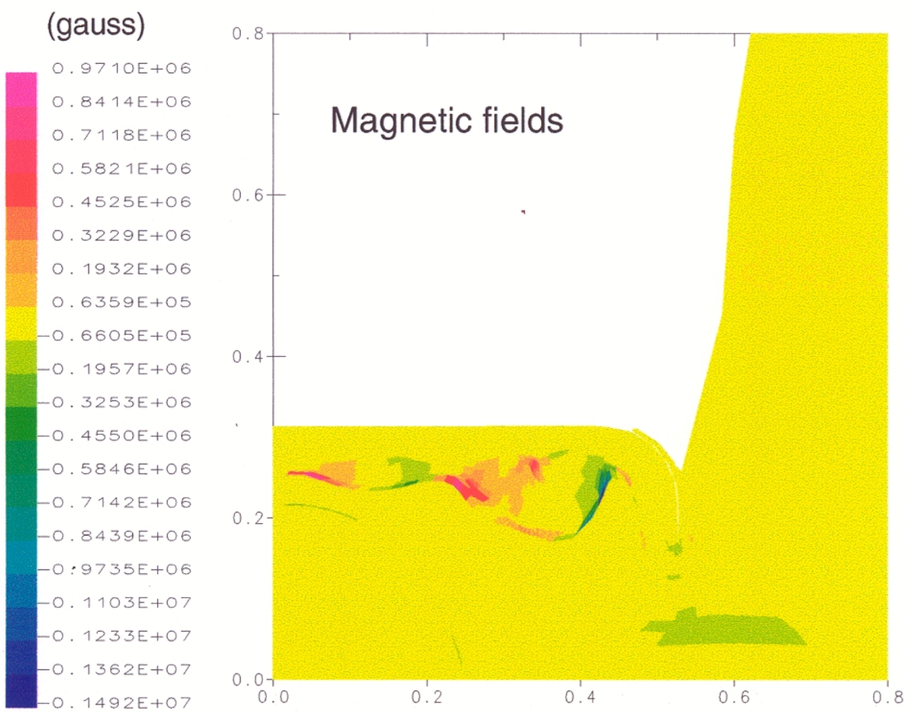

➲ We expect some modifications for

✓ electron température

✓ ion température

✓ density

✓ionization

✓ hydrodynamic speed

✓ ...

Electron temperature color map at t = 16ns

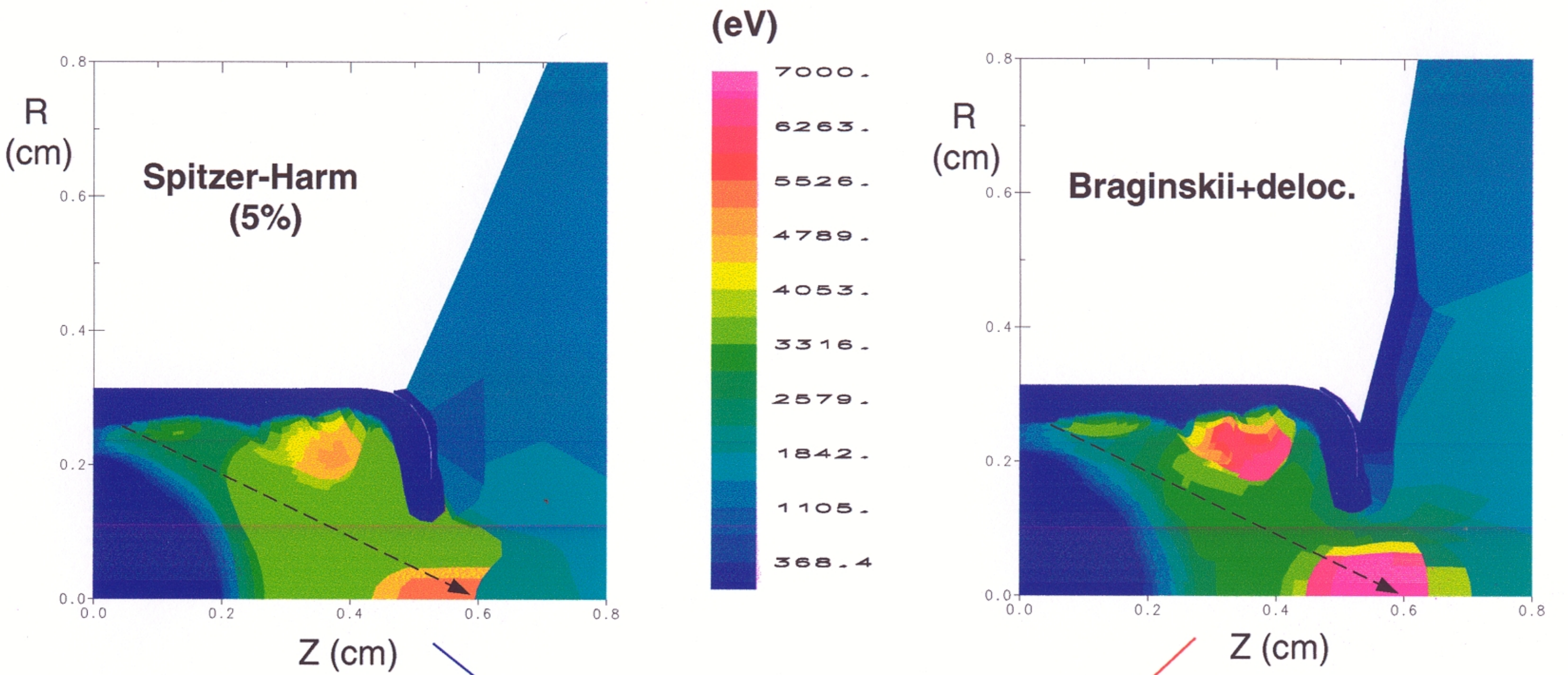

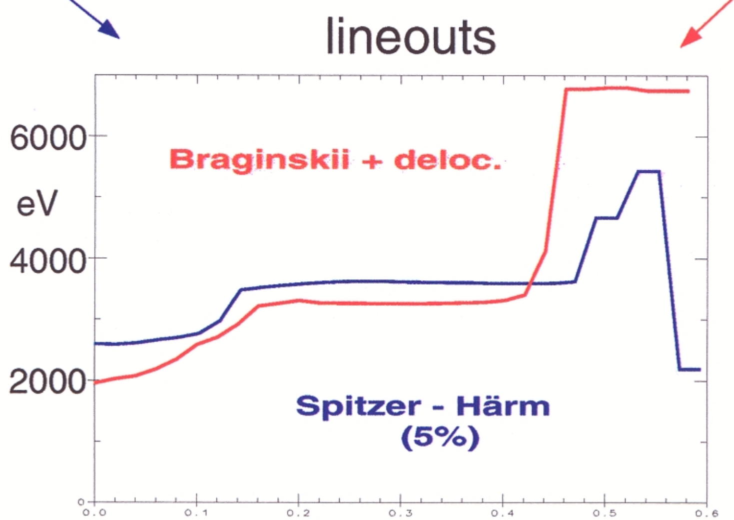

Electron density map at t = 16ns

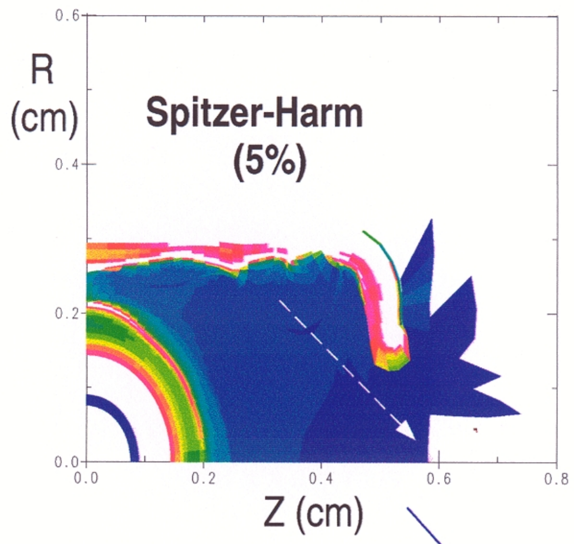

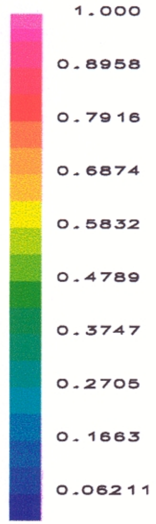

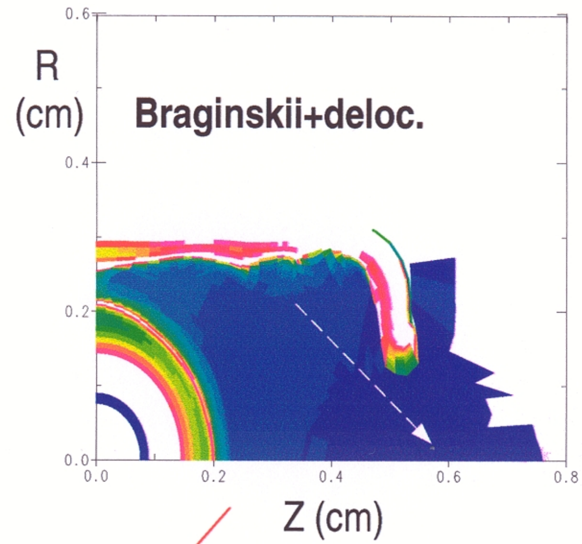

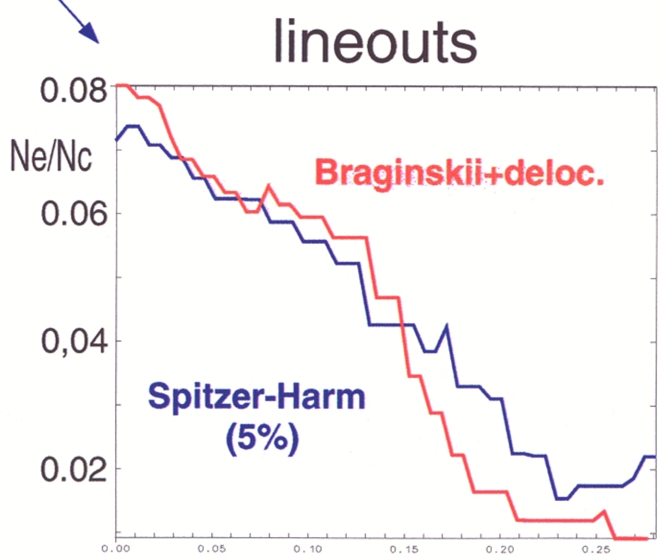

X-rays non uniformities on the ablation front

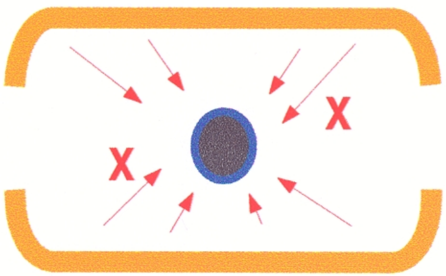

❍ Expansion of the X-ray flux on a Legendre polymomial basis

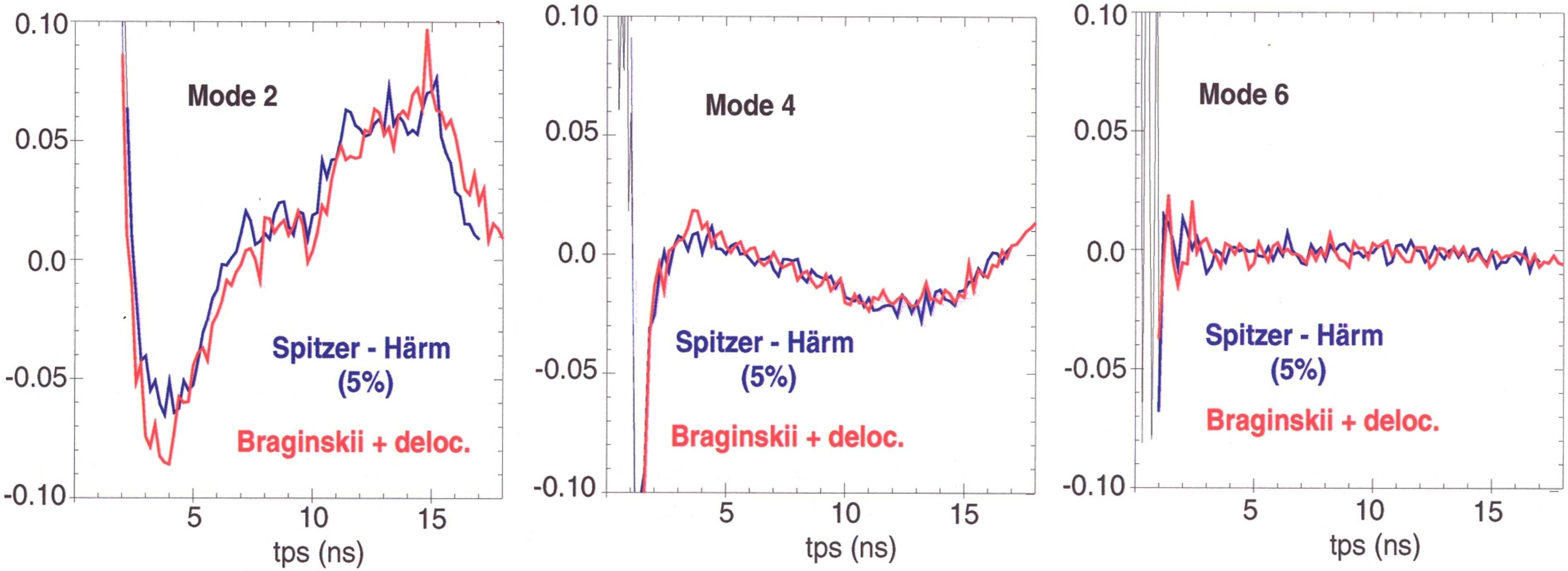

!neither beam-phasing nor pointing optimization !

Cavity : summary

- Simulations using magnetic fields and nonlocal fluxes match Thomson scattering results unlike simulations with S-H fluxes.

- The fields diffusion inside cavity reduce non-local effects.

  ➡ Using Braginskii fluxes, simulation passes through expérimental error bars

- Hydrodynamics quantities (Te,Ti,Ne,V,...) can be hardly modified by magnétics fields ⇨ effects on others processes (Laser Plasma Interaction)

- The radiation temperature and the irradiation symetry of micro-ballon are not affected by our model ⇔ limited Spitzer-Harm (f~5%)

Spherical target (Omega facility)

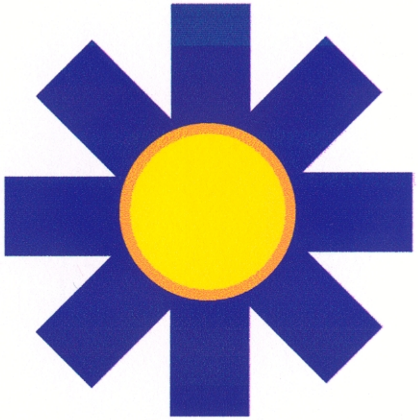

✔ CH targets (950µm) cover with gold (2.5µm)

✔ laser : - 3ω
- intensities from 1e13 to 1e15 W/cm2
- square pulses for from 1 to 4ns
- fwhm ≈ 500µm

simplified expérimental configuration

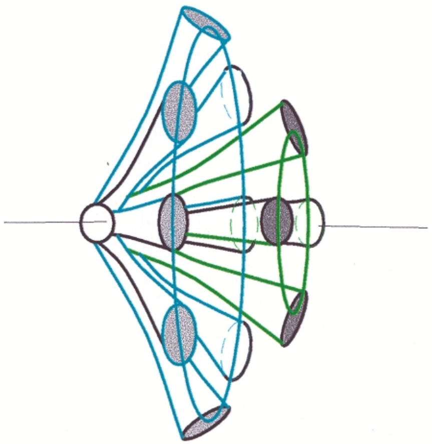

simplified 2D simulation

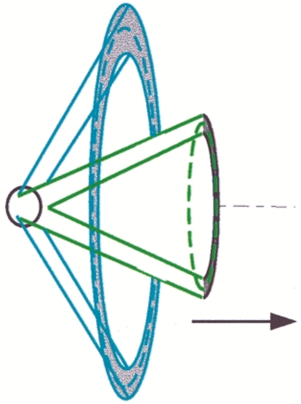

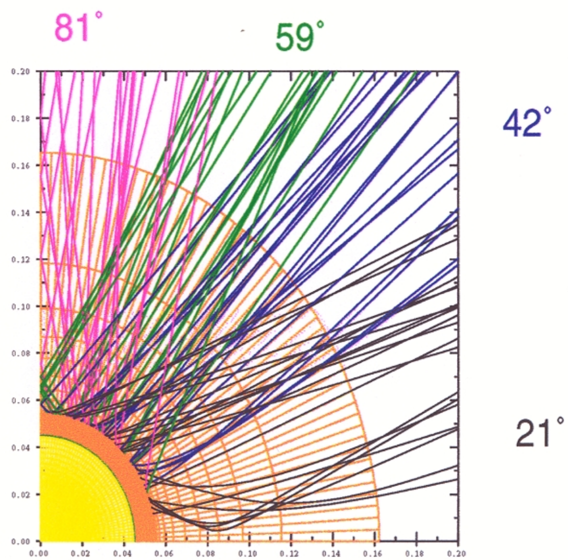

✔ X-ray Diagnostics : spectrum, conversion efficiency, imaging with spectral resolution

Influence of self-generated magnetic fields

✔Crossed gradients Te-Ne can create B-fields

✔ For this geometry, with an isotropic irradiation, gradients are collinear -> no B-fields

✔ In experiment, we can have unbalanced laser power between beams (cones)

I=1.4e14, at 21° (-14%), at 42° (+2%) at 58° (-0.3%) at 81° (+6%) *worst case*

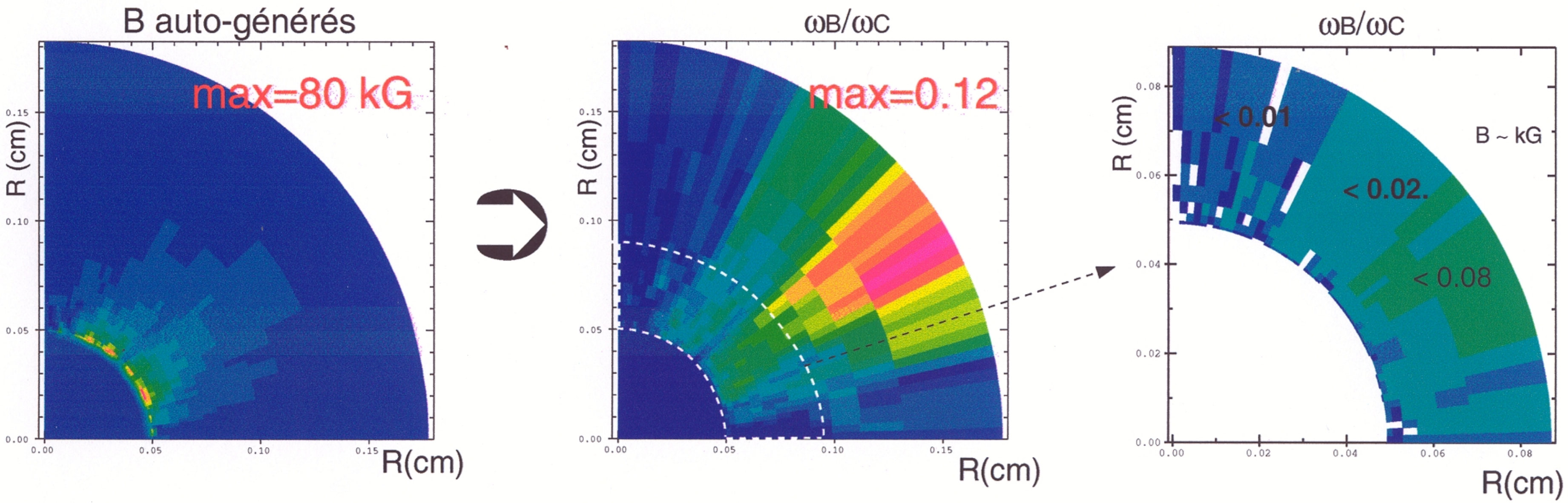

➥ **No influence of magnetic fields (same res. w or w/o B)**

➥ **Only nonlocal flux acts on plasma in these experiments**

X-ray Conversion

X-ray Energy / Absorbed laser energy

✔ We test the influence of heat flux on X-ray conversion

✔ Expérimental data come from several experiments

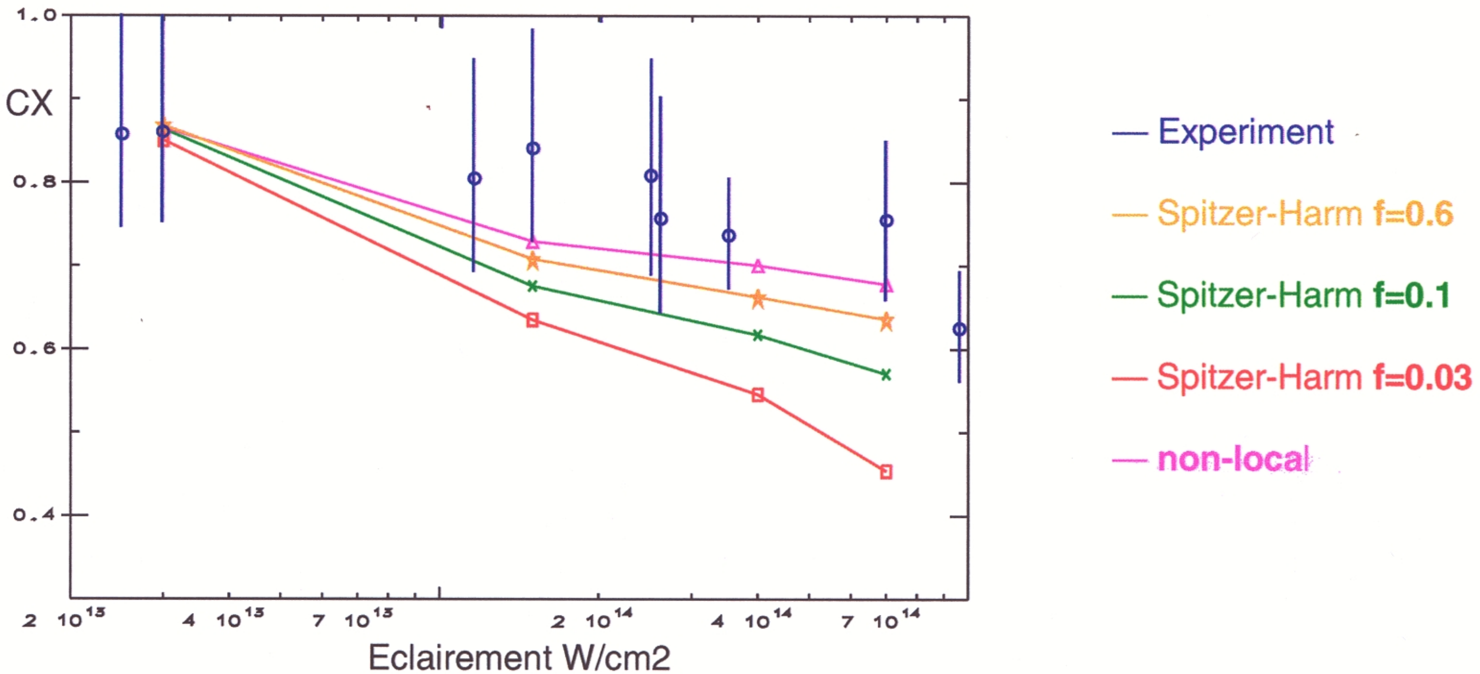

✔ The slightly limited SH flux and the nonlocal flux reproduce experimental data

Heat fluxes for high and low laser intensities

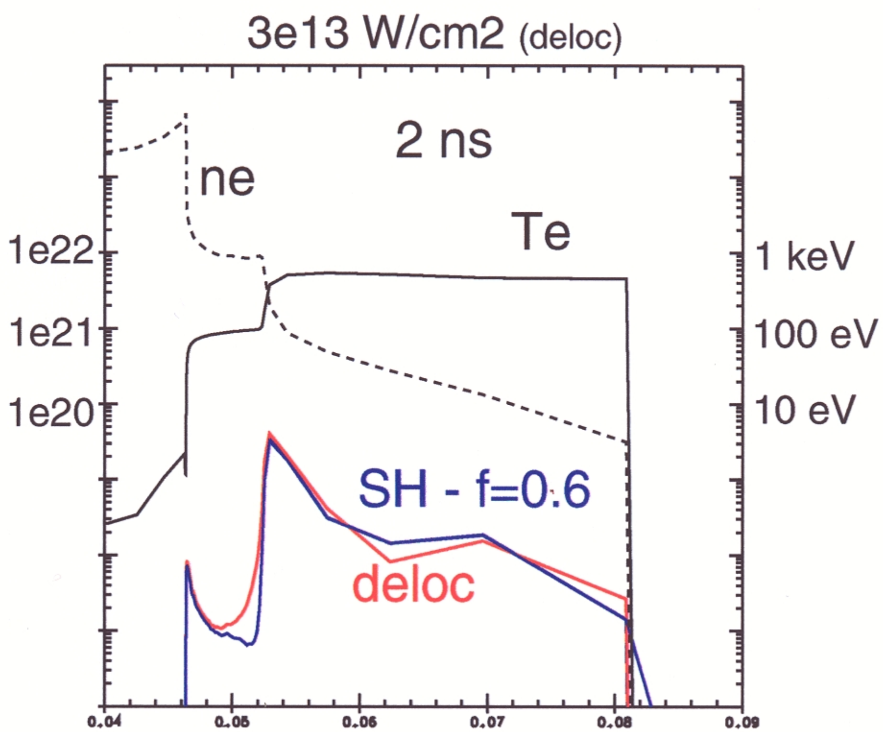

$lpm / L_T << 1$

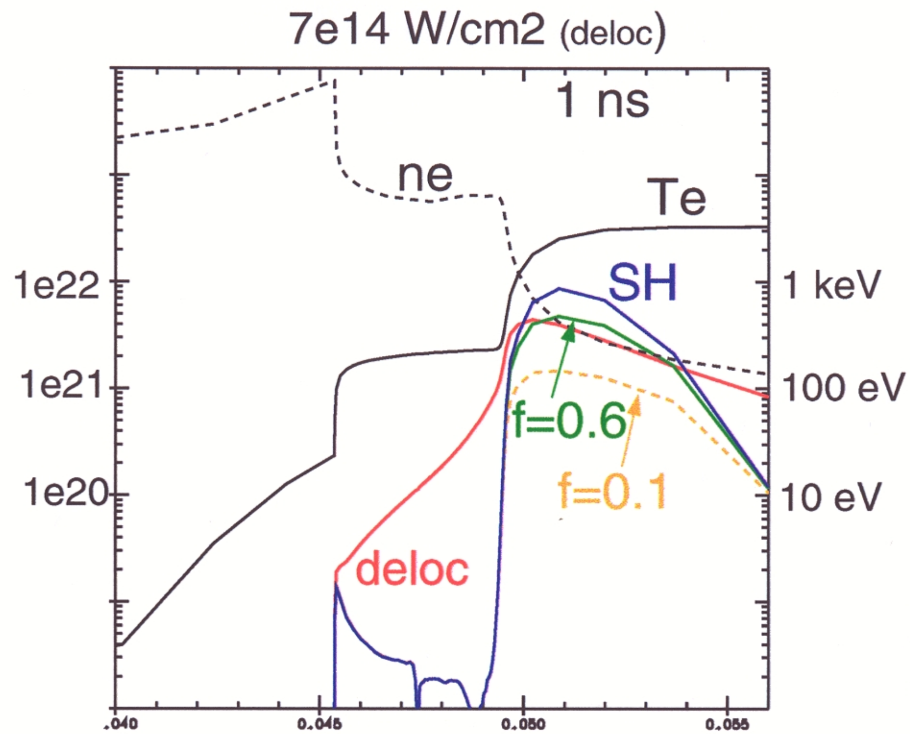

$lpm / L_T < 1$

- low temperature, smooth gradient, short e.m.f.p, the nonlocal flux tends towards Spitzer-Harm flux.
- high température, sharp gradient, long e.m.f.p., the flux is nonlocal and different from Spitzer-Harm flux.

Simulation of X-ray imaging

Characterize plasma expansion

- ❑ From 2D hydrodynamic computations, we can simulate diagnostic (post-process)

emission at 2 keV

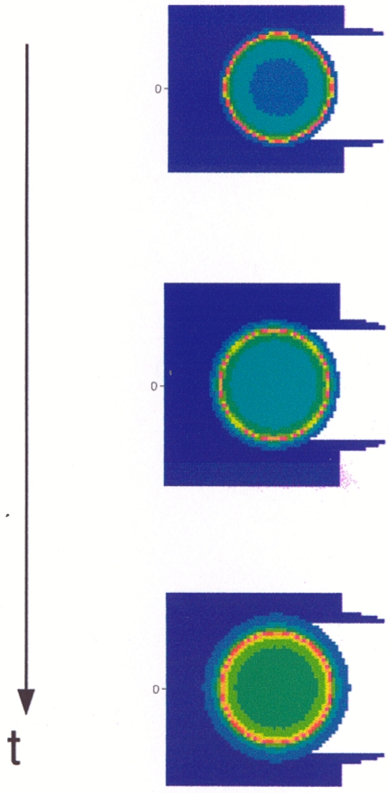

D 1/2
t=500 ps

D 1/2
t=1 ns

D 1/2
t=2 ns

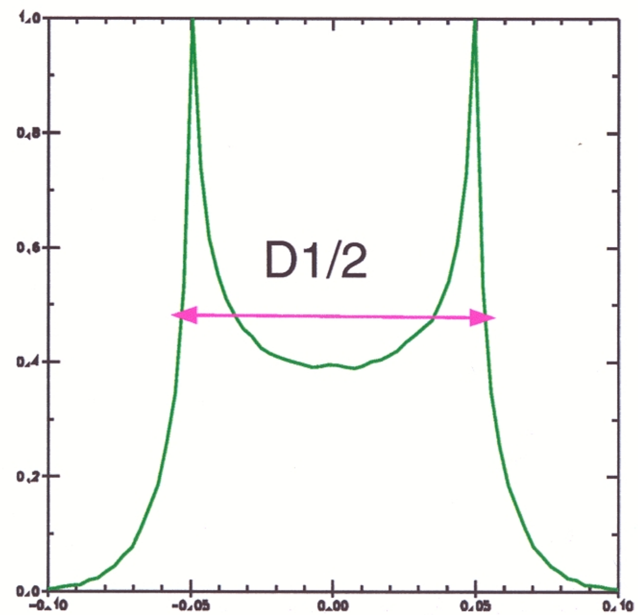

Emitting zones movement for I=7e14W/cm2

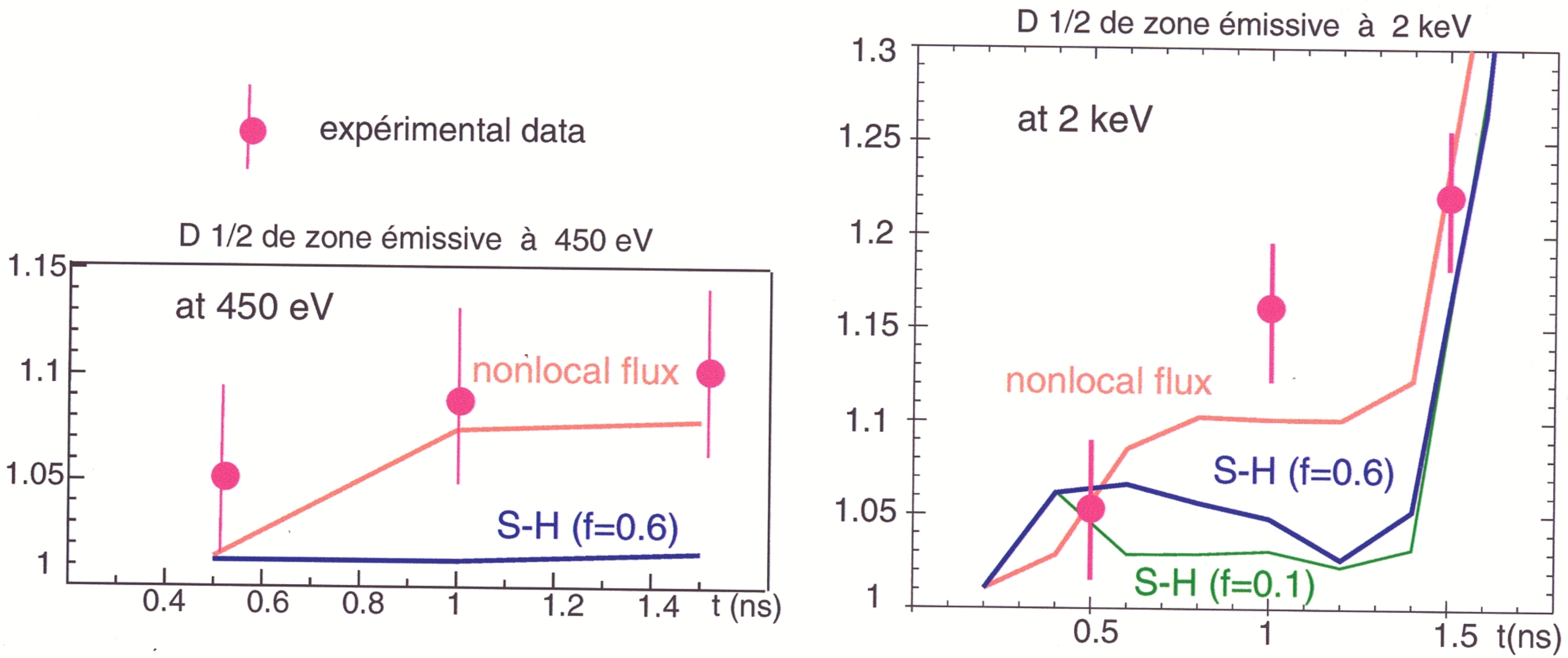

✔Spitzer-Harm fluxes do not be able to reproduce experiment

✔A flux limiter does not improve results

✔Using nonlocal fluxes, we get simuation closer to experimental data

Emitting zones movement for I = 4e14W/cm2

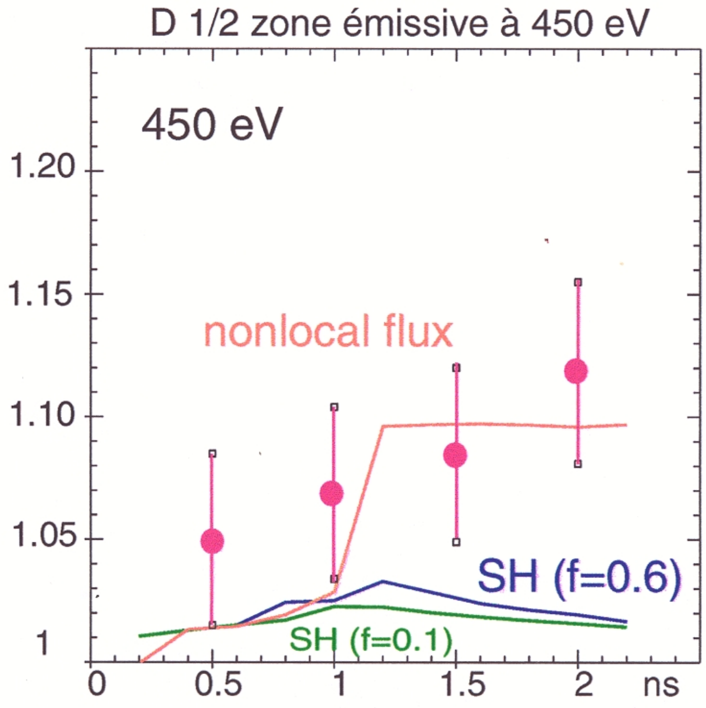

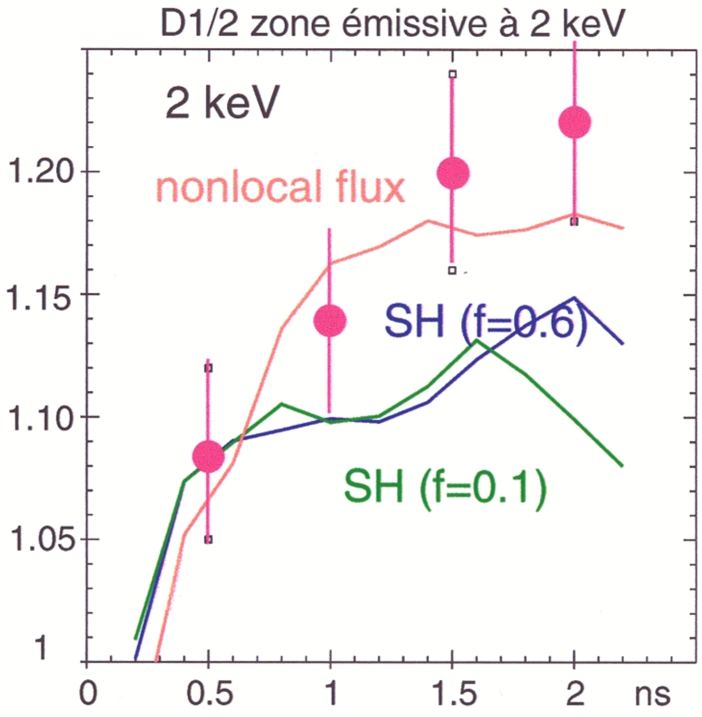

✔ Discrepancies between S-H and nonlocal fluxes are reduced but only nonlocal simulation passes through experimental data.

Emitting zones movement for I = 1e14W/cm2

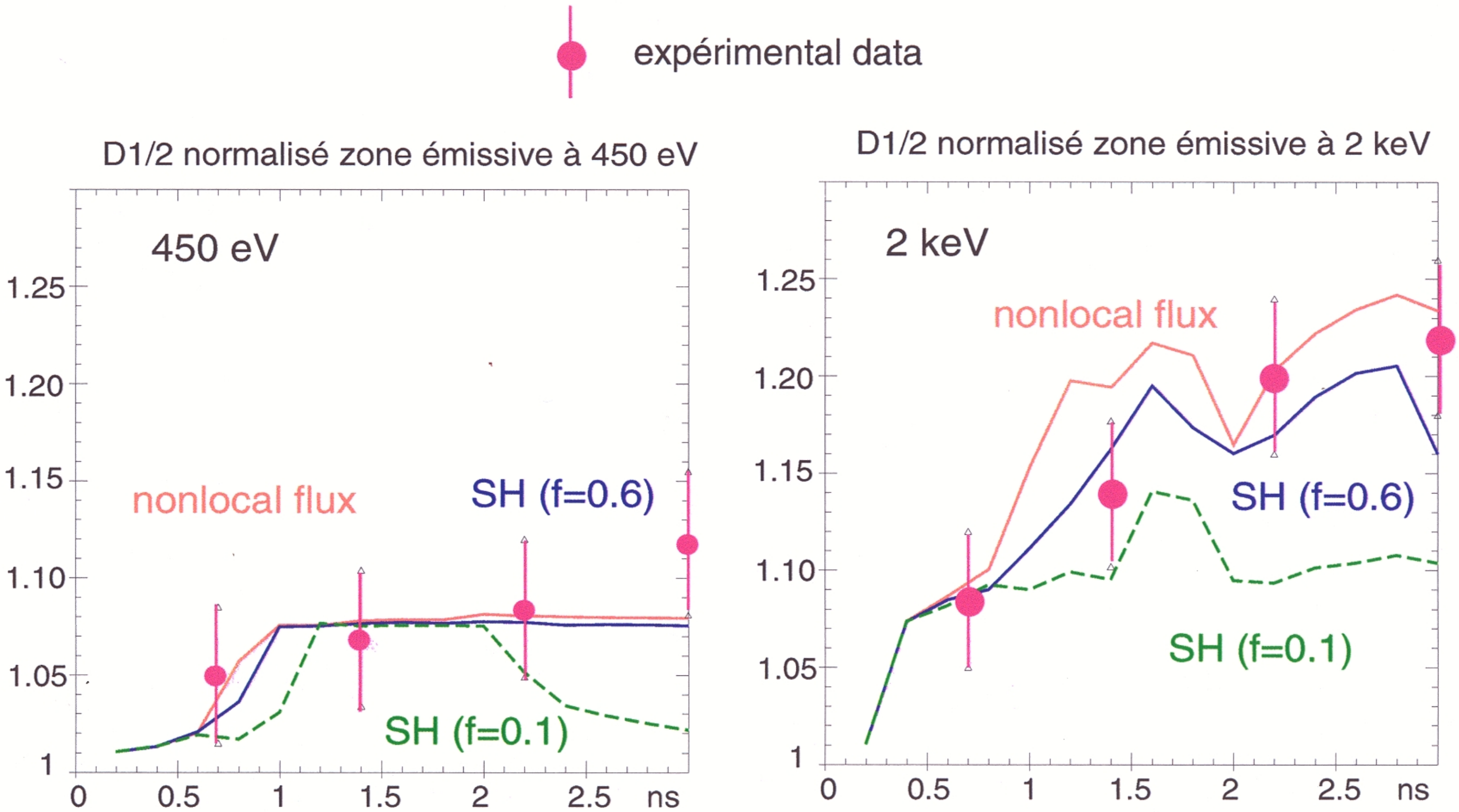

✔Non local flux tends towards SH flux for low intensity

✔ Both models reproduce experiment

Spherical target : summary

- Unlike cavity experiments, only nonlocal effetcs act on heat fluxes

- If some results like X-ray conversion efficiency can be explain by the use of Spitzer-Harm fluxes, only the nonlocal fluxes reproduce the movement of emitting zones.

- The variation of laser intensity in experiment allows us to test the convergence of our model to Spitzer-Harm model (low flux).

Conclusion

- The use of Spitzer-Harm fluxes, limited or not, does not allow us to reproduce some experimental results.

- From one experiment to another, and even from one diagnostic to another, the flux limiter value can be different : interpretation $\Longleftarrow\!\!\Longrightarrow$ prevision

- Nonlocal fluxes combined with magnetic fields improve simulations and so our understanding of laser plasma experiments

(up to now...)

Modelling electron heat conduction in FCI2

Guy Schurtz
Philippe Nicolai
Michel Busquet

CEA/DAM/DIF

G.Schurtz, Ph.Nicolai, M.Busquet - Phys.of Plasmas 7, 10 Oct 2000

G.Schurtz- APS - DPP conference - Montreal (2000)

Ph.Nicolai, M.Vandenboomgaerde, B.Canaud & F.Chaigneau Phys.of Plasmas 7, 10 Oct 2000

Hydro simulations : scale lengths

- **Spatial scales** : micron < l< cm
  Time scales : ps < τ < ns
  ==> 1 fluid, 2 températures
  Local Thermal Equilibrium
  NLTE radiation transport
- **Euler Equations** coupled to
  - rad. & fast ions transport
  - laser light propagation
- **Transport coefficients**
  - LTE : EOS, ionisation, material strength, conductivities,opacities)
  - NLTE : approximated models (e.g. : Radiom)

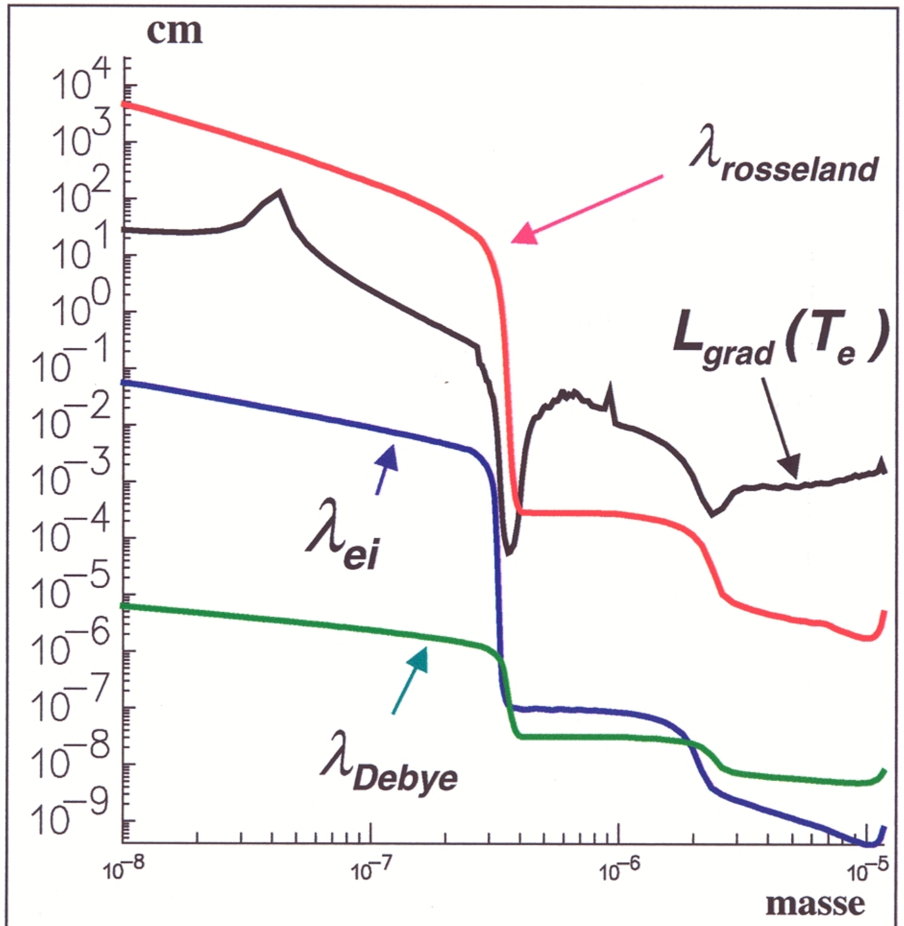

Gold foil irradiated at 10^{15} w/cm^2

2

Energy flow in a laser irradiated gold target

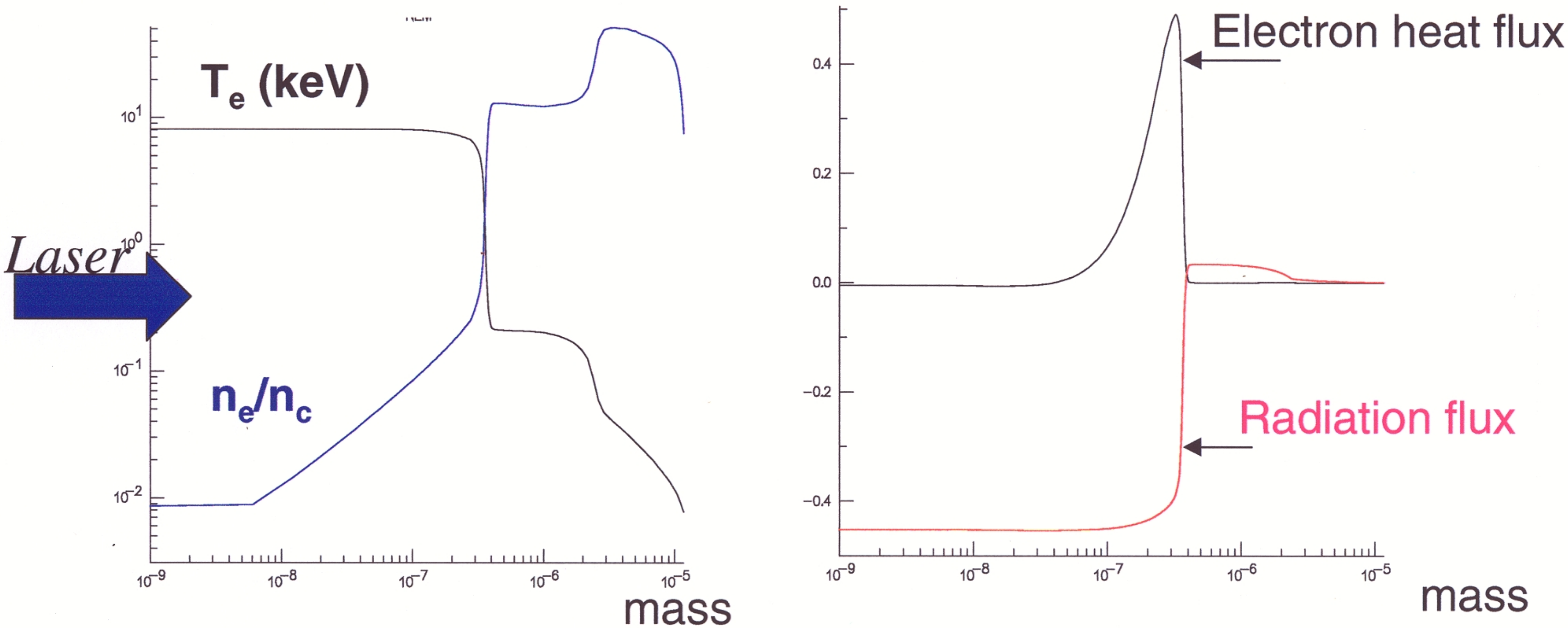

- Energy is transported to the emissive zone by the heat flux
- Electron heat conduction determines the X-ray conversion efficiency of the target

FCI2

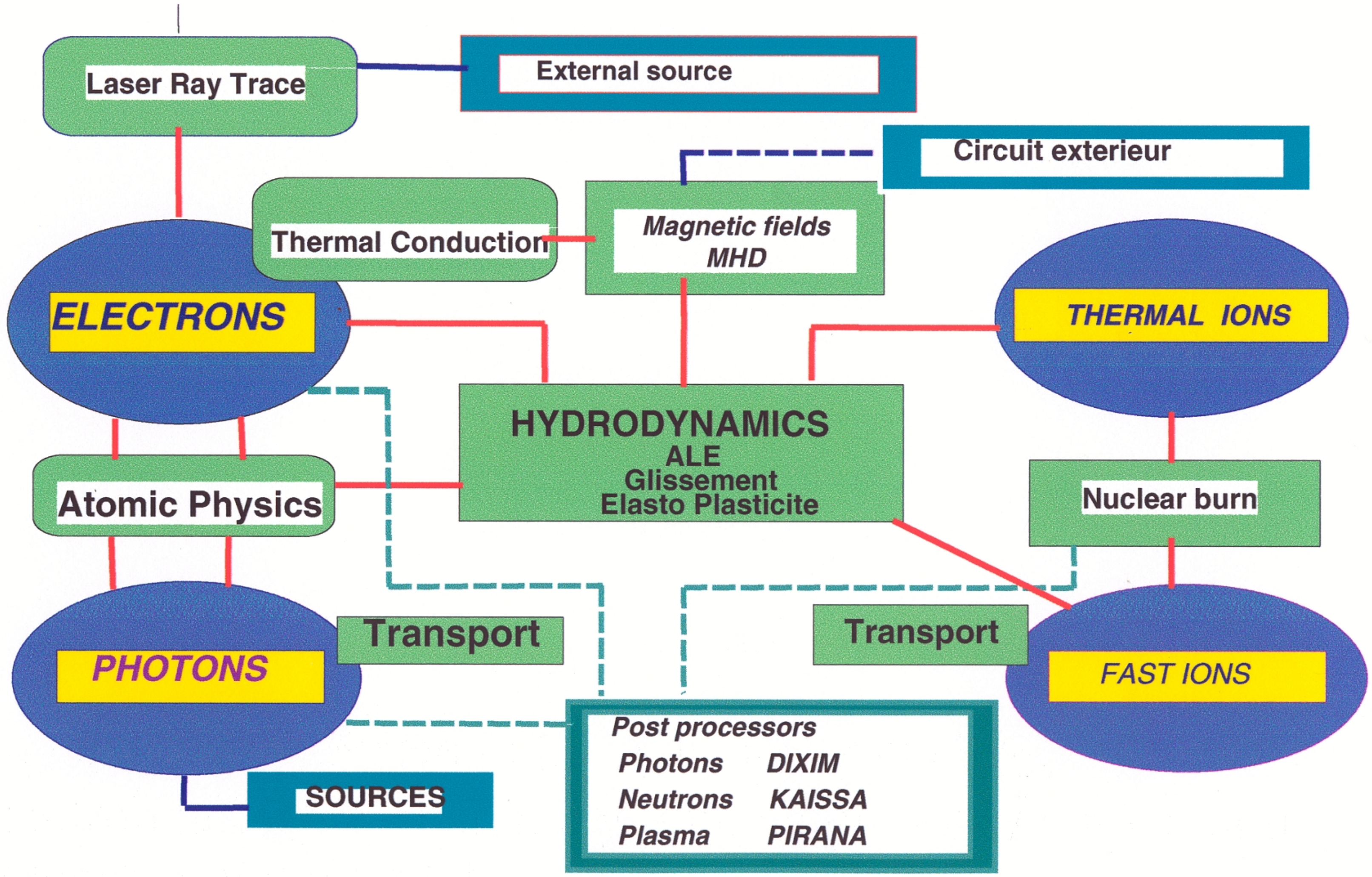

Laser Ray Trace
External source
Circuit exterieur
Thermal Conduction
Magnetic fields
MHD
ELECTRONS
THERMAL IONS
HYDRODYNAMICS
ALE
Glissement
Elasto Plasticite
Atomic Physics
Nuclear burn
Transport
Transport
PHOTONS
FAST IONS
Post processors
Photons DIXIM
Neutrons KAISSA
Plasma PIRANA
SOURCES

A « venerable old kludge » *(L. Suter dixit)* : the flux limited Spitzer Harm heat conduction

- The classical Spitzer Harm theory fails at restituting observed data

- In order to reproduce experiments one limits the heat flux to some fraction f of the free streaming limit

$$Q_{fs} = \frac{3}{2} n_e k T_e v_{th}$$

- f is the main adjustable parameter of numerical simulations

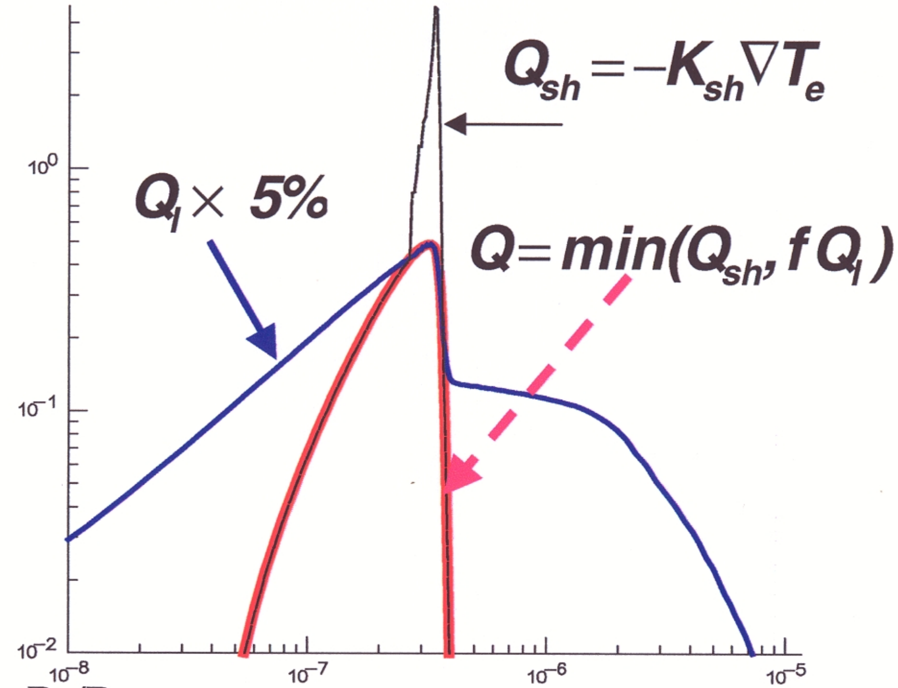

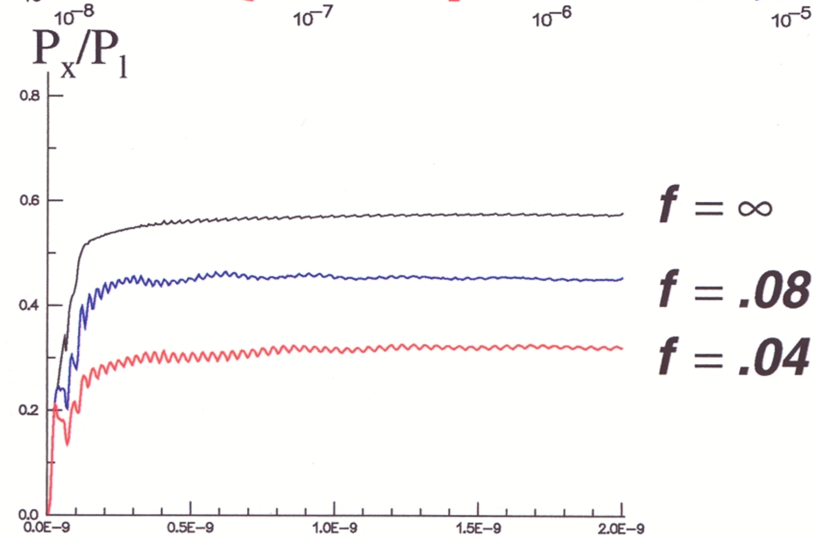

5

A few good reasons why the heat flux should be inhibited

- Electrons cannot move freely between collisions.
  - Self generated magnetic fields
    - » measurements inidicate B in the range [0.1,1] MG
- Collisions are enhanced
  - Ion acoustic turbulence
    - » no real experimental evidence
    - » no general agreement among theoreticians
- Free electrons depart significantly from LTE
    - » non maxwellian d.f. predicted by *Fokker Planck* codes
    - » Non Local heat flux theories

Validity of Spitzer linear theory

- the perturbation calculation

$$f(v,\Omega) = f_0^{mb}(v) + \Omega . f_1(v)$$

is valid as long as $|f_1| << f_0$

$$\lambda_e << T / |\nabla T|$$

- As $\lambda_e(v) \approx \left(v / v_{th} \right)^4 \lambda_{ei}$,

this condition cannot be fullfilled for all velocities

- major contributions to the heat flux occur at ~3,7 V_{th}

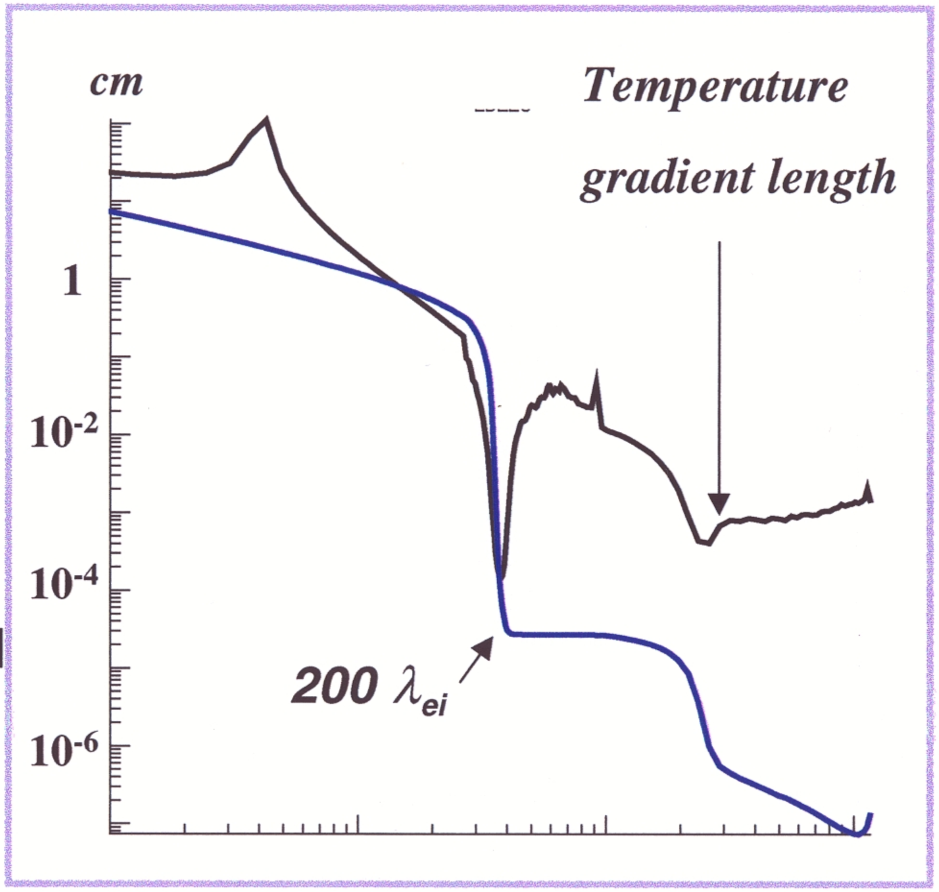

- f_0 cannot be maxwellian any more in case of sharp gradients

Non local heat flux

- 1D non local practical formula

$$Q_{nl}(x) = \beta_{1d} \int_{-\infty}^{\infty} Q_{sh}(x')W(x,x')\frac{dx'}{a\lambda(x')}$$

$$LMV : W(x,x') = e^{-\tau(x,x')} \text{ avec } \tau(x,y) = \frac{\left|\int_x^y n_e(z)dz\right|}{an_e(y)\lambda_e(y)}$$

- Difficulties
  - Formulation limited to 1D slab geometry
  - Boundary conditions

- Simple rationale for an heuristic extension to other geometries
  - fluxes are vectors $Q \rightarrow \vec{Q}$
  - kernels become tensors $W \rightarrow \vec{\Omega}\, W\, \vec{\Omega}$

---

* J.F.Luciani et al., Phys.Rev.Lett.51,1664 (1983)

** E.Epperlein et al., Phys.Fl. B3,3082 (1991)

The equivalent 3D kernel is a tensor

✔ Computation of non local flux at r requires summation over all contributing points r'

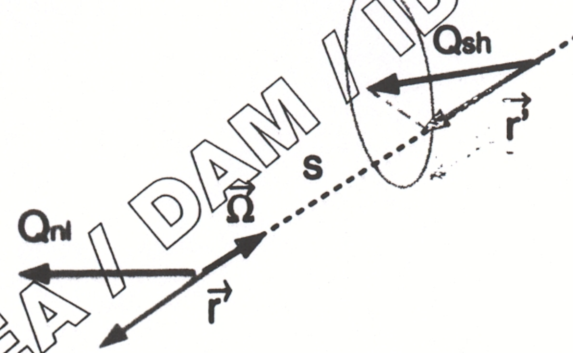

In spherical coordinates :

$$\vec{Q}_{nl}(r) = \int_{4\pi} \vec{\Omega}\, d^2\Omega \int_0^\infty contribution(r + s\Omega)\, W(r, r + s\Omega)\, \frac{ds}{\lambda^*(\vec{r}_0 + s\vec{\Omega})}$$

✔ If we assume that the distribution function has the azimuthal symmetry around the direction of grad T (i.e. P1 approximation) , contribution in direction Ω is $Q_{sh}.\Omega$

$$\boxed{\vec{Q}_{nl}(\vec{r}) = \int_{4\pi} \vec{\Omega}\,\vec{\Omega}\, d^2\Omega \int_0^\infty \vec{Q}_{SH}(\vec{r} + s\vec{\Omega})\, W(\vec{r}, \vec{r} + s\vec{\Omega})\, \frac{ds}{\lambda^*(\vec{r}_0 + s\vec{\Omega})}}$$

✔ Compares to classical 1D results

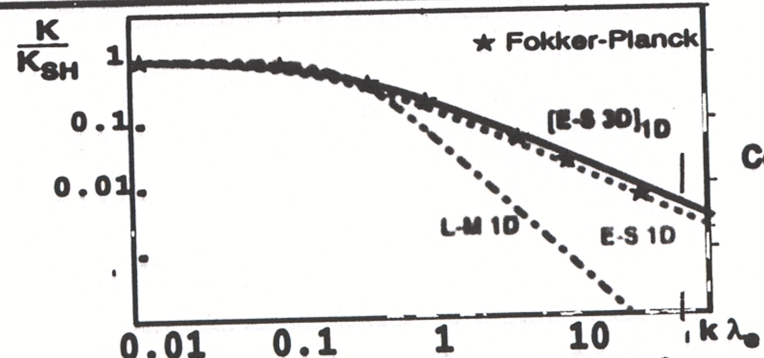

Conductivity reduction

Introduction in a 2D code

- 2 approches :
  - 1 : Direct calculation of Q on a given mesh point i from contributions of all other mesh points j
    - drawbacks :
      - high computationnal cost, ray effects
      - reflective boundary conditions difficult to handle
    - advantages :
      - accept différent kernels
  - 2 : « adjoint » method : start from « source points » and reformulate Q_{nl} as the integral solution of a transport problem.
    - advantages :
      - Numerical Analysis provide standard tools
      - clear link to kinetic equations (Fokker Planck)
    - drawbacks
      - requires a symetrical kernel
      - complex but for an exponentiel kernel (LMV-like)

Equivalent transport equation for the exponential kernel

- Introduce the scalar q (r,Ω) solution de $\vec{\Omega}.\vec{\nabla} q(r,\Omega) = \frac{1}{\lambda(r)}\left(\frac{3}{4\pi}\vec{\Omega}.\vec{Q}_{sh} - q(r,\Omega)\right)$

  and let Q be its 1st order angular moment $\vec{Q} = \int_{4\pi} q\,\vec{\Omega}\, d^2\Omega$

- We have $\vec{Q} = \frac{3}{4\pi}\int_{4\pi} \vec{\Omega}\, d^2\Omega \int_{-\infty}^{\infty} \vec{Q}_{sh}(r+s\Omega).\vec{\Omega} \quad \exp-\left|\int_{r}^{r+s\Omega} \frac{dr'}{\lambda(r')}\right| \quad \frac{ds}{\lambda(r+s\Omega)}$

- Approximated Sn quadratures
  - 1D slab : the S2 ($\mu\pm = \pm\frac{1}{\sqrt{3}}$) solution is the non local LMV flux
  - more generally, S2 is equivalent to P1:

$$H = \int_{4\pi} q(\Omega)\, d^2\Omega$$

$$\vec{Q} = \int_{4\pi} q(\Omega)\vec{\Omega}\, d^2\Omega$$

$$\boxed{\begin{aligned}&\left(\frac{1}{\lambda} - \vec{\nabla}.\frac{\lambda}{3}\vec{\nabla}\right)H = -\vec{\nabla}.\vec{Q}_{sh}\\ &\vec{Q} = \vec{Q}_{sh} - \frac{\lambda}{3}\vec{\nabla} H\end{aligned}}$$

The 3D n.l. flux as the solution of a transport equation

✔ Introduce the scalar q solution of the steady state transport equation

$$\vec{\Omega}.\vec{\nabla}q(r,\vec{\Omega}) = \frac{1}{\lambda(r)}\left\{\frac{3}{4\pi}\,\vec{\Omega}.\vec{Q}_{SH}(r) - q(r,\vec{\Omega})\right\}$$

✔ Define the optical depth as : $\tau(r,r') = \int_{r}^{r'} dr''/\lambda(r'')$

✔ The solution is $q(r,\Omega) = \frac{3}{4\pi}\int_{0}^{\infty} \frac{\exp\left[-\tau(r-s\Omega,r)\right]\,\Omega.Qsh\,(r-s\Omega)\,ds}{\lambda(r-s\Omega)}$

✔ Form the first order angular momemtum of q : $\vec{Q} = \int_{4\pi} q(r,\vec{\Omega})\,\vec{\Omega}\,d^2\Omega$

$$\vec{Q} = \frac{3}{4\pi}\int_{4\pi}\vec{\Omega}\,\vec{\Omega}\,d^2\Omega\int_{0}^{\infty}\frac{W(r,r+s\Omega)\,Qsh\,(r+s\Omega)\,ds}{\lambda(r+s\Omega)}$$

The LMV flux is the S2 solution of the transport equation

✔ Solve the 1d transport equation along directions $\mu = \pm 1/\sqrt{3}$

$$Q(x) = 1/2 \int_{-\infty}^{\infty} \frac{\exp\left[-\sqrt{3}\,\tau(x,x')\right] Qsh(x')\,dx'}{\lambda(x')/\sqrt{3}} \quad = \text{LMV formula with } \lambda = \sqrt{3}\,\lambda_{lmv}$$

✔ if S2 is correct, P1 is o.k. : $q(r,\Omega) = H(r)/4\pi + 3\,\Omega.Q/4\pi$

$$H = \int_{4\pi} q(r,\Omega)\, d^2\Omega \qquad \vec{Q} = \int_{4\pi} q(r,\vec{\Omega})\,\vec{\Omega}\, d^2\Omega$$

✔ H and Q are solutions of the moment equations

$$\boxed{\begin{aligned} &\left(\frac{1}{\lambda} - \nabla \frac{\lambda}{3} \nabla\right) H = -\nabla . Q_{sh} \\ &Q_{nl} = Q_{sh} - \frac{\lambda}{3} \nabla H \end{aligned}}$$

Comparison to LMV : multigroup diffusion

✔ The transport kernel is symmetric whereas the LMV kernel is non symmetric

$$W_{lmv}(x,y) = \exp[-\tau(x,y)] \qquad \tau_{lmv}(x,y) = \int_x^y ds/\lambda(ne(s),T(y))$$

===> electrons are transported from y to x at the hot thermal velocity

✔ the transport equation must be solved for different energy groups : $\lambda_g = 2\left(\frac{Eg}{kT}\right)^2 \lambda_e$

$$\left(\frac{1}{\lambda_g} - \overrightarrow{\mathrm{div}}\,\frac{\lambda_g}{3}\,\overrightarrow{\mathrm{grad}}\right) H_g = -\overrightarrow{\mathrm{div}}\left\{\frac{1}{24}\,\overrightarrow{Q}_{sh}\int_{\frac{E_{g-1}}{T}}^{\frac{E_g}{T}} u^4 \exp(-u)\,du\right\}$$

$$\overrightarrow{Q}_{nl} = \overrightarrow{Q}_{sh} - \sum \frac{\lambda_g}{3}\,\overrightarrow{\mathrm{grad}}\,H$$

$\varphi(x) = \int \varphi_{?}(x')\, w(x,x')$

✔ reduction to 1d is equival … tor w2 of Luciani & Mora ❶

❶ J.F. Luciani , P.Mora in Lase & part. beams 12, 387 (1994)

H is the departure from the maxwellian d.f.

- Fokker Planck
  - P1
  - steady state
  - Lorentz model pour C1

$$\boxed{\begin{aligned} &v\nabla.f_1 - \frac{eE}{m_e v^2}\frac{\partial(v^2 f_1)}{\partial v} = C^0 \\ &\frac{v}{3}\nabla f_0 - \frac{eE}{3m_e}\frac{\partial f_0}{\partial v} = -\upsilon_{ei}' f_1 \end{aligned}} \quad (1)$$

- Solve (1) near the maxwellian : $f_0 = f_0^m + \Delta f_0 \quad ; \quad f_1 = f_1^m + \Delta f_1$
  - from definition $Q_{sh} = \int f_1^m v^5 dv\,, \quad et \quad C^0(f_0^m) = 0$
  - let $\lambda(v) = \sqrt{\lambda_{ei}(v)\lambda_{ee}(v)} \approx \sqrt{Z}\,\lambda_{ei}(v), et\ C^0(\Delta f_0) = -\frac{v\,\Delta f_0}{\lambda_{ee}(v)}$
- Multiply System (1) by $m_e v^4/2$ and eliminate Δf1 :

$$\boxed{\begin{aligned} &\left[\frac{1}{\lambda} - \nabla.\frac{\lambda}{3}\nabla\right]\frac{m_e\sqrt{Z}}{2}v^5\Delta f_0 = -\nabla.(g(v)Q_{sh}) \\ &Q = Q_{sh} - \frac{m_e\sqrt{Z}}{2}\int\frac{\lambda}{3}\nabla(\Delta f_0)v^5 dv \end{aligned}}$$

Par identification,

$$H = \frac{m_e\sqrt{Z}}{2}v^5\Delta f_0$$

Electric fields

✔ Electric fields

- slow down fast electrons (limit the range of delocalization propagator)
- accelerate low energy electrons (return current : Already included in SH theory)

✔ LMV & Bendid solution ❶ : multiply the kernel by $\exp(-e\,|\Phi(X)-\Phi(X')|\,/\,kT)$

- the electrical potential is given by Spitzer : $e\mathcal{E} = kT[\,\mathrm{grad}(\log n) + \gamma\,\mathrm{grad}(\log T)\,]$

  (shown to be reasonably accurate, even in sharp gradients)

- taking the spatial derivative gives the the equivalent transport mean free path λ'

$$\frac{1}{\lambda'} = \frac{1}{a\lambda} + \frac{|e\mathcal{E}|}{kT} \longleftarrow$$

Harmonic mean of collision mean free path and stopping length at energy kT

- At group energy Eg, the stopping length should be taken as $\dfrac{E_g}{|e\mathcal{E}|}$

th

❶ A. Bendid, J.F. Luciani, J.P. Matte. Phys. Fluids 31,711 (1988)

Effects of a non local heat flux

- **Reduces the maximum heat flux**
- **Preheat of dense target**
- **Non isothermal corona and counter streaming fluxes**

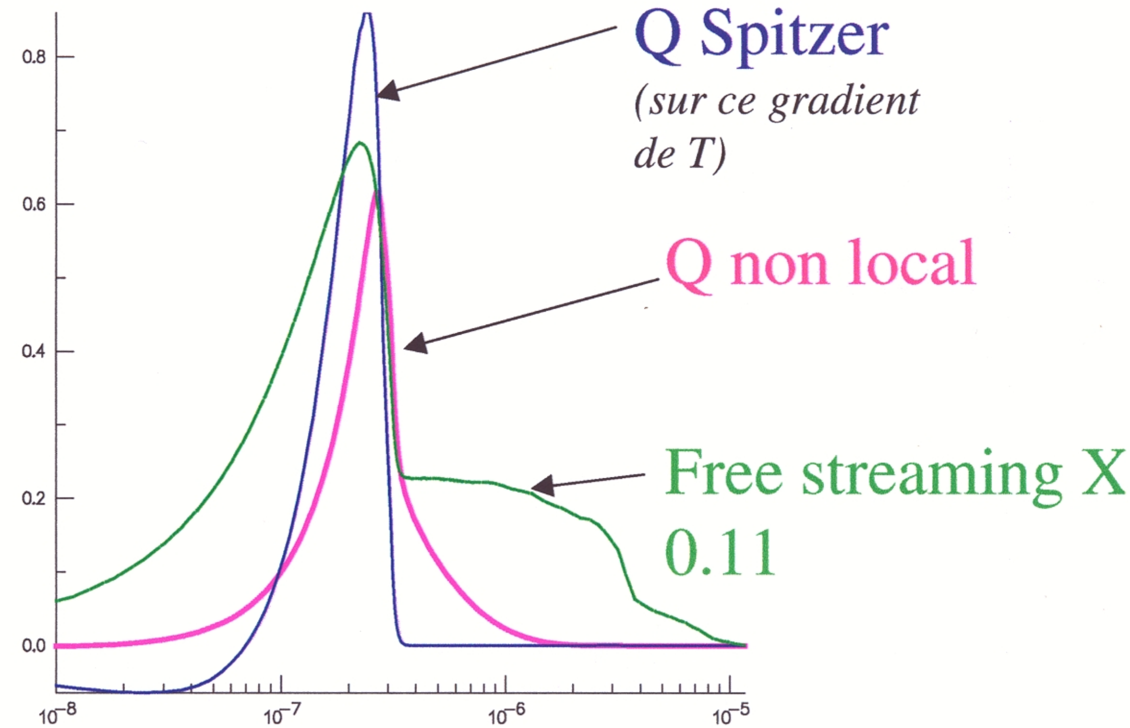

- **All effects cannot be reproduced with a single flux limiter**

Summary of multigroup equations

- Define energy dependant transport coefficients :

$$\lambda_{ei}^{g} = \lambda_{ei}\left(\frac{u_g}{kT}\right)^2, \quad \frac{1}{\lambda_{nl}^{g}} = \frac{1}{\lambda_{ei}^{g}} + \frac{e|E|}{u_g}$$

$$\lambda_{ee}^{g} = Z^* \lambda_{ei}^{g}, \quad \gamma_g = \frac{1}{24}\int_{u_{g-1/2}/kT}^{u_{g+1/2}/kT} \beta^4 e^{-\beta} d\beta$$

- Get the local flux Q_{loc} from linear theory (Spitzer, Braginskii,..)

- Solve for all groups

$$\left[\frac{1}{\lambda_{ee}^{g}} - \nabla.\frac{\lambda_{nl}^{g}}{3}\nabla\right] H^g = -\nabla.(\gamma^g Q_{loc})$$

- Compute the heat flux from

$$Q_{nl} = Q_{loc} - \sum_g \frac{\lambda_{nl}^{g}}{3} \nabla H^g$$

- Compute distribution functions from

$$f^0 v^5 = f_{mb}^0 v^5 - H(v)$$

How accurate NL distribution functions are ? Comparison to FP results

- *Test problem : 1D, Z=4, ne=10^{21}, initial temperature gradient problem run with 1D Fokker Planck code C2M2*
  Fluid code FCi2 + nl model

- *Numerical results at 0.5 ps :*

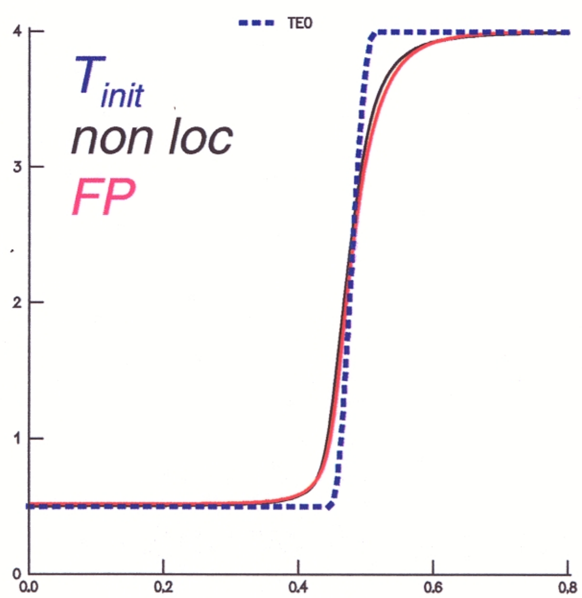

Temperatures

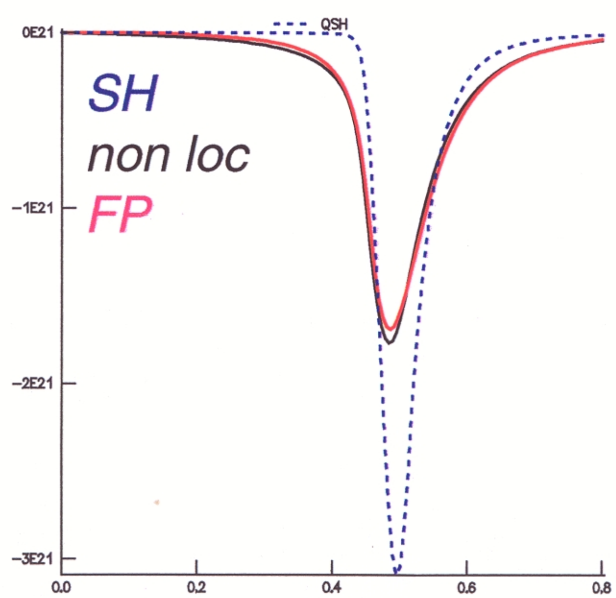

Heat fluxes

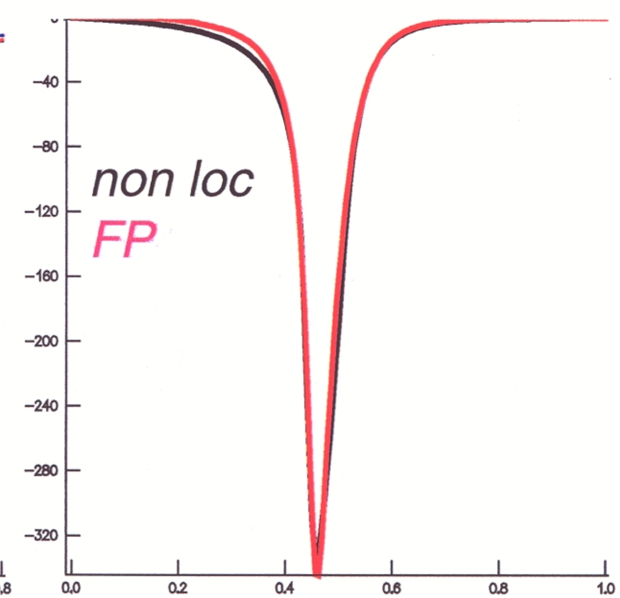

Electric fields

Distribution functions

- *Distribution function predicted by the non local model agree reasonably well with Fokker Planck calculations*

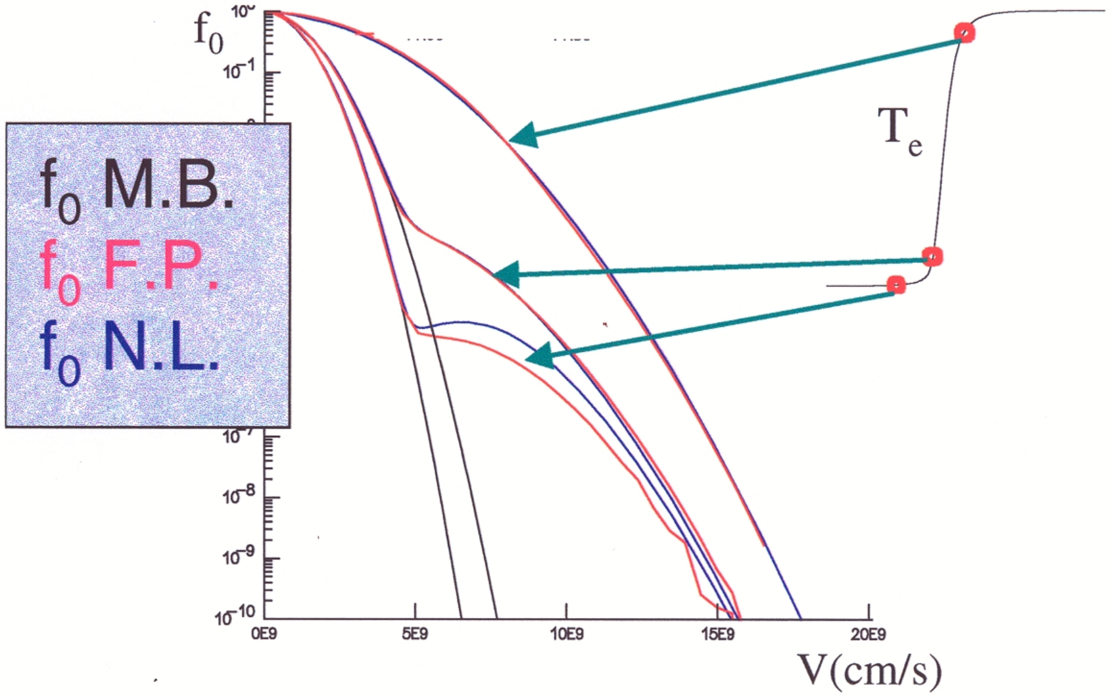

- *Computing moments of f0 exhibit other non local effects (e.g. Non Local Efields)*

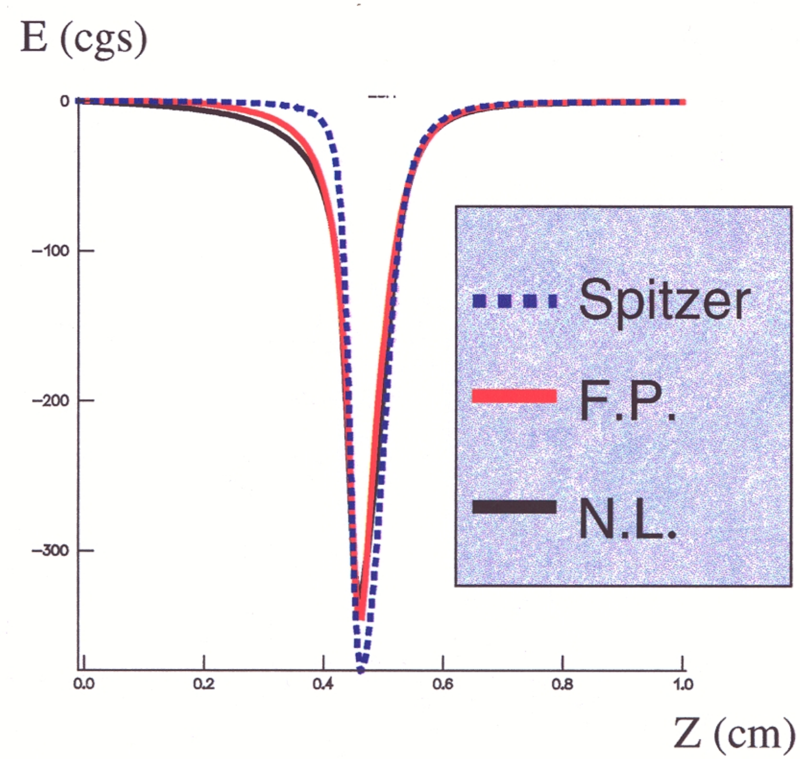

Non local heat equation in Fourier variables: eigen values of $\rho C_v \, dT/dt = - \text{div}.Q$

- **Conditions**
  - uniform density, harmonic temperature perturbation of wave number k
  - 1 group diffusion, a=32

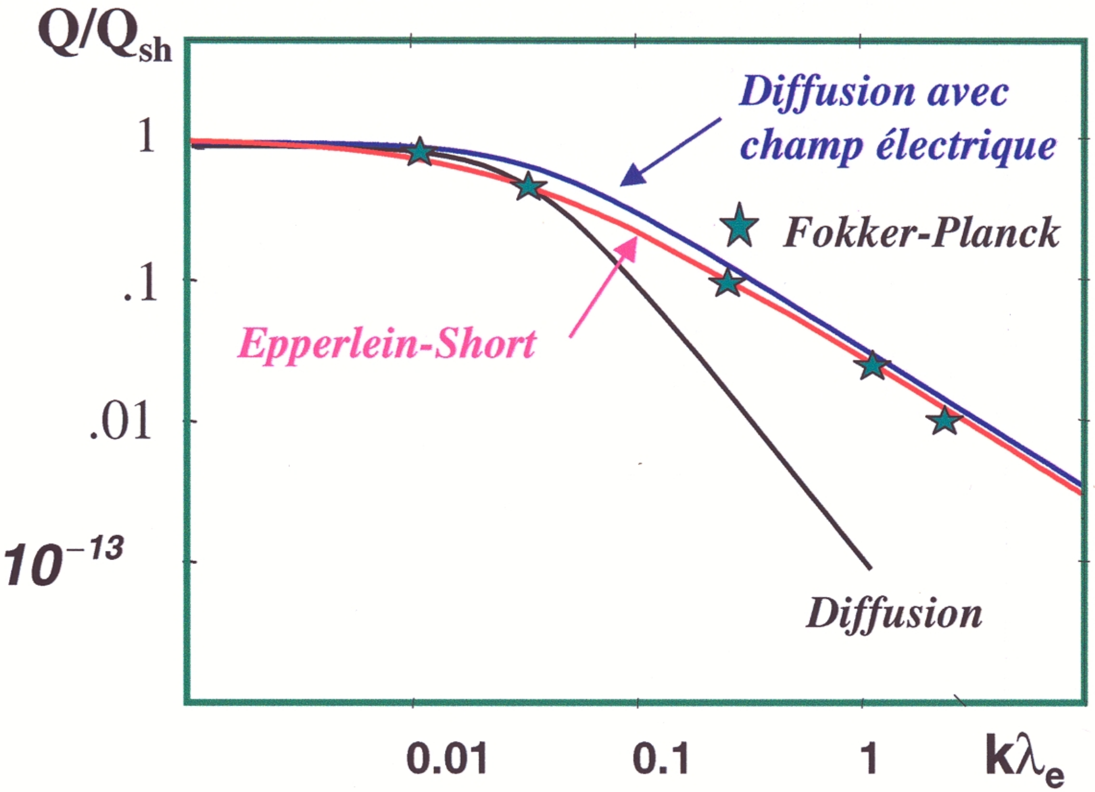

- **Spitzer Harm**

$$\omega \approx v_{th} \lambda k^2 \Rightarrow 10^{-15} < \tau(s) < 10^{-13}$$

- **Non local, no E field**

$$\frac{Q_{nl}}{Q_{sh}} \approx \frac{1}{1+(a\lambda k)^2} \qquad \lim_{\lambda k \to \infty}(\omega) \propto \nu_{ei}$$

- **Including E-field « a la Bendid-Luciani »**

$$\frac{Q_{nl}}{Q_{sh}} \approx \frac{1+b\lambda k}{1+b\lambda k+(a\lambda k)^2} \qquad \lim_{\lambda k \to \infty}(\omega) \approx k v_{th}$$

Planned improvements

- Probably needed
  - Introduce the Nernst term in Faraday equation

$$\left(\frac{\partial \boldsymbol{B}}{\partial \boldsymbol{t}}\right)_{Nernst} = \nabla \times (\boldsymbol{u}_{nernst} \times \boldsymbol{B}), \text{ with } \boldsymbol{u}_{nernst} \propto \frac{\boldsymbol{Q}}{n_e T_e}$$

  - Second order space differencing

- Achievable with a yet unknown (accuracy/cost) ratio
  - improve treatment of collisions (e.g. $\frac{1}{\lambda} v\partial_v H$ *instead of* $\frac{H}{\lambda}$)
  - Improve introduction of E and B fields ($E\partial_v f^0$ *and* $B \times f^1$ *instead of* $\left[\frac{1}{L_E} + \frac{1}{L_B}\right] f^1$)
  - full P1 steady state FP equations for H ?

Numerical Implementation of the model

Spitzer & Harm : Conduction matrix

- energy balance of a cell $\rho\, c_v \frac{dT}{dt} = -\nabla . Q \Rightarrow M_i\, c_v \frac{dT_i}{dt} = -\sum_j A_{ij} Q_{ij}$

Area of interface   Normal component of Q

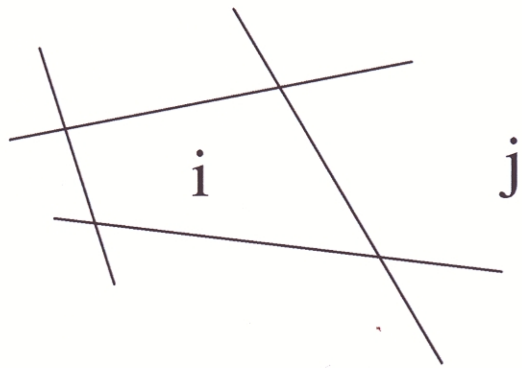

- SH fluxes $Q_{sh} = -K \nabla T \Rightarrow Q_{ij} = G_{ij}(T_i - T_j)$

- space differenced heat flux equation $[M\, c_v] \frac{d\tilde{T}}{dt} = [D]\, \tilde{T}$

Diagonal matrix   Symmetric 5 diag matrix   Vector of temperatures

- Only 1st order accurate . May be extended to 2nd order (9 diagonals)

Time differencing

- eigen values of the SH heat flux equation
  - let k be the wave number of an harmonic temperature spatial mode
  - this mode is damped with the characteristic time

$$\tau = \frac{1}{v_{th}\lambda k^2}$$

  - The largest wave number one can sample on a mesh of width Δx is $k_{max} \sim 1/\Delta x$
- if we integrate the heat equation as $[M\,c_v]\dfrac{\tilde{T}^{n+1}-\tilde{T}^{n}}{\Delta t} = [D]\,\tilde{T}^{n}$ (explicit scheme), the code becomes unstable unless we satisfy the very restrictive criterion $\Delta t < \tau_{min}$
- Implicit time differencing : $[M\,c_v]\dfrac{\tilde{T}^{n+1}-\tilde{T}^{n}}{\Delta t} = [D]\,\tilde{T}^{n+1}$ is unconditionnally stable

The non local conduction matrix

- Matrices
  - Let *[D_{sh}]* be the finite difference analog of *div. K_{sh} grad*
  - and *[Δ]* the finite difference analog of λ *div. $\lambda/3$ grad*

- The 1 group non local heat flux verifies

$$\begin{cases} (V-[\Delta])\tilde{H} = -\lambda[D_{sh}]\tilde{T} \\ Q_{nl} = Q_{sh} - \dfrac{\lambda}{3}\nabla H \end{cases}$$

  (V=matrix of volumes)

- the non local heat flux equation thus writes

$$[M\,c_v]\frac{\tilde{T}^{n+}-\tilde{T}^{n}}{\Delta t} = \left(I-\Delta[V-\Delta]^{-1}\right)[D_{sh}]\tilde{T}^{n+1}$$
$$= [D_{nl}]\tilde{T}^{n+1}$$

  - Usual diffusion matrices are sparse (+other desirable properties as M-matrices) whereas D_{nl} is a full matrix
  - eigen values of D_{nl} look like $\dfrac{v_{th}\lambda_{ei}k^2}{1+(a\lambda_{ei}k)^2}$ (bounded for large λk !)

===> an implicit solution involves a large amount of linear algebra and may not be necessary

practical solution

- Look for a numerical solution in the form $\left[\boldsymbol{M}\, \boldsymbol{c}_v\right] \dfrac{\tilde{\boldsymbol{T}}^{n+1} - \tilde{\boldsymbol{T}}^{n}}{\Delta \boldsymbol{t}} = \left[\boldsymbol{D}\right] \tilde{\boldsymbol{T}}^{n+1} + \tilde{\boldsymbol{S}}$

  where D is a diffusion-like matrix

  (5 or 9 diagonals + I-D is a symmetric M-matrix)

- For each cell boundary (ij), compute $\left[\boldsymbol{D}_{sh}\right], \boldsymbol{Q}_{sh}^{i,j}, \boldsymbol{Q}_{nl}^{i,j}$ from the temperatures at the beginning of the time step T^n ,and set S to zero

- Compute D and S as follows :
  - Whenever $\boldsymbol{Q}_{sh}^{i,j} . \boldsymbol{Q}_{nl}^{i,j} > 0$, set $\boldsymbol{D}^{i,j} = \boldsymbol{D}^{j,i} = \boldsymbol{D}_{sh}^{i,j} \dfrac{\boldsymbol{Q}_{nl}^{i,j}}{\boldsymbol{Q}_{sh}^{i,j}}$

    (this multiplier must be bounded in order to avoid excentric values)

  - Otherwise, set $\boldsymbol{D}^{i,j} = \boldsymbol{D}^{j,i} = 0$, $\boldsymbol{S}_i = \boldsymbol{S}_i - \boldsymbol{Q}_{nl}^{ij}$, $\boldsymbol{S}_j = \boldsymbol{S}_j + \boldsymbol{Q}_{nl}^{ij}$

Non Local Heat Conduction

- **Substitution of a simplified Fokker Planck equation to the classical concept of delocalization kernel allows the extension of non local theory to 2 or 3D flows. This model is implemented in FCI2.**

- **Heat flow predictions agree qualitatively and quantitatively with Fokker Planck in both 1D and 2D**
    - reduction of the heat flow at maximum
    - preheat of dense cold zones
    - counter streaming fluxes in the corona

- **Electric fields are accounted for at two steps of the model**
    - the computation of linear fluxes that are sources for delocalization include E fields
    - The delocalization operator is modified (mfp limited to stopping length)
    - This modification ensures a correct asymptotic behavior of eigen values.

- **Distribution functions are a by product of the model**
    - comparison to F.P. indicate the NL distr. funct. are reasonnably accurate.
    - Allow calculation of other non local moments (e.g. E and B fields)

Self Generated Magnetic Fields in FCI2

- A- MHD model implemented in FCI2

- B- Coupling Bfields to non local transport

Magnetohydrodynamics : équations of motion

- Ions

$$\left(\frac{\partial}{\partial t} + u_i.\nabla\right)u_i - \frac{Ze}{m_i}\left(E + \frac{u_i}{c}\times B\right) + \frac{1}{m_i n_i}\nabla P_i = \frac{R_{ie}}{m_i n_i}$$

- Électrons

$$\left(\frac{\partial}{\partial t} + u_e.\nabla\right)u_e + \frac{e}{m_e}\left(E + \frac{u_e}{c}\times B\right) + \frac{1}{m_e n_e}\nabla P_e = \frac{R_{ei}}{m_e n_e}$$

- **Hypotheses**
  - momentum conservation $R_{ei}=-R_{ie}$
  - plasma neutrality : $n_e = Z^* n_i$
  - $m_e << mi$: $j = en_e(u_i-u_e)$ est steady
  - linear perturbation calculations ⇒ $$\frac{\vec{R}_{ei}}{e n_e} = \overline{\overline{\alpha}}.\vec{j} - \frac{\overline{\overline{\beta}}}{e}.\vec{\nabla} T_e$$
  - 2 transport coefficients

α = electrical resistivity tensor

β = thermo-electric tensor

Ohm 's law

- **Sum : momentum balance**

$$\rho\frac{du}{dt}+\nabla(P_e+P_i)=\frac{1}{c}\,j\times B$$

- **Différence : Ohm 's law**

$$(cE+u\times B)+\frac{c}{en_e}\nabla P_e=\frac{1}{en_e}\,j\times B+c\vec{\vec{\alpha}}\;j-\frac{c}{e}\vec{\vec{\beta}}\;\nabla T_e$$

Advection Source Hall Diffusion

- **Simplified equation used in FCI2**

$$(cE+u\times B)+\frac{c}{en_e}\nabla P_e=c\alpha_{\perp}\;j$$

Induction equation

- **Ohm 's law** $$cE = -u \times B - \frac{c}{en_e} \nabla P_e + c\alpha\ j$$
- **Ampère** $$j = \frac{c}{4\pi} \nabla \times B - \cancel{\frac{1}{4\pi} \frac{\partial E}{\partial t}}$$
- **Faraday** $$\frac{\partial B}{\partial t} = -c\nabla \times E$$

$$\boxed{\frac{\partial B}{\partial t} - \nabla \times (u \times B) = \frac{c}{en_e} \nabla kT_e \times \nabla n_e - \frac{c^2}{4\pi} \nabla \times (\alpha \nabla \times B)}$$

« Lagrangian » variation of the magnetic flux — *Thermal source* — *Resistive diffusion*

- **Boundary conditions : B=0 (** ***sauf Zp*** **)**

Effects of magnetic fields

- **Laplace force is most often negligible :**
  - magnetic pressure : $P_{(Mbar)} \approx 0.04\, B^2_{(Mgauss)}$
  - B ~1 Mg $\Longrightarrow$ P_{mag} ~ 40 kb to compare to P_e (Mb-Gb)
- **The heat flux is strongly affected**
  - electrons rotate aroung field lines and cannot participate to a heat flux any more
  - appearance of a heat flux orthogonal to the temperature gradient (Righi Leduc)
  - Bfield effects are characterized by the dimensionless number

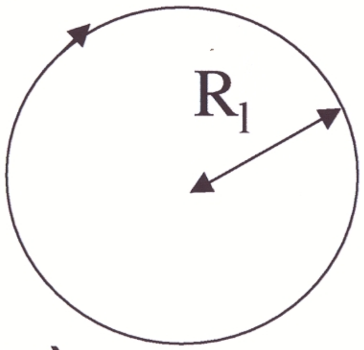

$$R_l = \frac{m_e v}{eB}$$

$$\omega_c = \frac{eB}{m_e}$$

$$\omega\tau = \frac{\lambda_{ei}}{R_l} = \frac{\omega_c}{\nu_{ei}}$$

Model implemented in FCI2

- **Resistive MHD , scalar electrical conductivity (Spitzer)**
  - **in 2D axisymmetric geometry** $\boldsymbol{B} \equiv \boldsymbol{B}_\theta$

- **Braginskii heat fluxes including modified heat conductivities according to Epperlein, Haines, Nicolai**

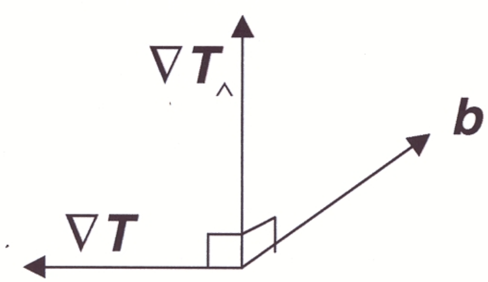

$$Q = -\chi_\perp \nabla T_e - \chi_\wedge b \times \nabla T_e - \frac{\beta_\perp T_e}{e n_e} j - \frac{\beta_\wedge T_e}{e n_e} b \times j$$

- **For B=0,** $j = 0, \;\; \chi_\wedge = 0, \;\; \chi_\perp = K_{sh}$

- **Absence of the Nernst term (though probably necessary because $v_{nernst} \sim 0.1\, v_{th}$)**

Coupling the non local model to magnetic fields ...

- Bfields effects : the relevant parameter is the Hall number $\Omega=\omega\tau$
  - at reduced velocity w, the number to consider is Ωw^3
  - perturbation terms like $w^4(w^2 - 4)$
    become $w^4(w^2 - ..)/(1+ \Omega^2 w^6)$
      - » the perturbation calculus is valid again, even in sharp gradient conditions
      - » non local effects are cancelled by B fields

- Heuristic used in FCI2
  - use Braginskii instead of SH fluxes as delocalization source
  - Limit the delocalisation mfp to the Larmor radius $r_l = mv/eB$
      - » for small Ω, smooth gradients : Q ---> Spitzer Harm
      - » for small Ω, sharp gradients : Q ---> non local flux
      - » for large Ω : Q---> Braginskii « relocalized »

Delocalisation mfp in presence of magnetic fields

- Delocalization mfp are strongly reduced in presence of magnetic fields
- A priori reduction factors are $c_\perp = \dfrac{1}{1+\Omega^2 w^6}$ $\quad c_\wedge = \dfrac{\Omega\, w^3}{1+\Omega^2 w^6}$
- Our non local model only uses a single scalar non local mfp

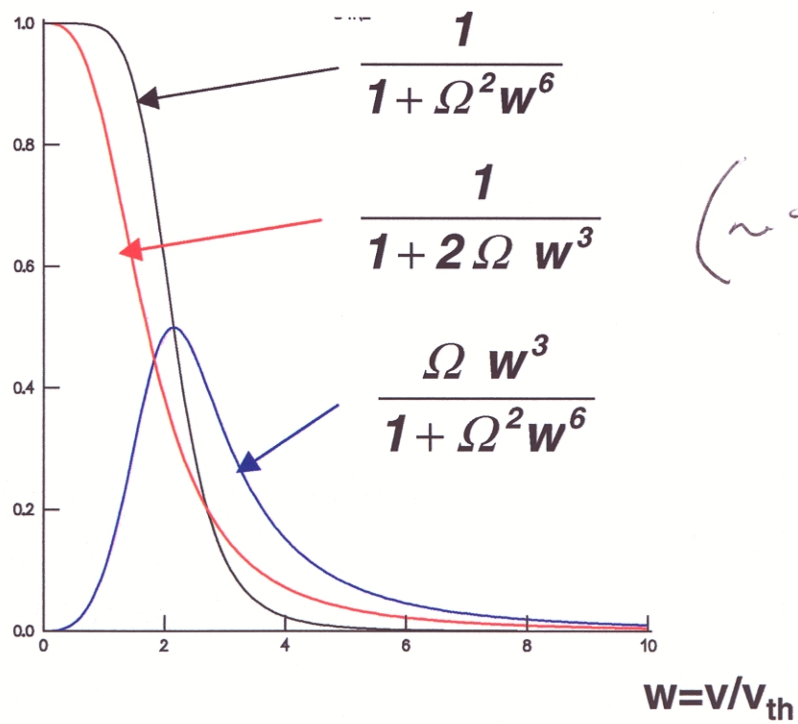

(~ harmonic average of λ_{ei} and r_{Larmor}

Cas test d 'Epperlein et Rickard

Spitzer Harm

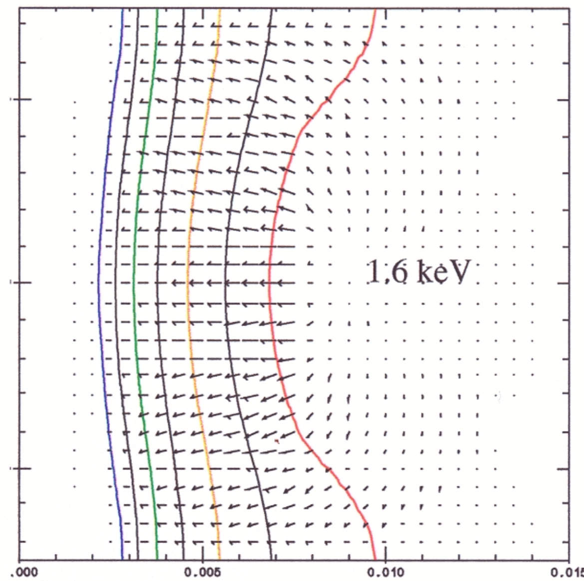

Flux de chaleur non local

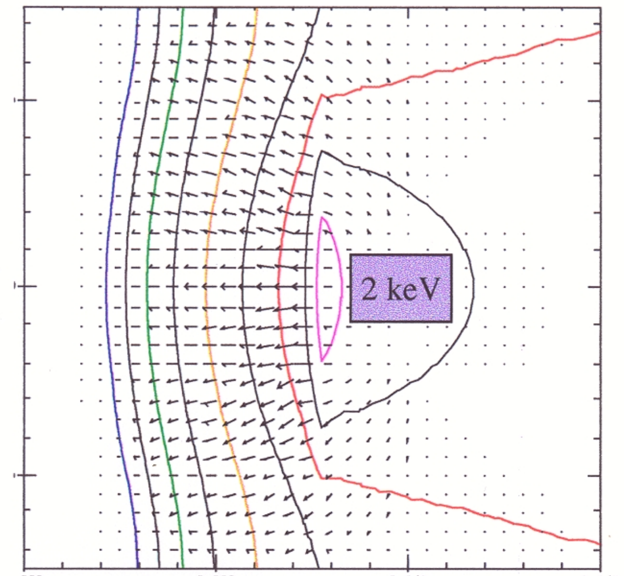

Braginskii

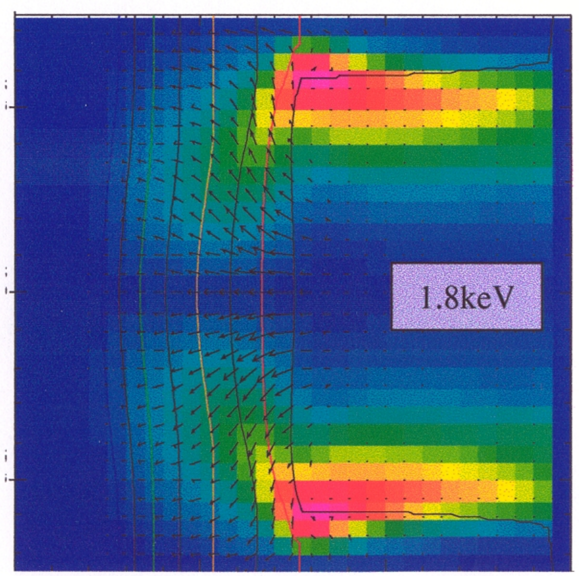

Délocalisation de Braginskii

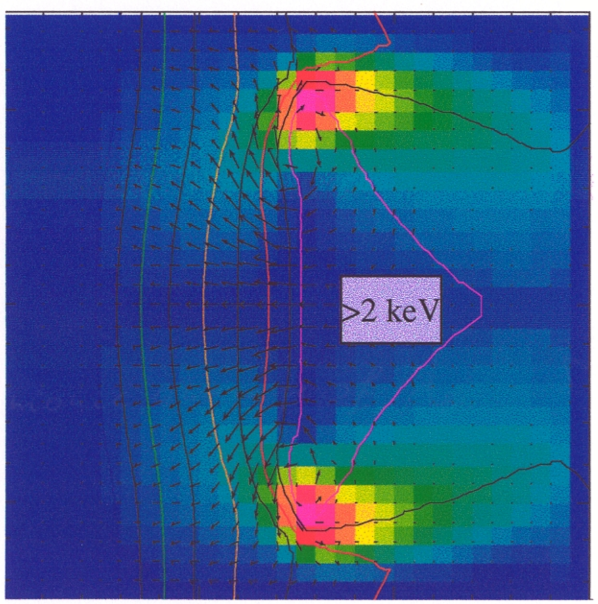

Computing fields

- « zero current » electric fields
  - may be computed from the non local distribution function f_0^{nl}

$$E_{nl}^0 = -\frac{m_e}{6e}\frac{\nabla\int f_0 v^7 dv}{\int f_0 v^5 dv}$$

  - degenerates to the Spitzer null current electric field for $f_0 = f_0^{mb}$

$$E_{sh}^0 = -\frac{kT_e}{e}\left(\nabla \ln(n_e) + \frac{5}{2}\nabla \ln(T_e)\right)$$

- Magnetic fields sources : $\left(\frac{\partial B}{\partial t}\right)_s = -c\nabla\times E^0$
  - degenerates to the classical thermal source $-\frac{c}{en_e}\nabla n_e \times \nabla kT_e$
  - non local effects may appear (e.g.: Kingham & Bell PRL 88-2002)

Non local effects cause kinetic sources to depart significantly from thermal sources

- Sources for B fields $\left(\frac{\partial B}{\partial t}\right)_s^{kin} = \frac{cm_e}{6e}\nabla\times\frac{\nabla\int f_0 v^7 dv}{\int f_0 v^5 dv} \rightarrow -\frac{c}{en_e}\nabla n_e \times \nabla T_e$
- Epperlein & Rickard

B_θ at 120 ps

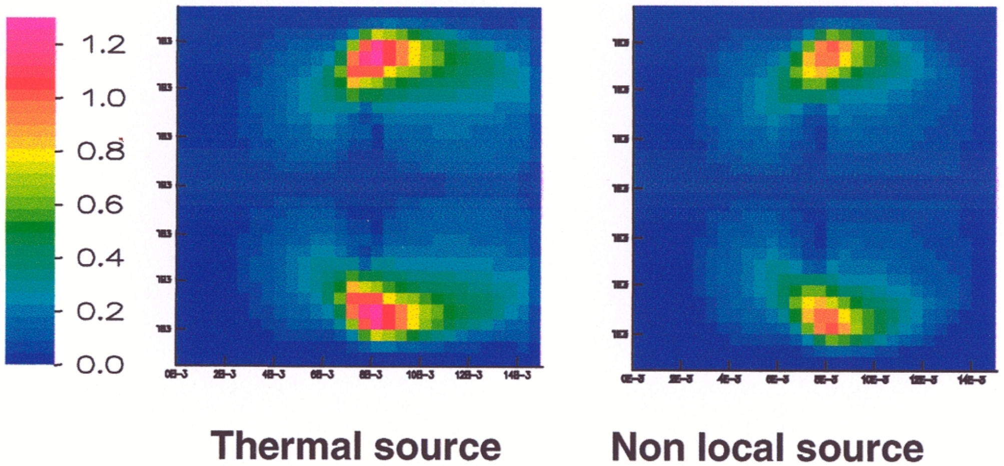

- Kingham & Bell

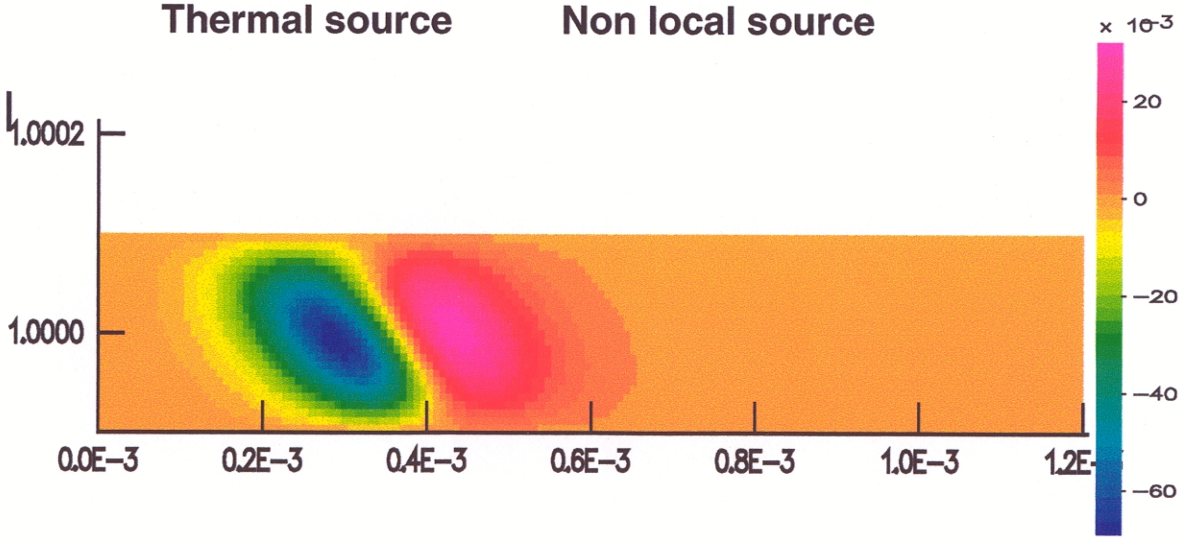

Missing terms in the induction equation

- Epperlein problem

B1

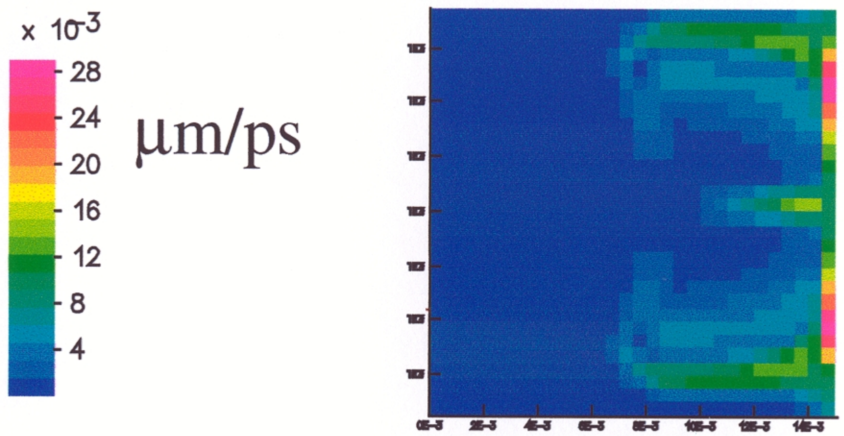

Hall velocity j/en_e

The Hall term is negligible

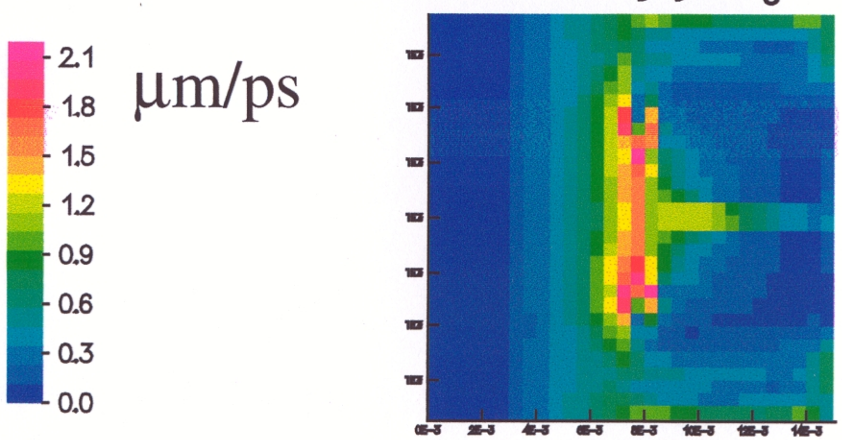

Nernst velocity $0.72\ Q/n_eT_e$

Nernst velocity ~ 0.07 thermal velocity

==> Nernst advection time scale is shorter than growth time scale

Coupling non local model to magnetic fields

- **We delocalize Braginskii fluxes with a modified diffusion operator**
  - Respects limit regimes
    - for B=0 , SH or non local fluxes according to gradient lengths
    - At moderate $\omega\tau$, non local effects are cancelled and we find Braginskii
  - Interpolation in intermediate situations is unclear : needs to be validated with 2D FP simulations including B fields.

- **Calculating sources with non local distribution functions exhibit new effects.**
    - Non local sources may be reduced because f_0v^7 has smoother gradients (e.g. Epperlein problem).
    - Non local sources may be enhanced because grad(f_0v^7) and grad(f_0v^5) have larger angles (eg.: Kingham & Bell)

- **The coupled model needs being improved**
    - Introduction of Nernst in the induction equation
    - Further theoretical investigation and numerical validation are

Numerical Investigation of Recent Laser Absorption and Drive Experiments of CH Spherical Shells on the OMEGA Laser

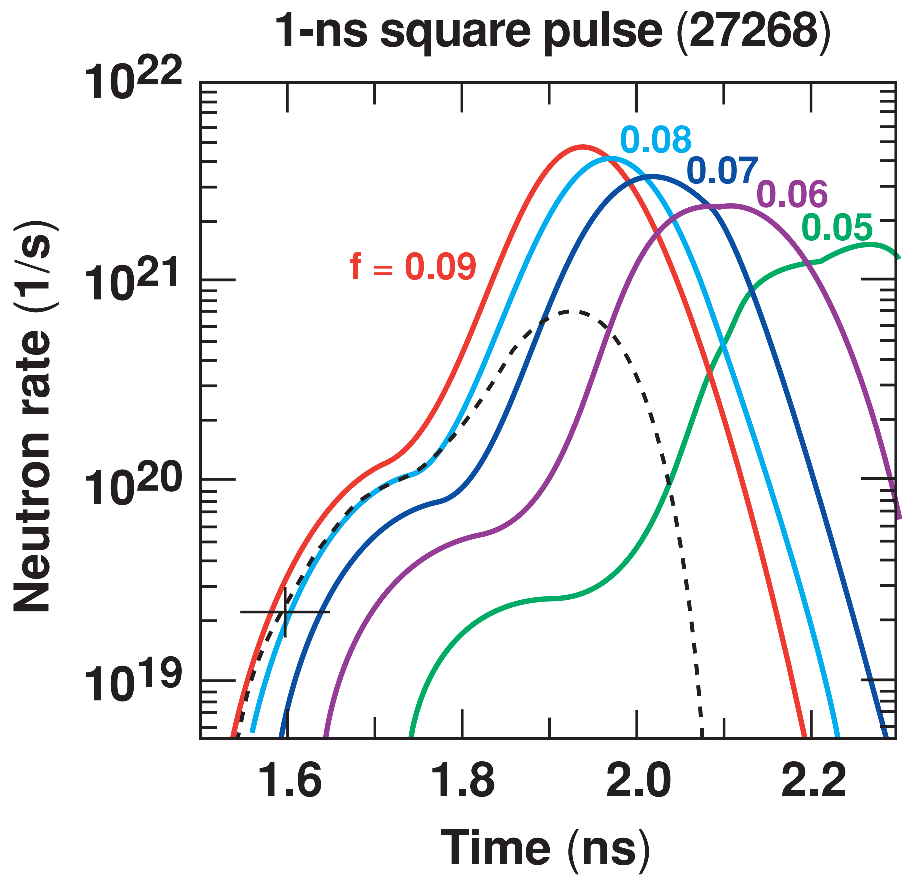

J. A. Delettrez
Laboratory for Laser Energetics
University of Rochester

32nd Anomalous Absorption Conference
Oahu, Hawaii
21–26 July 2002

Contributors

J. P. Knauer, W. Seka, P. Jaanimagi, and C. Stoeckl

Laboratory for Laser Energetics
University of Rochester

Summary

Dedicated experiments on the OMEGA laser have measured absorption fraction and implosion timing

UR LLE

- Neutron temporal diagnostics (NTD), shell trajectory, and temporal x-ray emission measured the drive efficiency.
- Laser absorption was measured with improved diagnostics.
- The timing and the level of both the shock yield and the onset of the compression yield are sensitive to the flux limiter.
- Absorption measurements require a flux limiter value below 0.06 (harmonic).
- A flux limiter between 0.07 and 0.08 gives general agreement with implosion timing.
- Work is ongoing to reconcile the two results.

The flux limiter affects independently the drive and the laser absorption fraction

- The flux limiter controls the flow of the absorbed energy into the target and affects
  - the drive though the mass ablation rate and
  - the absorption fraction through the electron temperature in the corona.
- It is active at and inside the critical surface.
- Two methods are used to compute the thermal flux:
  - the sharp cutoff: $Q = \max(Q_{SH}, Q_{FS})$
  - the harmonic mean: $Q = (Q_{SH} Q_{FS})/(Q_{SH} + Q_{FS})$

The absorbed energy was measured with two independent diagnostics

- **Two differential plasma calorimeters measure the plasma and scattered light reaching the tank wall (time integrated).**
- **Two full-aperture backscatter stations (FABS, *f*/6) measure the scattered and refracted light through two focusing lenses (time integrated and time resolved).**
- **Two subsidiary scattered light diagnostics measure the scattered/ refracted light between the lenses (time integrated and time resolved).**
- **The signals from all six calorimeters are very consistent with overall errors estimated at 2% (absolute) from shot to shot.**

The drive timing was obtained from x-ray and neutron diagnostics

- The shell trajectory was measured with an imaging streak camera and a framing camera.
- The onset of stagnation was via the shock yield measured with the neutron temporal diagnostic (NTD).
- The temporal x-ray emission was obtained from a diamond detector.

The neutron burn history shows details of the shock arrival and the stagnation phase of the implosion

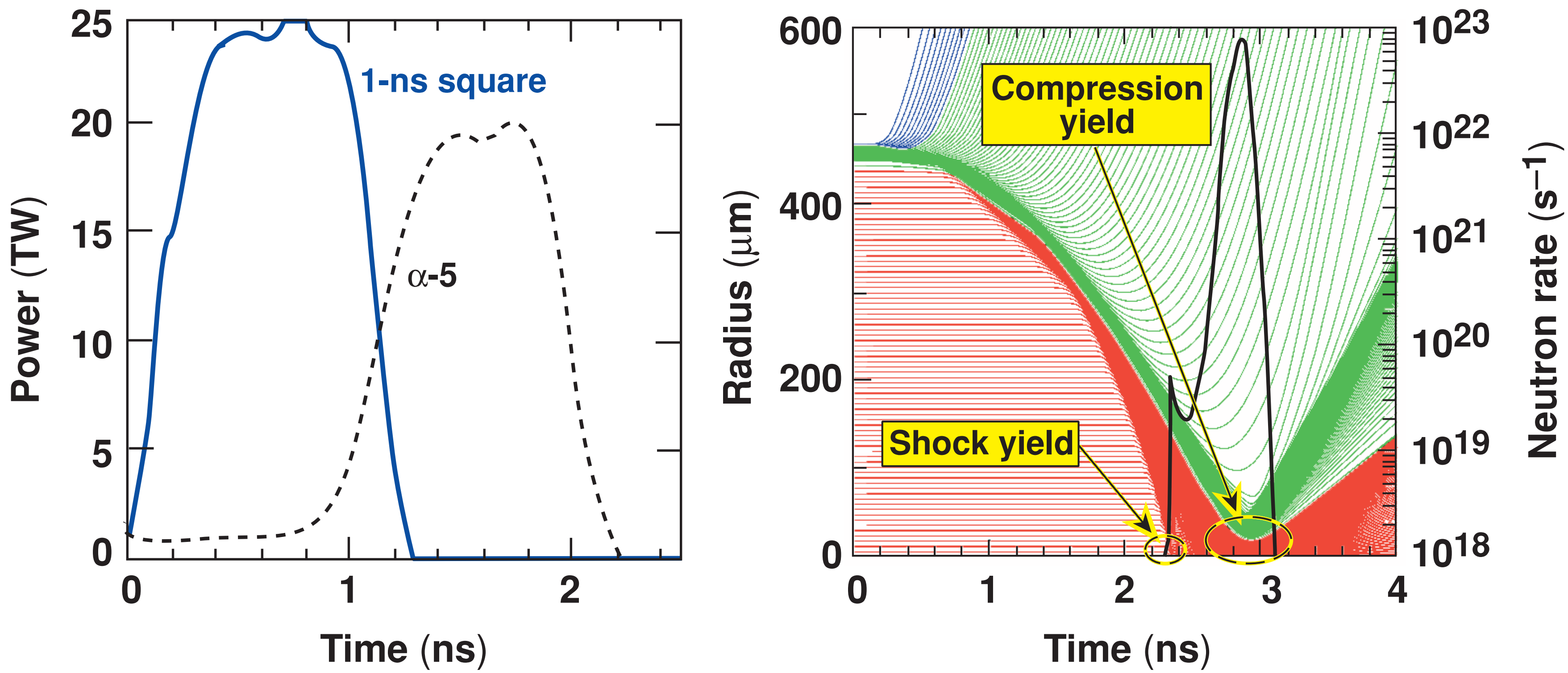

Targets are 15 μm CH or CHSi shells filled with 15 atm D_2, D_2/Ar, or D_2 ^{3}He, and diameters 930 μm and 1100 μm.

TC5961

The laser absorption is modeled in *LILAC* with 2-D ray tracing and classical inverse bremsstrahlung

- The ray trace uses the measured DPP spatial distribution, including the effect of SSD and PS.
- The absorption model includes the Langdon effect.
- The density profile at and below the critical surface is zoning dependent.
- The harmonic mean method is less sensitive to zoning than the sharp-cutoff method.

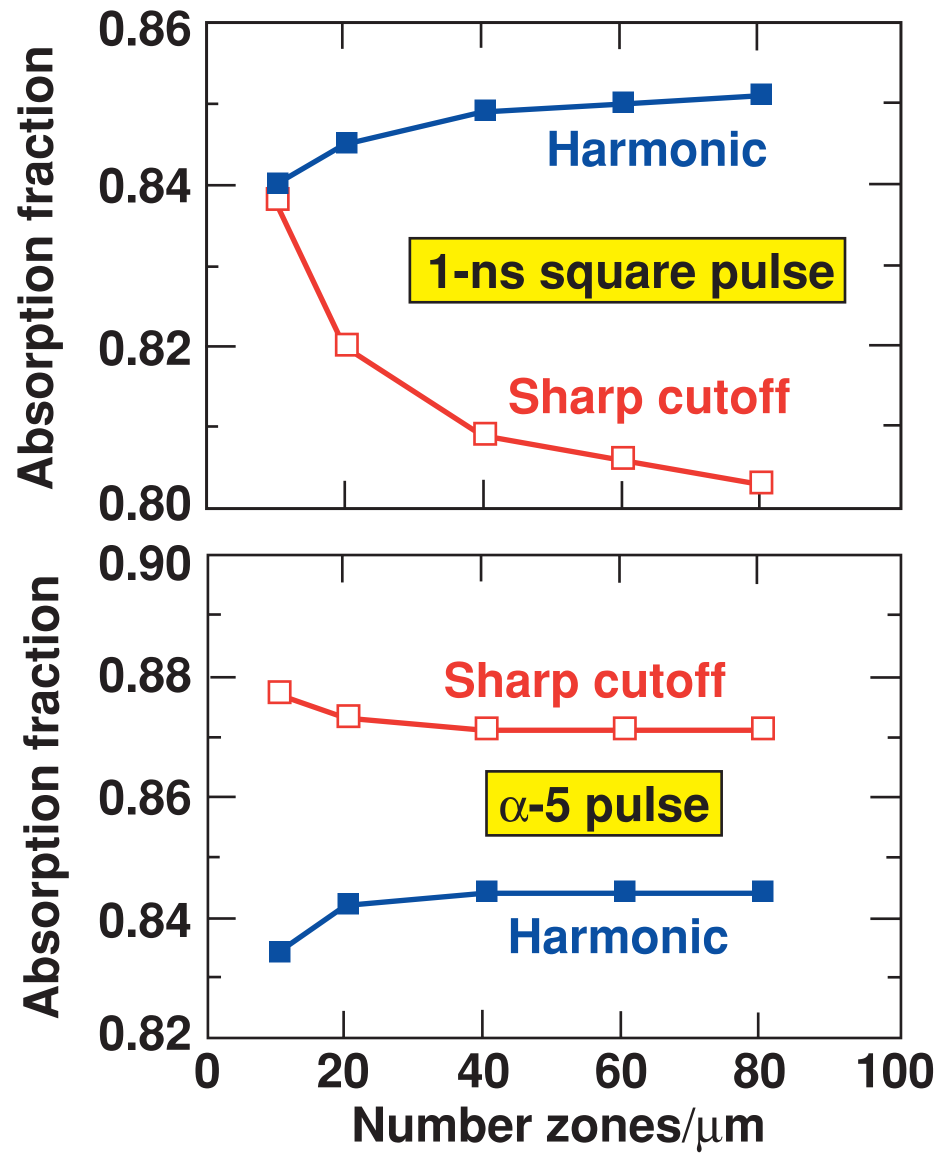

TC5962

The measured and simulated absorption fractions show the same trend over a wide range of experimental conditions

Scattered light absorption

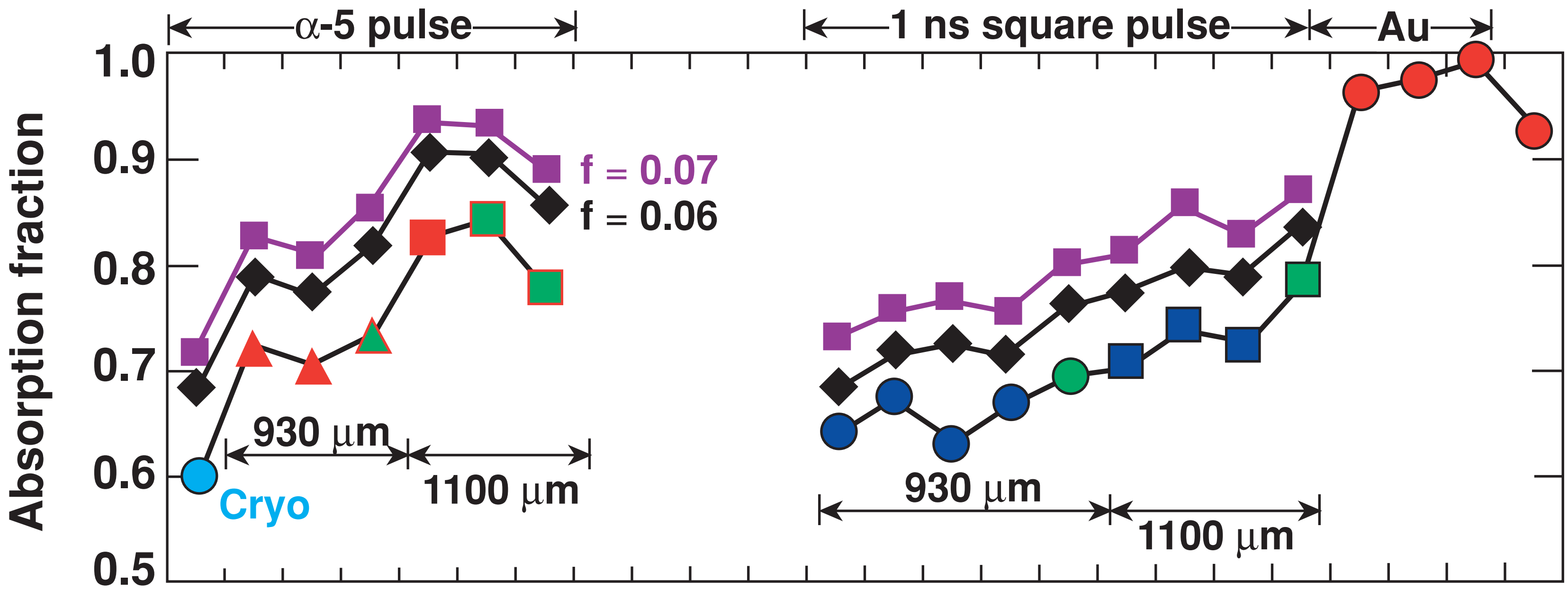

Green fill: CHSi shells

Experimental error bars are size of symbols

TC5969

For CH shells and generic conditions *LILAC* needs a low value of flux limiter to match the experimental measurements

UR LLE

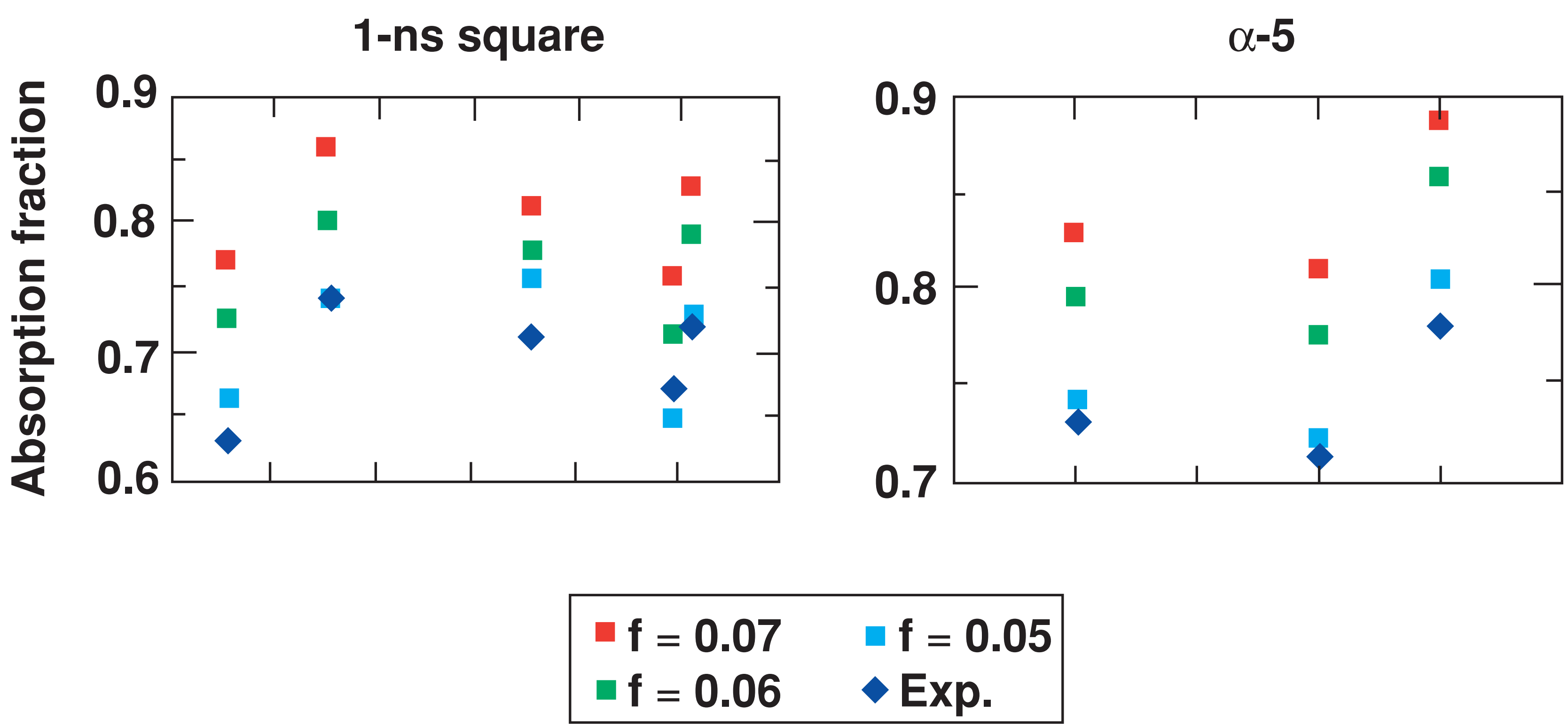

TC5963

The NTD timing is best matched by a flux limiter between 0.07 and 0.08 harmonic

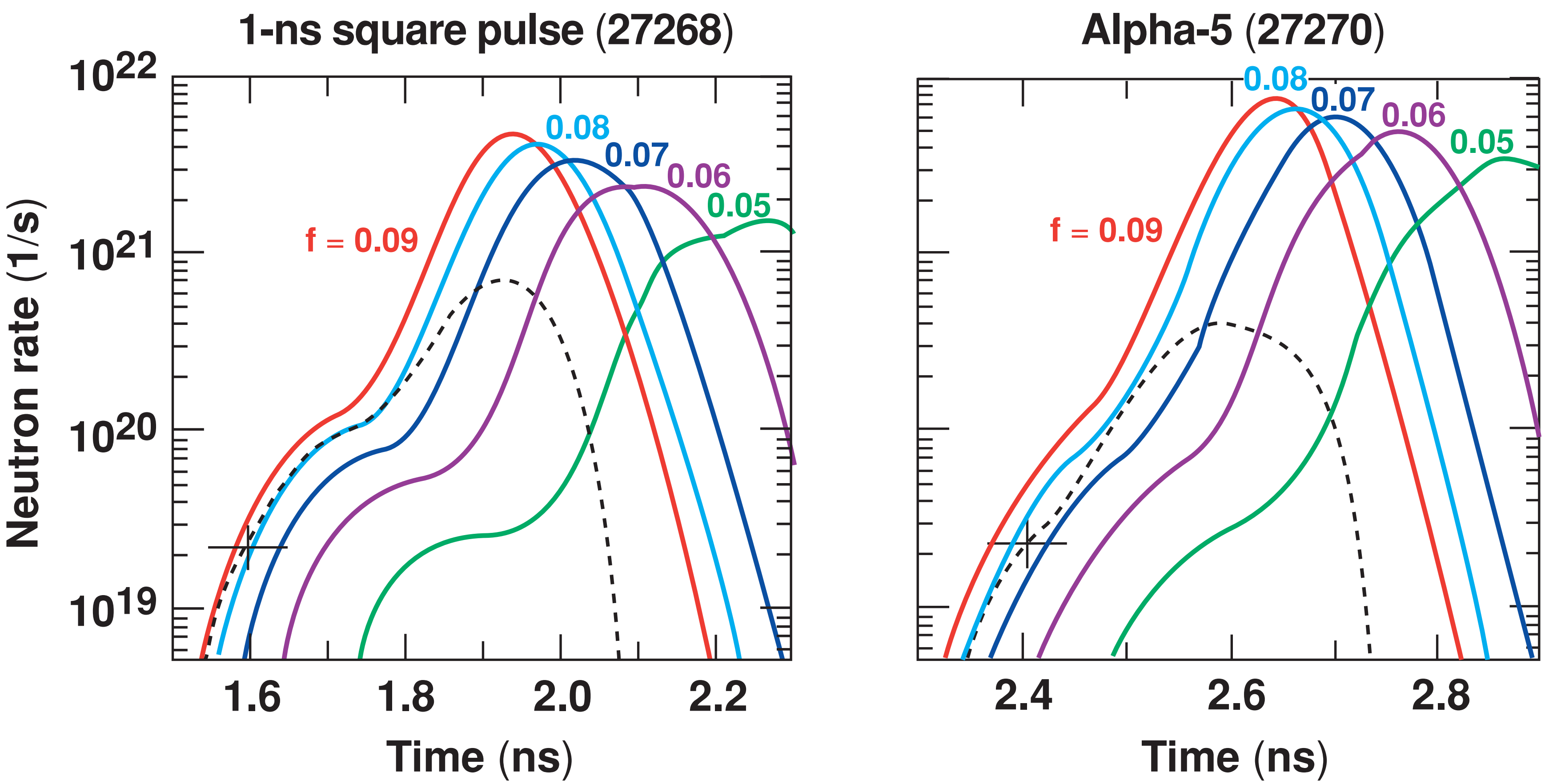

TC5964

The shell trajectories confirm the results of NTD

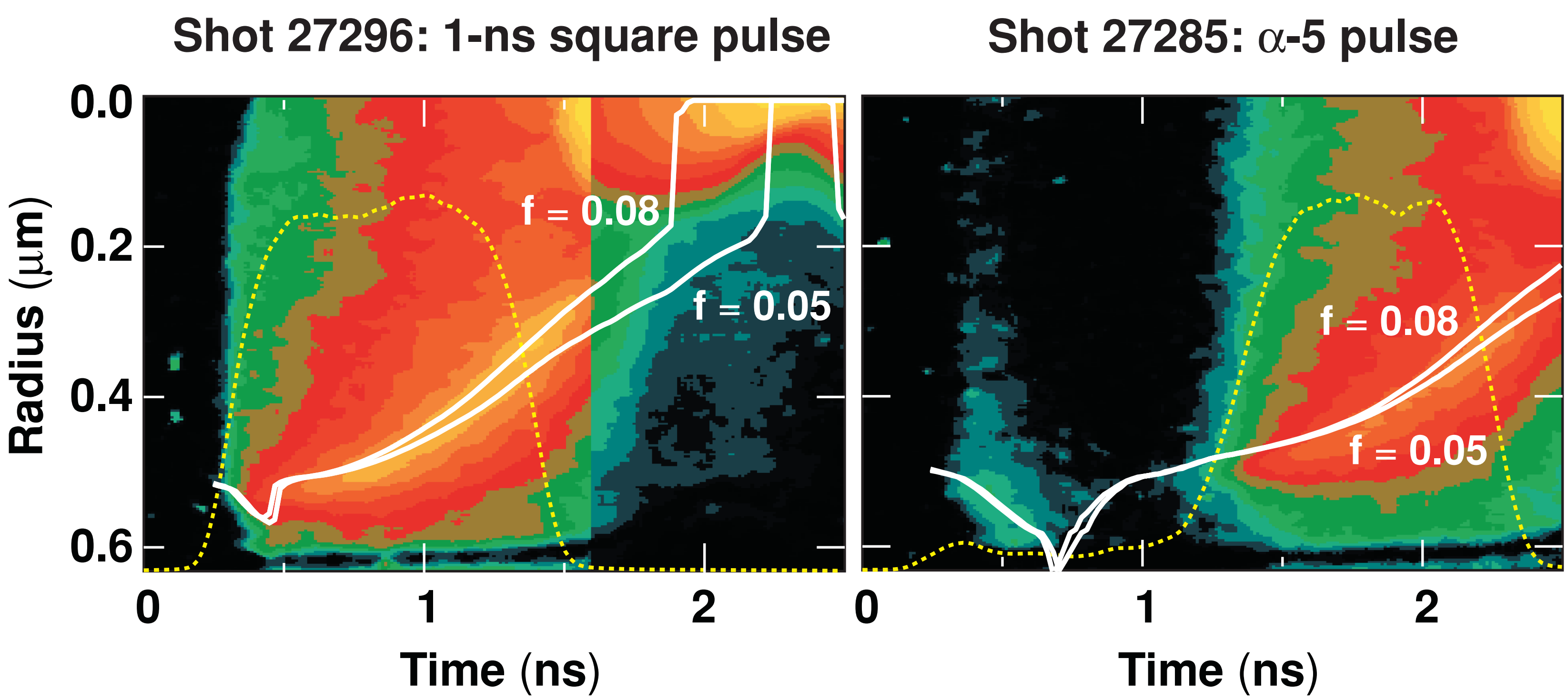

Reconciliation between the results of the absorption and implosion timing is difficult

- Flux-limiter values between 0.07 and 0.08 are supported by
  - NTD and x-ray timing in the experiments reported here,
  - Ar emission timing in doped-core mix experiments,[1] and
  - Fokker-Plank calculations of the thermal flux.[2, 3]
- Absorption measurements agree with a flux limiter below 0.06.
- Time-dependent flux limiter[3] goes the wrong way.
- Many considered scenarios failed because of the coupling between absorbed energy and drive efficiency through the flux limiter.

[1] S. P. Regan *et al.*, Phys. Plasma 9, 1357 (2002).
[2] J. P. Matte *et al.*, Phys. Rev. Lett. 53, 1461 (1980).
[3] A. Sunahara, Bull. Am. Phys. Soc, 46, 181 (2001).

Summary/Conclusions

Dedicated experiments on the OMEGA laser have measured absorption fraction and implosion timing

- Neutron temporal diagnostics (NTD), shell trajectory, and temporal x-ray emission measured the drive efficiency.
- Laser absorption was measured with improved diagnostics.
- The timing and the level of both the shock yield and the onset of the compression yield are sensitive to the flux limiter.
- Absorption measurements require a flux limiter value below 0.06 (harmonic).
- A flux limiter between 0.07 and 0.08 gives general agreement with implosion timing.
- Work is ongoing to reconcile the two results.

A brief review of 2D Fokker-Planck codes without B-fields

Richard P J Town

LLNL

Most 2D FP codes have used the diffusive approximation in the high Z limit[1]

- **SPARK keeps only f_0 and f_1:**

$$\frac{\partial f_0}{\partial t} + \frac{v}{3}\underline{\nabla} \cdot \underline{f_1} =$$

$$\frac{1}{v^2}\frac{\partial}{\partial v}\left[\frac{v^2}{3}\underline{a} \cdot \underline{f_1} + Y\left(Cf_0 + D\frac{\partial f_0}{\partial v}\right) + \frac{YnZ}{6v}\upsilon_0^2\frac{\partial f_0}{\partial v}\right]$$

$$\underline{f_1} = \tau\left(v\nabla f_0 - \underline{a}\frac{\partial f_0}{\partial v}\right)$$

where:

$$\underline{a} = e\,E\big/m, \tau = v^3\big/\left[(Z+1)nY\right],$$

$$Y = 4\pi\left(e^2\big/m\right)^2 \ln\Lambda, C = I_0^0 f_0, D = \tfrac{1}{3}v\left(I_2^0 + J_{-1}^0\right)$$

---

[1]P. Shkarofsky et al, "The Particle Kinetics of Plasmas" (1966).

The Japanese have developed a 2-D FP code called KEICO[1]

- The code expands to f_0 and f_1 only and retains the electron inertia term (df_1/dt).
- Preheating due to nonlocal electron thermal transport suppresses the Rayleigh-Taylor growth rate:

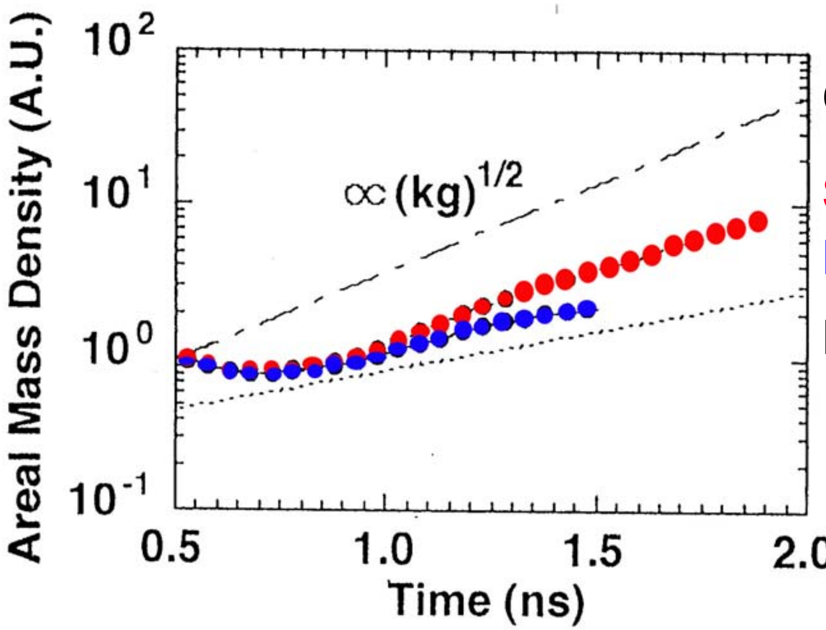

Classical: 2.6 ns^{-1}

Spitzer-Harm: 2.1 ns^{-1}

Fokker-Planck: 1.4 ns^{-1}

Experiment: 1.2 ns^{-1}

---

[1] M. Honda et al, ECLIM 1996

The SPARK code uses the ADI scheme to invert the Fokker-Planck equation[1]

$$\frac{\partial f_0}{\partial t} = \underline{\nabla} \cdot \left[\chi \left(\nabla f_0 - \underline{a}\alpha \frac{\partial f_0}{\partial v} \right) \right] +$$

$$\frac{1}{v^2} \frac{\partial}{\partial v} \left[\chi \left(\underline{a} \cdot \underline{a} \frac{\partial f_0}{\partial v} + v \underline{\beta} \cdot \underline{a} f_0 \right) + Y \left(C f_0 + \left(D + \frac{YnZ\upsilon_0^2}{6v} \right) \frac{\partial f_0}{\partial v} \right) \right]$$

- **Finite difference the above using Chang-Cooper weighting.**
- **Two alternatives for calculating the electric field were tried:**
    - **Implicit moment method (*curl* E = 0)**
    - **Total current equals zero.**
- **When J=0 there was a deterioration in quasineutrality.**

---

[1] **E. M. Epperlein et al, *Comput. Phys. Commun*. 52, P7 (1988)**

SPARK modeled the interaction of a short pulse laser with a solid target

- **Thermal smoothing becomes less effective in smoothing small scale (<80λ_{mfp}) temperature modulations when the electron transport is modeled by Fokker-Planck.**

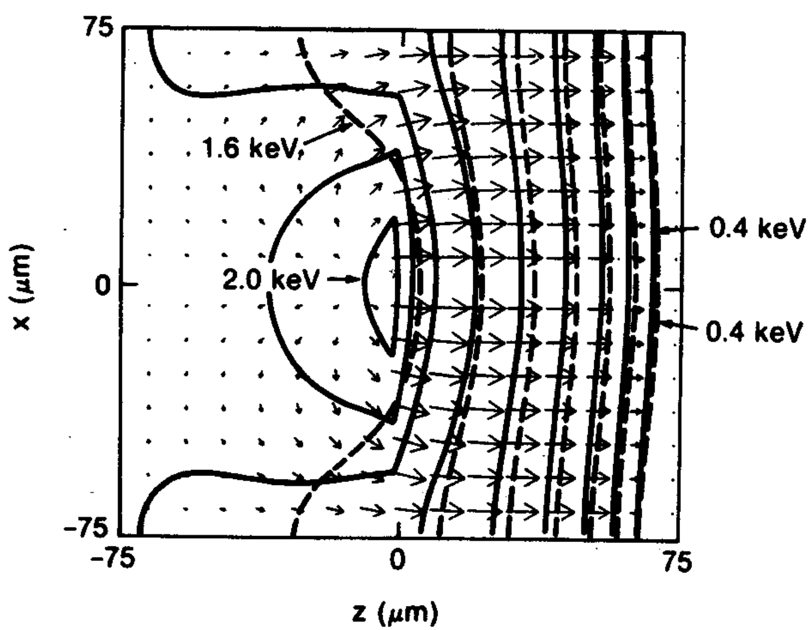

---

[1]E. M. Epperlein et al, *Phys. Rev. Lett.* 61, P2453 (1988)

SPARK simulations showed the heat flow was preferentially directed into the target

- The heat flow into the target did not exceed 0.1 q_{fs}
- The heat flow laterally was much less than 0.1 q_{fs}
- Large angle between q and grad T were found

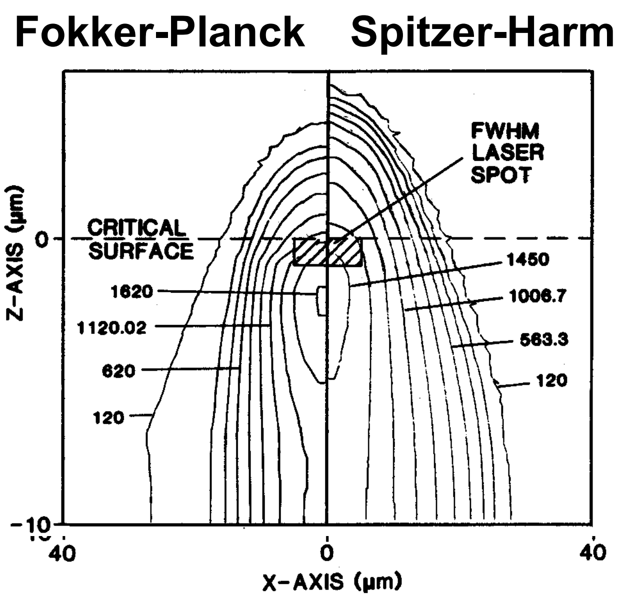

Temperature contours

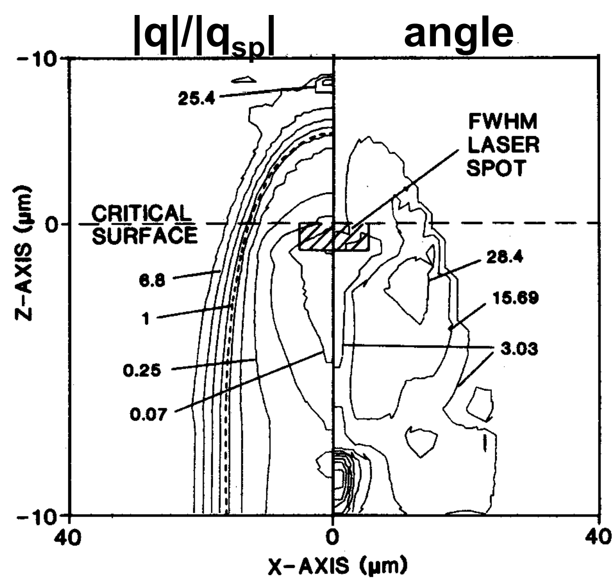

[1]G. J. Rickard et al, *Phys. Rev. Lett.* 62, P2687 (1989)

SPARK has been used to model filamentation

- Nonlocal heat flow was found to enhance the laser filamentation rate.
- Enhanced levels of self focusing, with filaments following the ray trajectories, was found when an f/2 lens was modeled.

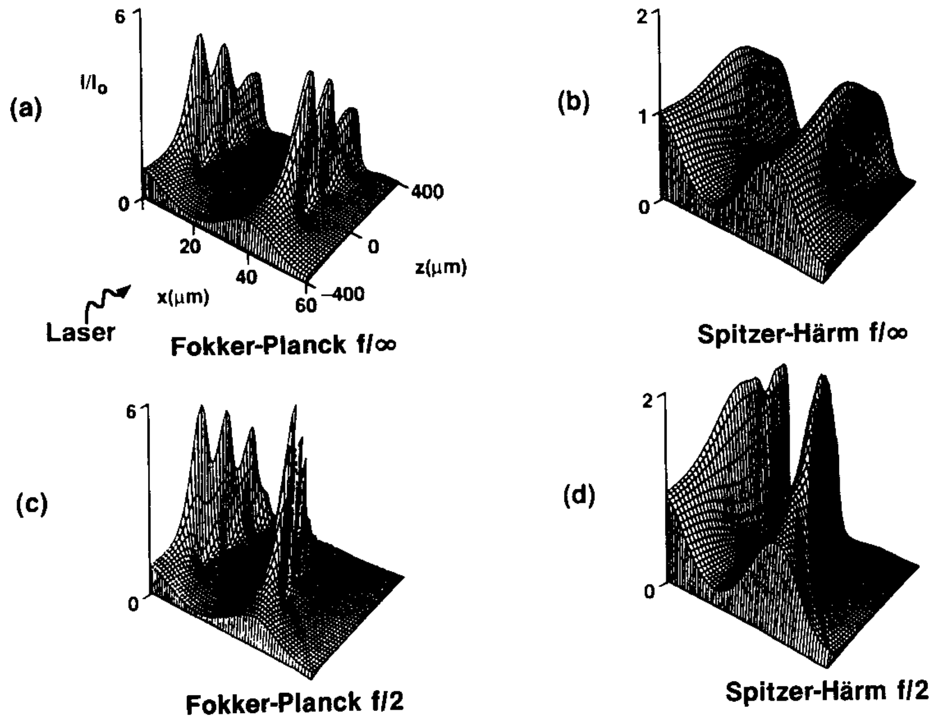

[1]E. M. Epperlein, *Phys. Rev. Lett.* 65, P2145 (1990)

One-dimensional simulations have been performed to assess how the foam alters the behavior of the target

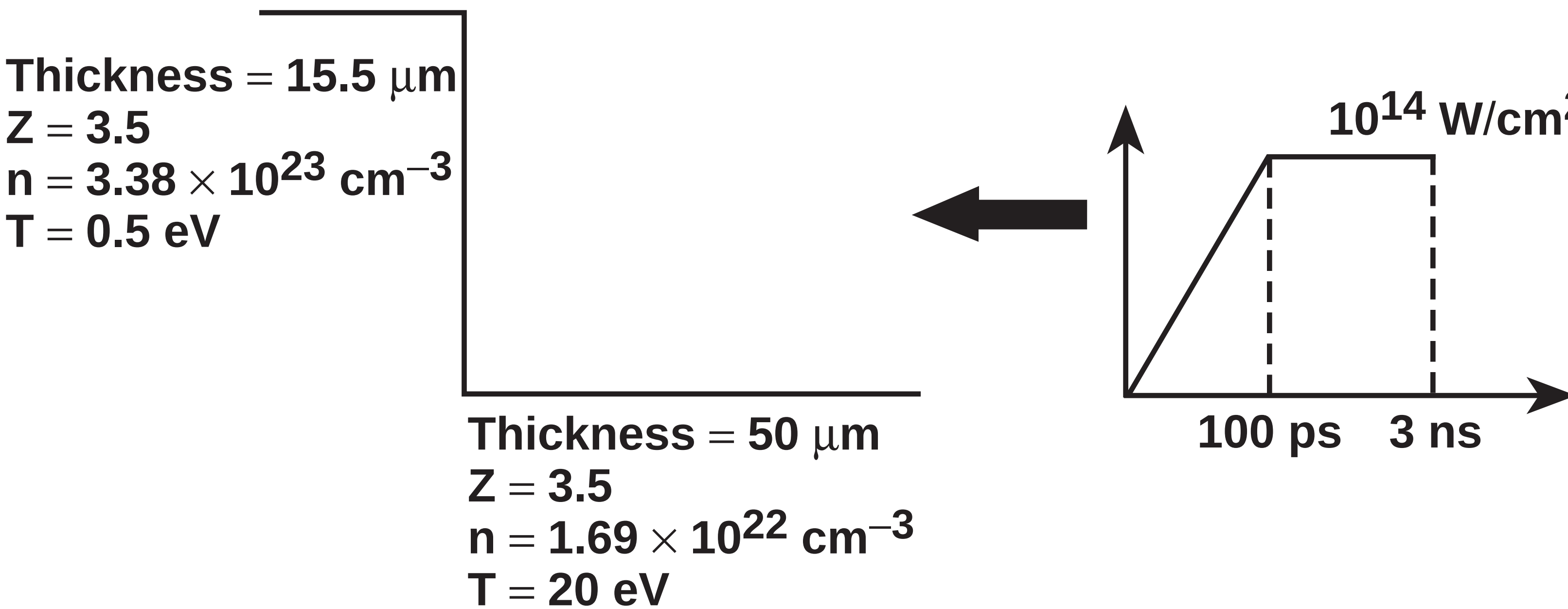

The Fokker-Planck simulations have higher ablation velocities than equivalent Spitzer simulations

Fokker-Planck simulations show:

- larger preheat of foam and bare targets

- lower peak densities

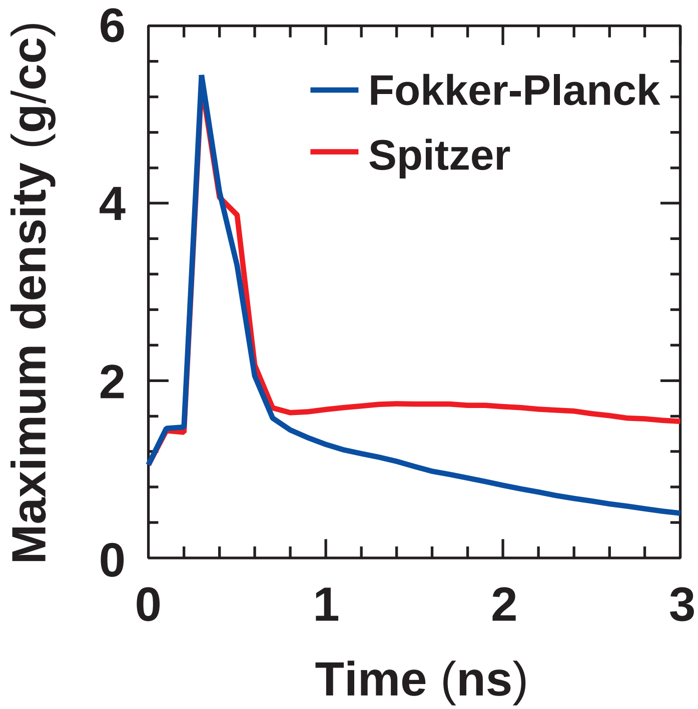

- higher ablation velocities

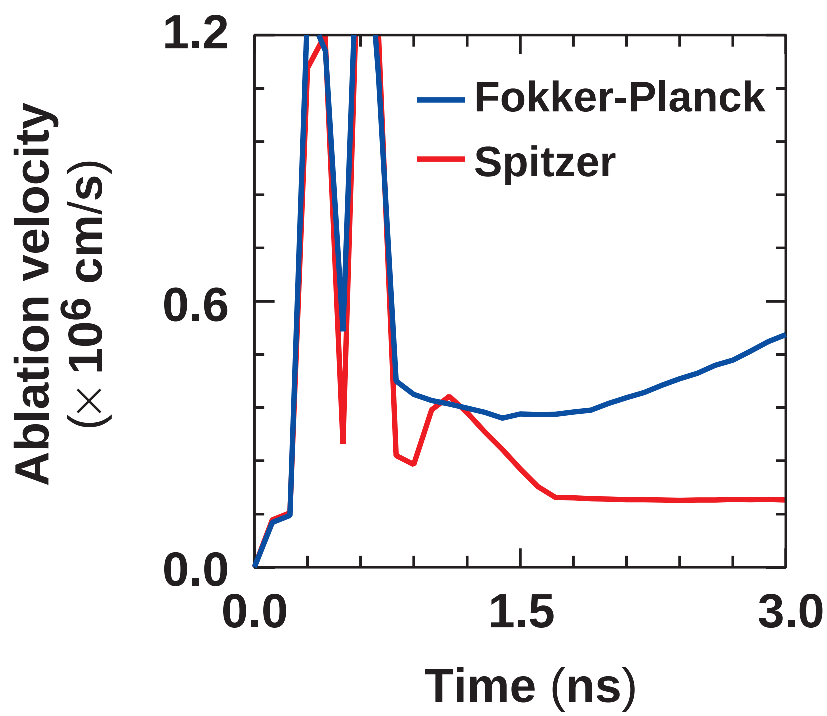

TC4253

Temperature contour plots show enhanced heat front penetration into the foam for the Fokker-Planck simulation

- The Fokker-Planck temperature contours are less smooth where the energy is being absorbed.
- The Spitzer temperature contours are less smooth at the heat front.

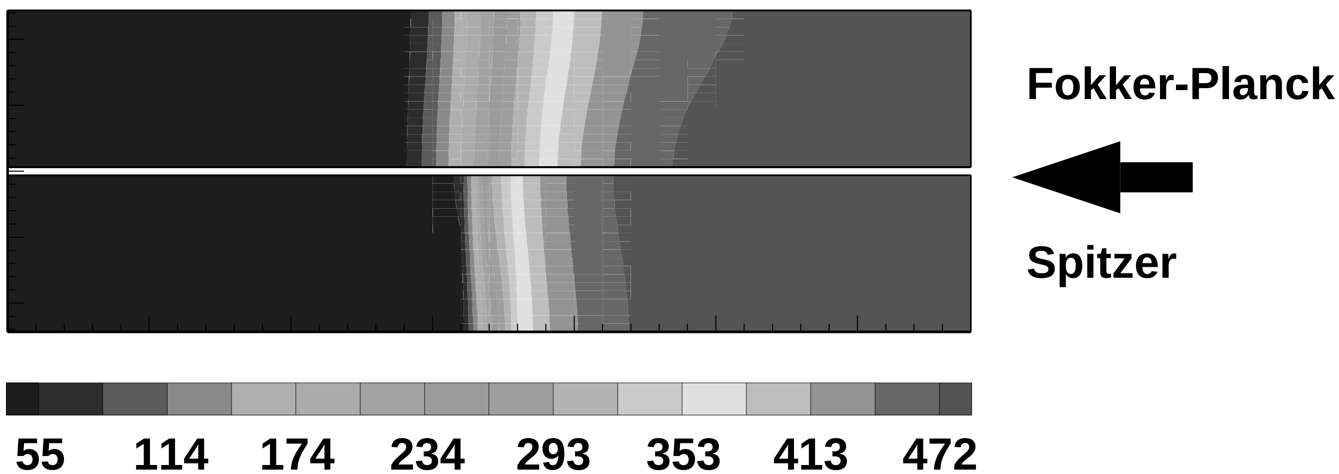

σ_{rms} is a measure of the nonuniformity at a particular distance in the foam

Defining:

$$\sigma_{rms}^2 = \frac{\int \left(T - \langle T \rangle\right)^2 dx}{\int \langle T \rangle^2 dx}$$

- The Fokker-Planck is less smooth in the energy-absorbing region but is more smooth than Spitzer in the main body of the foam.

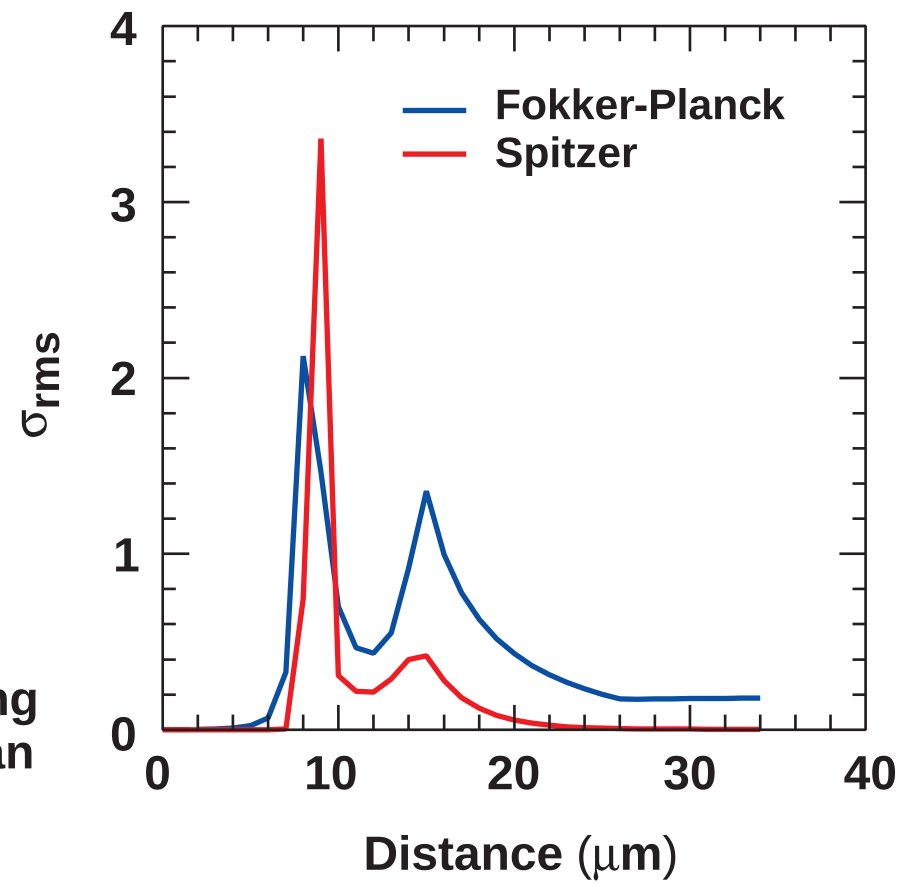

TC4256

Two-dimensional Fokker-Planck calculations of an idealized hohlraum were performed

- All boundaries were reflective, apart from the outer radial wall, which was kept at a fixed temperature.
- The laser propagated radially outward from 200 μm from the axis and escaped from the outer radial wall.

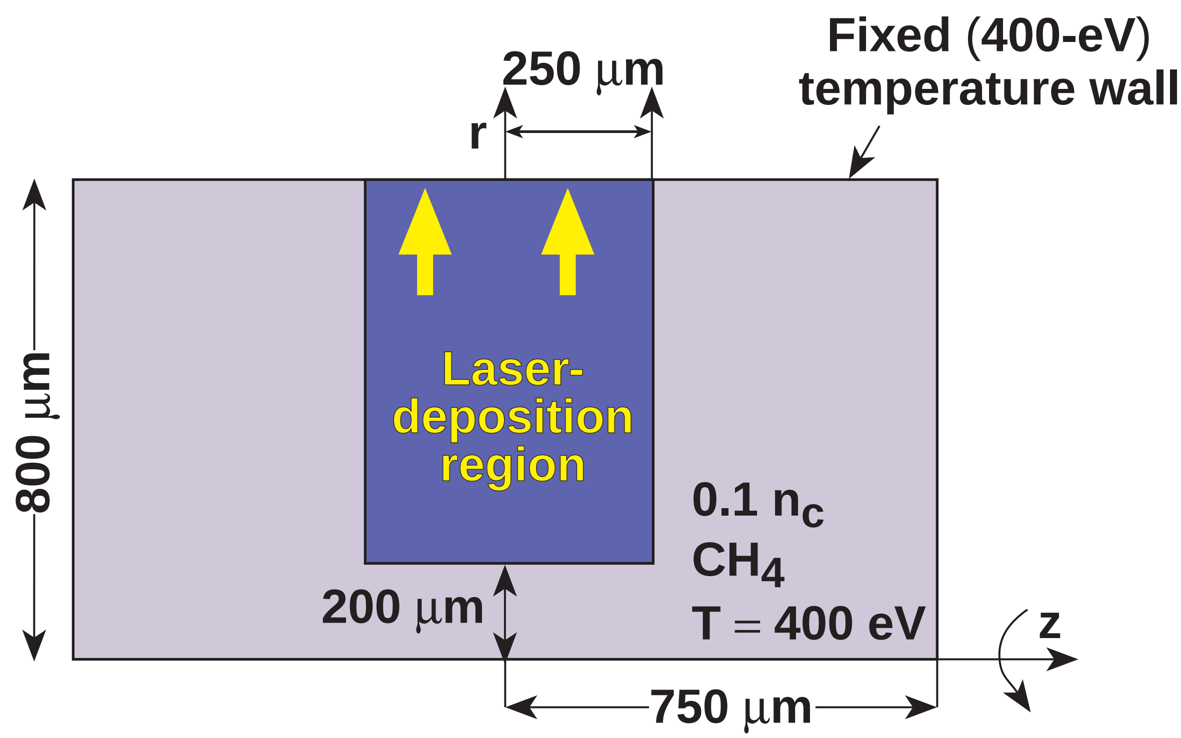

TC4503

Fokker-Planck calculations show a cooler, but more dispersed heated region than f = 0.01 Spitzer calculations

- Contour plot of electron temperature after 200 ps shows the f = 0.01 Spitzer calculations bottles up the absorbed laser energy.

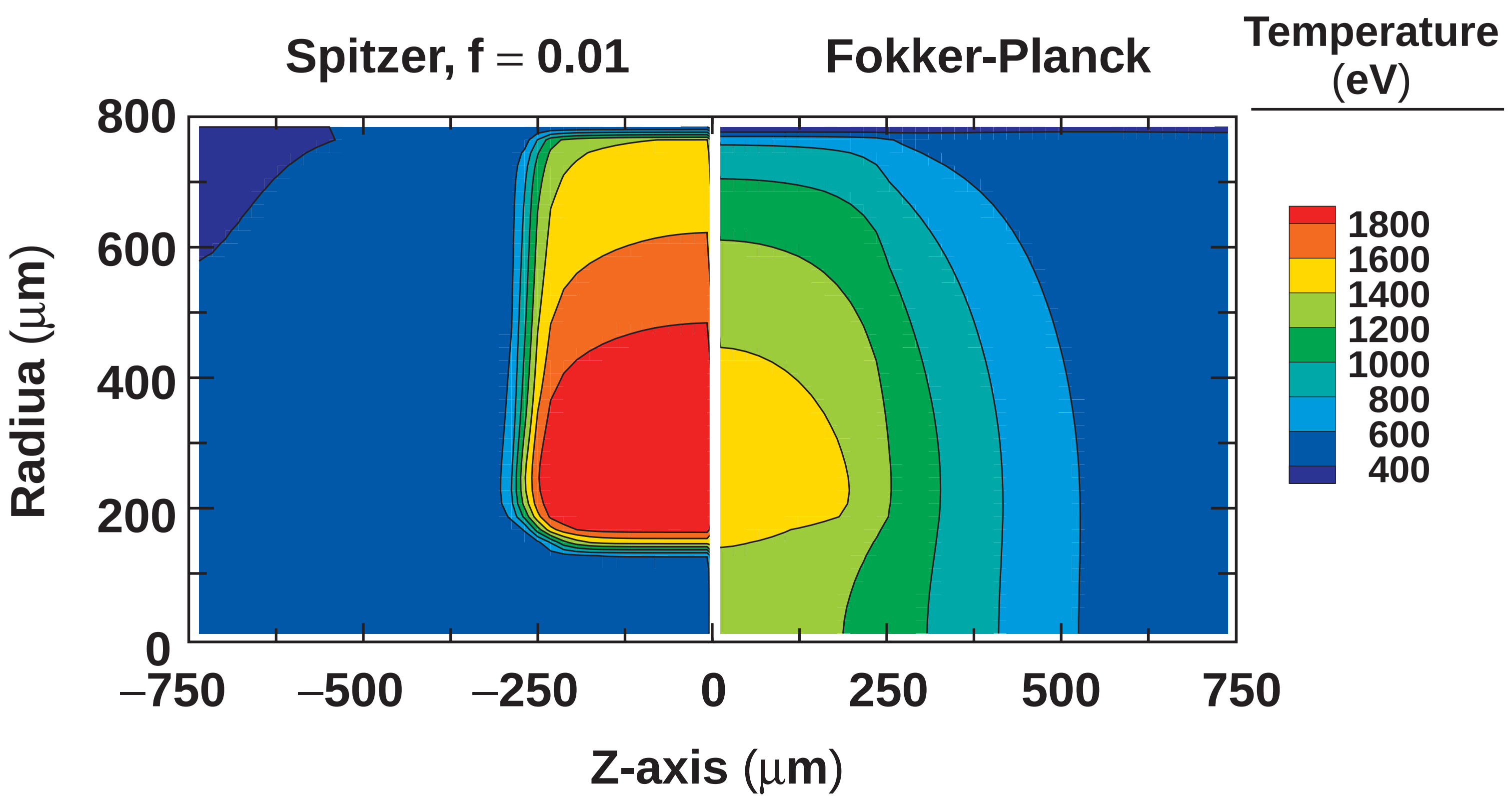

TC4509

A depletion of low-velocity electrons leads to a higher inferred electron temperature

- The electron distribution is non-Maxwellian and can be approximated by the DLM formula:

$$f(v) = K_n \exp\left(-v^n / v_n^n\right).$$

- The flat-top electron distribution reduces the number of electrons at low velocity, which leads to an overestimate of the temperature:

$$C_s^{FP} = A\, C_s^{Maxwellian}.$$

- Afeyan[1] calculated the over-estimate to depend on the parameter n:

$$A^2 = \frac{3\Gamma^2(3/n)}{\Gamma(1/n)\,\Gamma(5/n)}$$

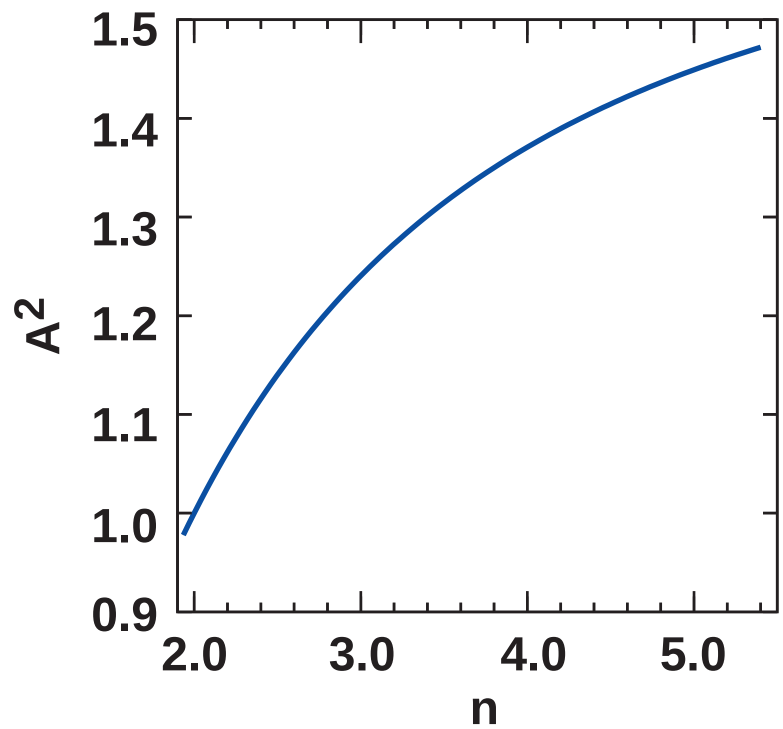

[1] B. B. Afeyan (submitted to Phys. Rev. Lett.)

The distribution function is non-Maxwellian throughout the hohlraum

UR LLE

- In the energy-absorption region there is a deficit of low- and high-velocity electrons.
- In the thermal-conduction region there is an excess of high-velocity electrons.
- The “n” has a peak value of 2.8.

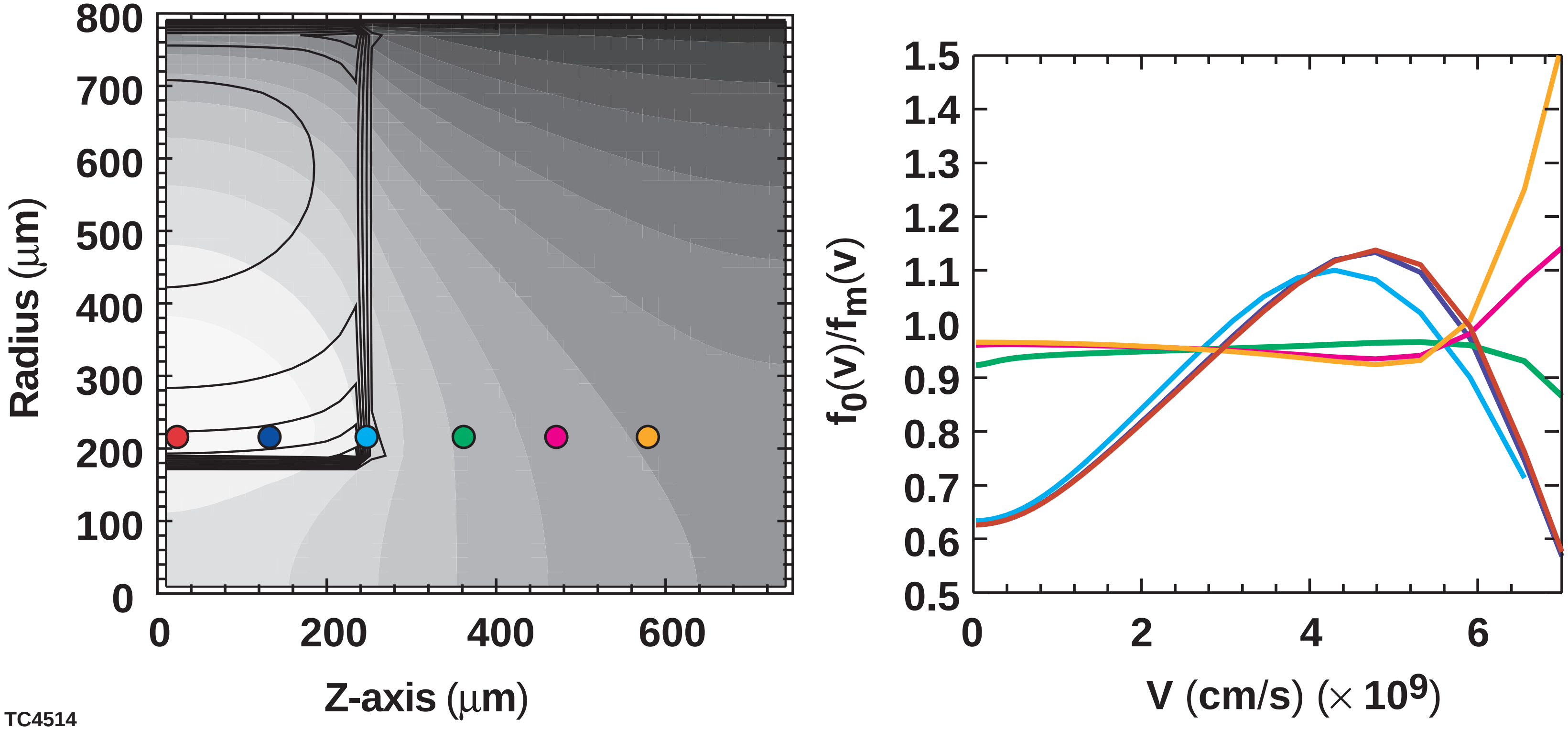

TC4514

Fokker–Planck Calculation of ICF Implosions

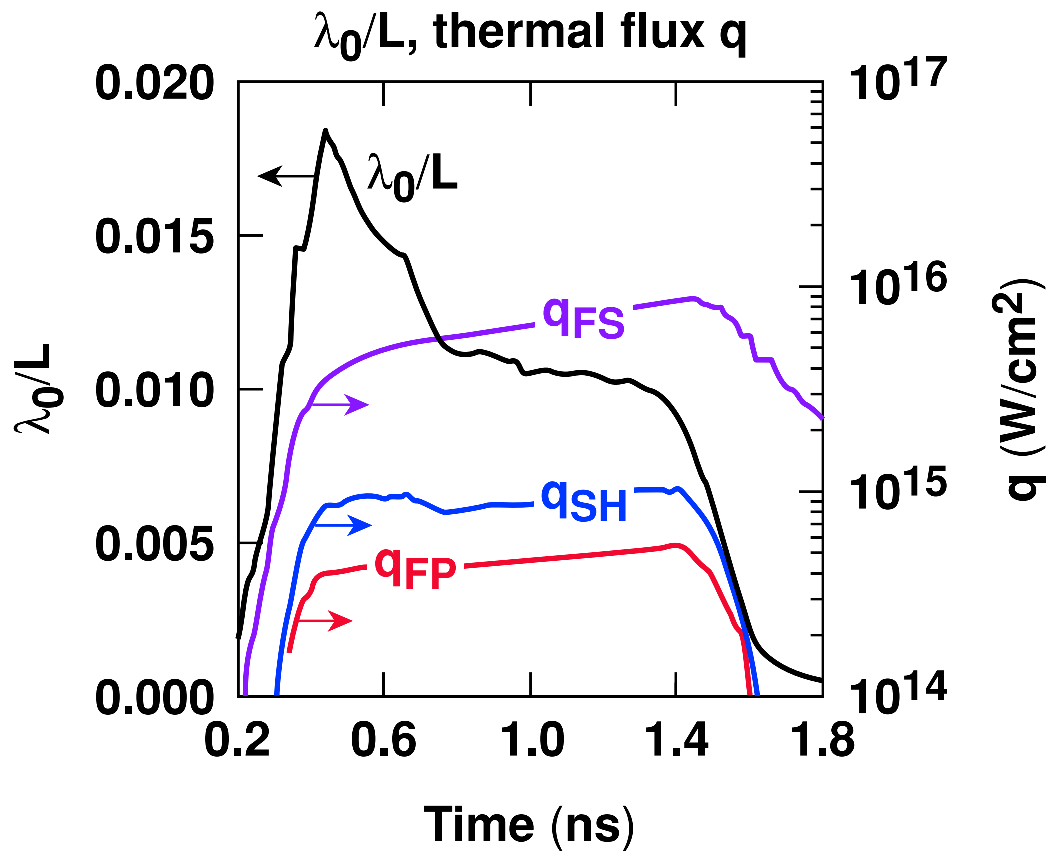

A. Sunahara, J. A. Delettrez,
R. W. Short, and S. Skupsky
University of Rochester
Laboratory for Laser Energetics

43rd Annual Meeting of the
American Physical Society
Division of Plasma Physics
Long Beach, CA
29 October–2 November 2001

Summary

We have developed a 1-D Fokker–Planck Code and combined it with the 1-D hydrodynamic code *LILAC*

UR LLE

- For CH implosions, comparison of Fokker–Planck (FP) with flux-limited Spitzer–Härm (SH) diffusions shows that
  - the flux inhibition factor is time dependent
  - with FP, the laser absorption is higher than with SH due to a longer density scale length at the critical surface
  - in the acceleration phase, FP gives a density-scale length at the ablation surface 50% longer than SH
  - FP gives good agreement with the experimental bang time.

FP Code Equations

The distribution function is expanded in Legendre modes to second-order

- $f(z, \vec{v}, t) = f_0 + f_1\cos(\theta_z) + f_2\left\{3\cos^2(\theta_z) - 1\right\}/2$
- The Fokker–Planck equations for f_0, f_1, and f_2 are calculated with e-i and e-e collisions.
- For closure, a simplified f_3 equation is used.
- The electric field is calculated based on the current free condition.
- ΔT_e and Δn_e are calculated from the hydrodynamics equations without $\nabla \cdot q_e$
- $T_{eff} = \frac{4\pi m_e}{3n_e}\int_0^\infty v^4 f_0 dv$ is computed from FP using ΔT_e and Δn_e as source terms.

In the FP calculation the flux inhibition factor ($f = q_{FP}/q_{FS}$) is time dependent

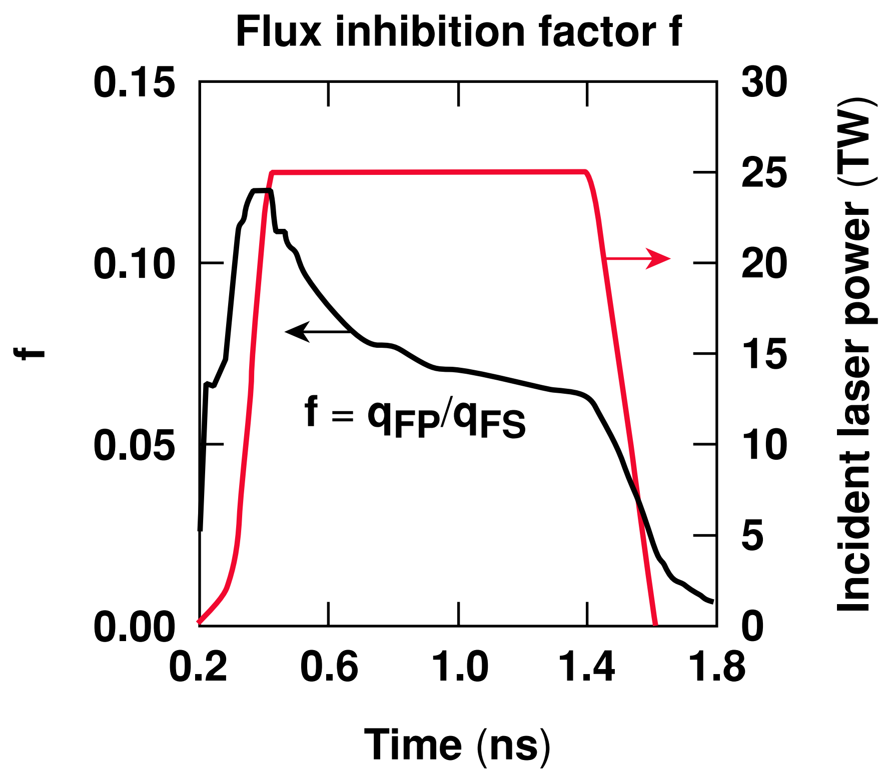

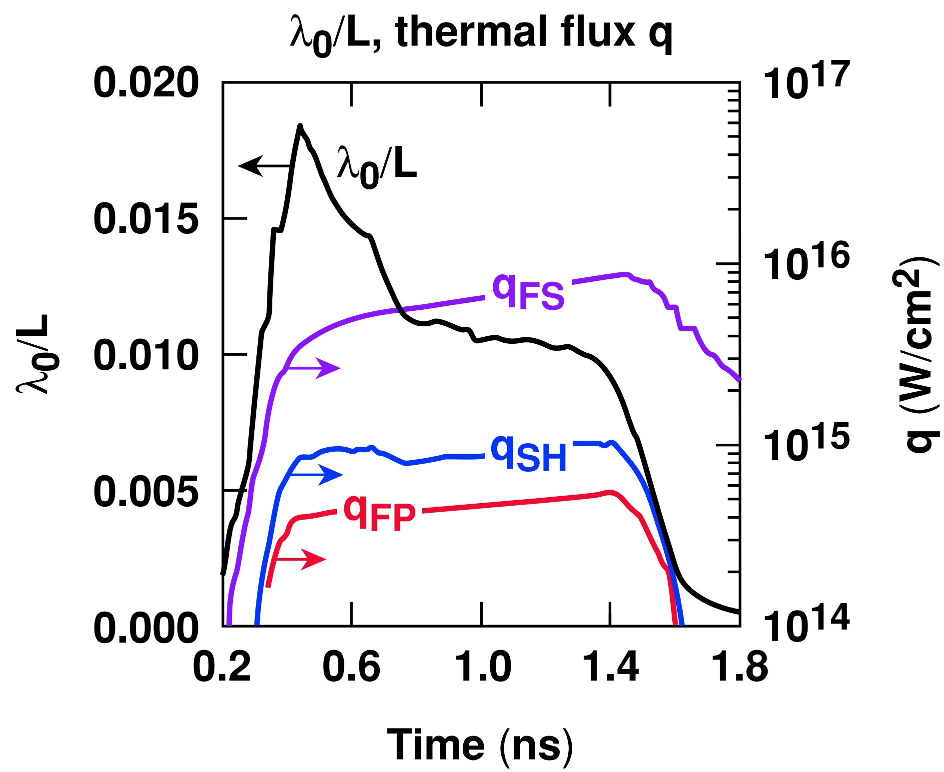

- Quantities measured at the critical surface
  - λ_0: electron mean free path for 90° collision scattering
  - L: electron temperature scale length $L = L_{Te} = T_e \Big/ \frac{\partial T_e}{\partial x}$

TC5812

To match the flux-limited SH flux with FP, the flux limiter should be changed in time

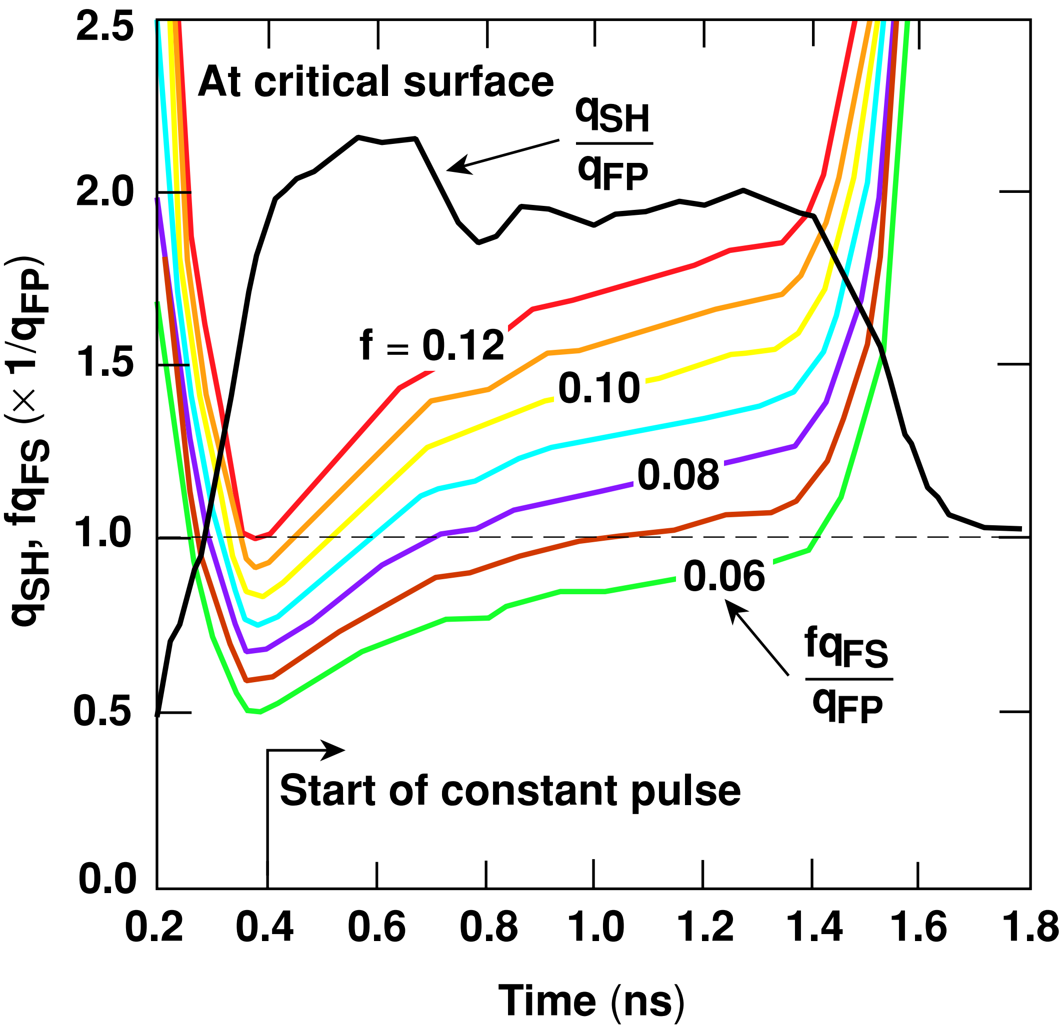

q_{FP} = min (fq_{FS}, q_{SH})

f : flux-inhibition factor

q_{FS}: Free-streaming flux

$$q_{FS} = n_e T_e v_{th}$$

$$v_{th} = \left(\frac{T_e}{m_e}\right)^{\frac{1}{2}}$$

q_{SH}: Spitzer-Härm flux

Absorbed laser power-averaged flux limiter

$$\langle f \rangle = \frac{\int f I_A dt}{\int I_A dt} = 0.075$$

I_A: Absorbed laser power

The inhibition factor is larger early in the pulse.

TC5813

Early in the pulse, FP gives a large density scale length at the critical surface than SH

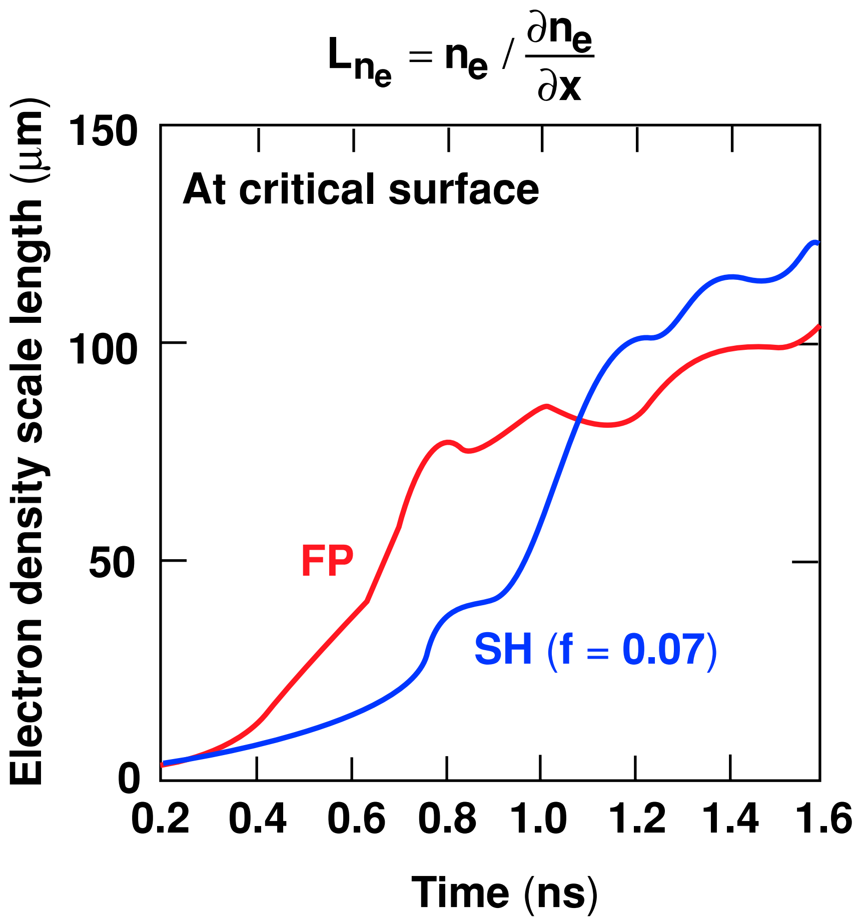

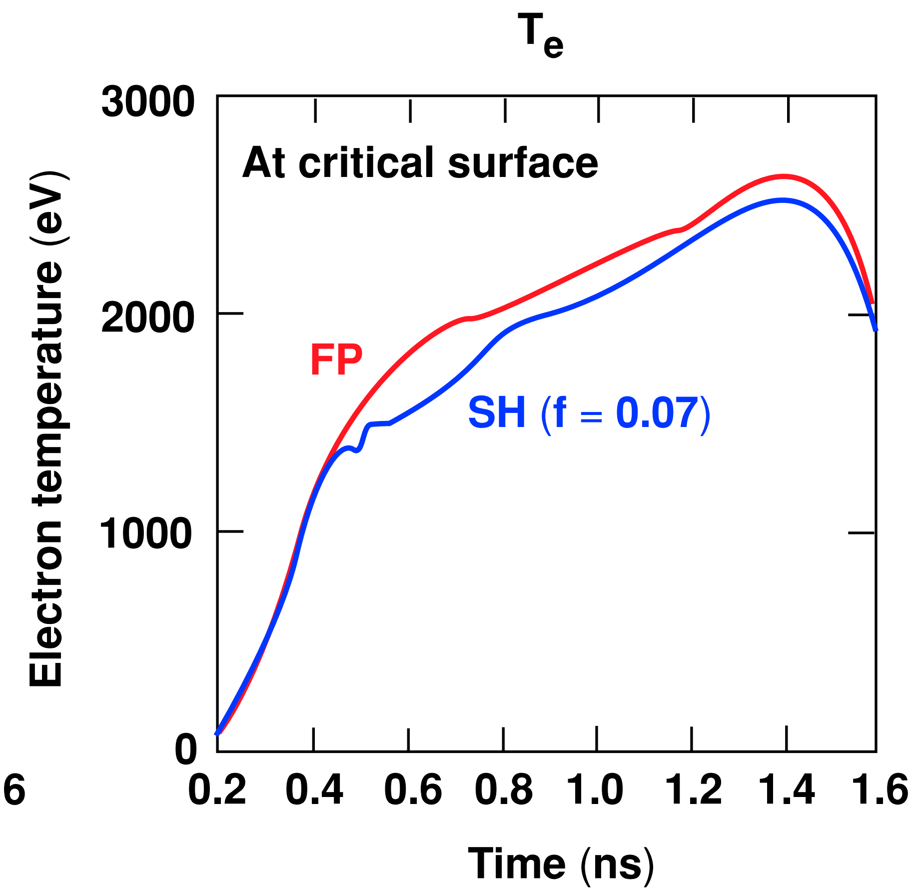

The larger early L_{ne} in the FP case gives rise to a larger absorption fraction than in the SH case.

TC5814

FP gives a large laser absorption early in the pulse and results in an increase of the total laser absorption fraction

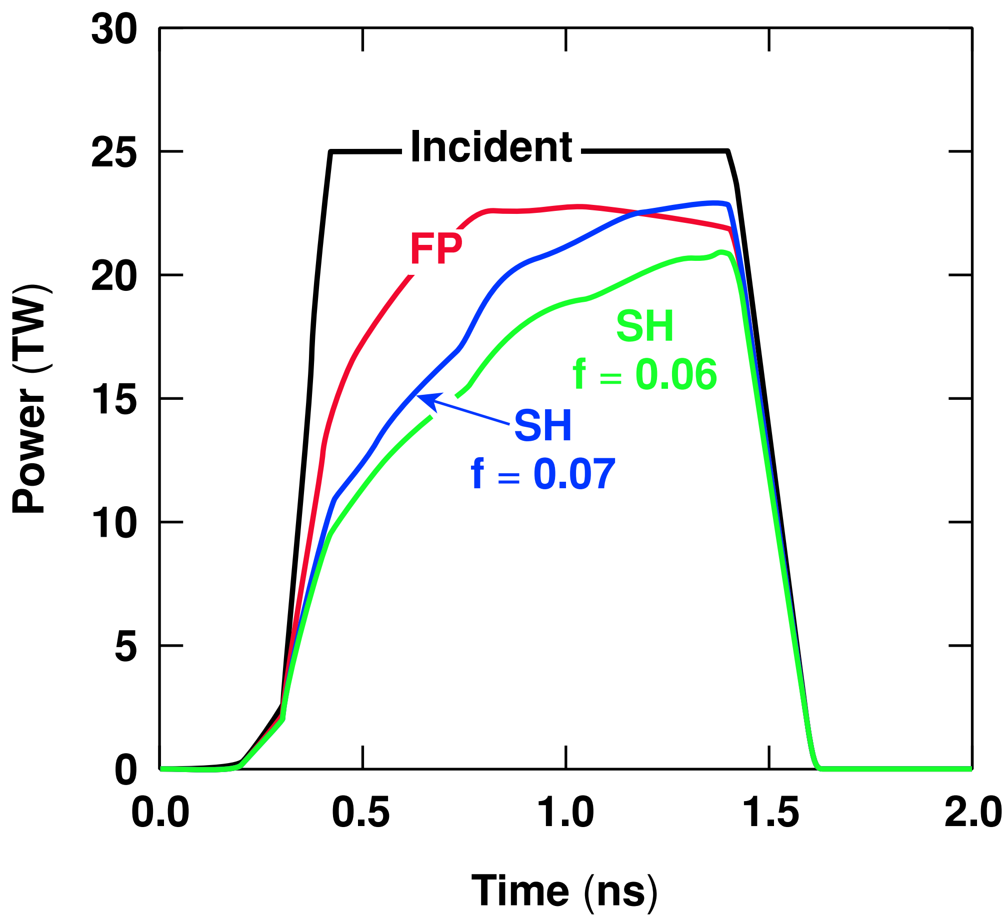

Total absorption fraction

FP: 0.83

SH f = 0.07: 0.76

SH f = 0.06: 0.68

TC5815

During the acceleration phase, FP gives a relatively low value for the mass ablation rate

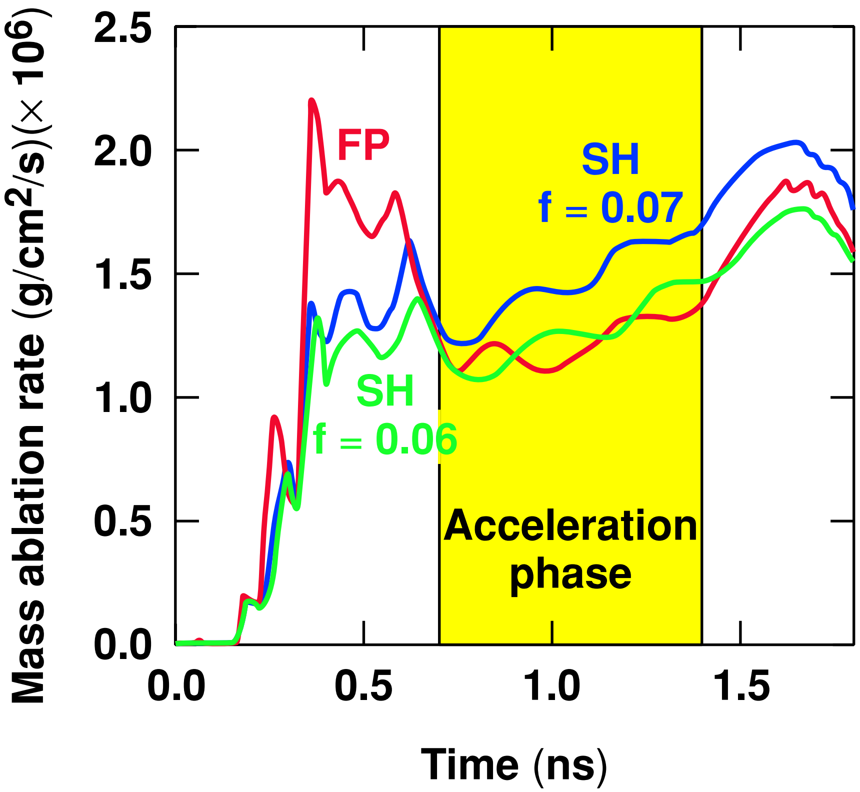

Time-averaged values over the acceleration phase

	FP	SH
Ablation density $<\rho_a>$ (g/cm^3)	3.06	3.77
Ablation velocity 10^5 $<V_a>$ (cm/s)	4.01	3.99
Minimum density gradient scale length $<L_m>$ (μm)	1.31	0.83

The early large mass ablation rate causes the large scale length in the FP case.

TC5816

For the 1-ns square pulse, both the SH f = 0.07 and FP show good agreement with experimental results

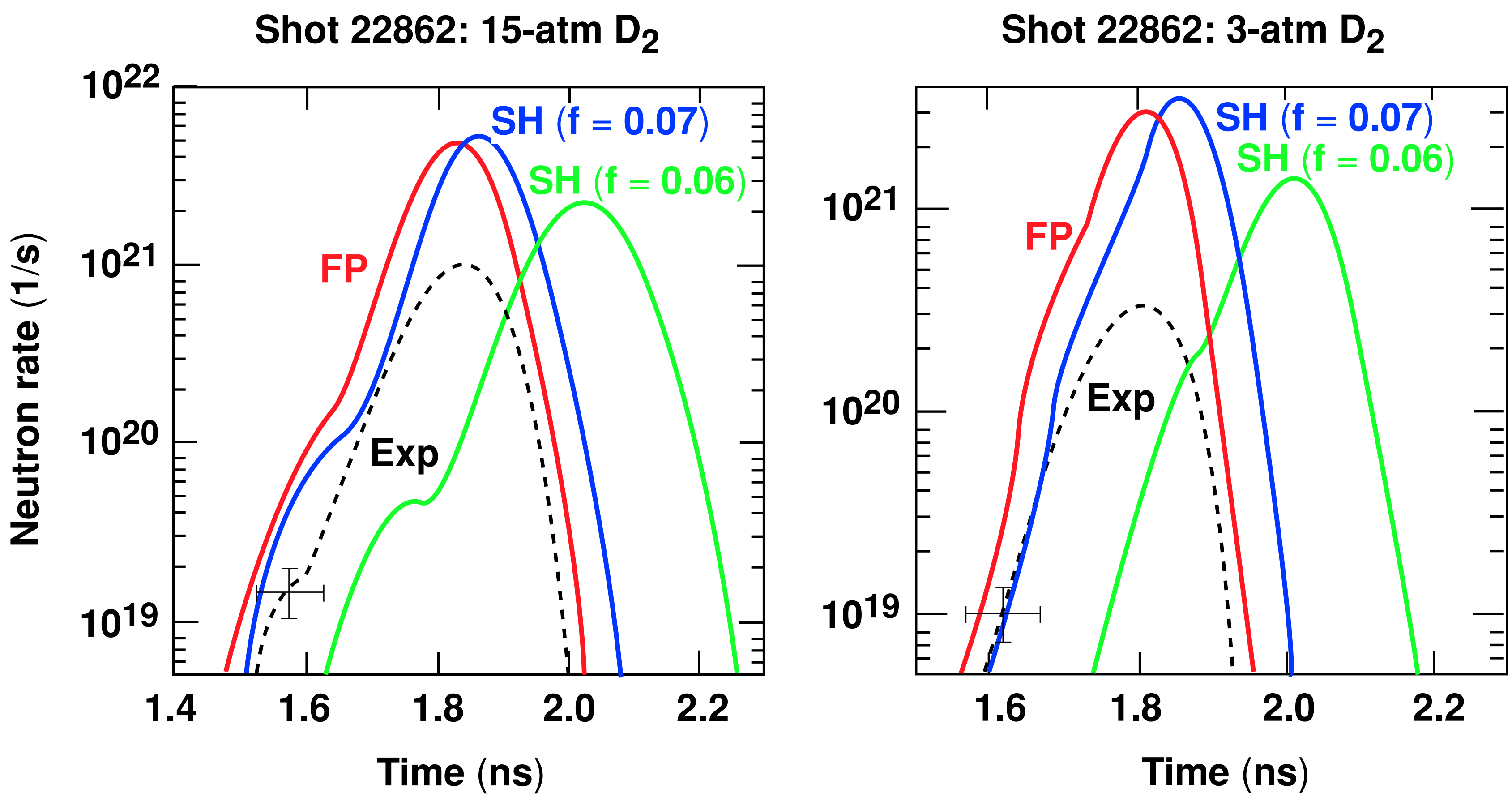

From FP, $\langle f \rangle = 0.075$

TC5817

For the 400-ps square pulse, the FP bang time coincides with SH f = 0.09 case, confirming that a larger flux limiter is needed for the short pulse

UR LLE

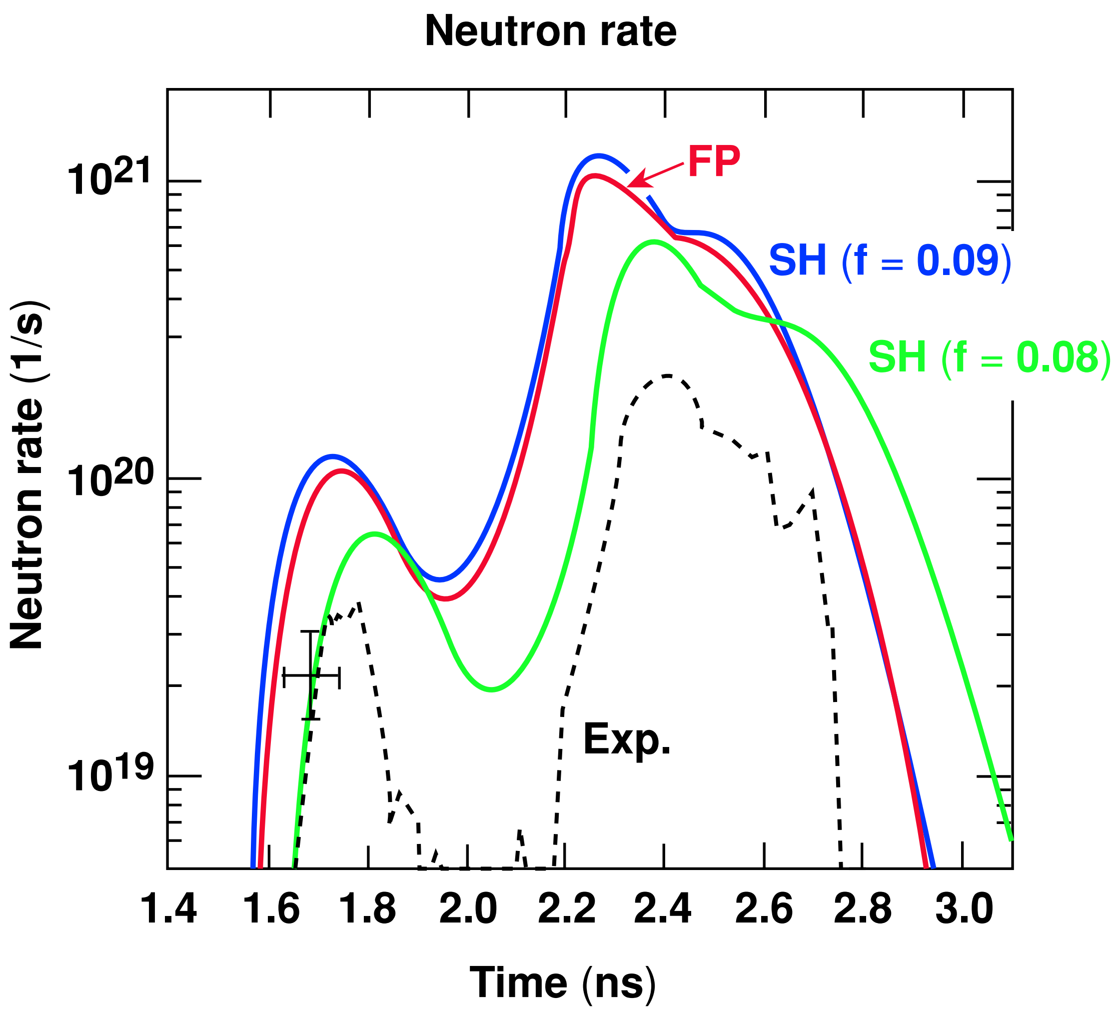

Absorbed laser-power-averaged flux limiter

$$\langle f \rangle = \frac{\int f I_A dt}{\int I_A dt} = 0.087$$

I_A: Absorbed laser power

TC5818

Conclusions

We have developed a 1-D Fokker–Planck code and combined it with the 1-D hydrodynamic code *LILAC*

- For CH implosions, comparison of FP with the flux-limited SH model
  - The flux inhibition factor is time dependent.
  - With FP, the laser absorption is higher than with SH due to a longer density scale length at the critical surface.
  - In the acceleration phase, FP gives a density-scale length at the ablation surface 50% longer than SH.
  - FP gives good agreement with the experimental bang time.
  - Calculations for cryogenic targets with shaped pulses are planned.

The Collisional Delta-f Method

Stephan Brunner, John Krommes and Ernest Valeo

presented at

LLNL Electron Transport Workshop

Sept. 9-11, 2002

1. Summary

- Objective: Development of low noise MC techniques for transport applications:

$$f = f_0 + \delta f, \quad \frac{\delta f}{f_0} \ll 1$$

where f_0 satisfies simplified equations and δf is solved by MC techniques.

- First applied to microturbulence problems in MFE: Kotchenreuther, Lee, Lin, Dimitz, Cohen, where f_0 was taken fixed.

- Our contribution:

  – Evolution of f_0, which enables transport time scale simulations.

  – Algorithm for computation of quasineutral $\vec{E}$.

  – Introduction of noise reductions techniques.

$\boxed{\text{1. Combined Fluid-Kinetic Equations. [Barnes (91)]}}$

Fokker–Planck Equation for Electrons:

$$\boxed{\frac{\partial}{\partial t} f + \vec{v} \cdot \frac{\partial}{\partial \vec{x}} f + \frac{(-e)}{m} \vec{E} \cdot \frac{\partial}{\partial \vec{v}} f = - \{ C_{ee}[f, f] + C_{ei} f \} .}$$

Decomposition of the distribution uniquely determined by:

$$f(\vec{x}, \vec{v}; t) = f_{\mathrm{SM}}(\vec{x}, \vec{v}; t) + \delta f(\vec{x}, \vec{v}; t),$$

$$f_{\mathrm{SM}} = \frac{N/\overline{N}}{[2\pi T/m]^{3/2}} \exp\left(-\frac{1}{2} \frac{[\vec{v} - \vec{u}]^2}{T/m} \right).$$

Constraints: $\int \delta f \, \vec{v}^{\,j} \, d\vec{v} = 0, \quad j = 0, 1, 2.$

1. **Taking the first three velocity moments of the F-P equation $\Longrightarrow$**

   $\boxed{\text{Fluid Equations}}$ **for Background Parameters** $[N(\vec{x}; t), \vec{u}(\vec{x}; t), T(\vec{x}; t)]$.

2. **Rewriting the F-P equation $\Longrightarrow$** $\boxed{\text{Effective equation for } \delta f}$**:**

$$\frac{D}{Dt} \delta f = - \left\{ \frac{D}{Dt} f_{\mathrm{SM}} + C_{ee}[\delta f, f_{\mathrm{SM}}] \right\},$$

$$\frac{D}{Dt} \doteq \frac{\partial}{\partial t} + \vec{v} \cdot \frac{\partial}{\partial \vec{x}} + \frac{(-e)}{m} \vec{E} \cdot \frac{\partial}{\partial \vec{v}} + C_{ee}[f_{\mathrm{SM}}, \ ] + C_{ei},$$

Approximation : "Linearizing" the self-collision operator:

$$C_{\mathrm{ee}}[f, f] = \underbrace{C_{\mathrm{ee}}[f_{\mathrm{SM}}, f_{\mathrm{SM}}]}_{=0} + \underbrace{C_{\mathrm{ee}}[\delta f, \delta f]}_{\textbf{neglect}} + C_{\mathrm{ee}}[f_{\mathrm{SM}}, \delta f] + C_{\mathrm{ee}}[\delta f, f_{\mathrm{SM}}]$$

Fluid-Kinetic Equations Cont'd

Fluid Equations for Background Parameters

- $j = 0 \Longrightarrow$ **Continuity equation:**

$$\frac{\partial N}{\partial t} + \frac{\partial}{\partial \vec{x}} \cdot (N \vec{u}) = 0.$$

- $j = 1 \Longrightarrow$ **Momentum equation:**

$$m\,N\left(\frac{\partial \vec{u}}{\partial t} + \vec{u} \cdot \frac{\partial \vec{u}}{\partial \vec{x}}\right) = -\frac{\partial}{\partial \vec{x}}(N\,T) - \frac{\partial}{\partial \vec{x}} \cdot \Pi(\delta f) + (-e)N\vec{E} + \vec{R}_{ei}(f_{\mathrm{SM}}) + \vec{R}_{ei}(\delta f).$$

- $j = 2 \Longrightarrow$ **Heat equation:**

$$\frac{\partial}{\partial t}\left(\frac{3}{2}N\,T + \frac{1}{2}m\,N\,u^2\right) + \frac{\partial}{\partial \vec{x}} \cdot \left[\frac{5}{2}N\,T\,\vec{u} + \frac{1}{2}m\,N\,u^2\,\vec{u} + \Pi \cdot \vec{u} + \vec{q}\,(\delta f)\right] = (-e)N\vec{u} \cdot \vec{E}.$$

CLOSURE to the fluid equations from moments of δf:

Stress tensor: $\quad \Pi(\delta f) = m\overline{N}\int \vec{v}\,\vec{v}\,\delta f\,d\vec{v}$

Drag of δf on ions: $\quad \vec{R}_{ei}(\delta f) = -m\overline{N}\int \vec{v}\,C_{ei}\,\delta f\,d\vec{v}$

Heat flux in δf: $\quad \vec{q}\,(\delta f) = \frac{m}{2}\overline{N}\int (\vec{v} - \vec{u})^2\vec{v}\,\delta f\,d\vec{v}$

$\boxed{\text{Fluid-Kinetic Equations Cont'd}}$

Representing δf using the Collisional δf method

$$\frac{D}{Dt}\delta f = -\left\{\frac{D}{Dt}f_{\rm SM} + C_{ee}[\delta f, f_{\rm SM}]\right\},$$

$$\frac{D}{Dt} \doteq \frac{\partial}{\partial t} + \vec{v}\cdot\frac{\partial}{\partial \vec{x}} + \frac{(-e)}{m}\vec{E}\cdot\frac{\partial}{\partial \vec{v}} + C_{ee}[f_{\rm SM},\ ] + C_{ei},$$

Representation of δf with Marker Particles:

$$\delta f(\vec{x},\vec{v};t) \simeq \sum_{i=1}^{n_p} w_i(t)\,\delta(\vec{x}-\vec{x}_i(t))\,\delta(\vec{v}-\vec{v}_i(t)).$$

Marker Distribution: $g(\vec{x},\vec{v};t) \simeq \sum_i \delta(\vec{x}-\vec{x}_i(t))\,\delta(\vec{v}-\vec{v}_i(t))$.

MARKER EQUATIONS:

$$\frac{d\vec{x}}{dt} = \vec{v},$$

$$\frac{d\vec{v}}{dt} = \frac{(-e)}{m}\vec{E} + \frac{\delta\vec{v}_{ee}}{\delta t} + \frac{\delta\vec{v}_{ei}}{\delta t},$$

$$\dot{w} \doteq \frac{dw}{dt} = -\frac{1}{g}\left\{\frac{D}{Dt}f_{\rm SM} + C_{ee}[\delta f, f_{\rm SM}]\right\}.$$

- **Random Increments $\delta\vec{v}_{ee}$ and $\delta\vec{v}_{ei}$ reproduce $C_{ee}[f_{\rm SM},\delta f]$ and $C_{ei}\,\delta f$. $\Longrightarrow$ Monte Carlo Simulation.**
- **Collisions in PIC and δf, including approximations on $C[\delta f, f_{\rm SM}]$:**

  Takizuka & Abe (77); Xu & Rosenbluth (91); Dimits & Cohen (94); Lin et.al(97); Chen & White (97).
- **Two weighted δf scheme [Hu & Krommes (94)]**

  $\Longrightarrow$ Avoids evaluating g.

Study Case: Relaxation Through Self-Collisions.

DISCARDING terms in the weight equation:

MOTIVATION: They require evaluating partial derivatives in velocity space of g and δf, which is costly in computation time and demanding statistically.

CONSEQUENCE: Different markers, having undergone different stochastic trajectories, can end up at the same point in phase space with different weights w_i. $\Longrightarrow$

- The initial definition $w_i(t) = W[\vec{v}_i(t), t]$ is violated.
- SPREADING Δw OF MARKER WEIGHTS
  $\Longrightarrow$ INCREASING NUMERICAL NOISE.

JUSTIFICATION: By reinterpreting the weight field W at a given point in phase space as the average over all particle weights in the vicinity of that point, it can be proven that the system of marker equations REMAINS EXACT [Chen & White (97)].

ELECTRIC FIELD $\sim$ RUNAWAY FIELD

Electric field: $E = 5 \cdot 10^{-2}\ m\overline{\nu}_{\rm ee}(0)v_{\rm th}(0)/e$,

Runaway field: $E_c = 0.11\ m\overline{\nu}_{\rm ei}v_{\rm th}/e$,

$Z = 1, \qquad n_p = 10^4, \qquad \Delta t = 10^{-2}\overline{\nu}_{\rm ee}(0)^{-1}$.

TEMPERATURE

(Ohmic heating)

AVERAGE VELOCITY

$\sim$ CURRENT

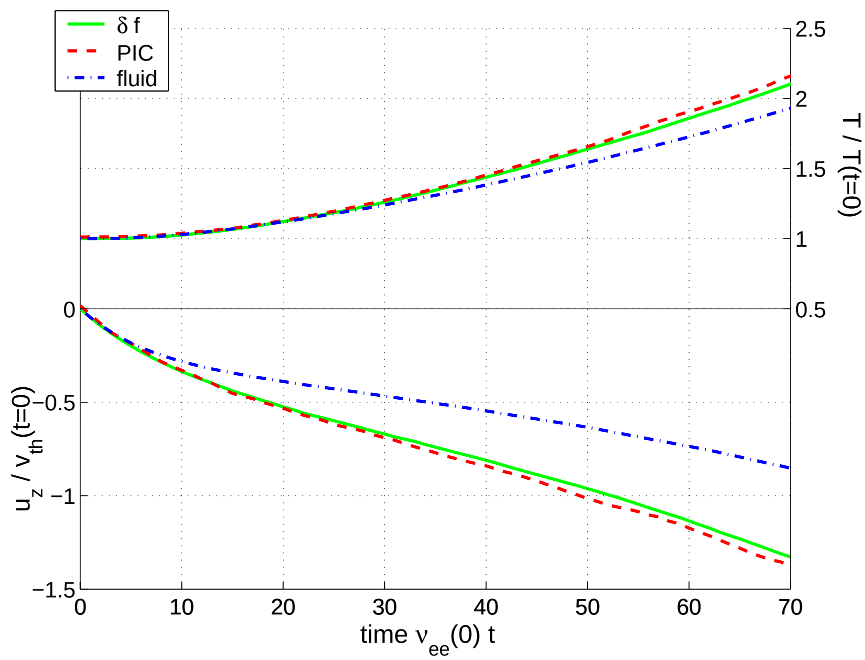

DISTRIBUTIONS

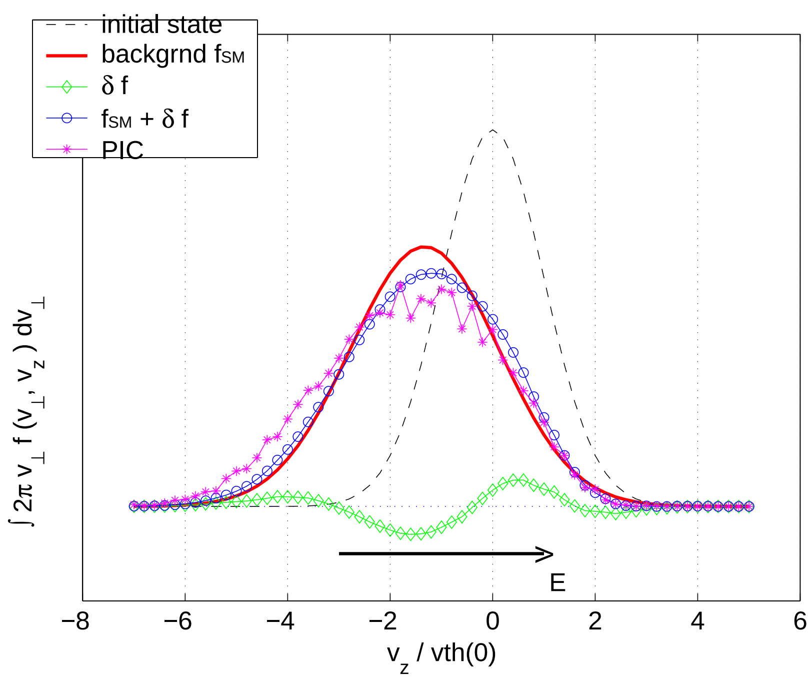

ELECTRIC FIELD $\ll$ RUNAWAY FIELD

Electric field: $E = 10^{-4}\ m\overline{\nu}_{\rm ee}(0)v_{\rm th}(0)/e$,

AVERAGE VELOCITY

$\sim$ **CURRENT**

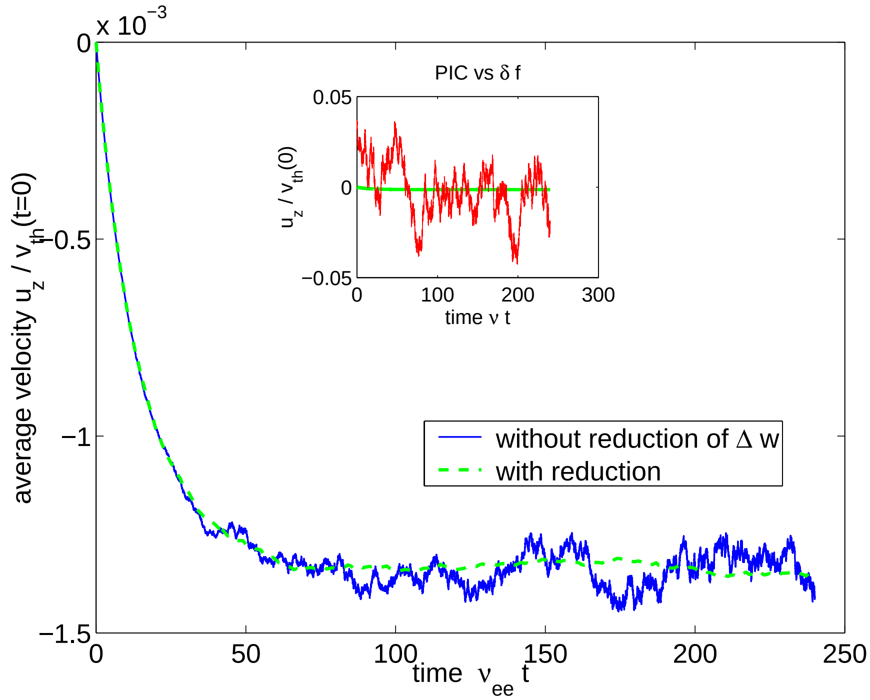

SOURCES/SINKS $\Longrightarrow$

GOOD RESOLUTION

MAINTAINED AT $|\vec{v}| \gg v_{\rm th}$

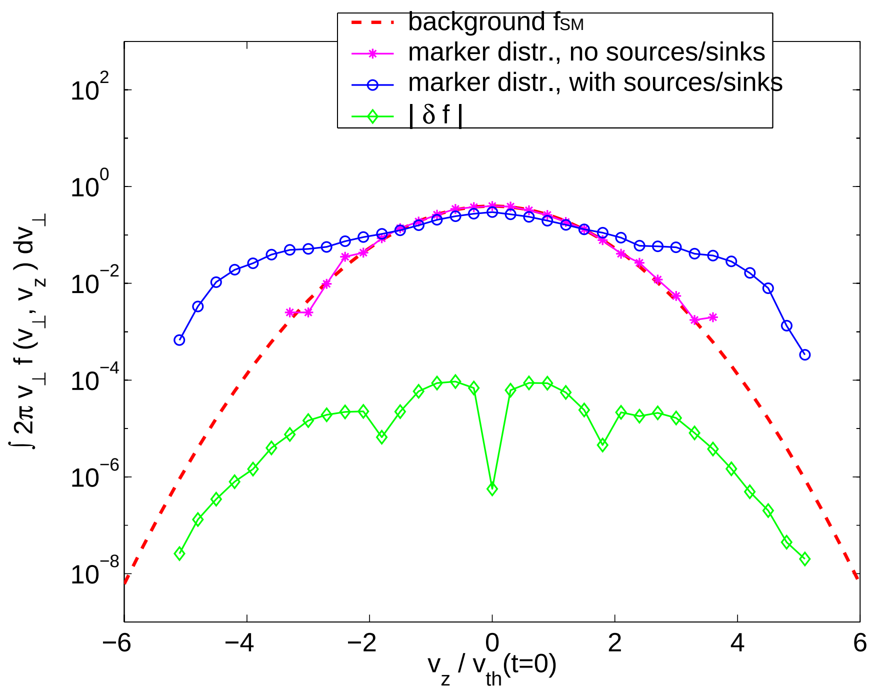

ELECTRIC FIELD $\ll$ RUNAWAY FIELD, Cont'd.

LINEAR REGIME

$$\Longrightarrow$$

SPITZER CONDUCTIVITY

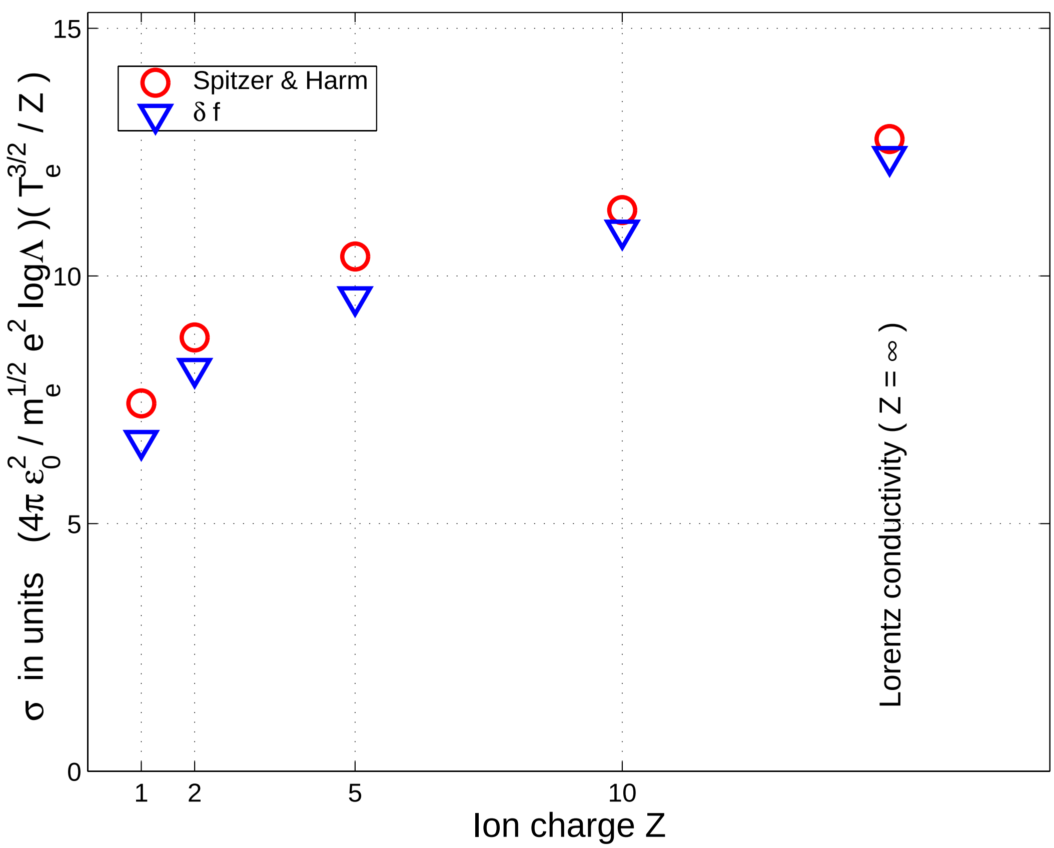

Illustration 2: Linear, NonLocal Electron Heat Transport

Assuming small amplitude, 1-Dim perturbations of the electron dist.:

$$f(x, \vec{v}; t) = f_{\mathrm{M}}(|\vec{v}|) + \delta f(x, \vec{v}; t), \qquad \delta f / f \ll 1.$$

- Only the linearized F-P equation is solved.
- No evolution of the background required.

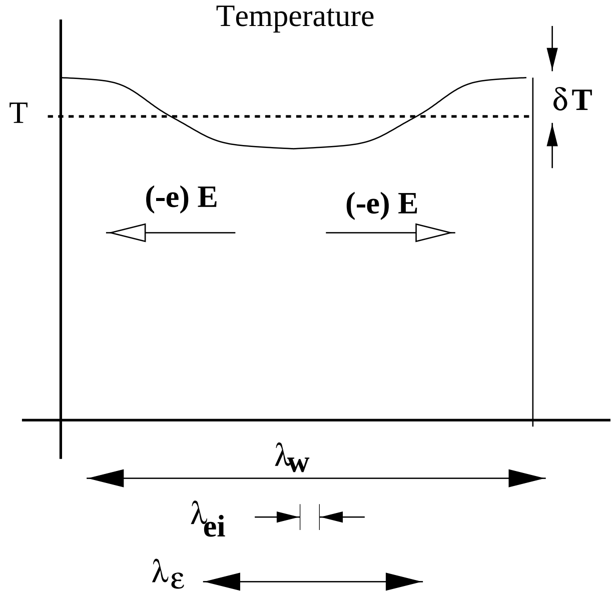

Initial Condition:

$$\delta f(t=0) = \delta T \frac{\partial}{\partial T} f_{\mathrm{M}},$$

$$\delta T = \cos \frac{2\pi}{\lambda_w} x.$$

Periodic boundary conditions.

Assuming high Z plasma, $Z \gg 1 \Longrightarrow$ Varaiables (x, v).

- $\overline{\lambda}_{ei} / \lambda_{\mathrm{wave}} \ll 1 \;\Longrightarrow\; \delta f = \delta f_0(x, |\vec{v}|) + \delta f_1(x, |\vec{v}|) \dfrac{v_x}{|\vec{v}|} + \ldots$
- Stopping Length: $\overline{\lambda}_\epsilon = \sqrt{\dfrac{\tau_{ee}}{\tau_{ei}}}\, \overline{\lambda}_{ei} = \sqrt{Z}\, \overline{\lambda}_{ei} \;\Longrightarrow\; \overline{\lambda}_\epsilon / \lambda_w \sim 1.$

Linear, NonLocal Electron Heat Transport. Cont'd

The linearized F-P equation:

$$\frac{\partial \delta f}{\partial t} + v_x \cdot \frac{\partial \delta f}{\partial x} + \frac{(-e)}{m} E \cdot \frac{\partial f_{\mathrm{M}}}{\partial v_x} = -\{ C_{ee}[f_{\mathrm{M}}, \delta f] + C_{ee}[\delta f, f_{\mathrm{M}}] + C_{ei}\delta f \},$$

is expanded in the small parameter $\overline{\lambda}_{ei}/\lambda_{\mathrm{wave}}$.

The lowest order anisotropy: $\delta f_1 = -\frac{\lambda_{ei}(v)}{2}\left(\frac{\partial\, \delta f_0}{\partial x} + \frac{e\, E}{T} f_{\mathrm{M}}\right),$

is used for obtaining an effective equation for $\delta f_0(x, |\vec{v}|)$:

$$\frac{\partial\, \delta f_0}{\partial t} - \frac{\partial^2}{\partial x^2}\left(\frac{v\lambda_{ei}(v)}{6}\, \delta f_0\right) + C_{ee}[f_{\mathrm{M}}, \delta f_0] = \frac{v\lambda_{ei}(v)}{6}\frac{e}{T}\frac{\partial E}{\partial x}\, f_{\mathrm{M}} - C_{ee}[\delta f_0, f_{\mathrm{M}}].$$

This equation is then solved using the collisional δf scheme.

Computing the Self-Consistent Electric Field

Continuity Eq.: $\dfrac{\partial}{\partial t}\delta N + \dfrac{\partial}{\partial x}\Gamma = 0$ **+ Quasineutrality** $\Longrightarrow \dfrac{\partial \Gamma}{\partial x} = 0$

$$\Gamma = \frac{1}{3}\int_0^\infty (4\pi v^2)\, dv\; v\,\delta f_1 = -\int_0^\infty (4\pi v^2)\, dv\; \frac{v\,\lambda_{ei}(v)}{6}\left(\frac{\partial\,\delta f_0}{\partial x} + \frac{e\,E}{T}\, f_{\mathrm{M}}\right).$$

METHOD 1: $$\frac{\partial E}{\partial x} = -\frac{T}{e}\frac{\sqrt{2\pi}}{96}\,\frac{\partial^2}{\partial x^2}\left[\int_0^\infty dv\,(4\pi v^2)\left(\frac{v}{v_{\mathrm{th}}}\right)^5 \delta f_0\right].$$

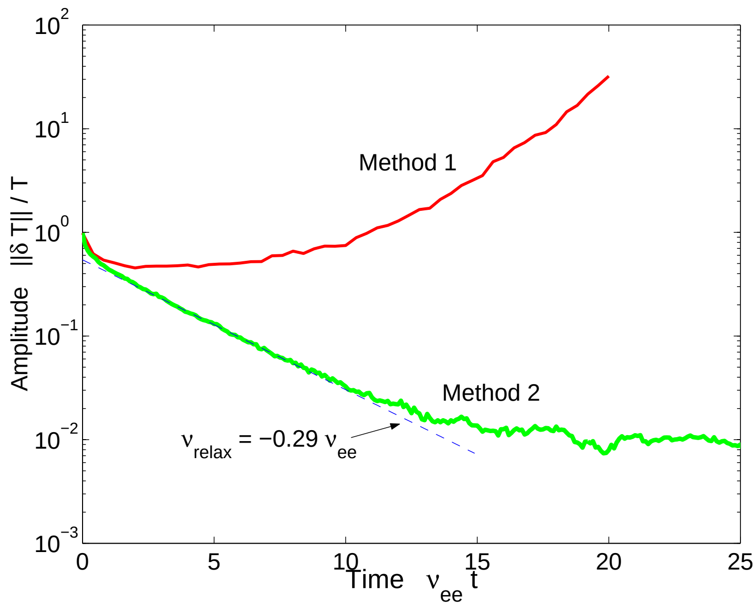

$\overline{\lambda}_\epsilon/\lambda_w = 0.1$

Solution to Numerical Instability:

Impose Numerical Invariance of Density on the Spatial Grid $\{X_k\}$:

$$\delta N_k^{j+1} = \sum_{i=1}^{n_p} w_i^{j+1} S(X_k - x_i^{j+1}) = \sum_{i=1}^{n_p} w_i^j\, S(X_k - x_i^j) = \delta N_k^j.$$

$$\frac{d\,w_i}{dt} \simeq \frac{w_i^{j+1} - w_i^j}{\Delta t} = \frac{1}{g}\left\{\frac{v\lambda_{ei}(v)}{6} f_{\mathrm{M}} \frac{e}{T}\sum_{l=1}^{n_x}\left(\frac{\partial E}{\partial x}\right)_l^{j+1/2} S(X_l - x_i) - C_{ee}[\delta f, f_{\mathrm{M}}]\right\}.$$

METHOD 2 = Linear System: $$\sum_{l=1}^{n_x} M_{kl}\left(\frac{\partial E}{\partial x}\right)_l^{j+1/2} = A_k.$$

Comparison with NonLocal Hydrodynamic Approach

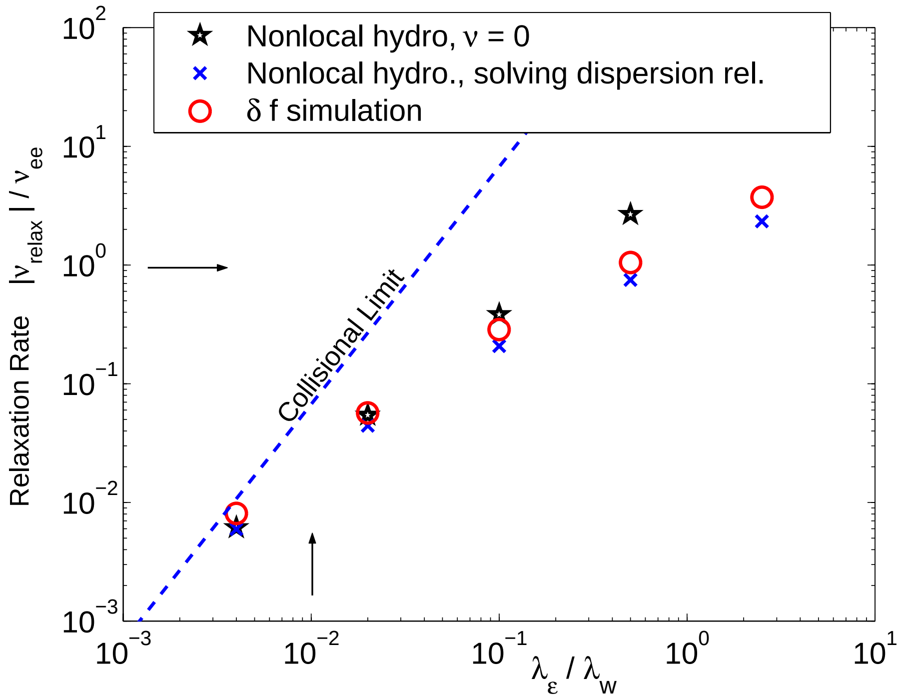

Collisional Limit OK for:

$$\overline{\lambda}_\epsilon/\lambda_w \stackrel{\sim}{<} 10^{-2}$$

Transport is nonlocal both in space and in time.

NONLOCAL HYDRODYNAMIC APPROACH: [Bychenkov et.al (95)]

Solves the same linearized F-P equation for δf_0 as in δf simulations, however using a generalized Laguerre polynomial decomposition. The solution is then applied for deriving closure relations to the fluid Eqs.,valid for all regimes of collisionality.

In reciprocal space (k, ν):

$$j_x = (-e)\Gamma_x = \ \sigma(k,\nu)\, E^\star + \alpha(k,\nu)\ ik\,\delta T,$$

$$q_x = -\alpha(k,\nu)\, T\, E^\star - \chi(k,\nu)\ ik\,\delta T,$$

Heat Eq.: $\displaystyle \frac{3}{2}N\frac{\partial}{\partial t}\delta T + \frac{\partial}{\partial x}\left(q_x + T\,\Gamma_x\right) = 0 \implies \nu_{\mathrm{relax}} = -\frac{2}{3}\frac{k^2}{N}\left(\chi - T\frac{\alpha^2}{\sigma}\right).$

Illustration 3: NonLinear, NonLocal Electron Heat Transport

Considering large amplitude, 1-Dim temperature perturbations of the electron distribution:

$$f(x, \vec{v}; t) = f_{\mathrm{M}}[v|N_e(x), T(x,t)] + \delta f(x, \vec{v}; t).$$

Requires:

- Solving the full nonlinear F-P equation.
- Evolving the background when applying the δf method.
- Enforcing quasineutrality $\Longrightarrow$ Equation for $\vec{E}$ (Similar algorithm as in linear code).

HERE: No assumption on $Z \Longrightarrow$ Variables $(x, v, \mu = \cos\theta)$.

NonLinear, NonLocal Electron Heat Transport. Cont'd

Computing Background Temperature

TWO ALTERNATIVES:

1. **"Stiff" constraint on kinetic energy $\mathrm{Kin}(\delta f)$:**

$$\mathrm{Kin}(\delta f) = \frac{m}{2} \int \delta f \, v^2 \, d\vec{v} = 0.$$

$\Longrightarrow$ **Heat Eq. for background temperature:**

$$\frac{3}{2} N_e(x) \frac{\partial}{\partial t} T(x,t) + \frac{\partial}{\partial x} q_x(\delta f) = 0.$$

2. **"Soft" constraint on kinetic energy $\mathrm{Kin}(\delta f)$:**

$$0 \;\simeq\; \mathrm{Kin}(\delta f) \;\ll\; \mathrm{Kin}(f_{\mathrm{M}}).$$

"Numerical feed-back" of $\mathrm{Kin}(\delta f)$ back into f_{M}:

$$\frac{3}{2} N_e \frac{\partial}{\partial t} T(x,t) = \alpha_{\mathrm{relax}} \; \mathrm{Kin}(\delta f).$$

BENCHMARKING NonLinear Code with Linear NonLocal Hydrodynamic Approach

---

Relaxation of Small Amplitude Sinusoidal Perturbations in the Background Temperature: $\delta T/T = 0.1$.

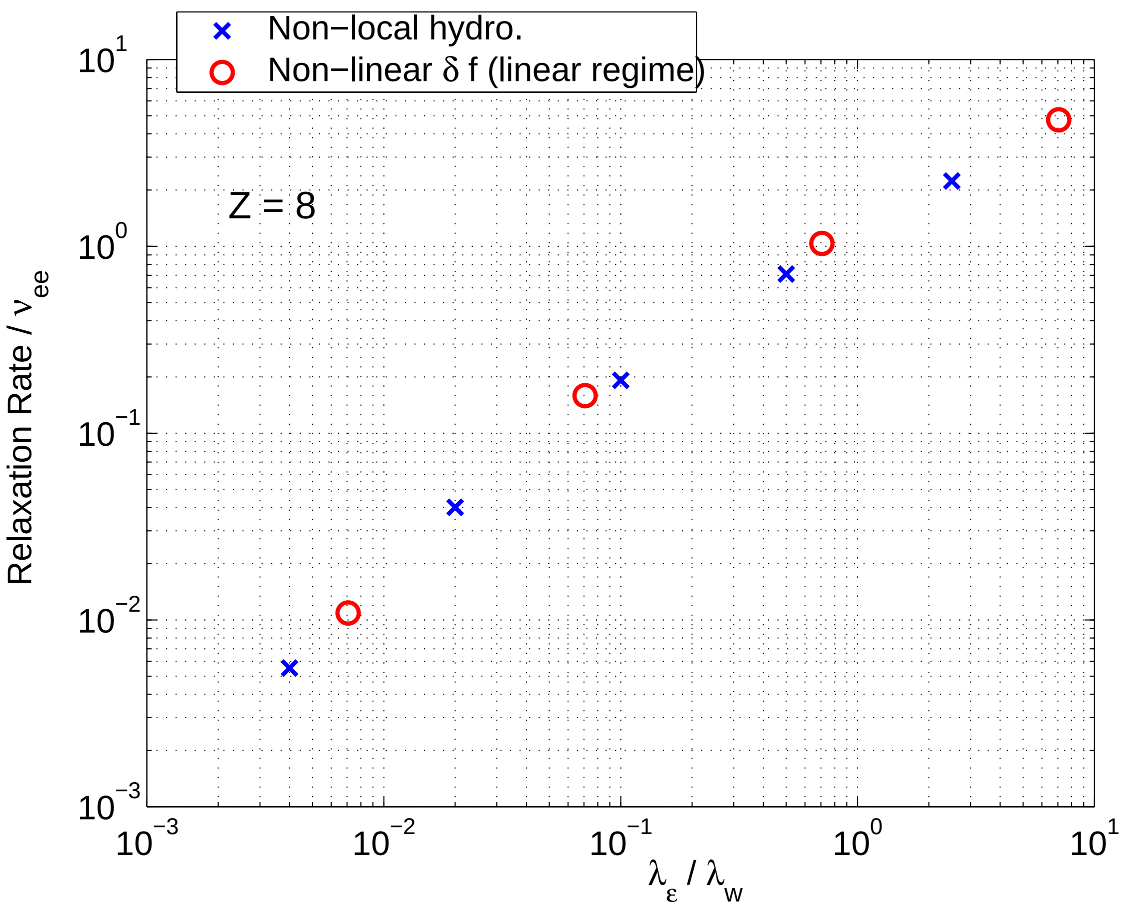

Relaxation of Gaussian Temperature Peak

TEMPERATURE:

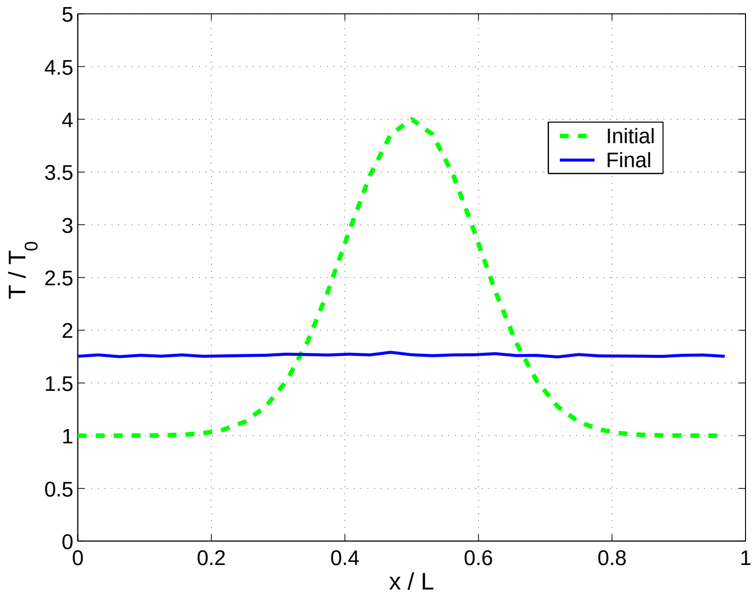

INITIALLY:

$$T(x, t = 0) = T_0 + \delta T \exp\left[-\frac{1}{2}\left(\frac{x - 0.5\,L}{\Delta x}\right)^2\right],$$

$$\delta f \equiv 0.$$

Parameters:

$\lambda_{ee}(0)/L = 10^{-1}$ **(Evaluated at base of peak)**

$Z = 3$

$\Delta x/L = 10^{-1}$, $\delta T/T_0 = 3$

Uniform density: $N \equiv N_0$

COMPARING f_{M} AND δf AT TIME $t = 5.0\,\nu_{ee}(0)$

Hot Peak

$X/L = 0.5$

Cold Boundary

$X/L = 0.0$

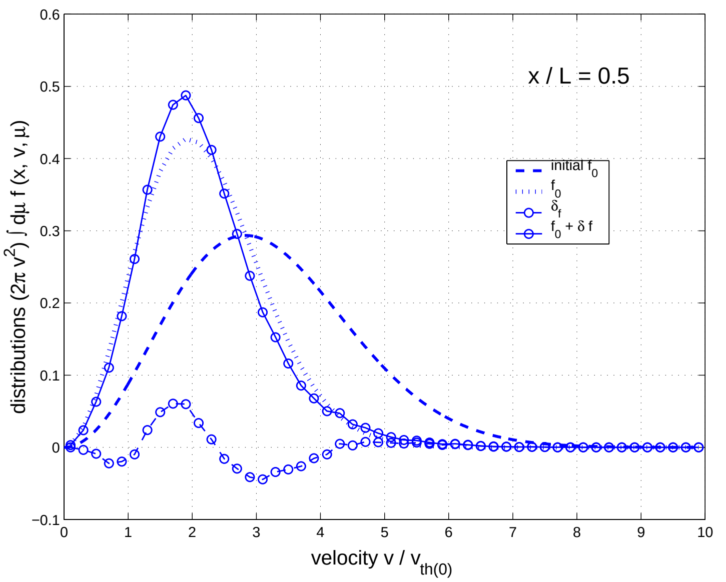

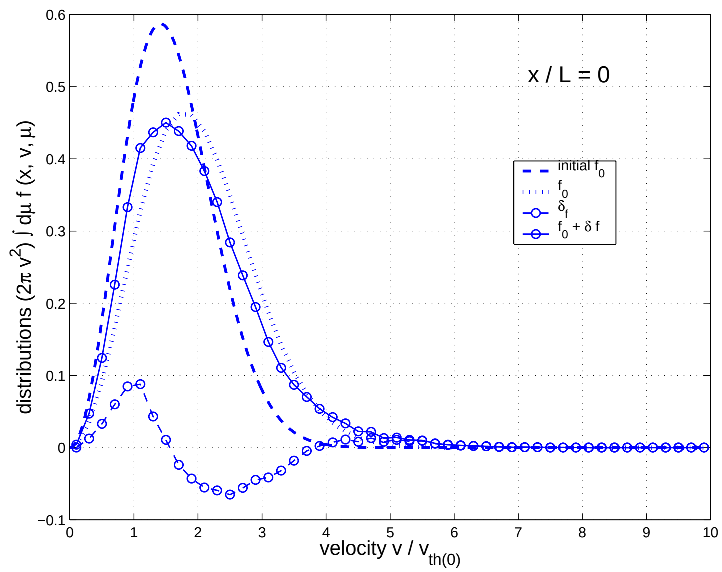

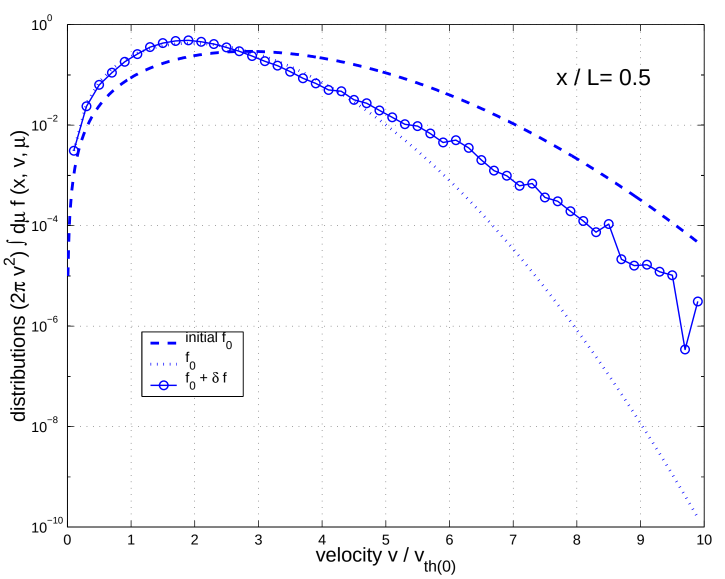

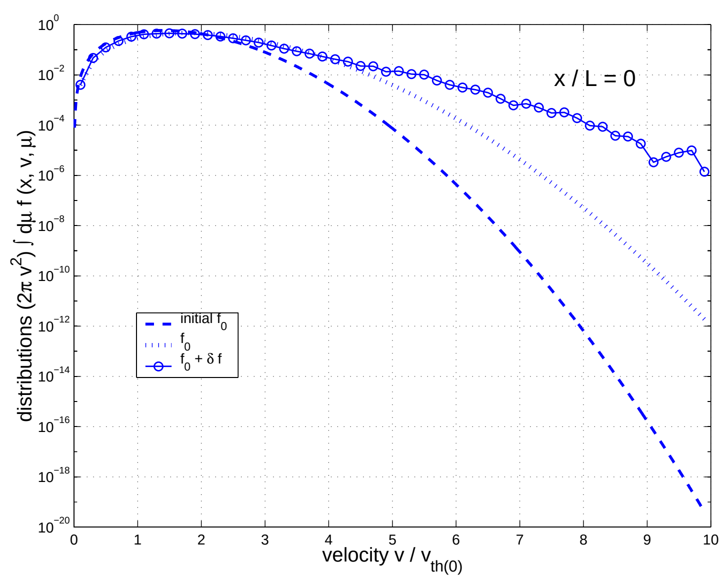

SCALING ON PARALLEL COMPUTER

- **Code is Parallelized using MPI.**
- **Running on Origin 2000 and Linux Cluster.**
- **Implements a high-quality, parallel pseudo-random number generator (C.Karney).**

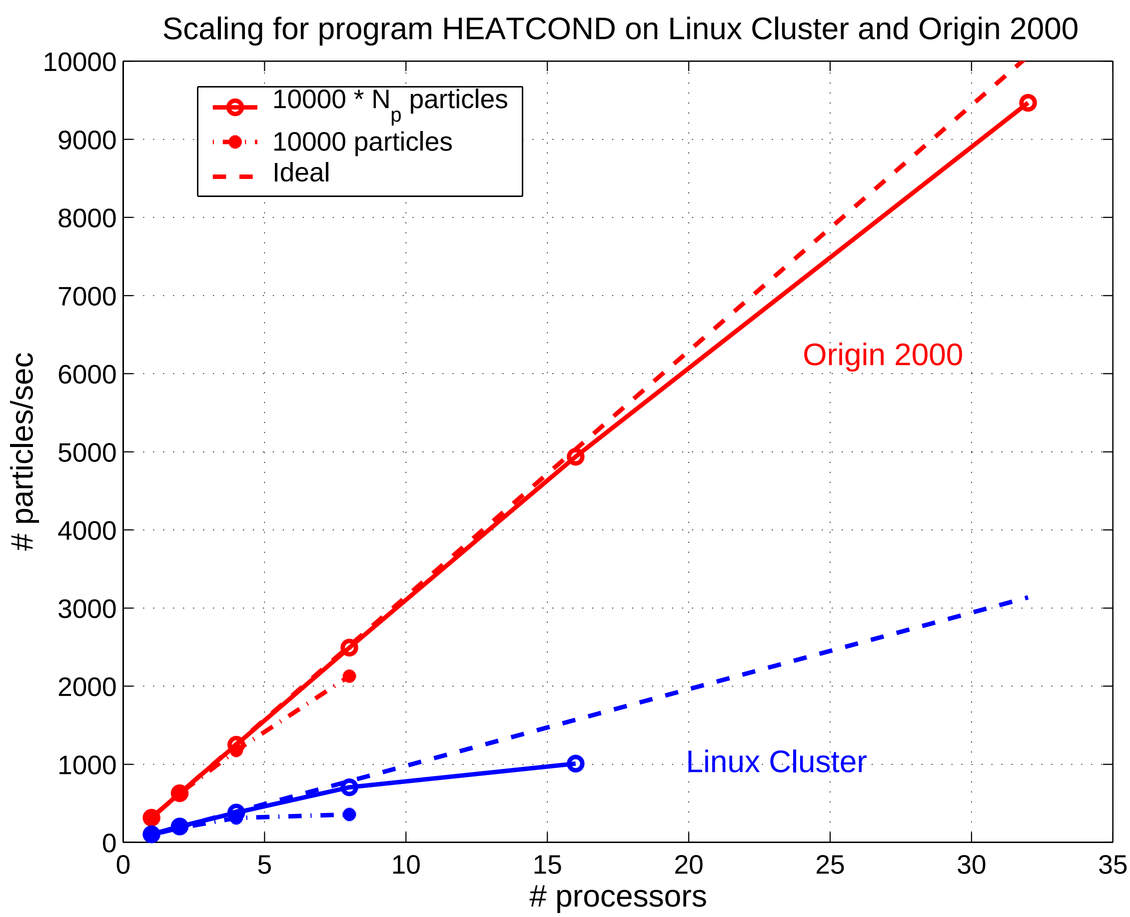

REFERENCES:

Xu & Rosenbluth (91); Dimits & Cohen (94); Lin et al.(97)

S. Brunner, E. Valeo, and J. A. Krommes, Physics of Plasmas 6, 4504 (1999); 7, 2810 (2000).